# Decrypting the role of HSP90α and β isoforms in BCR-ABL1$^{+}$ leukemia and Characterization of Small Molecule HSP90 Inhibitors and Degraders

**Inaugural-Dissertation**

zur Erlangung des Doktorgrades (Dr. rer. nat.)
der Mathematisch-Naturwissenschaftlichen Fakultät
der Heinrich-Heine-Universität Düsseldorf

vorgelegt von

**Melina Vogt**

aus Mülheim an der Ruhr

Düsseldorf, Februar 2024

Aus der Klinik für Kinder-Onkologie,- Hämatologie und Klinische Immunologie
der Universitätsklinik Düsseldorf

Gedruckt mit der Genehmigung der
Mathematisch-Naturwissenschaftlichen Fakultät der
Heinrich-Heine-Universität Düsseldorf

Berichterstatter:
1. Prof. Dr. Arndt Borkhardt
2. Prof. Dr. Thomas Kurz
Tag der mündlichen Prüfung: 18.11.2024

## Acknowledgments

I would like to thank all the people who have contributed to the success of this work.

First, I would like to thank Dr. Sanil Bhatia for the opportunity to write this thesis in his group. I would like to thank you for the excellent scientific supervision, your constant optimism, and the opportunity to promote my independent way of working. You have been a great mentor and our joint efforts on this project has always kept my enthusiasm and motivation high.

Furthermore, I extend my appreciation to Prof. Dr. Arndt Borkhardt for granting me the opportunity to conduct my dissertation within the Department of Pediatric Oncology, Hematology, and Clinical Immunology. I am particularly grateful for his comprehensive reviews of my progress and his willingness to assume the role of my primary supervisor.

Additionally, I express my gratitude to Prof. Dr. Thomas Kurz for assuming the responsibility of my secondary supervision and for the informative discussions and great cooperation.

I would like to thank all the co-authors and collaborators who have played a crucial role in shaping this research project. Their contributions, ranging from experimental expertise to critical feedback, have been essential in making this work a success.

I extend my gratitude to the entire 'Team Target' for their unwavering support and camaraderie throughout our three-year journey. Special thanks go to Kati and Jia for conducting the in vivo experiments and to Julian for the analysis and visualization of the bioinformatic data. Our friendship and mutual support created a really valuable and motivating atmosphere within the lab. I would also like to thank Philip for the imaging and microscopy. Silke's constant support in all aspects of laboratory operations played a crucial role in ensuring our smooth workflow and success. I would like to thank the entire HSP90 team including Vitalij, David, Julian H. and Berna and especially Niklas for the incorporation into the HSP90 project and the great teamwork. I am truly grateful to all members of the KMT-lab for creating such a great and supportive environment.

I would like to thank all members of the Düsseldorf School of Oncology (DSO) for the financial and professional support and the numerous opportunities for scientific exchange.

Many thanks also go to my family and friends, who have always encouraged and supported me.

# Table of Contents

## List of Abbreviations

| | |
|---|---|
| ABL | Abelson leukemia virus |
| ADP | Adenosine diphosphate |
| AHA1 | Activator of HSP90 ATPase homolog 1 |
| ALDH4A1 | Aldehyde dehydrogenase 4 family member A1 |
| ALL | Acute lymphoblastic leukemia |
| AML | Acute myeloid leukemia |
| APOBR | Apolipoprotein B receptor |
| AR | Androgen receptor |
| ATP | Adenosine Triphosphate |
| AX | Aminoxyrone |
| BCR | Breakpoint cluster region |
| BMFZ | Biological-Medical Research Center |
| B-PLL | B-cell prolymphocytic leukemia |
| BSA | Bovine serum albumin |
| CA2 | Carbonic anhydrase 2 |
| CDK | Cyclin-dependent kinase |
| CLL | Chronic lymphocytic leukemia |
| CmA1 | Coumermycin A1 |
| CML | Chronic myeloid leukemia |
| CRBN | Cereblon |
| CTD | C-terminal domain |
| CTG | CellTiter Glo |
| CXCR4 | C-X-C chemokine receptor type 4 |
| dDSS | Differential drug sensitivity score |
| Dip G | Diptoindonesin G |
| DLT | Dose-limiting toxicity |
| DMEM | Dulbecco's modified eagle medium |
| DMSO | Dimethyl sulfoxide |
| DSMZ | German Collection of Microorganisms and Cell Cultures |
| e.g. | Lat: *exempli gratia* (for example) |

| | |
|---|---|
| ECD | Phycoerythrin-texas red conjugate (energy-coupled dye) |
| et al. | Lat: *et alii* (and others) |
| FACS | Fluorescence-activated cell sorting |
| FCS | Fetal calf serum |
| FDA | Food and drug administration |
| FDR | False discovery rate |
| fGSEA | Fast gene set enrichment analysis |
| FITC | Fluorescein isothiocyanate |
| FP | Fluorescence polarization |
| FSC | Forward scatter |
| GFP | Green fluorescent protein |
| GIST | Gastrointestinal stromal tumours |
| GRP94 | Glucose-regulated protein |
| HCH1 | High-copy HSP90 suppressor |
| HER2 | Human epidermal growth factor receptor 2 |
| HOP | HSP70-HSP90 organizing protein |
| HRC | Histidine-rich calcium-binding protein |
| HSP | Heat shock protein |
| i.v. | Intravenously |
| IAP | Inhibitor of apoptosis |
| $IC_{50}$ | Half maximal inhibitory concentration |
| IFN-α | Interferon α |
| KD | Knockdown |
| kDa | Kilo Dalton |
| KI | Knock in |
| KO | Knockout |
| LCP2 | Lymphocyte cytosolic protein 2 |
| MAGEB1 | Melanoma-associated antigen B1 |
| MD | Middle domain |
| MDM2 | Mouse double minute 2 homologue |
| MoA | Mode of action |

| | |
|---|---|
| NES | Normalized enrichment score |
| NK cells | Natural killer cells |
| NSCLC | Non-small-cell lung carcinoma |
| NSG | NOD scid gamma |
| NTD | N-terminal domain |
| PBMC | peripheral blood-derived mononuclear cells |
| PBS | Phosphate-buffered saline |
| PDGF-R | Platelet-derived growth factor receptor |
| PEG | Polyethylene glycol |
| Ph | Philadelphia chromosome |
| PKC | Protein kinase C |
| POI | Protein of interest |
| PROTACS | Proteolysis targeting chimeras |
| PTGR1 | Prostaglandin Reductase 1 |
| PTGS1 | Cyclooxygenase 1 |
| PTPRC | Protein tyrosine phosphatase |
| RNP | Ribonucleoprotein |
| ROI | Region of interest |
| SCID | Severe combined immune deficiency |
| SLL | Small lymphocytic lymphoma |
| SSC | Sideward scatter |
| TFPI | Tissue factor pathway inhibitor |
| TKI | Tyrosine kinase inhibitors |
| TL | Triptolide |
| TOP2A | DNA topoisomerase 2 α |
| TPD | Targeted protein degradation |
| TRAP1 | TNF Receptor Associated Protein 1 |
| VHL | Von Hippel-Lindau |

# Abstract

Heat shock protein 90 (HSP90) is involved in various cellular processes and fulfils a crucial role as a molecular chaperone in the folding, stabilization, and regulation of client proteins. Their role in stabilizing oncoproteins, such as BCR-ABL1 and increased expression in cancer cells makes HSP90 a promising therapeutic target. Despite tremendous treatment success using tyrosine kinase inhibitors (TKIs), the prognosis in the BCR-ABL1$^+$ leukemia subtype is unfavourable and treatment-free remission is limited, leading to the ongoing occurrence of resistance. Various inhibitors targeting the N-terminal domain (NTD) of HSP90 have been developed but have shown limited clinical benefit. This is mainly due to the induction of the pro-survival resistance mechanism, the heat shock response (HSR) and dose-limiting toxicity. This study aims to tackle the prevailing issues related to HSP90 inhibitor therapy through (i) comprehending the influence of cytosolic HSP90 isoforms (HSP90α and HSP90β) in the development of resistance and (ii) advancing the progression of C-terminal domain (CTD) targeting HSP90 inhibitors, which have been recognized to prevent HSR induction.

(i) CRISPR/CAS9 or siRNA-mediated targeting of (constitutively expressing) HSP90β isoform resulted in an enhanced HSR and demonstrated consistent upregulation of the inducible isoform, HSP90α. Deletion of HSP90α resulted in an increase in BCR-ABL1 activity and associated pro-survival signalling. Interestingly, previously reported client proteins of HSP90α/β, such as CDK4, CDK6, and SURVIVIN, showed no altered expression in HSP90α/β-KO cells. When HSP90α/β-KO cells were transplanted into mice, there was a notable reduction in the transplantation efficiency specifically observed in HSP90α-KO cells, which was confirmed by the prolonged survival of mice. Proteogenomic profiling, including RNA sequencing, mass spectrometry, and secretome analysis, provided insights into molecular mechanisms and revealed differences in HSP90α/β-KO cells. Upon the ablation of HSP90α, a decrease in PTPRC (CD45) and LCK expression was observed in BCR-ABL1$^+$ leukemia cells. Furthermore, increased sensitivity of HSP90α-KO cells to CDK7 inhibition was identified. Notably, combined inhibition of HSP90 and CDK7 displayed synergistic effects against therapy-resistant BCR-ABL1$^+$ leukemia cells, blocking pro-survival HSR and HSP90α overexpression.

(ii) This research builds on an existing strategy that specifically targets HSP90 CTD dimerization by employing novel protein-protein interaction inhibitors. Biochemical and biophysical assays showed that the inhibitors (α-helix mimetics based on substituted pyrimidine and pyrimidone amides) bind and disrupt the CTD dimerization interface of HSP90. Remarkably, the inhibitors **2** (VWK346) and **3** (VWK141) showed anti-leukemic activity against CML and ALL leukemia cell lines and patient-derived leukemia cells. As an alternative approach for targeting HSP90, first-in-class cereblon-recruiting Geldanamycin-based Proteolysis targeting chimeras (PROTACs) were evaluated.

These PROTACs demonstrated successful degradation of HSP90α and HSP90β, offering a promising approach to circumvent HSP90 inhibitor-induced resistance.

# Zusammenfassung

Das Hitzeschockprotein 90 (HSP90) ist an einer Vielzahl von zellulären Prozessen beteiligt und erfüllt eine entscheidende Rolle als molekulares Chaperon in der Faltung, Stabilisierung und Regulation von Klient-Proteinen. Die Bedeutung bei der Stabilisierung von Onkoproteinen, wie BCR-ABL und der erhöhten Expression in Krebszellen, machen HSP90 zu einem vielversprechenden therapeutischen Ziel. Trotz des bedeutenden Behandlungserfolges durch den Einsatz von Tyrosinkinase Inhibitoren (TKIs), ist die Prognose bei dem BCR-ABL1$^+$ Leukämie Subtyp ungünstig und die behandlungsfreie Remission ist begrenzt, wodurch es fortlaufend zum Auftreten von Resistenzen kommt. Eine Vielzahl von Inhibitoren, welche die N-Terminale Domäne (NTD) von HSP90 adressieren wurden entwickelt, jedoch zeigte sich ein begrenzter klinischer Nutzen. Dieser ist hauptsächlich der Induzierung des überlebens-fördernden Resistenzmechanismus, der hitzeschock Reaktion (HSR) und der dosis-limitierende Toxizität geschuldet. Diese Arbeit zielt darauf ab, die bestehende Problematik im Zusammenhang mit der Therapie mit HSP90 Inhibitoren anzugehen, indem (i) der Einfluss der zytosolischen HSP90-Isoformen (HSP90α und HSP90β) auf die Entwicklung der Resistenz verstanden wird und (ii) die Entwicklung von C-terminalen (CTD) HSP90-Inhibitoren vorangetrieben wird, von denen bekannt ist, dass sie die HSR-Induktion verhindern.

(i) CRISPR/Cas9 oder siRNA-vermitteltes Targeting der (konstitutiv exprimierenden) HSP90β-Isoform verstärkte die HSR und zeigte eine konsistente Hochregulierung der induzierbaren Isoform, HSP90α. Die Deletion von HSP90α führte zu einem Anstieg der BCR-ABL1-Aktivität und der damit verbundenen überlebens-fördernden Signalübertragung. Interessanterweise zeigten relevante Klient-Proteine von HSP90α/β, wie CDK4, CDK6 und SURVIVIN, keine veränderte Expression in HSP90α/β-KO Zellen. Bei der Transplantation von HSP90α/β-KO-Zellen in Mäuse wurde eine bemerkenswerte Verringerung der Transplantationseffizienz speziell bei HSP90α-KO-Zellen beobachtet, was durch das verlängerte Überleben der Mäuse bestätigt wurde. Die proteogenomische Profilierung, einschließlich RNA-Sequenzierung, Massenspektrometrie und Sekretomanalyse, ermöglichte Einblicke in die molekularen Mechanismen und zeigte Unterschiede in den HSP90α/β-KO-Zelllinien. Insbesondere wurde nach der Ablation von HSP90α eine Abnahme der PTPRC (CD45) und LCK-Expression in BCR-ABL1$^+$ Leukämiezellen beobachtet. Darüber hinaus wurde eine erhöhte Empfindlichkeit von HSP90α-KO Zellen gegenüber CDK7-Inhibition festgestellt. Insbesondere zeigte die kombinierte Inhibierung von HSP90 und CDK7 synergistische Effekte gegen Therapieresistente BCR-ABL1$^+$ Leukämiezellen, indem die überlebens-fördernd HSR und HSP90α Überexpression gehemmt wurde.

(ii) Diese Forschung baut auf einer bestehenden Strategie auf, die speziell auf den C-Terminus von HSP90 abzielt, indem neuartige Protein-Protein-Interaktions-Inhibitoren einsetzt werden.

Biochemische und biophysikalische Tests zeigten, dass die Inhibitoren (α-Helix-Mimetika auf der Basis von substituierten Pyrimidin- und Pyrimidonamiden) die C-terminale Dimerisierungsschnittstelle von HSP90 binden und unterbrechen. Bemerkenswerterweise zeigten die Inhibitoren **2** (VWK346) und **3** (VWK141) eine leukämiehemmende Wirkung in CML- und ALL-Leukämiezelllinien sowie in von Patienten-stammenden Leukämiezellen. Als alternativer Ansatz für die Adressierung von HSP90 wurden *first in-class* Cereblon-rekrutierende *Proteolysis targeting chimeras* (PROTACs) auf der Basis von Geldanamycin evaluiert. Diese PROTACs zeigten einen erfolgreichen Abbau von HSP90α und HSP90β, was einen vielversprechenden Ansatz zur Umgehung der HSP90-Inhibitor-induzierten Resistenz darstellt.

# List of Publications

This thesis is based on the following Publications:

**I. Co-targeting HSP90 alpha and CDK7 overcomes resistance against HSP90 inhibitors in BCR-ABL1+ leukemia cells**

**Vogt, M.;*** Dienstbier, N.;* Schliehe-Diecks, J.; Scharov,, K.; Tu, J.; Gebing, P.; Hogenkamp, J.; Furlan, S.; Picard, D.; Remke, M.; Yasin, L.; Bickel, D.; Kalia, M.; Iacoangeli, A.; Lenz, T.; Stühler, K.; Pandyra, A. A.; Hauer, J.; Fischer, U.; Wagener, R.; Borkhardt, A.; Bhatia, S.
Cell Death Dis. 2023, 14, 799.

**II. Development of a First-in-Class Small-Molecule Inhibitor of the C-Terminal Hsp90 Dimerization.**

Bhatia, S.; Spanier, L.; Bickel, D.; Dienstbier, N.; Woloschin, V.; **Vogt, M.;** Pols, H.; Lungerich, B.; Reiners, J.; Aghaallaei, N.; Diedrich, D.; Frieg, B.; Schliehe-Diecks, J.; Bopp, B.; Lang, F.; Gopalswamy, M.; Loschwitz, J.; Bajohgli, B.; Skokowa, J.; Borkhardt, A.; Hauer, J.; Hansen, F. K.; Smits, S. H. J.; Jose, J.; Gohlke, H.; Kurz, T.
ACS Central Science 2022, 8 (5), 636-655.

**III. Development of the first Geldanamycin-Based HSP90 Degraders.**

Wurnig, S.;* **Vogt, M.;*** Hogenkamp, J.; Dienstbier, N.; Borkhardt, A.; Bhatia, S.; Hansen, F. K.
Front. Chem. 2023, 11.

* contributed equally to this work

Publications not included in this thesis:

**IV. Solid-Phase Synthesis of Cereblon-Recruiting Selective Histone Deacetylase 6 Degraders (HDAC6 PROTACs) with Antileukemic Activity.**

Sinatra, L.;* Yang, J.;* Schliehe-Diecks, J.; Dienstbier, N.; **Vogt, M.;** Gebing, P.; Bachmann, L. M.; Sönnichsen, M.; Lenz, T.; Stühler, K.; Schöler, A.; Borkhardt, A.; Bhatia, S.; Hansen, F. K.
Journal of Medicinal Chemistry 2022, 65 (24), 16860-16878.

**V. Unleashing T cell anti-tumor immunity: new potential for 5-Nonloxytryptamine as an agent mediating MHC-I upregulation in tumors.**

Stachura, P.; Liu, W.; Xu, H. C.; Wlodarczyk, A.; Stencel, O.; Pandey, P.; **Vogt, M.;** Bhatia, S.; Picard, D.; Remke, M.; Lang, K. S.; Häussinger, D.; Homey, B.; Lang, P. A.; Borkhardt, A.; Pandyra, A. A.
Molecular Cancer 2023, 22 (1), 136.

**VI. High-throughput screening as a drug repurposing strategy for poor outcome subgroups of pediatric B-cell precursor Acute Lymphoblastic Leukemia.**

Athanasios Oikonomou, A.; Valsecchi, L.; Quadri, M.; Watrin, T.; Scharov, K.; Procopio, S.; Tu, J.; **Vogt, M.;** Savino, A. M.; Silvestri, D.; Valsecchi, M. G.; Biondi, A.; Borkhardt, A.; Bhatia, S.; Cazzaniga, G.; Fazio, G.; Bardini, M.; Palmi, C.
Biochemical Pharmacology 2023, 217 (3).

**VII. A brain organoid/ALL coculture model reveals the AP-1 pathway as critically associated with CNS involvement of BCP-ALL**

Gebing, P.; Loizou, S.; Hänsch, S.; Schliehe-Diecks, J.; Spory, L.; Stachura, P.; Jepsen, V. H.; **Vogt, M.;** Pandyra, A. A.; Wang, H.; Zhuang, Z.; Zimmermann, J.; Schrappe, M.; Cario, G.; Alsadeq, A.; Schewe, D. M.; Borkhardt, A.; Lenk, L.; Fischer, U.; Bhatia, S.
Blood Adv 2024; 8 (19): 4997–5011.

**VIII. Small-molecule inhibitor of C-terminal HSP90 dimerization modulates autophagy and functions synergistically with mTOR inhibition to kill cisplatin-resistant cancer cells.**

David, C.; Sun, Y.; Woloschin, V.; **Vogt, M.;** Dienstbier, N.; Schlütermann, D.; Berning, L.; Lungerich, B.; Friedrich, A.; Akgün, S.; Mendiburo, M. J.; Borkhardt, A.; Wesselborg, S.; Bhatia, S.; Kurz, T.; Stork, B.
Manuscript in preparation

* contributed equally to this work

Oral presentation:

**IX. S153: DECRYPTING THE ROLE OF HSP90A AND B ISOFORMS TO OVERCOME RESISTANCE IN BCR-ABL1 LEUKEMIA.**

**Vogt, M.;** Dienstbier, N.; Schliehe-Diecks, J.; Scharov, K.; Tu, J. W.; Gebing, P.; Hogenkamp, J.; Picard, D.; Lenz, T.; Stühler, K.; Wagener, R.; Pandyra, A.; Hauer, J.; Fischer, U.; Borkhardt, A.; Bhatia, S.
HemaSphere 2022, 6.

# 1. Introduction

## 1.1 Leukemia

Despite the advancing state of medical development, as well as novel discoveries and treatment options, cancer remains the second most common cause of death after cardiovascular diseases in the industrialized world. In 2022 alone, 239,948 deaths were attributable to cancer and malignant neoplasms in Germany.[1]

Cancer, defined as a disease of the genome, can occur in any cell type of the body.[2] When precursor white blood cells are affected by genetic alterations, this leads to leukemia, a malignant disease of the hematopoietic system. More than 10,000 new cases are diagnosed annually, and the relative 10-year survival rate is approximately 50 % in 2020, with an apparent deterioration of the prognosis with increasing age.[3] In fact, 4 % of all new cases diagnosed were among children under 15 years of age, with an incidence peak at 3 to 5 years of age. This makes leukemia one of the most common cancers in children.[4]

In general, leukemia diseases are classified based on the rapidity of disease progression and the cell type from which they originate.[5] A distinction is made between the acute and chronic forms of progression. Acute leukemia proceeds more rapidly and usually more aggressively. There is often a fast progressive reduction in bone marrow function, i.e., reduced healthy blood formation with a red and white blood cell deficiency. Over time, an increasing number of immature, dysfunctional white blood cells are formed, and, at the same time, healthy blood cells are replaced. For those suffering from the disease, this leads to a weakened immune system and, thus, to persistent and frequent infections. In general, many patients suffer from fatigue, weight loss, fever, bone and joint pain and associated reduced performance. Furthermore, the lack of red blood cells leads to anaemia.[6]

Chronic leukemia, on the contrary, usually progresses more slowly, and often there are almost no symptoms in the beginning, which also progresses very slowly. The chronic initial phase is characterized by a proliferation of immature white blood cells in the peripheral blood and in the hematopoietic bone marrow. The first signs are persistent fatigue and reduced performance. In the further course, there is a steady increase of leukocytes and thus a decreasing number of red blood cells. Classic anaemia signs thus characterize the acceleration phase. In the final phase of the disease, also known as the blast crisis, a blast thrust releases large quantities of immature blood cells.[7] The high concentration in the bone marrow and blood leads to severe disease symptoms in patients, similar to those of an acute form of the disease.[8]

Furthermore, a distinction is made between myeloid and lymphoid leukemia. Both precursors arise from multipotent hematopoietic stem cells (Figure 1).

Myeloid cells give rise to red blood cells, granulocytes, monocytes, and platelets, whereas lymphoid cells give rise to T and B lymphocytes and natural killer cells (NK cells).[9]

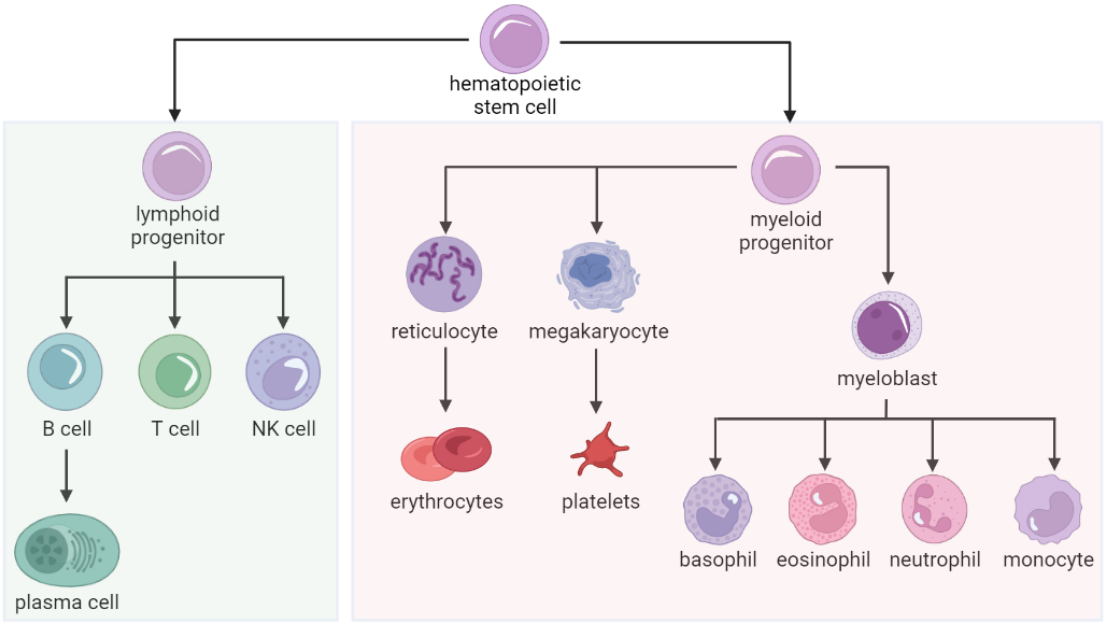


**Figure 1: Schematic overview of the normal hematopoiesis.**

Normal hematopoiesis shows the differentiation in the bone marrow originating from multipotent hematopoietic stem cells into lymphoid (left) and myeloid (right) progenitor cells and resulting effector cells. The leukemia subtypes are classified depending on the originating progenitor cell. Figure: Created with BioRender.com, following Jagannathan-Bogdan, M. and Zon, L. I. [10]

Based on previously described criteria, the four most common forms that occur are acute myeloid leukemia (AML), chronic myeloid leukemia (CML), acute lymphoblastic leukemia (ALL), and chronic lymphocytic leukemia (CLL). The most frequent forms are CLL, with about 37 % of newly diagnosed cases, and AML, with about 23 % of cases.[11] In childhood, ALL is the most common form of leukemia. It occurs due to risk factors such as genetic factors that contribute to the development of the disease such as Down syndrome and Fanconi anemia.[12] Furthermore, there are several genes whose mutation predisposes carriers to the development of ALL (e.g. ETV6, IKZF1, and PAX5).[13] Other studies revealed immunodeficiency, viral infections, or environmental influences as potential risk factors.[14,15]

### 1.1.1 BCR-ABL1$^+$ leukemia

Cancer development, in general, is based on a modification of the genome, more precisely by genetic defects, such as mutations, which lead to the activation of oncogenes or inactivation of tumour suppressor genes or repair genes. Furthermore, chromosomal alterations such as deletions, insertions, inversions, duplications, or translocations can lead to cell degeneration. In hematological diseases, chromosomal translocations are very frequent and a typical cause.[16]

A prominent example is the BCR-ABL1 fusion gene, which encodes the oncoprotein BCR-ABL1.

It is generated by a reciprocal translocation between the Abelson leukemia virus (ABL or ABL1) gene, located on the long arm of chromosome 9 (q34.1), and the breakpoint cluster region (BCR) gene, located on the long arm of chromosome 22 (q11.2).[17] The severely truncated chromosome 22, resulting from the translocation t(9;22)(q34;q11), is also known as the Philadelphia chromosome (Ph). It was named after its discoverers, Peter Nowell and David Hungerford, who first found it in the leukemia cells of a patient in Philadelphia in 1960.[18]

There may be breakpoints at different locations in the BCR gene, resulting in fusion genes of different sizes. The ABL1 gene is always the same, and the BCR gene size can vary. The most common isoforms are $p190^{BCR\text{-}ABL1}$ and $p210^{BCR\text{-}ABL1}$, named after their molecular weight. In rare cases, the isoform $p230^{BCR\text{-}ABL1}$ may arise.[19]All three isoforms have in common that they encode a tyrosine kinase (TK), which is hyperactivated under the influence of translocation. Tyrosine kinases, in general, catalyze the transfer of phosphate groups to other proteins and thus play a key role in signal transduction by modulating the activity of other proteins. Therefore, they influence cellular processes, such as cell growth, proliferation, differentiation, migration, and many others mediated *via* RAS, STAT1-5 or AKT signalling (Figure 2). It has been shown that the biological activity of the kinase decreases with the increasing size of the BCR-ABL1 construct. Furthermore, the different BCR-ABL1 isoforms are associated with different forms of leukemia.

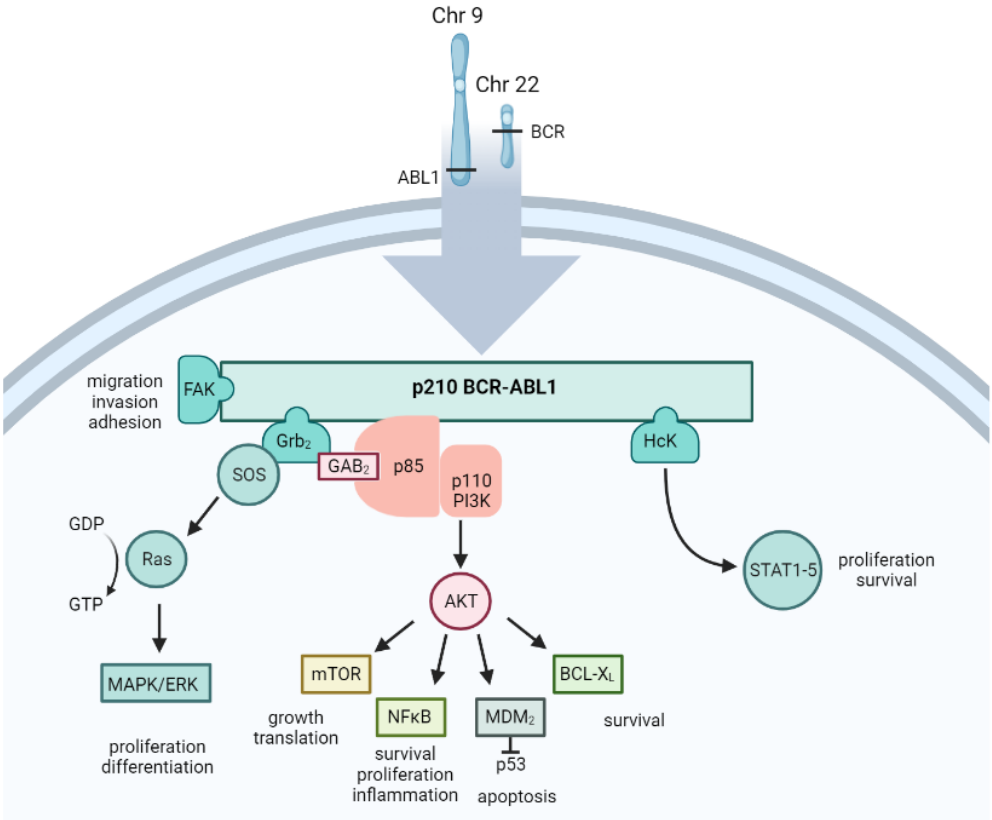


**Figure 2: Role of $p210^{BCR\text{-}ABL1}$ in leukemogenesis.**

The tyrosine kinase BCR-ABL1 is involved in several cellular processes, such as cell growth, proliferation, differentiation, or migration mediated *via* RAS, STAT1-5 and AKT signalling. Figure: Created with BioRender.com.

P210$^{BCR-ABL1}$ can be found in 95 % of all hematopoietic cells from patients with CML and is therefore considered a hallmark of CML.[20] P190$^{BCR-ABL1}$, on the other hand, is mainly expressed in Philadelphia-positive acute B-cell precursor acute lymphoblastic leukemia ($Ph^+$ BCP-ALL) and is rarely found in CML (1-2 % of patients). Approximately 20-30% of all patients with B-ALL harbour the BCR-ABL1 fusion protein.[21]

### 1.1.2 Tyrosine kinase inhibitors (TKIs)

The treatment of leukemia patients depends primarily on the clinical picture and the stage of the disease. Cytogenetic analyses can help to identify abnormal chromosomal origins.[22] Standard procedures in the conventional sense are chemotherapy with cytostatics, radiation therapy, or stem cell transplantation.[23] Furthermore, there are directed therapy approaches, such as immunotherapy with monoclonal antibodies or targeted therapy with small molecules. Targeted therapy is based on a precise knowledge of the genetic profile of a tumour and is thus part of personalized medicine. It is crucial to search for biomarkers, such as mutations or fusion genes, before treatment. In the best case, this can be exploited, and tumour cells can be targeted without affecting the healthy surrounding tissue. The discovery of the BCR-ABL1 fusion protein as a driver oncogene in mainly CML and BCP-ALL provided a starting point for developing inhibitors against tyrosine kinases (TKIs).

In 2001, the inhibitor Imatinib was approved by the U.S. Food and drug Administration (FDA) as a first-line treatment for CML under the trade name Gleevec.[24] Later, Imatinib was also approved for treating patients with relapsed or refractory $Ph^+$ ALL and children with $Ph^+$ ALL. This revolutionized the prognosis of patients in terms of survival from about 20% to 80-90% and quality of life. Previously, CML was treated with classical chemotherapeutic agents, such as hydroxyurea and interferon α (IFN-α), in addition to allogeneic stem cell transplantation.[25] However, Imatinib was also shown to have inhibitory activity against tyrosine kinase c-KIT and platelet-derived growth factor receptor (PDGF-R). Docking studies and crystallization experiments later showed that Imatinib interacts with the hinge region of the kinase. It binds competitively to the inactive confirmation of the adenosine triphosphate (ATP)-binding pocket.[26]

Despite the good response rate to Imatinib, it was found that treatment did not achieve a long-term response in approximately one-third of the patients.[27] Intolerances and the development of resistance could justify this. There are BCR-ABL1-independent mechanisms, mainly increased drug efflux or decreased drug uptake and activation of other oncogenic signalling pathways.[28, 29] BCR-ABL1-dependent mechanisms mainly include point mutations but also gene amplifications or hyperexpression of BCR-ABL1.[30-32] In response, new inhibitors have been developed to circumvent point mutations.

These second-generation inhibitors are Nilotinib and Dasatinib, approved in 2006 and 2007. Both inhibitors also bind competitively to the inactive confirmation of BCR-ABL1 to the ATP-binding pocket. These inhibitors could overcome various resistance-mediating mutations but not the gatekeeper mutation T315I.

Therefore, other inhibitors were explicitly developed to circumvent this particular mutation, and in 2012 the third-generation inhibitor Ponatinib was approved. This inhibitor also binds ATP competitively to the inactive confirmation but is active against all mutant forms of BCR-ABL1 to date.[33] Clinically, Ponatinib was shown to have high activity in patients with resistance to other inhibitors, making it a good alternative for the treatment of T315I-positive CML and $Ph^+$ALL.[34, 35] Nevertheless, the clinical application shows that new mutations keep appearing and new forms of resistance occur, which requires ongoing development of TKIs.[36] Furthermore, most patients need to continue treatment indefinitely, as only about 20% of patients achieve molecular remission.[37] This poses difficulties for particular young patients. All TKIs approved for CML are multikinase inhibitors and thus inhibit other kinases besides BCR-ABL1. This can be associated with various side effects, such as nausea, cytopenia, fatigue, rash, diarrhea, and liver damage.[38-40] While long-term treatment with Imatinib does not cause severe toxicity, it may lead to clinically significant reductions in the estimated glomerular filtration rate, hemoglobin levels, and instances of renal dysfunction.[41, 42]

## 1.2 HSP90

Cells can be exposed to stressful external influences and stress factors, such as radiation, heat, hypoxia, or infections. Under such conditions, cellular processes must remain intact. This essential function in the cells is fulfilled by a family of chaperone proteins known as heat shock proteins (HSPs), discovered in the 1960s. [43] They were first described in connection with heat shocks and thus carry their name. It is now known that such proteins also play an essential role in other stress-related exposures, as mentioned previously. The HSPs are upregulated and, with the help of their chaperone function, cause protein stabilization, protect them from denaturation, and accelerate the degradation of non-functional proteins.[44] There are many HSPs, which are named and differentiated according to their molecular weight, such as HSP70, HSP40 or HSP27. The most studied and characterized member is HSP90. Overall, HSP90 makes up 1-2% of the protein under normal conditions and can make up 4-6% under stress conditions.[45] A large amount of the protein under normal conditions indicates that it also plays other essential roles in cells. Molecular chaperones, such as HSP90, continue to serve in the transport, translocation and folding of proteins, thus maintaining protein homeostasis. HSP90 is highly conserved and expressed in a variety of organisms. In mammalian cells, there are two dominant cytosolic isoforms, HSP90α (*HSP90AA1* gene; located at 14q32–33) and HSP90β (*HSP90AB1* gene; located at 6p21).[46] The human forms show an 85% sequence identity to each other.

HSP90β is constitutively expressed, whereas HSP90α is the stress-inducible isoform. Both isoforms have similar preferences regarding their client proteins and can compensate for each other. However, exceptions have also been reported, as differences in the non-coding regions allow for different regulations of HSP90α and β.[46] For example, knockout (KO) of HSP90β in mice has been shown to result in embryonic lethality, whereas HSP90α-KO mice develop largely normally.[47, 48] Furthermore, different binding preferences concerning client proteins have been reported. For example, A-RAF (rapidly accelerated fibrosarcoma), c-SRC (cellular SRC, short for sarcoma), hERG (human ether-à-go-go-related gene) channels, and ERK-5 bind preferentially to HSP90α. In contrast, cyclin-dependent kinases (CDK4 and CDK6), cellular inhibitor of apoptosis (cIAP1), and C-X-C chemokine receptor type 4 (CXCR4) are HSP90β-specific clients.[49-52]

There is a third cytoplasmic isoform called HSP90N. With a size of 75 kDa, the protein is significantly smaller and fulfils other cellular functions. For example, it is involved in the activation of Raf and thus influences downstream ERK kinases.[53] Two other functional isoforms are glucose-regulated protein (GRP94) and TNF receptor-associated protein 1 (TRAP1), which are localized in the endoplasmic reticulum and mitochondria, respectively. The chaperone activity depends on ATP and the dimerization of the flexible homodimers, which undergo a high conformational rearrangement during the functional cycle (Figure 3). HSP90 consists of three structural domains, the N-terminal domain (NTD), which is connected to the middle domain (MD) *via* a charged linker, and a C-terminal domain (CTD). The NTD has a binding pocket for ATP and shows homology to members of the Gyrase, HSP90, Histidine kinase, MutL (GHKL) ATPase superfamily. The MD is essential for client protein binding and recognition and ATP hydrolysis. Specific substrates, such as activators of HSP90 ATPase homolog 1 (AHA1) and high-copy HSP90 suppressor (HCH1), have been shown to increase the ATPase activity of HSP90. The CTD has an additional ATP-binding pocket and is further responsible for dimerization. At the C-terminal end is a conserved MEEVD motif, which is essential for interaction with cofactors.[54, 55]

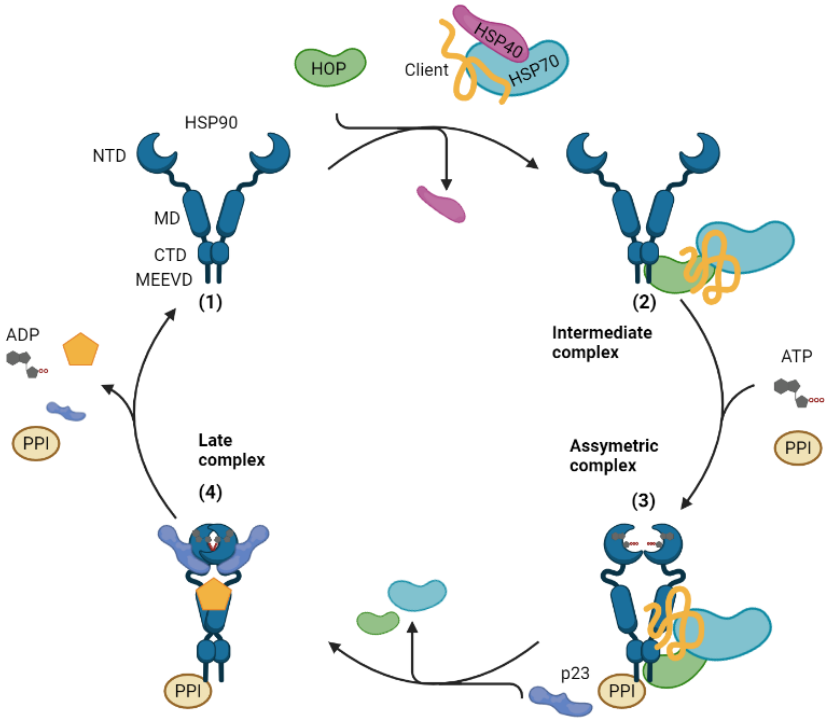


**Figure 3: Schematic representation of the HSP90 chaperone cycle.**

The four main steps show the loading of HSP90 with the client protein and the subsequent binding of ATP as an energy supplier. The client protein gets folded and afterwards released from the complex. HSP90 is back in its initial state, and the catalytic cycle can start again. Figure: Created with BioRender.com, following Mielczarek-Lewandowska, A. *et al*.[56]

In the apo-state, HSP90 is in an open V confirmation (1). In this open confirmation, some hydrophobic residues are exposed so that unfolded and misfolded proteins can be recruited. The recruitment is done with the help of HSP40 and HSP70, which bind client proteins. Furthermore, HOP (HSP70-HSP90 organizing protein), responsible for the binding between HSP70 and HSP90 and transfers client proteins, aids recruitment (2). In the next step, ATP gets bound, resulting in a conformational change by bringing the N-terminal domains closer together and forming a closed confirmation (3). Subsequently, p23 stabilizes the closed and twisted state of HSP90 so that HSP70 and HOP can leave the complex (4). In the final step, ATP gets hydrolysed to ADP, and the released energy enables the folding of a bound client protein. Subsequently, the folded protein, and all co-chaperones and ligands, are released from the complex, and HSP90 gets accessible for the next cycle.

### 1.2.1 HSP90 in Cancer

Cytosolic HSP90 isoforms fulfil several roles in cellular physiology. The described client proteins, which exceed 400 and keep increasing, fulfil essential roles in cellular pathways. They belong to different classes, such as transcription factors (steroid receptors, p53, BCL-6) and kinases (AKT, MAP-kinases, CDKs).[57, 58] Such proteins can contribute to carcinogenesis by driving uncontrolled proliferation, acting anti-apoptotic, promoting genome instability and mutations, facilitating tumor-promoting inflammation, and contributing to angiogenesis.

Thus, HSP90 is involved in all processes considered hallmarks of cancer (Figure 4).[59] An increased HSP90 level, accompanied by a shortened survival of the patients has been found for example in breast cancer and lung cancer.[60] Particularly in the case of NSCLC, a variety of HSP90-dependent client proteins are affected. These include mutant EGFR, MET, and the EML4-ALK translocation product.[61, 62] Recently, inhibition of HSP90 in trastuzumab-resistant HER2-positive breast cancer was shown to be effective by inducing apoptosis and inhibiting tumor growth and angiogenesis.[63] Furthermore, the HSP90 inhibitor AUY922 was shown to induce apoptosis and inhibit proliferation of lung cancer cells. This occurs through the down-regulation of HSP90 client proteins such as EGFR, MET, and AXL, thereby inhibiting AKT signaling.[64]

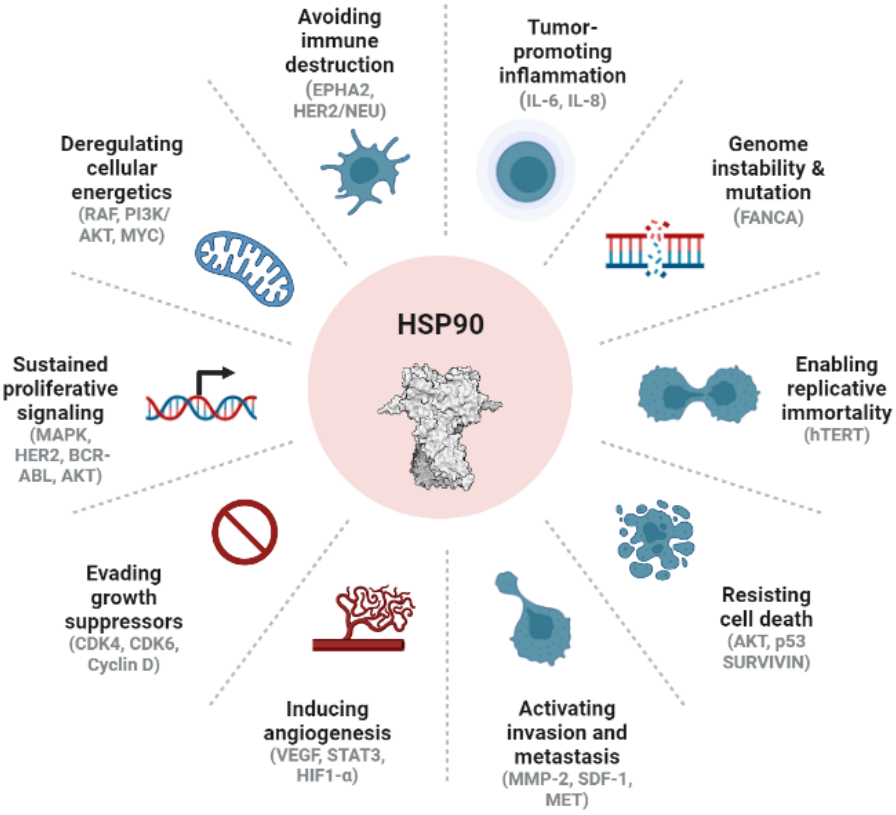


**Figure 4: Targeting HSP90 as a strategy to address the hallmarks of cancer.**
Original hallmarks proposed by Hanahan and Weinberg in 2000[65] and emerging hallmarks (deregulating cellular energetics, avoiding immune destructions) and enabling factors (genome instability & mutation, tumor-promoting inflammation) introduced in 2011.[66] Figure: Created with BioRender.com.

The inhibition of HSP90 can thus suppress tumor-promoting signalling pathways and provide a treatment option for a variety of cancer entities.[59]

### 1.2.2 HSP90 in Leukemia

In addition to overexpression of HSP90 in lung and breast cancers, increased expression levels have been observed in several leukemic subtypes. HSP90 is involved in the stabilization of the FLT3-ITD fusion protein, which is the most common form of FLT3 mutation and is found in 25% of all AML cases.[67, 68] This mutation leads to the production of an overactive protein that promotes the growth of leukemic cells. As a result, patients with FLT3-ITD mutations often have a high leukemia burden and a poor prognosis. Moreover, HSP90 is involved in the stabilization of anaplastic lymphoma kinase (ALK) fusion proteins that occur in ALK-positive non-Hodgkin's lymphoma (ALK-NHL). The treatment with the HSP90i 17-AAG was shown to destabilize the HSP90/NPM-ALK complex, which leads to downregulation of NPM-ALK kinase.[69] Other relevant oncogenic proteins stabilized by HSP90 include c-MYC and BCL2, which are frequently overexpressed in B-ALL cells and lead to improved cell survival and increased proliferation.[70, 71]

High levels of HSP90 were also found in CML cell lines and in patients which suffer from therapy resistance and relapse.[72] The molecular cause is the involvement of HSP90 in the stabilization of the translocated protein BCR-ABL1.[73] HSP90 inhibitors, such as the CTD targeting inhibitor novobiocin, were shown to induce apoptosis in HL-60/BCR-ABL1 and K562 cell lines and disrupt BCR-ABL1/HSP90 and BCR-ABL1/HSP70 binding.[74] Furthermore, Imatinib-resistant cell lines were shown to exhibit increased sensitivity to novobiocin. Remarkably, the efficacy of aminoxyrone (AX), an inhibitor targeting the dimerization of HSP90 CTD, was demonstrated in multi-TKI resistant CML and BCP-ALL cells, without triggering a pro-survival HSR.[75]

Therefore, targeting HSP90 is of great therapeutic interest and enables molecular targeting of different leukemia subgroups, particularly BCR-ABL1$^+$-dependent leukemias.

### 1.2.3 HSP90 inhibitors

There are different ways to target HSP90, addressing the C-terminal domain (CTD), the N-terminal domain (NTD), or the middle domain (MD).[76]

Furthermore, HSP90 can be addressed using isoform selective inhibitors targeting preferentially the cytosolic isoforms HSP90α or HSP90β. In addition, HSP90 can be inhibited dependent on the localization, for example with selective inhibitors targeting GRP94 or TRAP1. The mode of action of the inhibitors is either based on binding competitive to the ATP binding pocket in the NTD or CTD, the allosteric binding or by inhibiting protein-protein interactions between HSP90 and clients proteins or between HSP90 domains, like the CTD monomers.

Selected inhibitors are presented based on their lead structure in the following section.

### 1.2.3.1 N-terminal domain (NTD) targeting HSP90 inhibitors

The development of N-terminal HSP90 inhibitors is based on addressing the ATP binding pocket. This binding pocket has the peculiarity that the hydrophobic adenine moiety of the nucleotide is localized deep in the binding pocket on the helical face of the N-domain. ATP/ADP thus adopts a curved confirmation.[77] This unique feature allows the inhibitors to be designed with a particular specificity compared to other enzymes with ATP binding pockets. The following describes three different scaffold classes of NTD HSP90 inhibitors.

It has long been known that ansamycin antibiotics, such as Geldanamycin, possess anti-tumor properties by reducing the activity of tyrosine kinases and reversing tyrosine kinase-induced oncogenic transformation.[78] The macrocyclic antifungal antibiotic radicicol is another natural product with anti-tumor properties that can suppress malignant cell transformation.[79] Initially, these inhibitors were thought to address and inhibit tyrosine kinases directly. However, it was later shown that the actual target is HSP90.[80] Both inhibitors bind ATP competitively and prevent the formation of a closed, asymmetric complex of HSP90. This prevents protein folding and results in the accumulation of unfolded, nonfunctional proteins, like $p210^{BCR\text{-}ABL1}$, which gets degraded *via* the proteasome.

Geldanamycin showed good efficiency in cellular systems in inhibiting cell growth and proliferation and leading to apoptosis and was therefore evaluated for clinical use. However, the therapeutic index, which describes the ratio between toxic to anti-tumour doses, was found to be low.[81] Furthermore, in pre-clinical trials, Geldanamycin exhibited strong hepatotoxicity, metabolic instability, and inadequate water solubility.[82]

Therefore, structural modifications were made, and analogues based on Geldanamycin were developed. One of these compounds is 17-AAG (Tanespimycin), which is more hydrophilic and has better toxicological properties. These better properties could be achieved by introducing an allylamino group on the quinone ring at C-17 (Figure 5A). A further improvement of water solubility was achieved using the hydrochloride salt IPI-504 (Retaspimycin), produced by the allylamine protonation and the quinone reduction. Also, introducing a dimethylaminoethyl group at C-17, in the case of 17-DMAG (Alvespimycin), improved the solubility. All of these analogues have been tested in several clinical trials, including human epidermal growth factor receptor 2 (HER2) positive breast cancer, non-small-cell lung carcinoma (NSCLC), multiple myeloma and relapsed CLL/ small lymphocytic lymphoma (SLL) and B-cell prolymphocytic leukemia (B-PLL). [83,84,85,86] However, the inhibitors showed only limited efficacy response and thus modest clinical activity. Despite some improvements in physicochemical properties, the Geldanamycin-based inhibitors did not lead to a breakthrough and have not yet been approved as anticancer agents.

The second inhibitor class is based on the resorcinol structural motif, and the first identified inhibitor was radicicol. This inhibitor has a greater affinity for HSP90 *in vitro*. However, it cannot be administrated *in vivo* due to the rapid metabolism of the allyl epoxide moiety and α-, β-, γ-, and δ-unsaturated ketones. Therefore, analogues with the resorcinol moiety were developed (Figure 5B). X-ray crystallography studies revealed the importance of resorcinol as a critical pharmacophore. It showed that this moiety forms important hydrogen bonds in the ATP binding pocket.[87] Based on this knowledge, the analogue Ganetespib was developed, as well as Luminespib, which emerged from a structure-based approach. Ganetespib has been tested in 38 clinical trials of phase I-III as mono- or combination-therapy, including NSCLC[88], breast cancer[89], Melanoma[90] and AML, CML, MDS and myeloproliferative disorders.[91,92] Luminespib has been tested in clinical trials for NSCLC[93], gastrointestinal stromal tumours (GIST)[94] and myeloproliferative neoplasms.[95] Overall, both inhibitors showed adverse events and the efficacy as a single agent was not given. Therefore, there are also studies investigating Luminespib in combination with bortezomib, a proteasome inhibitor for the treatment of relapsed or refractory multiple myeloma.[96]

In addition to the natural product-inspired and derived inhibitors, small molecules based on the endogenous ligand ATP were also developed. The purine moiety of ATP was used as a starting point for the structure-based design. Finally, the first inhibitor of this class was PU3, which showed anti-proliferative activity against breast cancer cell lines in the low micromolar range.[97] Some substitutions, such as introducing a sulfur-linker, which proved to be very valuable, and introducing a 3-isopropylamino-propyl chain, led to a significant improvement in affinity and bioavailability. The resulting inhibitor Zelavespib (PU-H71) has a binding affinity for HSP90 in the low nanomolar range (Figure 5C).[98] Zelavespib has been evaluated in seven clinical trials, including metastatic breast cancer and myeloproliferative neoplasms.[99,100] Recently, PU-H71 was granted orphan drug status by the U.S. Food and Drug Administration (FDA) for treating myelofibrosis.[101] Furthermore, good results were achieved using PU-H71 in AML. Inhibition of HSP90 was shown to induce cell death in AML leukemia cell lines and primary samples. In particular, apoptotic sensitivity was observed in cell lines with constitutive activation of PI3K-AKT/JAK-STAT signaling pathways.[102]

Another class of N-terminal HSP90 inhibitors is based on the benzamide motif, which includes Pimitespib (TAS-116). This inhibitor is an oral, small molecule inhibitor of HSP90α/β with antitumor activity and high efficacy in solid tumors, including gastrointestinal stromal tumors (GIST).[103] In addition, TAS-116 demonstrated a good safety profile with minimal ocular toxicity and prolonged progression-free survival (phase III trial).[104] Therefore, this inhibitor was recently approved by the FDA in Japan for its application in GIST.[105]

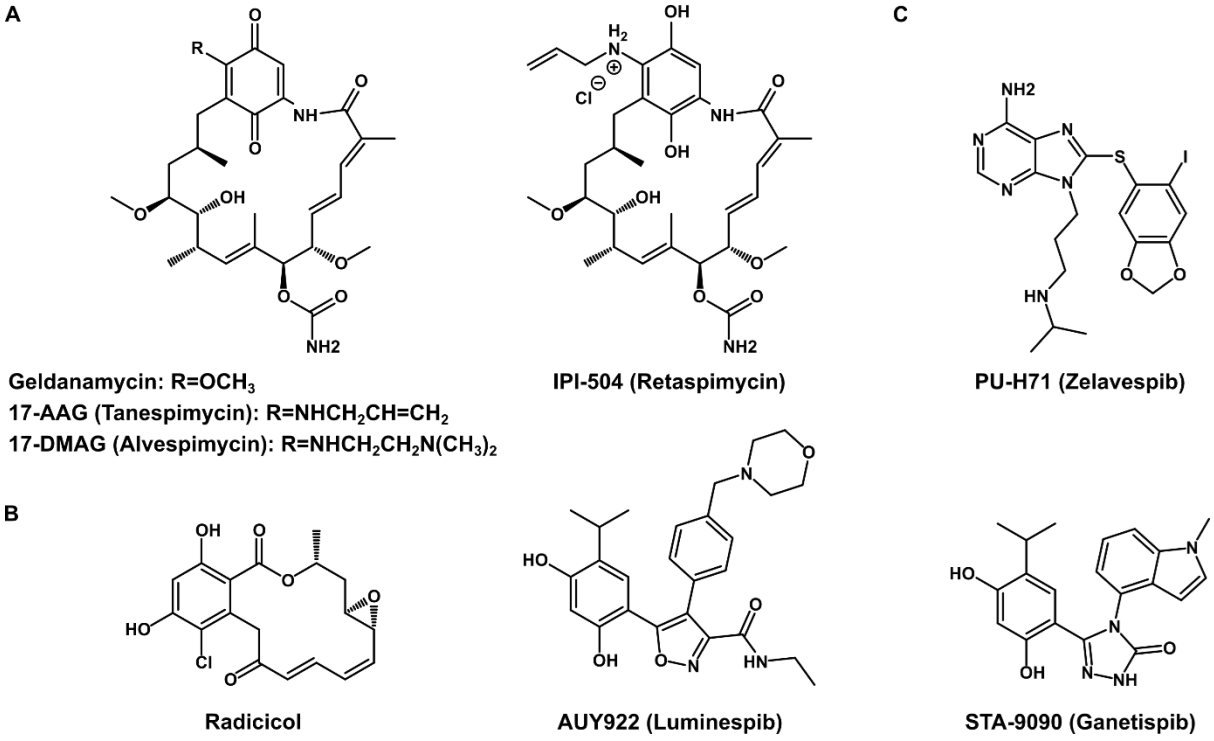


**Figure 5: Selected N-terminal HSP90 inhibitors.**

The N-terminal HSP90 inhibitors are either based on ansamycin (**A**), resorcin (**B**) and purine (**C**).

More than 30 HSP90 inhibitors targeting the N-terminal domain and, thus, the ATP binding pocket have made it into clinical trials.[106] Common to all inhibitors is that they exhibit specific toxicities, such as ocular, cardio, and hepatotoxicities.[107] Phase II clinical trials further showed that treatment as a single reagent has low efficacy, whereas combination therapies offer a much more promising outcome and may provide clinical benefits.[108]

### 1.2.3.2 Middle domain (MD) targeting HSP90 inhibitors

The MD of HSP90 is essential for client protein binding and recognition. The natural product diptoindonesin G (dip G) is a small molecule modulator that directly acts on the middle domain of HSP90.[109] In a cell-free fluorescence polarization (FP) assay, deoxy-dip G showed direct binding to HSP90 with high affinity. In hematologic cancers, in particular, AML cells were sensitive to dip G and it exhibits potential antiproliferative activity by inducing differentiation of AML cells *via* ERK signalling.[110]

Another inhibitor, which is targeting HSP90, is the natural compound triptolide (TL). TL acts at different sites of HSP90, for instance by regulating the ATPase activity and thus influencing the dimerization of the N-terminal domain, resulting in a loss of chaperone activity. Furthermore, it was shown that TL targets the MD of HSP90 and can inhibit the interaction of HSP90β and CDC37. Inhibition of HSP90 with TL leads to induction of apoptosis in cancer cells *via* kinase client protein degradation and cell cycle arrest.[111]

#### 1.2.3.3 C-terminal domain (CTD) targeting HSP90 inhibitors

Another approach is to address the CTD of HSP90. As mentioned, the CTD also has an ATP-binding site structurally different from the N-terminal domain. Where the N-terminal domain has increased specificity towards adenine-based nucleotides, the C-terminal domain can bind purine- and pyrimidine-based nucleotides.[112] The first reported inhibitor was the amino-coumarin antibiotic Novobiocin in 2000 (Figure 6A). Originally, aminocoumarins were inhibitors of bacterial DNA gyrase and are produced by the actinomycete *S. niveus*. Studies showed that novobiocin binds to HSP90 with reduced affinity.[113] The binding does not occur to the N-terminal ATP binding pocket of HSP90 but to the C-terminal ATP binding pocket under the condition that the N-terminal binding pocket is occupied.[114] Furthermore, Novobiocin was shown not to induce HSR and causes degradation of HSP90 clients, such as HER2, RAF-1, and mutant p53.[113] Important structural analogues are Clorobiocin and Coumermycin A1 (CmA1) (Figure 6B/C). CmA1 has a 10-fold improved IC50 (70 µM) against the breast cancer line SkBr3.

Another mechanism of action is inhibiting the association of HSP90 with cochaperones, including cell division cycle 37 protein (CDC37). The cochaperone CDC37 is essentially involved in the stabilization of HSP90-kinase complexes and inhibiting the interaction can sensitize the cells for other inhibitors and synergistic approaches.[115, 116] A modulator of the HSP90-CDC37 interaction is Celastrol, a plant-derived quinone methide triterpene (Figure 6D).[117] Studies have shown that Celastrol exhibits anticancer effects and induces cell death in pancreatic, prostate, and melanoma cancer cells.[118, 119] However, Celastrol was shown to induce HSR through activation of HSF1.[120] Another inhibitor of HSP90-CDC37 interaction is Withaferin A, a natural product derived steroidal lactone. This inhibitor possesses antiproliferative and antiangiogenic activity against pancreatic cancer cells and treatment leads to the inhibition of HSP90 activity and degradation of HSP90 clients, like AKT and CDK4.[121]

One more important cochaperone associated with HSP90 is HOP. This protein mediates the interaction between the HSP70-HSP40 complex and the CTD of HSP90. This binding can occur *via* protein-protein interactions between the tetratricopeptide repeat (TPR) domains of HOP and the highly conserved MEEVD motif of HSP90. A modulator of the HSP90-HOP interaction is Sansalvamide A, a fungal depsipeptide (Figure 6E). This cyclic inhibitor revealed antiproliferative activity against colon and melanoma cancer cell lines.[122] Later, this inhibitor was improved in terms of stability, which leads to the inhibitor Sansalvamide A-amide (Figure 6F). Mechanistic studies revealed that this inhibitor binds to the NTD and MD of HSP90 and acts allosterically to modulate interactions with cochaperones at the CTD of HSP90.[123]

The cyclopeptide exhibits 10-fold improved activity against the colon cancer cell line HCT-116 compared to the Sansalvamide A, however, the inhibitor induces HSR, indicated by the overexpression of HSP70.[124]

In a structure-based approach, peptides were produced based on the TPR sequence. The peptide was shown to inhibit the interaction between HSP90 and the TPR2A domain of HOP. The Antp-TPR peptide showed antitumor activity *in vitro* and *in vivo* in a xenograft model of human pancreatic cancer.[125] This approach was subsequently combined with the macrocyclic peptide scaffold resulting in the inhibitor LB76 (Figure 6G). Studies showed that this Sansalvamide A-amide analogue inhibited the interactions of HSP90 with HOP and Cyp40.[126]

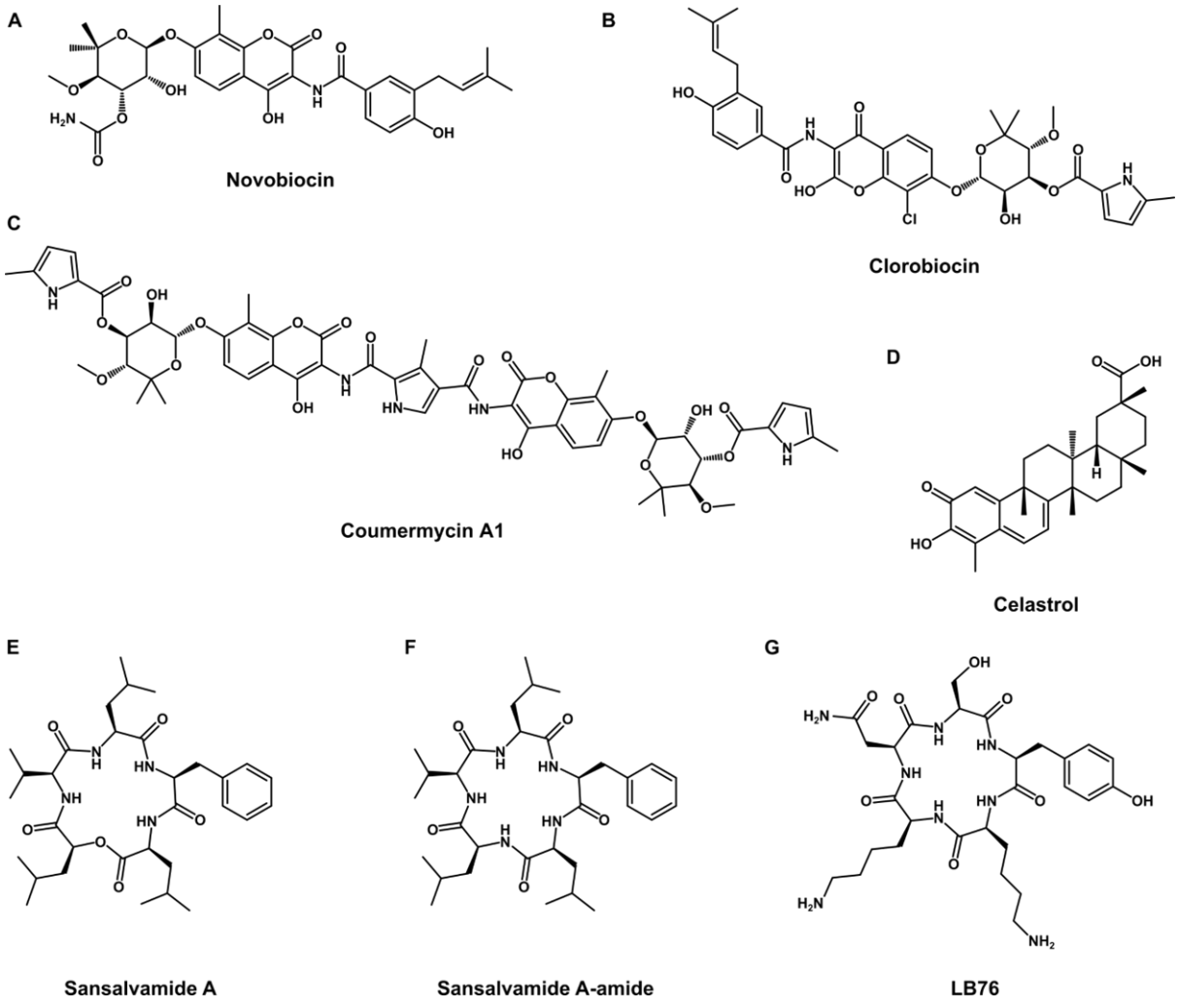


**Figure 6: Selected C-terminal HSP90 inhibitors.**

The C-terminal inhibitors Novobiocin, Clorobiocin, and Coumermycin A were based on aminocoumarin (**A-C**), Celastrol a quinone methide triterpene (**D**), Sansalvamide a cyclic depsipeptide, and the derivatives Sansalvamide A-amide (**F**) and LB76 (**G**).

Another possibility to inhibit HSP90 is the inhibition of C-terminal dimerization. This is essential for HSP90 activity and can be addressed as the C-terminal dimers constantly exchange between open and closed conformation.[127]

A structure-based approach by identifying hot spot residues at the dimerization interface resulted in the first-in-class C-terminal peptide-based dimerization inhibitor Aminoxyrone (AX) (Figure 7C).[128] α-aminoxypeptides can adopt a helical conformation and thus form a secondary structure (Figure 7B).[129] AX can mimic the amino acid side chains on helix 5 due to its side chain functionalization.

AX was effective in BCR-ABL1$^+$ precursor cells and highly resistant BCP-ALL cells by investigating cell lines and patient-derived cells. Furthermore, a low toxicity profile and no initiation of HSR were shown.[75] In addition, treatment with AX reduced the tumor burden in mice and reduced the BCR-ABL1 amount and activity.

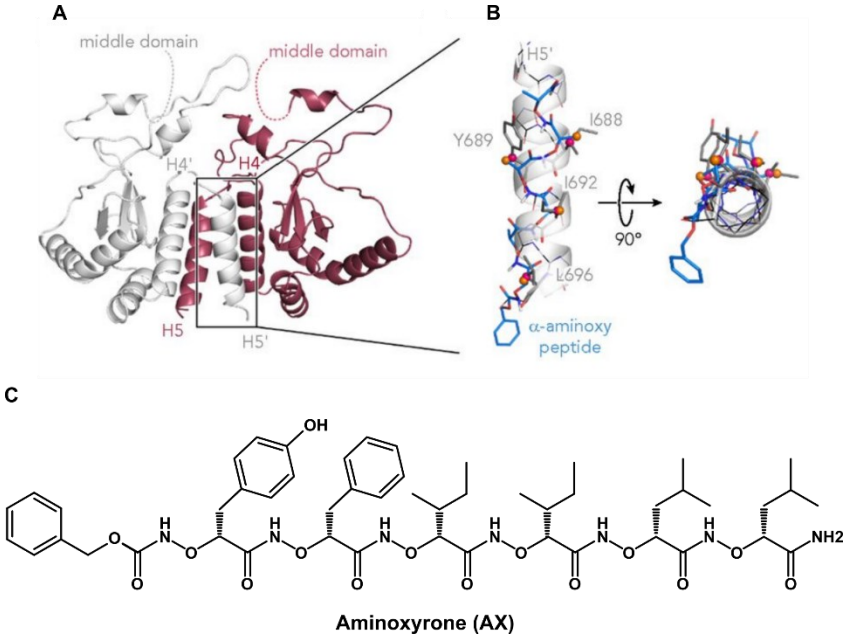


**Figure 7: Design of the peptidomimetic C-terminal HSP90 dimerization inhibitor Aminoxyrone (AX)**
(**A**) Dimeric crystal structure of HSP90 CTD (PDB: 3Q6M) showing helices H4, H4′, and H5, H5′ form the CTD dimerization interface. (**B**) Overlay of a hexameric α-aminoxy peptide with the $C_\beta$ atoms of four hot spot amino acids on helix H5′. Figure adapted from Bhatia, S. *et al*.[75] (**C**) The structure of the C-terminal HSP90 inhibitor AX.

In the last decades, various HSP90 inhibitors based on different lead structures have been developed and evaluated in combination with either standard chemotherapy or targeted inhibitors in over 60 clinical trials.[76, 130] Furthermore, great efforts were made in the design and evaluation of isoform selective inhibitors.

However, the clinical relevance and utility are still low, whereby there is still a great need for novel HSP90 inhibitors with vigorous anticancer activity and good safety profiles.

#### 1.2.3.4 Isoform-selective HSP90 inhibitors

Most of the designed HSP90 inhibitors are not selective for a specific isoform due to the high structural similarity. Due to the different localization of the isoforms, it is possible to develop inhibitors that preferentially target the cytosolic isoforms HSP90α/β. Such an inhibitor with a higher affinity to cytosolic HSP90 over GRP94 and TRAP1 is Luminespib (NVP-AUY922). In a cell-free FP assay, Luminespib showed an IC50 value of 7.8 nM/ 21 nM against HSP90α/β, whereas the IC50 values against GRP94 and TRAP1 were 535 nM/ 85 nM.[131]
In addition, inhibitors were developed that preferentially address TRAP1. The mitochondrial localization of TRAP1 enables selective targeting through the introduction of mitochondria-targeting moieties. The inhibitor SMTIN-P01 is a purine-based analogue of PU-H71 and has a positively charged triphenylphosphine (TPP) moiety to target mitochondria. It could be shown that SMTIN-P01 has cytotoxic effects related to mitochondrial membrane depolarization and has no effect on client protein levels. Furthermore, no initiation of the HSR was observed.[132]

A major challenge is to develop inhibitors that exhibit selectivity between the cytosolic isoforms HSP90α and HSP90β. Recently, an Hsp90α selective inhibitor was developed using a structure-based approach based on Geldanamycin. This inhibitor has an IC50 value against HSP90α of 460 nM (FP assay) and thus a 50-fold selectivity over the closely related isoform HSP90β. Furthermore, it could be shown that treatment of the NSCLC cell line NCI-H522 leads to a dose-dependent decrease of the HSP90 client proteins HER2, RAF-1, SURVIVIN and AKT. Interestingly, treatment with the HSP90α selective inhibitor increased the total level of HSP90 at low concentrations, similar to Geldanamycin, and decreased the expression level at higher concentrations.[133]

Furthermore, there were different approaches to develop HSP90β selective inhibitors. In 2019, the first N-terminal isoform-selective inhibitor of HSP90β was developed with an IC50 of 180 nM in a cell-free assay and with > 50-fold selectivity over closely related isoforms Hsp90α and GRP94. This inhibitor, named KUNB31, further showed anti-proliferative activity in NSCLC, urothelial bladder and colorectal cancer cell lines and treatment induced the degradation of HSP90β-dependent clients (CDK4, CDK6 and AKT) without concomitant induction of total HSP90 levels.[50] Recently, another HSP90β selective inhibitor was developed based on the structure of SNX-2112. SNX-2112 is an NTD HSP90 inhibitor that equally targets both cytosolic isoforms HSP90α and HSP90β. Structural modifications enabled an up to 300-folds selectivity over HSP90α, as well as IC50 values for GRP94 and TRAP1 over 5μM.[134]

## 1.2.4 Problems associated with HSP90i-based therapy

### 1.2.4.1 Heat shock response (HSR)

One mechanism contributing to poor HSP90 inhibitor efficacy is the pro-survival heat shock response (HSR) induction. Inhibition of the ATPase function of HSP90 leads to the release of the transcription factor named heat shock factor 1 (HSF1). This plays a central role in the transcriptional activation of HSR and is considered a significant factor in regulating heat shock proteins. Heat shock and other cellular stress factors, such as oxidative stress, proteosome inhibitors, and HSP90 inhibitors, induce this conserved cell defence mechanism to maintain proteostasis.[135, 136] In the inactive form, HSF1 is present as a monomer in the cytoplasm. When HSF1 is triggered, it becomes phosphorylated and translocates to the nucleus, where it gets activated by trimerization. In the nucleus, it subsequently binds to heat-shock responsive DNA elements (HSEs), and upregulation of some HSPs, including HSP70, HSP40, and HSP27, occurs.[137] Regulation of HSF1 proceeds *via* a negative auto-regulatory feedback loop, as some of the HSF1-induced HSPs can directly inhibit HSF1. Proteins such as HSP70, HSP72, and HSP90 can bind to the trimerization domain of HSF1 to inhibit activation. Thus, activating pro-survival HSPs by inhibiting HSP90 may reduce the activity of HSP90 inhibitors.[138, 139] Therefore, it is of great interest to develop inhibitors that do not induce HSR.

### 1.2.4.2 Dose-limiting toxicities (DLTs) and resistance incidences

HSP90 inhibitors induce apoptosis and inhibit tumor growth in a variety of cancer entities and thus exhibit anti-tumor activity. This effect is mainly driven by the downregulation of client proteins and the concomitant regulation of cellular pathways through the inhibition of HSP90. The use of HSP90i in clinical studies resulted in adverse side effects, such as hepatotoxicity, myelosuppression, and retinal dysfunction. These intolerable effects lead to the need to pursue new approaches, such as the administration of low doses. To achieve a desired effect, combinational treatment approaches are a promising alternative, as for example the combination of 17-DMAG with the proteasome inhibitor bortezomib showed. The dual inhibition leads to a high accumulation of ubiquitinated proteins resulting in proteotoxic stress for the tumor cells. Therefore, combining both inhibitors with lower doses led to greater efficacy than single agent treatment.[140] Another combination represented in clinical trials is IPI-504 with the cytostatic drug Docetaxel. Dual treatment resulted in anti tumor effects in NSCLC xenograft models.[141] In general, knowledge of the molecular mechanisms is essential and therefore it is important to identify potential predictive biomarkers for a better selection of responsive patients to HSP90i therapy.[142] For example, sensitivity can be increased by selecting patients with tumors that are highly dependent on HSP90 accompanied by overexpression. Furthermore, higher specificity can be achieved by characterizing the subcellular localization of HSP90 in more detail.

The localization is quite different between tumor and normal tissues, especially in mitochondria and the extracellular matrix.[143, 144] To overcome DLTs there is the possibility to use FDA approved drugs for the combination with HSP90 inhibitors. Furthermore, it is of great interest to identify new vulnerabilities associated with HSP90 to develop novel combination approaches. In addition to DLTs, HSP90 inhibitor treatment also leads to the development of resistance, which limits the benefits. A key factor in the development of resistance is HSP90 itself. As mentioned in section 1.2.4.1, HSP90 inhibition in many cases leads to initiation of HSR and thus upregulation of other chaperones and HSP90α. Studies investigating resistance development to PU-H71 in human breast adenocarcinoma cells have shown that the resistant cell lines exhibited HSP90AA1 gene amplification. Furthermore, a point mutation (Y142N) in the N-terminal ATP binding pocket led to a lower affinity towards the inhibitor. Both eventually lead to overexpression of the HSP90α Y142N variant with restored HSP90 chaperone function.[145] Another mechanism, which was found in PU-H71 resistance cell lines, was a gain in the ABCB1 gene encoding for the multi-drug resistance 1 (MDR1) protein, which leads to enhanced drug export.[146] Other studies exploring resistance mechanisms against the HSP90 inhibitor Ganetespib in KRAS-mutant NSCLC, showed hyperactivation of RAF/MEK/ERK/RSK and PI3K/AKT/mTOR pathways. Inhibition with a PI3K/mTOR, a PI3K, or an ERK inhibitor resulted in synthetic lethality, demonstrating strong dependence on those pathways.[147]

For the development of new inhibitors with improved efficacy and specificity, it is of great importance to understand the molecular mechanisms of action and subsequent mechanisms of response. In recent years, several insights have been gained that are crucial for further HSP90i development.

### 1.2.5 Targeting HSP90 with proteolysis targeting chimeras (PROTACs) or degraders

Besides the conventional targeting of proteins with small molecules, another technology is undergoing rapid development. The so-called proteolysis targeting chimeras (PROTACs) form a new class of chemical tools and potential therapeutics and were first described in 2001.[148] Structurally, they are based on three elements, a ligand of the E3 ligase, a ligand of the protein of interest (POI), and a linker connecting both entities. Thus, PROTACs are heterobifunctional small molecules, usually with a molecular weight between 0.7 and 1.1 kDa. The two functional moieties cause the generation of spatial proximity between the E3 ubiquitin ligase and the POI, and an E3 ligase:PROTAC:POI ternary complex is formed.[149] This leads to polyubiquitylation of the surface-exposed lysine at the POI, thus marked for degradation by the proteasome.[150]

PROTACs enable targeted protein degradation (TPD) *via* ubiquitin-dependent proteolysis (Figure 8).

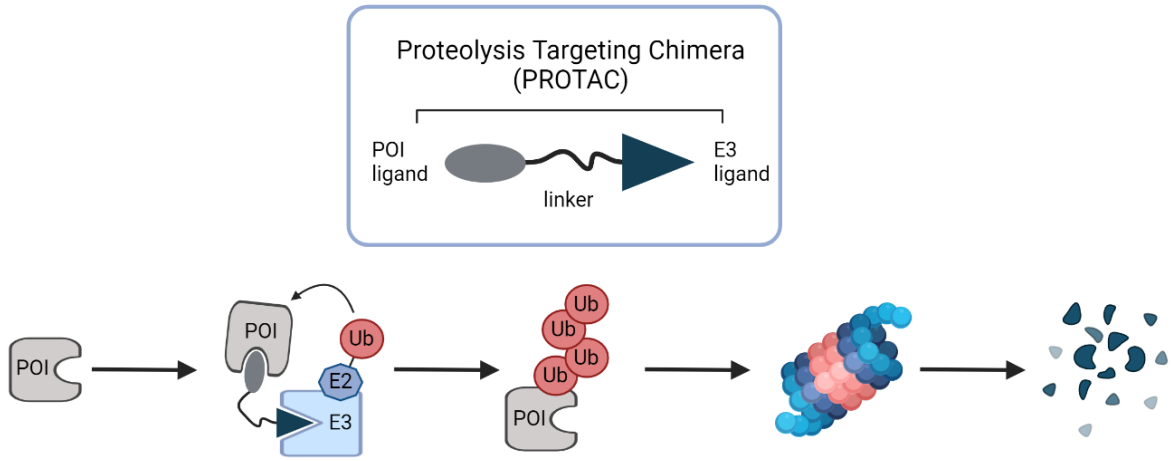


**Figure 8: Schematic representation of PROTAC degraders.**

PROTACs are heterobifunctional small molecules consisting of a POI ligand, an E3 ligase ligand and a connecting linker, which enables proximity and leads to polyubiquitylation and proteasomal degradation of the POI. Figure: Created with BioRender.com.

There are hundreds of E3 ligases, although only some can be successfully exploited as PROTACs.[151] The most prominent and mostly reported compounds are those using cereblon (CRBN) or Von Hippel-Lindau (VHL) ligases. More examples include using nutlin compounds to recruit MDM2 (human murine double minute 2) and cellular inhibitor of apoptosis (cIAP) ligands.[152] The advantages of these ligases are that those specific ligands have a well-characterized binding mode and a good physicochemical profile. Nevertheless, many E3 ligases have not been explored yet, offering considerable potential for further development in selectivity for tumour tissue or subcellular localization.[153] As already mentioned, the ligands of the E3 ligases are linked to the ligand of the POI *via* a linker. This usually consists of polyethylene glycol (PEG) or linear alkane chains. The linker can have a decisive influence on stability, bioavailability and permeability and, thus, must be optimized in terms of length, mobility, and hydrophilicity. In addition, it is essential at which site of the ligands the linker is chemically bound so that the ligands continue to have affinity and specificity for their target. With the help of PROTACs, it is possible to target all proteins that can be degraded *via* the ubiquitin-proteasome system (UPS). The UPS is an essential pathway for protein homeostasis in cells; many proteins, including transcription factors, oncogenes, and tumour suppressors, can be regulated by it.[154] The mode of action (MoA) of small molecules is based on the modulation of protein function *via* temporary inhibition of enzymatic activity. PROTACs, on the other hand, cause a complete degradation of the target proteins and thus also modulate non-enzymatic functions, such as regulatory or scaffolding functions. Furthermore, PROTACs are catalytically active and lower doses are theoretically possible, which can also reduce off-target effects. A common issue with

small molecule inhibitor treatment is the occurrence of resistance caused by mutations, deletions, or exon skipping. The use of PROTACs can overcome this since no active site is necessary.
Furthermore, the use offers new possibilities to influence the so-called “undruggable” proteome. Potentially, proteins without an active site, such as transcription factors, receptors, and membrane-associated proteins, can be addressed.[155]

Meanwhile, the concept of PROTACs has even entered preclinical and early clinical development programs. In 2019, the first PROTAC entered clinical trials. One year later, the first proof-of-concept of the two PROTACs (ARV-110 and ARV-471) for the estrogen and the androgen receptors in prostate and breast cancer patients was shown.[156,157] These PROTACs have shown promising results regarding safety, efficacy, and tolerability.[158] Currently, 15 candidates are in clinical trials, with an increasing trend.

# 2. Aims and Objectives

Introducing TKIs has led to outstanding clinical response in BCR-ABL1$^+$ leukemia. However, the occurrence of resistance is very common, as a result this entity is still associated with poor prognosis. HSP90 is a promising therapeutic target and plays an essential role in malignant transformation and tumour progression of cancer cells. However, HSP90 inhibitors have not been routinely used in the clinic, primarily due to the induction of HSR and associated resistance and the dose-limiting toxicity of NTD-HSP90 inhibitors. To improve the potential of HSP90 inhibitors for clinical application, gaining a better and more profound understanding of the HSP90 isoforms (α and β) is essential. To date, HSP90α/β isoform-specific dependence on client proteins has been determined mainly by isoform-specific HSP90i or transient knockdown approaches. Furthermore, the development of C-terminal HSP90i offers a promising approach. The first C-terminal HSP90 dimerization inhibitor has already been developed and published with collaborative partners of the working group *Kurz* (Department of Pharmaceutical and Medicinal Chemistry, Heinrich Heine University Düsseldorf) and *Gohlke* (Department of Pharmaceutical and Medicinal Chemistry, Heinrich Heine University Düsseldorf). The peptidomimetic aminoxyrone was rationally developed based on studies of hot spots at the HSP90 CTD dimerization interface.[128] Treatment with AX in a cellular context showed success in TKI-sensitive and refractory CML cell lines. Moreover, no HSR was induced.[75] However, the peptidomimetic nature of AX resulted in low water solubility, often leading to reduced oral bioavailability, and the challenges included its complex structure and the intricate process of chemical synthesis. Based on these limitations, the first small molecule HSP90 CTD dimerization inhibitors were developed by the *Kurz* group by rational drug design including structural simplification and optimization of AX. Another promising strategy explored in this thesis involves testing PROTACs based on the HSP90 inhibitor Geldanamycin. As a result, this work aims at the following objectives:

1) Decrypting the role of HSP90α and β isoforms utilizing CRISPR/CAS9 or siRNA technology to generate genetic knockout or knockdown models of HSP90 isoforms (α and β) in leukemia cell lines. The aim is to investigate these models at a molecular level, encompassing *in vitro* and *in vivo* analyses as well as multi-omics characterization to identify novel therapeutic vulnerabilities in BCR-ABL1$^+$ leukemia.

2) The biochemical evaluation of the tripyrimidonamides **1a** (LSK82) and **1b** (VWK147), as well as the structurally optimized bipyrimidone- and bipyrimidine-amides **2** and **3** (VWK346, VWK141), which were pre-selected based on cell-based cytotoxicity assays performed by colleagues from our working group (*Bhatia*). The focus is on the characterization of the com-

pounds in terms of activity and binding mode by establishing biochemical and biophysical assays to demonstrate that the compounds interact with the C-terminal domain (CTD) of HSP90 and thereby preventing/disrupting its dimerization.

3) The objective is to assess the biochemical and cellular properties of Geldanamycin-based HSP90 PROTACs, with a focus on their ability to induce degradation of HSP90 in leukemia cells. These potential HSP90 degraders, designed and synthesized by the *Hansen* (Department of Pharmaceutical and Cell Biological Chemistry, University of Bonn) working group are built on a CRBN-recruiting pomalidomide-derived ligand and feature diverse alkyl- or PEG-based linkers of varying lengths. Additionally, the study aims to differentiate between the cytosolic isoforms HSP90α and HSP90β, and to explore any isoform-specific effects.

# 3. Material and Methods

## 3.1 Material

### 3.1.1 Used machines and devices

**Table 1:** List of used devices.

| Device | Company |
|---|---|
| CFX Connect Real-Time System | BioRad |
| Heraeus Multifuge 4 KR | Thermo Scientific, Rockford, Illinois, USA |
| Heraeus Multifuge 3SR+ | Thermo Scientific, Rockford, Illinois, USA |
| Thermomixer comfort | Eppendorf |
| TECAN Spark 10M | Tecan Group LTD., Maennedorf, Switzerland |
| TECAN D300e Dispenser | Tecan Group LTD., Maennedorf, Switzerland |
| JESS | Protein simple |
| Multidrop Reagent Dispenser | Thermo Scientific, Rockford, Illinois, USA |
| CytoFLEX Flow Cytometer | Beckman-Coulter, Inc., Brea, California, USA |
| Cell Counter Vi-CELL BLU | Beckman-Coulter, Inc., Brea, California, USA |
| L-46 Vortex mixer | Scientific Industries, Bohemia, USA |
| Fresco 21 centrifuge | Thermo Scientific, Rockford, Illinois, USA |
| Nanodrop | Thermo Scientific, Rockford, Illinois, USA |

### 3.1.2 Cell lines

**Table 2:** Cell lines used for the cell biological experiments.

| Cell line | Entity | Source |
|---|---|---|
| HEK293T | Human embryonic kidney cells | DSMZ |
| K562 | CML | DSMZ |
| KCL-22 | CML | DSMZ |
| SUP-B15 | BCP-ALL | DSMZ |
| JURKAT | T-ALL | DSMZ |
| LOUCY | T-ALL | DSMZ |
| TALL1 | T-ALL | DSMZ |
| MOLT13 | T-ALL | DSMZ |
| RCH-ACV | BCP-ALL | DSMZ |
| Kasumi-2 | BCP-ALL | DSMZ |
| SEM | BCP-ALL | DSMZ |
| NALL1 (Null-cell ALL1) | ALL | - |

### 3.1.3 Cell culture media and supplements

**Table 3:** List of used cell culture media and supplements.

| Product | Company |
|---|---|
| DMEM GlutaMAX | Thermo Scientific, Rockford, Illinois, USA |
| RPMI 1640 GlutaMAX | Thermo Scientific, Rockford, Illinois, USA |
| Penicilin (10.000 U/mL)-Streptomycin (10 mg/mL) (P/S) | Sigma-Aldrich, St. Louis, Missouri, USA |
| Fetal Calf serum (FCS) | Biowest®, Nuaillé, France |
| Dulbecco's phosphate-buffered saline (PBS) | Sigma-Aldrich, St. Louis, Missouri, USA |
| MethoCult™ H4100 | StemCell Technologies, Vancouver, BC, Canada |
| TrypLE™ Express | Thermo Scientific, Rockford, Illinois, USA |

### 3.1.4 Antibodies

**Table 4:** Primary Antibodies used for conventional and digital Western Blotting.

| Target | Species | Dilution (conventional) | Dilution (JESS) | Cat. No. |
|---|---|---|---|---|
| β-actin | Mouse | 1:2000 | 1:50 | MAB8929 |
| GAPDH | Mouse | 1:2000 | - | CST#97166 |
| GAPDH | Rabbit | 1:2000 | - | CST#5174 |
| Nucleolin | Rabbit | - | 1:50 | CST#14574 |
| HSP90α | Rabbit | 1:2000 | 1:100 | CST#8165 |
| HSP90β | Rabbit | 1:1000 | 1:100 | CST#5087 |
| HSP90 | Rabbit | 1:2000 | 1:100 | CST#4877 |
| HSP70 | Rabbit | 1:1000 | - | CST#4872 |
| HSP27 | Mouse | 1:1000 | - | CST#2402 |
| HSP40 | Rabbit | 1:2000 | - | CST#4871 |
| HSF-1 | Rabbit | 1:1000 | - | CST#4356 |
| GRP94 | Rabbit | 1:1000 | - | CST#2104 |
| TRAP1 | Mouse | 1:1000 | - | SC-13557 |
| CDC37 | Mouse | 1:1000 | - | SC-13129 |
| AHA1 | Mouse | 1:1000 | - | SC-166065 |
| FKBP5 | Rabbit | 1:1000 | - | CST#12210 |
| p-AKT (S473) | Rabbit | 1:750 | 1:30 | CST#4060 |
| AKT (pan) | Mouse | 1:1000 | 1:50 | CST#2920 |
| p-STAT5 (Y694) | Rabbit | 1:1000 | 1:50 | CST#9351 |
| STAT5 | Rabbit | 1:1000 | 1:50 | CST#9363 |
| Survivin | Rabbit | 1:1000 | - | CST#2808 |

| | | | | |
|---|---|---|---|---|
| CDK4 | Rabbit | 1:1000 | - | CST#12790 |
| CDK6 | Rabbit | 1:1000 | - | CST#13331 |
| CDK7 | Mouse | 1:1000 | 1:30 | CST#2916 |
| BCR-ABL1 | Rabbit | 1:1000 | 1:50 | CST#2862 |
| p-BCR-ABL1 (Y412) | Rabbit | - | 1:10 | CST#2865 |
| CRKL | Mouse | 1:1000 | 1:30 | CST#3182 |
| p-CRKL (Y207) | Rabbit | - | 1:30 | CST#3181 |
| Aurora A | Rabbit | 1:1000 | - | CST#14475 |
| Aurora B | Rabbit | 1:1000 | - | CST#28711 |
| p-Aurora A/B/C (T288/T232/T198) | Rabbit | 1:1000 | - | CST#2914 |
| XIAP | Rabbit | 1:1000 | - | CST#2042 |
| c-IAP1 | Rabbit | 1:1000 | - | CST#7065 |
| SLP-76 (LCP2) | Rabbit | 1:1000 | - | CST#4958 |
| TOP2A | Rabbit | 1:1000 | - | CST#12286 |
| HiBiT | Mouse | 1:1000 | - | Promega |
| RPB1 | Mouse | 1:1000 | - | CST#2629 |
| p-RPB1 (S5) | Rabbit | 1:1000 | - | CST#13523 |
| PARP | Rabbit | 1:1000 | - | CST#9532 |
| LCK | Rabbit | 1:1000 | - | CST#2752 |
| p-LCK (Y505) | Rabbit | 1:1000 | - | CST#2751 |
| p-LCK (Y394) | Mouse | 1:1000 | - | #933101 |
| SRC | Rabbit | 1:1000 | - | CST#2109 |
| p-SRC (Y416) | Rabbit | 1:1000 | - | CTS#2101 |
| CD45 (intracellular domain) | Rabbit | 1:1000 | - | CST#13917 |
| LYN | Rabbit | 1:1000 | - | CST#2796 |
| p-LYN (Y507) | Rabbit | 1:1000 | - | CST#2731 |

**Table 5:** Secondary Antibodies used for Western Blotting.

| Target | Species | Dilution | Cat. No. |
|---|---|---|---|
| Rabbit HRP | Goat | 1:2000 | CST#7074 |
| Mouse HRP | Horse | 1:2000 | CST#7076 |
| Rabbit HRP | Goat | - | #042-206 |
| Mouse HRP | Goat | - | #042-205 |
| 20X Mouse NIR | Goat | 1:20 | #043-821 |

### 3.1.5 Kits

**Table 6:** List of used commercially available Kits.

| Kit | Company |
|---|---|
| CellTiter Glo® Luminescent Assay | Promega, Fitchburg, USA |
| ECL™ Western Blotting Detection Reagents | Cytiva, Marlborough, Massachusetts, USA |
| RealTime-Glo™ MT Cell Viability Assay | Promega, Fitchburg, USA |
| Pierce™ BCA Protein Assay | Thermo Scientific, Rockford, Illinois, USA |
| Nano-Glo® HiBiT Lytic Detection Kit | Promega, Fitchburg, USA |
| Lenti-X™ Packaging Single Shots | Takara, Shiga, Japan |
| Maxwell® RSC Blood DNA Kit | Promega, Fitchburg, USA |
| Maxwell® RSC simply RNA Cells Kit | Promega, Fitchburg, USA |

### 3.1.6 Buffers and solutions

**Table 7:** List of used buffers and solutions.

| Buffer | Composition |
|---|---|
| SDS gel running buffer (10X) | 250 mM Tris, 2 M Glycine, 35 mM SDS in $dH_2O$ |
| Transfer buffer (10X) | 250 mM Tris, 2 M Glycine in $dH_2O$ |
| Transfer buffer (1X) | 25 mM Tris, 200 mM Glycine, 20 % MeOH in $dH_2O$ |
| TBS (10X) | 200 mM Tris, 1.5 M NaCl |
| TBS-T (1X) | 20 mM Tris, 150 mM NaCl, and 5 % Tween20 |
| Blocking buffer | TBS-T, 5 % BSA |
| Stacking buffer | 0.5 M Tris, pH 6.8 |
| Separation buffer | 1.5 M Tris, pH 8.8 |
| Lyse buffer | RIPA 10 mL, cOmplete™ 1X, phosSTOP, 1 mM DTT |
| Denaturation buffer | 25 mM Tricine, pH 7.8, 8 mM MgSO4, 0.1 mM EDTA, 1% Triton X-100, 10% glycerol, and 10 mg/mL BSA in $dH_2O$ |
| Cold mix buffer | 100 mM Tris, pH 7.7, 75 mM $Mg(OAc)_2$, 375 mM KCl, and 15 mM ATP in $dH_2O$ |
| Control buffer | 20 mM Tris, pH 7.5, 150 mM NaCl, 1 % haemoglobin and 4 % BSA in $dH_2O$ |
| Assay buffer | 25 mM Tricine, pH 7.8, 8 mM MgSO4, 0.1 mM EDTA, 33 µM DTT, 0.5 mM ATP, and 0.5 mM luciferin in $dH_2O$ |
| Nicoletti assay buffer | 0.1 % sodium citrate, 0.1 % Triton X-100, 50 µg/mL PI |
| LB media | 5 g/L sodium chloride, 5 g/L yeast extract, 10 g/L peptone |

### 3.1.7 Oligonucleotides

**Table 8:** List of used primers.

| Name | Sequence (5'- 3') |
|---|---|
| c-For-HSP90aa1 | CAGCCGCCCTTCTATTTTCG |
| c-Rev-HSP90aa1 | TTAAGCATACAGCACCCCCAAG |
| c-For-HSP90ab1 | TCTTGAGGCTTTAGAACCAG |
| c-Rev-HSP90ab1 | AGTCTGAACTCACTGTCTAAGGT |

### 3.1.8 DNA- and Protein ladders

**Table 9:** List of used DNA- and protein ladders.

| Ladder | Supplier |
|---|---|
| GeneRuler™ 1 kb DNA ladder | Thermo Scientific (Rockford, Illinois, USA) |
| PageRuler™ Prestained Protein Ladder 10-180 kDa | Thermo Scientific (Rockford, Illinois, USA) |

### 3.1.9 Chemicals and Reagents

**Table 10:** List of used Chemicals and Reagents.

| Chemicals/Reagents | Supplier |
|---|---|
| Ammonium persulfate (APS) | Carl Roth, Karlsruhe, Germany |
| Bovine serum albumin (BSA) | Carl Roth, Karlsruhe, Germany |
| cOmplete™ Protease Inhibitor Cocktail | Roche, Basel, Switzerland |
| phosSTOP™ | Roche, Basel, Switzerland |
| Pierce™ RIPA lysis buffer | Thermo Scientific, Rockford, Illinois, USA |

### 3.1.10 Compound library for Drug screening

**Table 11:** List of compounds used for the library drug screening.

| Compound /Inhibitor | Drug class /Target |
|---|---|
| Coumermycin A1 | HSP90 |
| EC144 | HSP90 |
| Ganetespib | HSP90 |
| Geldanamycin | HSP90 |
| Tanespimycin | HSP90 |
| PU-H71 | HSP90 |
| KUNB31 | HSP90 |
| BIIB021 | HSP90 |
| AUY922 (LUMINESPIB) | HSP90 |
| Panobinostat | HDAC |

| | |
|---|---|
| Ricolinostat | HDAC6 |
| Romidepsin | HDAC |
| Belinostat | HDAC |
| Entinostat | HDAC |
| Givinostat (ITF2357) | HDAC |
| CI-994 (Tacedinaline) | HDAC |
| Dasatinib (Hydrochlorid) | BCR-ABL, Src |
| Imatinib (Mesylate) | BCR-ABL inhibitor |
| Ponatinib | BCR-ABL, FGFR, FLT3, VEGFR |
| Bosutinib | BCR-ABL, Src |
| Dinaciclib | CDK |
| LY2835219 (Abemaciclib) | CDK |
| Palbociclib | CDK |
| YKL-5-124 | CDK7 |
| SY-1365-THZ1 | CDK7 |
| Volasertib | Polo-like Kinase (PLK) |
| BI2536 | PLK |
| 6-Mercaptopurine (Monohydrate) | Antimetabolites |
| 6-Thioguanine | Antimetabolites |
| Clofarabine | Antimetabolites |
| Cyclocytidine HCL | Antimetabolites |
| Methotrexate | Antimetabolites |
| 5-Azacytidine | Antimetabolites |
| Cytarabine (Hydrochlorid) | Antimetabolites |
| Vinblastine (sulfate) | Antimitotics |
| Vincristine (sulfate) | Antimitotics |
| Alisertib | Aurora Kinase A |
| Barasertib | Aurora kinase B |
| Aurora A Inhibitor I | Aurora Kinase A inhibitor |
| Birabresib | BRD2/3/4 |
| Carfilzomib | Proteasome inhibitor |
| Bortezomib | Proteasome inhibitor |
| MLN-9708 (Citrate) | Proteasome inhibitor |
| Cobimetinib | MEK |
| MEK162 (Binimetinib) | MEK |

| | |
|---|---|
| Lonafarnib | RAS |
| Regorafenib (Monohydrate) | RAF |
| Tipifarnib | Farnesyl Transferase; RAS |
| Sorafenib (Tosylate) | RAF |
| Trametinib | MEK |
| AT9283 | JAK |
| CYT387 (Momelotinib) | JAK |
| Fedratinib (TG101348) | JAK; FLT3 |
| BSI-201 (Iniparib) | PARP |
| Olaparib | PARP |
| GSK343 | EZH2i/HMTasei |
| Ibrutinib (Ibruvica) | BTK |
| Tirabrutinib | BTK |
| Amsacrine (Hydochlorid) | Topoisomerase inhibitors |
| Daunorubicin (Hydrochloride) | Topoisomerase inhibitors |
| Mitoxantrone (dihydrochloride) | Topoisomerase inhibitors |
| Dovitinib | FLT3, PDGFR, VEGFR, c-KIT |
| Gilteritinib | FLT3/AXL |
| Lestaurtinib | FLT3 |
| Midostaurin | PKC, VEGFR2, PDGFR, FLT3 |
| Pacritinib | FLT3, JAK |
| Pexidartinib | FLT3, KIT, CSF1R |
| Quizartinib | FLT3 |
| Pacritinib | FLT3, JAK |
| Pexidartinib | FLT3, KIT, CSF1R |
| Quizartinib | FLT3 |
| Staurosporin | Multiple non-selective inhibitor of protein kinases |
| Omaveloxolone | NF-kB |
| QNZ (EVP4593) | NF-kB |
| Birinapant | XIAP and cIAP1 |
| AZD6738 | ATM/ATR |
| Omacetaxine Mepesuccinate (Homoharringtonine) | Ribosome inhibitor |
| Selinexor | CRM1 inhibitor |
| Nintedanib (BIBF1120) | LCK inhibitor |
| Ro 08-2750 | NGF inhibitor |

| | |
|---|---|
| Bexarotene | Retinoid inhibitor |
| ABT-199 (Venetoclax) | Bcl-2 Family |
| Obatoclax (Mesylate) | Bcl-2 Family |
| Temsirolimus | mTOR |
| PF-04691502 | mTOR, PI3K |
| ARQ-092 (Miransertib) | AKT |
| BAY 80-6946 (Copanlisib) | PI3K |
| Dactolisib (BEZ235) | PI3K, mTOR |
| Idelalisib | PI3K |
| Everolimus | mTOR |
| 5-nonyloxy-tryptamine | 5-HT1B receptor agonist |
| Tegaserod | 5-HT4/serotonin agonist |
| Axitinib | VEGFR |

## 3.2 Biochemical Methods

### 3.2.1 Thermal shift assay

Thermal shift assay was performed as previously described.[159] C-terminal or N-terminal of HSP90 (5 µM) and the indicated concentrations of the inhibitors were mixed in the assay buffer (1X PBS, pH = 7.5) and were incubated for 2 h. Then, 6X SYPRO Orange dye (Sigma) was added to make a final volume of 20 µL. 96-well polymerase chain reaction (PCR) plates and a PCR system (BioRad, CFX Connect™ Real-time system) were used to heat the samples from room temperature to 95 °C in increments of 0.5 °C for 10 seconds.

To determine protein melting temperature values (Tm), a melting curve for each data set was analysed by GraphPad Prism 8.0.2 and fitted with the sigmoidal Boltzmann fit. Melting temperatures without the inhibitors were used as a control.

### 3.2.2 Luciferase refolding assay

Luciferase refolding assay was performed as previously described[159] using recombinant firefly Luciferase from Photinus pyralis (Sigma Aldrich, St. Louis, MO, USA; $10x10^{10}$ Units/mg), which was diluted (1:100) in denaturation buffer (25 mM Tricine, pH 7.8, 8 mM MgSO4, 0.1 mM EDTA, 1% Triton X-100, 10% glycerol, and 10 mg/mL BSA). In the first step, the luciferase was denatured by heating at 38°C for 8 min. Rabbit reticulocyte lysate (Promega, Madison, WI, USA) was diluted 1:1 with cold mix buffer (100 mM Tris, pH 7.7, 75 mM $Mg(OAc)_2$, 375 mM KCl, and 15 mM ATP), creatine phosphate (10 mM) and creatine phosphokinase (16 U/mL) and was pre-incubated at 30°C with compound for 1h. Afterwards, 1µL denatured or active luciferase was added to a 20 µL rabbit reticulocyte mixture. As a control, denatured or active luciferase was incubated without reticulocyte lysate in a buffer containing 20 mM Tris, pH 7.5, 150 mM NaCl, 1 % haemoglobin and 4 % BSA. At desired time points, 1.5 µL samples were removed and added to 40 µL assay buffer (25 mM Tricine, pH 7.8, 8 mM MgSO4, 0.1 mM EDTA, 33 µM DTT, 0.5 mM ATP, and 0.5 mM luciferin) and luminescence was read using a Spark® microplate reader (Tecan). Percent luciferase refolding was determined using luminescence of DMSO at 120 min as 100%.

### 3.2.3 BS3 crosslinker assay

CTD-HSP90 (2 µM) was diluted in Na2HPO4 (25 mM; pH 7.4) and treated with different concentrations of the inhibitor to make a final volume of 25 µL. The reaction mixture was incubated at RT for 1 h. The amine-reactive crosslinker BS3 (bis(sulfosuccinimidyl) suberate, Pierce) was added to a final concentration of 62.5 µM, and the samples were incubated for 1 h at RT. Crosslinking was quenched by adding SDS sample buffer and heating for 5 min at 95 °C. Samples were run on 12% SDS-PAGE gels followed by western blotting. Blots were probed with anti-HSP90 or anti-GST antibodies.

## 3.3 Molecular biological Methods

### 3.3.1 Recombinant protein expression

Synthetic codon-optimized DNA (GeneScript, Piscataway, NJ) corresponding to the coding region of residues 563–732 of hHSP90 CTD was cloned into expression vector pTEV21-a in E. coli BL21 (DE3) (Agilent Technologies). Cultures were grown at 37°C in LB media with ampicillin to OD600 = 0.8–1.2. The production of recombinant protein was induced by adding 1 mM isopropyl β-D-1-thiogalactopyr-anoside (IPTG), and cells were grown for another 4 h at 28°C. Cells were harvested by centrifugation, suspended in binding buffer (40 mM HEPES, 20 mM KCl, 1 mM DTT, 1 mM EDTA, 0.002% PMSF, pH 7.5) and disrupted by sonification. Recombinant proteins were purified *via* a C-terminal His 6-tag by immobilized metal ion affinity chromatography to homogeneity.

To prepare the recombinant hHSP90α NTD (amino acids 9−236; Addgene #22481) protein, the E. coli strain BL21(DE3) was used. BL21-DE3 expression strains were grown overnight and used to inoculate LB medium at 37 °C supplemented with 100 μg/mL ampicillin. After an OD600 = 0.5−0.8 was reached, overnight induction of protein expression with 0.5 mM IPTG at 25 °C was done. After induction, cells were harvested by centrifugation at 5000g and lysed using B-PER bacterial protein extraction reagent (ThermoFisher Scientific, Wesel, Germany). GST-tagged HSP90α NTD protein was affinity purified using spin columns (ThermoFisher Scientific) and eluted using glutathione elution buffer.

### 3.3.2 Protein isolation

Cells were harvested by centrifugation at 300 x g for 5 min at 4°C, washed thrice with PBS, and then snap-frozen in liquid nitrogen. RIPA lysis buffer (Thermo Fisher Scientific, #89900) supplemented with cOmplete$^{tm}$ (Roche, #11697498001), PhosSTOP (Sigma-Aldrich, #4906845001) and DTT were used to lyse the cells. Cells were lysed on ice for 20 min, centrifuged (21000 x g for 30 min at 4 °C), and protein quantification was performed by BCA-Assay (Thermo Fisher Scientific, #23227).

### 3.3.3 SDS gel

For the SDS gel, 10 - 20 μg of the lysate was separated at 50 V for 30 min during the stacking phase and 100 V for 1.5h during the separation phase.

**Table 12:** Recipe for each stacking and separation gel.

| | Stacking gel | Separation gel 12 % |
|---|---|---|
| Acrylamide (30 %) | 450 µL | 4 mL |
| $dH_2O$ | 2.11 mL | 2.1 mL |
| Stacking buffer (0.5 M Tris pH 6.8) | 380 µL | - |
| Separation buffer (1.5 M Tris pH 8.8) | - | 3.6 mL |
| APS (10 %) | 30 µL | 98 µL |
| SDS (10 %) | 30 µL | 98 µL |
| TEMED | 5 µL | 8.1 µL |

## 3.3.4 Western Blotting

Blotting was done using 0.45 µm nitrocellulose membranes (Cytiva, #10600002) at 100 V for 1-2h, depending on the target protein size. Membranes were blocked with a 5% BSA (Sigma-Aldrich #A3294) TBS-T solution, washed three times with TBS-T and incubated with primary antibody solution in 5% BSA solution overnight at 4°C. The next day, membranes were washed three times with TBS-T, incubated for 2h with secondary HRP-conjugate in 5% BSA solution and rewashed three times in TBS-T. For visualization ECL-Solution (Cytiva, #GERPN2106) was used per manufacturer's instruction, and images were captured using a Quantitative simple western immunoassay (JESS).

## 3.3.5 Quantitative simple western immunoassay (JESS)

For the quantification and the visualization of low abundance proteins, like, for example, phosphorylated ones, digital western blotting was performed. Therefore, lysates were diluted with 0.1X sample buffer and mixed with 5X master mix (5:1) to obtain a final sample concentration of 0.4 µg/µl. The samples were vortexed and denatured for 5 min. at 95°C in a heat block. Afterwards, the plate was loaded with the prepared protein lysates, biotinylated ladder, antibody diluent, primary- and secondary antibody, streptavidin-HRP, and a luminol-peroxide mix according to manufacturer's instructions. The assay plate was centrifuged (2500 rpm, 5 min., RT), and wash buffer was added last to remove air bubbles. A 12-230 or 40-400 kDa separation module with 25 cartridges was used for the immunoassay. Separation took place at 375 V for 25 min, following blocking with antibody diluent and incubating with primary and secondary antibodies. The evaluation was done with JESS.

## 3.3.6 Proliferation assay

### 3.3.6.1 RealTime-Glo™ MT Cell Viability Assay

The cells were seeded (0.4*10^5 cells/mL) in a 384-well plate using a $CO_2$-independent medium (ThermoFisher, #18045088). To measure the proliferation of the cells, the RealTime-Glo™ MT Cell Viability Assay (Promega, #G9711) was used.

NanoLuc® enzyme and MT cell viability substrate were added according to the manufacture instructions. The luminescence signal was determined from each well every 30 min. for 24 hours in a Tecan plate reader at 37 °C.

#### 3.3.6.2 Manual cell counting

The cells were seeded (0.1*10^6 cells/mL) in a T25 flask. Each day cells were counted using the cell counter (Beckman Coulter).

### 3.3.7 FACS

For the flow cytometry, the cells were centrifuged (300 x g, 5 min.), washed once with PBS, resuspended in PBS and transferred to a 96-well plate.

### 3.3.8 Cell cycle analysis (Nicoletti assay)

For the cell cycle analysis, cells (1*10^5 cells) were washed once with PBS and resuspended in Nicoletti assay buffer (0.1 % sodium citrate, 0.1 % Triton X-100, 50 µg/mL PI). After incubating the cells for 10 min. at RT, they were measured with the CytoFLEX.

### 3.3.9 Caspase 3/7 Glo assay

To measure the Caspase 3/7 activity, the luminescent Caspase-Glo® assay system (Promega, #G8090) was used. Cells (100.000 cells/mL) were seeded into a white 96-well plate and treated with PU-H71, THZ1 and with both inhibitors together with the indicated concentrations. Cells were incubated for 24h and diluted with Caspase-Glo® 3/7 Reagent 1:1 (Caspase-Glo® 3/7 Substrate and Caspase-Glo® buffer was previously mixed according to manufacturer's instructions). The plate was incubated for 30 min at RT and luminescence was measured with the Tecan Spark.

### 3.3.10 RNA sequencing

RNA was isolated utilizing the Maxwell® RSC simplyRNA Cells Kit (Promega, #AS1390). Library preparation followed supplier’s guidelines using the VAHTs Stranded mRNA-Seq Library Prep Kit (Illumina Inc. San Diego, USA). Briefly, total RNA (500 ng) was used to capture mRNA, fragmentation, cDNA synthesis, ligation of the adapters and library amplification. Purified libraries were normalized and sequenced on the NextSeq550 (Illumina) with 1x76 bp read setup. Followed by using bcl2fastq2 tool to convert the bcl files to fastq files. The raw sequencing data were uploaded to galaxy, and initial quality control was performed by FastQC and aggregated *via* MultiQC. After cutting the adapters with FASTQ Trimmer, the reads were aligned to the reference genome GRCh38 with RNA STAR. FastQC determined that at least 85% of all reads were uniquely mapped. To quantify the gene expression featureCounts was used, followed by edgeR to normalize the data to the sequencing depth. Differentially expressed

genes were determined by an absolute log2 fold change of >1 / < -1 and a FDR < 0.05. Differentially expressed genes with a low log2CPM (normalized log2CPM < -1) were treated preferentially.

### 3.3.11 Mass Spectrometry (MS) based proteome analysis:

1.1) Sample preparation proteomes: K562 cells (EV, HSP90α-KO, and HSP90β-KO); five biological replicates) were washed three times with PBS and shock frozen in liquid nitrogen. Briefly, cells were lysed and homogenized in urea buffer using a TissueLyser (Qiagen) and after centrifugation (15 min, 16000 rcf, 4°C), supernatants were collected. After determination of protein concentration (Pierce 660 nm Protein Assay, Thermo Fischer Scientific), samples were adjusted to 0.5 mg/ml total protein concentration with SDS buffer (final 7.5% glycerol, 3% SDS, 37.5 mM Tris/HCl pH 7.0). 10 µl were reduced (20 mM dithiothreitol, 20 min, 56°C), alkylated (80 mM iodoacetamide, 15 min, r.t., protected from light) and finally underwent tryptic digestion (200 ng trypsin in 50 mM triethylammonium bicarbonate). Last, a slightly modified sp3 protocol was applied using 50 µg 1:1 mix Sera-Mag SpeedBeads. Peptides were reconstituted in 0.1% trifluoracetic acid and subjected to LC-MS analysis.

1.2) Sample preparation secretomes: K562 cells (EV, HSP90α-KO, and HSP90β-KO); five biological replicates, 0.8*10^6 cells/mL) were washed three times with PBS and three times with FCS-free medium and were seeded into 100 mm dishes in FCS-free medium. After 24 h, the conditioned medium was collected by centrifugation (800 x g, 5 min) and the supernatant was filtered (PALL Acrodisc 32 mm Syringe Filter with 0.2 µm Supor Membrane) and shock frozen in liquid nitrogen.

An aliquot (400 µl) per cell type and replicate was thawed on ice in the presence of a protease inhibitor cocktail (added 50 µl of a solution of 1 cOmplete ULTRA tablet, mini, EDTA-free in 2 mL water; Roche, #05892791001), supplemented with SDS buffer (added 50 µl of 30% glycerin, 12% SDS, 150 mM Tris base), reduced (added 40.5 µL of 100 mM dithiothreitol; 20 min at 56 °C under shaking), alkylated (added 54 µL of 300 mM iodacetamide; 15 min at r.t. protected from light), and quenched (added 40.5 µL of 100 mM dithiothreitol; 20 min at r.t.). Applying a slightly modified sp3 protocol, proteins were precipitated (added 10 µL of 20 mg/mL 1:1 bead-mix of pre-washed Sera-Mag SpeedBeads GE #45152105050250 and #65152105050250 in water; added 645 µL ethanol abs. p.a.; 15 min at 24 °C under shaking), washed (3x 80% ethanol, 1x acetonitrile) and digested (100 ng trypsin in 20 µL 50 mM triethylammonium bicarbonate). Peptides were reconstituted in 0.1% trifluoracetic acid and subjected to LC-MS analysis.

2) LC-MS analysis: For the LC-MS analysis, a Q Exactive Plus Hybrid Quadrupole-Orbitrap Mass Spectrometer (Thermo Fisher Scientific), operated in positive mode and coupled with a nano electrospray ionization source connected with an Ultimate 3000 Rapid Separation liquid chromatography system (Dionex / Thermo Fisher Scientific, Idstein, Germany) equipped with an Acclaim PepMap 100 C18 column (75 µm inner diameter, 25 cm length, 2 mm particle size from Thermo Fisher Scientific) was applied using a 120 min LC gradient. The capillary temperature was set to 250°C and the source voltage to 1.4 kV. MS survey scans ranged from 350 to 2000 m/z at a resolution of 140,000. The automatic gain control was set to 3,000,000, and the maximum fill time was 80 ms. The ten most intensive peptide ions per survey scan were isolated and fragmented by high-energy collision dissociation.
3) Data analysis: MaxQuant (version 2.0.3.0, Max Planck Institute for Biochemistry, Planegg, Germany) was used for peptide/protein identification and quantification employing a human sequence database (UniProtKB, downloaded on 01/27/2021, 75777 entries for proteomes or on 01/18/2022, 79038 entries for secretomes). Methionine oxidation, N-terminal acetylation, and a carbamidomethylation at cysteine residues were considered variable and fixed modifications, respectively. A false discovery rate of 1% on protein and peptide levels was set as the identification threshold. A total of 4676 identified protein groups were identified for proteomes and 2051 for secretomes after removing potential contaminants, reverse hits, proteins only identified by modified peptides, and proteins without the valid intensity or MS/MS count values.
Statistical analysis was performed based on experiment-pairwise median log2(fold change) normalized and log2 transformed MaxQuant protein group intensities and LFQ intensities using the "R" (v4.0.4 for proteomes and v4.2.1 for secretomes) programming language. Principal component analysis (PCA) was performed using the prcomp() function with centering and without scaling on protein groups with a complete set of valid values over all samples. Testing for significant protein up- or downregulation in differential analyses (HSP90α-KO vs. EV or HSP90β-KO vs. EV) was performed using the 'Significance Analysis of Microarrays' (SAM) analysis method within the siggenes package. For this approach, a minimum of four valid values had to be present in at least one group (EV or KO) and missing values were filled in with random values from sample wise downshifted normal distributions of the log2 transformed data (0.3 s.d. width, 1.8 s.d. downshift). Replicate three of the EV samples of the secretomes was excluded from statistical analysis because it differed substantially from the other four replicates.

### 3.3.12 Sanger sequencing

DNA was isolated from the pellet using the Maxwell® RSC Blood DNA Kit (Promega, #AS1400) and quantified *via* Nanodrop (Thermo Fisher Scientific).

For the sequencing, the cells were harvested by centrifugation (400 x g, 5 min.), washed thrice with PBS, and snap-frozen in liquid nitrogen. Afterwards, a PCR was performed using previously optimized primer and conditions. The products from the PCR were loaded on an agarose gel electrophorese to validate the specificity and correct size of the product. The band was cut out of the gel and purified using the QIAquick PCR Purification Kit (#28106) as per manufacturer's instructions, and samples were sent to BFMZ. Data analysis was done with ApE or Sequencher®.

**Table 13: Used primers for sequencing.**

| Name | sequence (5'- 3') |
|---|---|
| For seq U6 | GAGGGCCTATTTCCCATGATTCC |
| Rev seq U6 | GGAATCATGGGAAATAGGCCCTC |
| Hi-90AA1-F | AACTGCGCTCCTGTCTTCTG |
| Hi-90AA1-R | TCTTACAGTGCACGTTACCCC |
| Hi-90AB1-F | CTTCGGGACAACTCCACCAT |
| Hi-90AB1-R | TTGACACCCTTAGTTTACTG |

### 3.3.13 qPCR

For the qPCR, the cells were harvested by centrifugation (400 x g, 5 min.), washed three times with PBS, and snap-frozen in liquid nitrogen. RNA was isolated using the Maxwell® RSC viral total nucleic acid purification kit (Promega) with the Maxwell RSC 48, following manufacturer's instructions. 2 µg of total RNA was used for cDNA synthesis (QuantiTect Reverse Transcription kit, Qiagen) and quantitative real-time PCR was carried out using BioRad cycler (BioRad). The mean Ct values of the housekeeping genes B2M, GAPDH and β-Actin were used to normalize the mRNA expression levels of the target genes.

**Table 14: Used housekeeping primers for qPCR.**

| Name | sequence (5'- 3') |
|---|---|
| For B2M | GTATGCCTGCCGTGTGAAC |
| Rev B2M | AAAGCAAGCAAGCAGAATTTGG |
| For β-Actin | GCACTCTTCCAGCCTTCC |
| Rev β-Actin | CTCGAAGCATTTGCGGTG |
| For GAPDH | GTCTCCTCTGACTTCAACAGCG |
| Rev GAPDH | ACCACCCTGTTGCTGTAGCCAA |
| For TBP | TGTATCCACAGTGAATCTTGGTTG |
| Rev TBP | GGTTCGTGGCTCTCTTATCCTC |

## 3.4 Cell culture methods

The cell biological work was carried out under a sterile bench. The cells were cultivated at 37 °C, 5 % $CO_2$, and a humidity of 95 %. All media and reagents used were autoclaved or purchased sterilized.

### 3.4.1 Thawing cells

Cells were thawed by taking the cryo tubes from liquid nitrogen and incubating them in a water bath at 37 °C for 2 minutes. The cells were immediately transferred to a 50 mL falcon tube and diluted with pre-warmed PBS (30 mL) to reduce the concentration of DMSO. Afterwards, the cells were centrifuged (300 x g, 5 min.), the supernatant was removed, and the cells were resuspended in pre-warmed media and plated into a 6-well plate. On the next day, cells were again washed one time with PBS (30 mL) and resuspended in fresh media.

### 3.4.2 Cryo-conservation of cells

For the Cryo-conservation, 5 Mio cells were harvested and washed once with PBS. Afterwards, the cell pellet was resuspended in cryo media (FCS, 10 % DMSO), immediately transferred into a Mr. Frosty™ freezing container, and stored in a -80°C freezer. After 12 h, cryo tubes were removed from the container and transferred into liquid nitrogen.

### 3.4.3 Culturing leukemic cells

The leukemic suspension cell lines were cultured in RMPI 1640 + GlutaMAX supplemented with Penicilin-Streptomycin (1 %) and FCS (10-20 %). To prevent overgrowing and to maintain the nutrient level, cells were splitted twice a week up to 1:20 with preheated media.

### 3.4.4 Culturing HEK293T cells

The adherent HEK293T cells were cultured in DMEM + GlutaMAX supplemented with 1 % (v/v) Penicilin-Streptomycin and 10 % (v/v) FCS in a 10 cm dish or a horizontal T75 flask. Cells were splitted twice a week up to 1:20 with preheated media. For this, the old medium was removed, and TrypLE™ Express solution was added to the cells so that the bottom was barely covered. After the incubation time of 5 min., new media was added, and the cells were resuspended and isolated by pipetting the liquid up and down several times. Most of the old media was removed, and the remaining cells were filled with new media.

## 3.4.5 Lentiviral transduction of cells

### 3.4.5.1 Xfect transfection

#### 3.4.5.1.1 Transfection of HEK293T cells for lentivirus preparation

HEK293T cells were plated in 10 cm dishes and grown until they reached around 80 % confluence. The plasmid DNA (7 µg), containing the target plasmid and the three helper plasmids (6 µg; 2.4 µg; 1.4 µg), were diluted with Xfect reaction buffer (Takara) to a final volume of 600 µL and mixed by vortexing. Afterwards, Xfect polymer (Takara) was added to the diluted plasmid DNA (1 µg DNA: 0.3 µL polymer) and incubated for 10 min. The entire nanoparticle complex solution was added dropwise to the cell culture medium, and the plates were incubated at 37 °C overnight. The nanoparticle complex was removed from the cells, and new growth medium was added. The plates were returned to 37 °C and grown for 60 h to generate the virus.

#### 3.4.5.1.2 Lentiviral transduction

After 60 h, the supernatant was collected and centrifuged (1000 x g, 10 min, 4 °C) to remove cell debris. The supernatant was filtered through a 0.45 µm filter and added (1 mL viral supernatant: 1 mL cell suspension with 0.4*10^6 cells) to the cells, pre-seeded in a 12 well plate. The cells were incubated for 72 h at 37°C and afterwards washed with PBS. After the cells were recovered from the viral stress, antibiotic selection was started. Cells without antibiotic selection markers were grown and later selected for a fluorescent marker like GFP/mCherry.

### 3.4.5.2 LentiX™ Single Shots

Lenti-X HEK293T cells were plated in 10 cm dishes in 8 mL and grown until they reached around 80 % confluence. The lentiviral vector plasmid (7 µg) containing the target sequence was diluted in sterile water to a final volume of 600 µL. The mixture was added to a tube of Lenti-X Packaging Single shots (Takara), vortexed, and incubated for 10 min at RT. After short centrifugation of the tube, the entire 600 µL of nanoparticle complex solution was added dropwise to the cell culture medium and the plates were incubated at 37 °C overnight. The nanoparticle complex was diluted by adding 6 mL of fresh growth medium, and the plates were returned to 37 °C and grown for 48 h to generate the virus.

After incubating the cells for 72 h with the viral solution, cells were centrifuged and washed to remove any residual viral particles. After 72 h, the lentiviral supernatant was harvested, filtered through a 0.45 µm filter to remove cellular debris, and added to the cells (0.4*10^6 cells) in a 12-well plate (one volume cells: one volume virus-containing supernatant). Cells were grown and later selected for a fluorescent marker like GFP/mCherry.

**Table 15:** Used plasmids for lentiviral transduction.

| Function | Vector | Selection | Cat. No. |
|---|---|---|---|
| Lentiviral packaging | pMDLg/pRRE (125) | - | #12251 |
| Lentiviral packaging | pRSV-Rev (126) | - | #12253 |
| Lentiviral packaging | pMD2.G (127) | - | #12259 |
| CAS9 OE | LentiV_Cas9_puro | Puromycin | #108100 |
| HSP90α KO | LRG2.1 | GFP | #108098 |
| HSP90β KO | LRCherry2.1 | mCherry | #108099 |
| Luciferase OE | pS-Luc-GFP-W [160] | GFP | - |

**Table 16:** Used sgRNA for HSP90AA1/HSP90AB1 gene KO. Blue-marked bases indicate overlaps between the forward and reverse sequences. The black bases are overlaps for the cloning.

| Gene | sgRNA |
|---|---|
| For HSP90AA1 | CACCGGACCCAAGACCAACCGATGG |
| Rev HSP90AA1 | AAACCCATCGGTTGGTCTTGGGTC |
| For HSP90AB1 | CACCGCATTAGAGATCAACTCCCGA |
| Rev HSP90AB1 | AAACTCGGGAGTTGATCTCTAATG |

### 3.4.6 siRNA KD

To generate genetic knockdown, cells (0.25*10^6 cells/mL) were seeded in a 12-well plate in FCS-free Accell siRNA delivery media (Horizon, Dharmacon™ Reagents, Catalog ID: B-005000-500) without adding any supplements. siRNA targeting HSP90α/β or Non-targeting Control pool (Horizon, Dharmacon™ Reagents, Catalog ID: D-001910-10-20) was diluted in RNAse-free water (100 µM) and incubated at 37 °C for 1h in the shaker. Afterwards, siRNA was added to the cells (1 µM) and incubated for 48h. Cells were collected, centrifuged, and resuspended in RPMI GlutaMAX supplemented with 10% FSC and 1% P/S to let them recover for 48h. After 96h, cell pellets were taken, and the rest of the cells were again transferred to Accell siRNA delivery media containing respective siRNA. Again, cells were incubated for 48h and afterwards transferred to RPMI GlutaMAX supplemented with 10% FSC and 1% P/S to let them recover for 48h. After 192h in total, again cell pellets were taken for further analysis.

**Table 17:** Used siRNA SMARTpool for targeting HSP90α/β ordered from Dharmacon.

| | | |
|---|---|---|
| Accell Human HSP90AB1 | A-005187-14 | CGAUUAGGUUAGGAGUUCA |
| | A-005187-15 | GCUUCGAGGUGGUAUAUAU |
| | A-005187-16 | GCAGUAAACUAAGGGUGUC |
| | A-005187-17 | CCAUCACCCUUUAUUUGGA |
| Accell Human HSP90AA1 | A-005186-14 | GCUGUAUCUUGAUGUUUAG |
| | A-005186-15 | CUGUGAUCACCAAACAUAA |
| | A-005186-16 | GUGUCAAACCGAUUGGUGA |
| | A-005186-17 | CUUGGAGGAACGAAGAAUA |

### 3.4.7 RNP Nucleofection for gene knockout (KO)

Transfection was performed using the Amaxa Nucleofection system (SF Cell Line Kit, cat. no. V4XC-2032). For 2 X $10^5$ cells, 100 pmol of CAS9-GFP protein (Alt-R S.p. CAS9-GFP V3, #10008100; IDT) was mixed with 120 pmol of gRNA (crRNA:tracrRNA 1:1), which was previously annealed by heating to 95°C, and assembled for 20 min at RT. After the incubation, the cells (resuspended in Nucleofector solution SF) and the Alt-R CAS9 Electroporation Enhancer (#1075916) were added to the mixture. The complete volume was gently transferred to the Nucleocuvette module, placed in the 4D-Nucleofector system, and electroporated with the optimized program. Pre-warmed culture media was quickly added to the cells and transferred to a 96-well plate.

**Table 18:** Used crRNA for HSP90AA1/HSP90AB1 gene KO. Blue marked bases indicate overlaps between the crRNA and the tracrRNA.

| Gene | crRNA (5'- 3') | On-target score | Off-target score |
|---|---|---|---|
| For HSP90AA1 | GACCCAAGACCAACCGAUGG GUUUUAGAGCUAUGCU | 66 | 65 |
| Rev HSP90AB1 | CAUUAGAGAUCAACUCCCAG GUUUUAGAGCUAUGCU | 63 | 79 |
| Alt-R® CRISPR-CAS9 tracrRNA | Universal 67mer | | |

### 3.4.8 RNP Nucleofection for HiBiT-tag knock-In (KI)

Transfection was carried out using the Amaxa Nucleofection system (SF Cell Line Kit, cat. no. V4XC-2032). For 2 X $10^5$ cells, 100 pmol of CAS9 protein (Alt-R S.p. HiFi CAS9 nuclease V3, cat. no. 1081060; IDT) was mixed with 120 pmol of gRNA (crRNA:tracrRNA 1:1), which was previously annealed by heating to 95°C, and assembled for 20 min at RT.

Afterwards, the ssODN (100 pmol) was added, and the mixture was combined with the cell suspension (resuspended cells in Nucleofector solution SF) and the electroporation enhancer. The complete volume was gently transferred to the Nucleocuvette module, placed in the 4D-Nucleofector system, and electroporated with the optimized program. Pre-warmed culture media was quickly added to the cells and transferred to a 96-well plate.

**Table 19:** Optimized programs for the RNP Nucleofection.

| Cell line | program |
|---|---|
| K562 | CA-137 |
| KCL-22 | CA-137 |
| SUP-B15 | CV-104 |

**Table 20:** Used crRNA for HSP90AA1/HSP90AB1-HiBiT gene KI. Blue-marked bases indicate overlaps between the crRNA and the tracrRNA.

| Gene | crRNA (5'- 3') |
|---|---|
| HSP90AA1 | AGUAGACUAAUCUCUGGCUGGUUUUAGAGCUAUGCU |
| HSP90AB1 | UCGCAUGGAAGAAGUCGAUUGUUUUAGAGCUAUGCU |
| Alt-R® CRISPR-CAS9 tracrRNA | Universal 67mer |

**Table 21:** Used donor templates for HSP90AA1/HSP90AB1-HiBiT gene KI.

| Template | crRNA (5'- 3') |
|---|---|
| Ultramer DNA Oligo HSP90AA1 | T*G* CCA CCC CTT GAA GGA GAT GAC GAC ACA TCA CGC ATG GAA GAA GTA GAC GTG AGC GGC TGG CGG CTG TTC AAG AAG ATT AGC TAA TCT CTG GCT GAG GGA TGA CTT ACC TGT TCA GTA CTC TAC AAT TCC*T*C |
| Ultramer DNA Oligo HSP90AB1 | T*C* CCC CCT CTC GAG GGC GAT GAG GAT GCG TCT CGC ATG GAA GAA GTC GAT GTG AGC GGC TGG CGG CTG TTC AAG AAG ATT AGC TAA GTT AGA AGT TCA TAG TTG AAA AAC TTG TGC CCT TGT ATA GTG TCC*C*C |

## 3.4.9 Semi-solid cloning

After the genetic modification (KO or KI), monoclonal cells were isolated. This was done *via* semi-solid cloning. The cells were seeded (100 cells/mL) in methylcellulose medium for human cells (MethoCult™ H4100 STEMCELL, #04100) supplemented with FCS (Sigma-Aldrich) and penicillin/streptomycin (Invitrogen). After 10 days, the colonies were picked and transferred to a 96-well plate.

### 3.4.10 Colony forming unit assay (CFU)

To determine the colony formation capability, the cells were seeded (50 cells/mL) in methyl-cellulose medium for human cells (MethoCult™ H4100 STEMCELL, #04100) supplemented with FCS (Sigma-Aldrich) and penicillin/streptomycin (Invitrogen). Colonies were counted after 8 days (n=3)

### 3.4.11 Detection of HiBiT signal

To confirm the edited gene expression level, the Nano-Glo® HiBiT Lytic Detection System (#N3030; Promega) was used. 1 X $10^4$ cells were taken 48 hours post-electroporation and mixed 1:1 with Nano-Glo® HiBiT Lytic Reagent (LgBiT Protein 1:100 and Nano-Glo® HiBiT Lytic Substrate 1:50 in Nano-Glo® HiBiT Lytic Buffer). The mixture was incubated for 10 min at RT, and luminescence was measured using a Tecan Spark microplate reader. The background luminescence was measured using unedited cells and was subtracted from all readings.

### 3.4.12 Murine xenograft transplantation

Luciferase-GFP-positive K562 EV and HSP90α- or HSP90β-KO K562 (2.5 x $10^6$ cells) cells were transplanted *via* intravenous (i.v.) tail injection in NSG mice. At indicated time points, tumor engraftment and disease progression of human leukemia cell line models was monitored *via* bioluminescence imaging using IVIS Spectrum *in vivo* imaging system (PerkinElmer). The bioluminescence was initiated by intraperitoneal (i.p.) injection of 10 µl/kg D-Luciferin potassium salt in a concentration of 15 mg/ml solved in PBS. Animal experiments were conducted following the German Animal Welfare Act (LANUV) under the authorization of the animal research institute (ZETT) at Heinrich Heine University Düsseldorf.

### 3.4.13 Immunofluorescence imaging

The Lab-Tek II chamber slide w/Cover RS Glass slides (Thermo Fisher Scientific, #154534) was chosen for this experiment and was coated with a 50 µg/ml solution of Poly-D-Lysine (PDL; Thermo Fisher Scientific, #A3890401) and incubated for 24 h at 4°C. The wells were washed three times with PBS before adding cells. The micro slides with the cells were placed in the incubator for 60 min. After incubation, cell culture media was removed, and 200 - 300 µl of PBS was added to each well. For fixation, PBS was removed, and 4% formaldehyde was added to each well for 10 min at room temperature (RT). Next, 1x TBS was added to each well as a quencher for 5 min. For permeabilization, 200 - 300 µl of a 0.1 % Triton X-100 solution was added for 15 min. For blocking, 200 - 300 µl solution consisting of 10% BSA in 1x TBS was added for 1 hr at RT in a humidity cassette. Both primary and secondary antibodies were diluted in blocking solutions. Respective antibodies were added and incubated overnight at 4°C in a humidity cassette.

All wells were washed three times with 1x TBS for 15 min. 100 - 200 µl of secondary antibody (AlexaFluor, Thermo Fischer) was added for 1-1.5 h at RT, protected from light. A 300 nM solution of DAPI (hydrochloride) (StemCell Technologies, #75004) was added for 5 min, followed by a single 1x TBS wash. After removing the buffer from all wells, the chamber slide cover was removed, and 1-2 drops of ProLong Gold Antifade reagent (Invitrogen, #P36934) were added to each well. Finally, a rectangular coverslip was carefully placed on top. All samples were left to mount at 4°C overnight.
Immunofluorescence: Confocal laser scanning microscope, Fluoview3000, Olympus. UPLSAPO 60X2 Oil. Room Temperature. DAPI, AlexaFluor 488, 594, HSD GaAsP Detector. Software: FV31S-SW (Version 2.6.1.243).

Quantification of IF images was done with Fiji. Images were loaded, composite images were splitted into separate channels and Z-projection from all slices were set to maximum intensity. Afterwards, images were set to grayscale by changing current LUT to grays. Squares were set around the cells and mean gray values were measured. The background was subtracted from all values.

### 3.4.14 Plate printing

The plate design was done by using D300e control software. For the printing, white 384 well plates (Corning) were filled with indicated inhibitor concentrations and respective DMSO controls in a logarithmic distribution using a digital dispenser (TECAN D300e). For the high throughput screening, a library containing 93 compounds was created. The DMSO dissolved compound library was purchased from Selleckchem.

### 3.4.15 Drug screening

Cells were seeded (0.4*10^5 cells/mL) in the prepared plates utilizing Multidrop Combi Reagent Dispenser (Thermo-Fisher-Scientific) and incubated for 72h. CellTiter-Glo® Luminescent Cell Viability Assay (Promega) was performed per manufacturer's instructions to monitor ATP-based cell viability using microplate reader Spark 10M (Tecan). The calculation of $IC_{50}$ was determined by non-linear regression log(inhibitor) vs. norm. response (variable slope) using GraphPad Prism.

### 3.4.16 Synergy drug screening

As described above, the compounds were printed on white 384-well plates with increasing concentrations in a dose-response 8 by 8 matrices using a digital dispenser D300e. Cells were seeded (0.4*10^5 cells/mL for cell lines, 0.4*10^6 cells/mL for patient cells) in the prepared plates utilizing Multidrop (Thermo-Fisher-Scientific) and incubated for 72h.

Cell viability was monitored using CTG luminescent assay measured by microplate reader Spark 10M (Tecan). The ZIP synergy scores were determined using the online tool Synergyfinder.org.

### 3.4.17 Isolation of PBMCs

Whole blood was taken from three different healthy donors and subsequently processed by diluting with equal amount of PBS. The Ficoll® Paque Plus density gradient medium (Cytiva; #17-1440-03) was added to a fresh tube and the diluted blood was gently layered on top of the density gradient medium. The tube was centrifuged (800 x g; 30 minutes) and the cells were carefully harvest by inserting the pipette directly through the upper plasma layer to the mononuclear cells at the interface. The cells were washed twice with PBS and the pellet was resuspended two times in red blood cell lysis buffer for erythrolyse. The cells were counted, plated and subsequently used for downstream applications.

# 4. Results

## 4.1 Decrypting the role of HSP90α and β isoforms in BCR-ABL1$^+$ leukemia

### 4.1.1 Generation of HSP90α and HSP90β-KO cell lines

To elucidate the role of HSP90α and HSP90β, HSP90α/β-KO cell lines were generated using CRISPR/CAS9 technology. As a model system for the initial experiments, the well-characterized BCR-ABL1$^+$ K562 cell line established from CML cells was chosen. This cell line is highly relevant, as it displays high levels of HSP90 and strong dependency. In the first step, viral transduction was carried out using lentiviral particles, previously generated by HEK293T cells and respective packaging plasmids to generate stable CAS9-expressing K562 cells. Positive cells were enriched *via* puromycin selection und were subsequently monoclonal isolated. In a second step, monoclonal K562 CAS9-OE cells were again transduced using lentiviral particles containing the respective gRNAs coupled with a fluorescence selection marker targeting *HSP90AA1* and *HSP90AB1* or non-targeting empty vector control (EV) (Figure 9A).

Positive cells were enriched *via* cell sorting for either GFP in HSP90α-KO cells or mCherry in HSP90β-KO cells until the population reached almost 100 %, indicated by FACS analysis (Figure 9B). The genetically modified cell pool was afterwards monoclonal selected, and isolated clones were analysed for their HSP90 expression level *via* western blot. Positive clones should no longer have visible protein bands due to the presence of CAS9 and the gRNA, which form an RNP complex that causes a cut in the gene of interest. It was found that not all clones were positive, despite previous selection processes. Two clones were selected, each with an HSP90α-KO (Clone or C5 and C6) and an HSP90β-KO (C13 and C15). The cut was validated by Sanger sequencing and showed a one bp deletion for clones five and six in the *HSP90AA1* gene locus, a 13 bp deletion for clone 13, and a one bp deletion for clone 15 in the *HSP90AB1* gene locus. Western blot results showed a distinct KO and no residual protein expression. Expression of the respective other isoform showed no change of HSP90β levels in the HSP90α-KO cells, whereas overexpression of HSP90α was observed in the HSP90β-KO cells (Figure 9C).

qPCR analysis showed lower mRNA levels of *HSP90AA1* in HSP90α-KO clones and lower mRNA levels of *HSP90AB1* in HSP90β-KO clones. In line with western blot results, 2-fold higher mRNA levels of *HSP90AA1* in HSP90β-KO clones was observed (Figure 9D).

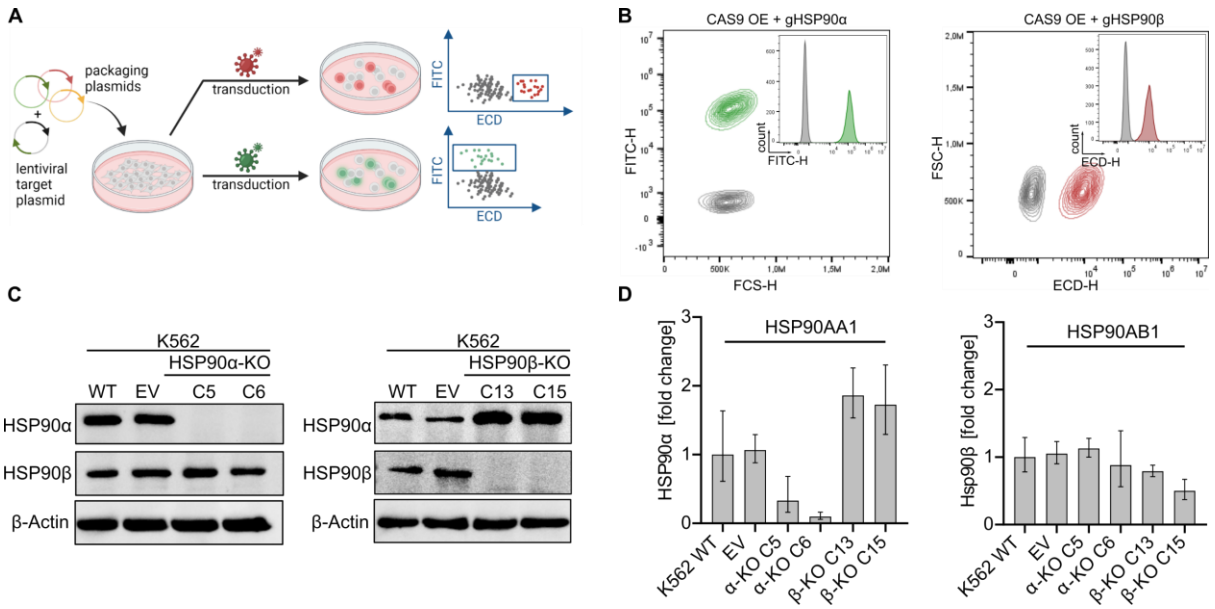


**Figure 9: Generation of HSP90α and HSP90β KO in K562 cells *via* viral transduction.**

K562 CAS9 OE cells were transduced with viral supernatant containing respective gRNAs targeting HSP90α and HSP90β. Afterwards, cells were sorted and monoclonal selected. (**A**) Schematic representation of viral transduction. Figure: Created with BioRender.com. (**B**) FACS data showed either GFP- or mCherry-positive K562 cells. (**C**) WB results showed a KO of HSP90α and HSP90β on the protein level in K562 cells. (**D**) qPCR data showed lower mRNA levels of *HSP90AA1* in K562 HSP90α-KO clones. Lower mRNA levels of HSP90AB1, as well as higher mRNA levels of *HSP90AA1* were observed in K562 HSP90β-KO clones. Results are shown as means ± error (N = 4).

The findings from the K562-KO models were corroborated in other cell lines to eliminate patterns unique to specific cell lines. As different model systems, the BCR-ABL1$^+$ KCL-22 cell line established from CML cells and the BCR-ABL1$^+$ SUP-B15 cell line established from BCP-ALL were chosen. Although lentiviral transduction offers some advantages for hard-to-transfect cells and increases efficiency by generating stable target expression, there is a possible risk of insertional mutagenesis, which can lead to off-target effects. Consequently, the transient method *via* ribonucleoprotein (RNP) nucleofection was used to generate further KO cell lines. This method offered faster modification and provided a selection by using GFP-tagged recombinant CAS9 (Figure 10A). Furthermore, the fact that CAS9 is not stably expressed helps to further reduce off-target effects. Positive cells were enriched *via* cell sorting for GFP until the population reached almost 100 % indicated by FACS analysis. Afterwards, the genetically modified cell pool was monoclonal selected *via* CFU assay, and growing clones were isolated. In the case of SUP-B15 cells, a monoclonal selection was not possible, as the resulting colonies were too small and stopped growing. However, the HSP90α expression level in the pool population was already low (Figure 10B). The generation of HSP90β-KO cells in SUP-B15 cells failed due to cell death after sorting, which indicated that this cell line is highly dependent on HSP90β expression. For KCL-22, the selection process was successful and isolated clones were analysed for their HSP90 level *via* western blot.

Three clones, each with an HSP90α-KO (C10, C14 and C15) and an HSP90β-KO (C10, C11 and C12), were selected. All clones showed a KO and no residual protein expression. The cut was validated by Sanger sequencing and showed a 14 bp deletion for clone 10, a one bp deletion for clone 14, a two bp deletion for clone 15 in the *HSP90AA1* gene locus and a three bp deletion for clone 10, an 11 bp deletion for clone 11, and an 11 bp deletion for clone 12 in the *HSP90AB1* gene locus. Expression of the respective other isoform showed no change of HSP90β levels in the HSP90α-KO cells, whereas overexpression of HSP90α was observed in the HSP90β-KO cells (Figure 10C).

qPCR analysis showed lower mRNA levels of *HSP90AA1* in HSP90α-KO clones and lower mRNA levels of *HSP90AB1* in HSP90β-KO clones. In line with western blot results, approximately 3-fold higher mRNA levels of *HSP90AA1* in HSP90β-KO clones was observed (Figure 10D).

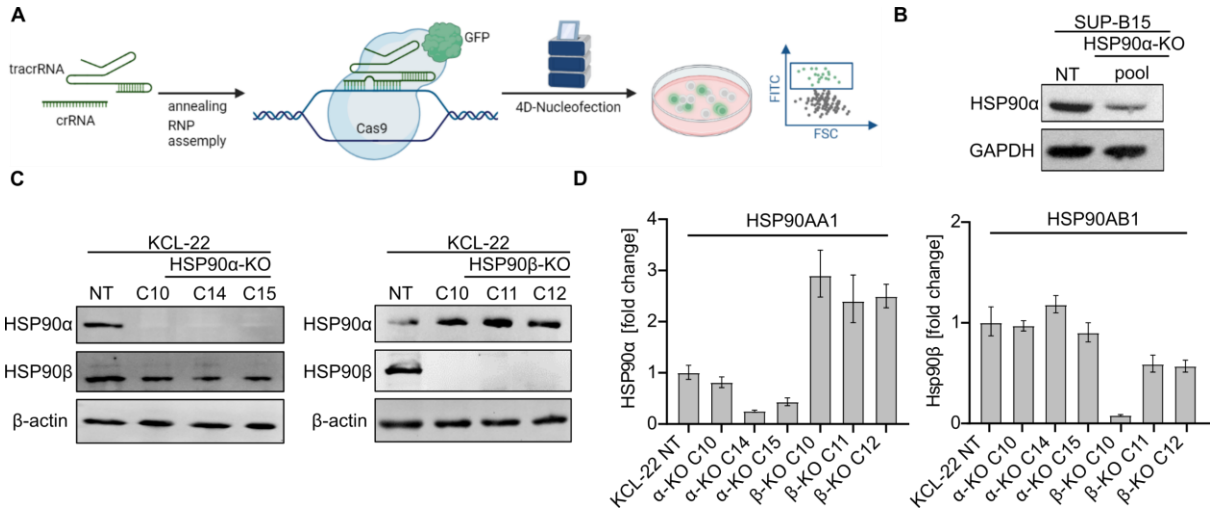


**Figure 10: Generation of HSP90α and HSP90β KO in KCL-22 and SUP-B15 cells *via* RNP nucleofection.** KCL-22 and SUP-B15 cells were nucleofected with an RNP complex containing CAS9-GFP and the respective gRNAs targeting HSP90α, HSP90β, and a non-targeting control. Afterwards, cells were sorted and monoclonal selected. (**A**) Schematic representation of RNP nucleofection. Figure: Created with BioRender.com. (**B**) WB results showed a reduced protein level of HSP90α in SUP-B15 HSP90α-KO pool cells. (**C**) WB results showed a clear KO of HSP90α and HSP90β on the protein level in KCL-22 cells. (**D**) qPCR data showed lower mRNA levels of *HSP90AA1* in KCL-22 HSP90α-KO clones, lower mRNA levels of HSP90AB1, as well as higher mRNA levels of *HSP90AA1* in KCL-22 HSP90β-KO clones. Results are shown as means ± error (N = 4).

Comparing K562 and KCL-22 KO cell lines, a consistent upregulation of HSP90α in the HSP90β-KO clones was observed on protein and mRNA levels. To investigate whether this effect is based exclusively on the translational level or also on the genetic level caused by an amplification of the HSP90AA1 locus, single nucleotide polymorphism (SNP) microarray analysis was performed on HSP90β-KO (K562) cells. However, no gain in DNA level was found (data not shown). Taken together the observations indicates, that an HSP90β-KO induces the overexpression of stress-inducible HSP90α isoform.

### 4.1.2 Investigation of heat shock response and client protein expression in HSP90α/β-KO K562 and KCL-22 cell lines

Given the consistent upregulation of HSP90α observed in HSP90β-KO cells, the overall HSP90 levels, including both HSP90α and HSP90β isoforms, were analyzed in the isoform-specific KO cell lines. Quantification by simple western immunoassay (JESS) showed that the total HSP90 level remained constant in all KO clones (Figure 11A). Next, the influence of the absence of HSP90α/β isoforms on other (isoform dependent) chaperones or HSP90 paralogues was probed. In the HSP90α-KO clones, no changes in the expression profile of GRP94 and TRAP1 were observed. Furthermore, no changes in the expression of HSR-related proteins, including HSF1, HSP70, HSP40 and HSP27, were observed (Figure 11B). The HSP90β-KO did not impact the expression of the two paralogues GRP94 and TRAP1 (Figure 11C); instead, it led to an increase in the expression of HSF1, HSP70, and HSP40, indicating that the isoform-specific HSP90β-KO induces a heat shock response (HSR).

Next, to see if the isoform-specific KO influences the induction of HSR, the KO cells were treated with the N-terminal HSP90 inhibitor AUY922, which is known to induce HSR. A strong increase in HSF1, HSP70, HSP40 and HSP27 could be observed in the EV control cells. Also, in the HSP90α-KO clones, the initiation of HSR was clearly shown, mainly due to the overexpression of HSF1, HSP70 and HSP40. HSR was also initiated in the HSP90β-KO clones, but the effect was less pronounced since the basal level was already increased. Quantification of the HSP70 level showed a 4-fold increase in the EV control cells and the HSP90α-KO clones, whereas HSP90β-KO clones indicated a 3-fold increase and a 3.5-fold increase from a two times higher basal level (Figure 11E).

For the KCL-22-KO clones, only changing targets were analysed. Specifically, for the HSP90β-KO clones, the HSR-related proteins HSF1, HSP70, HSP40, and HSP27 were examined, but no changes were observed (Figure 11F).

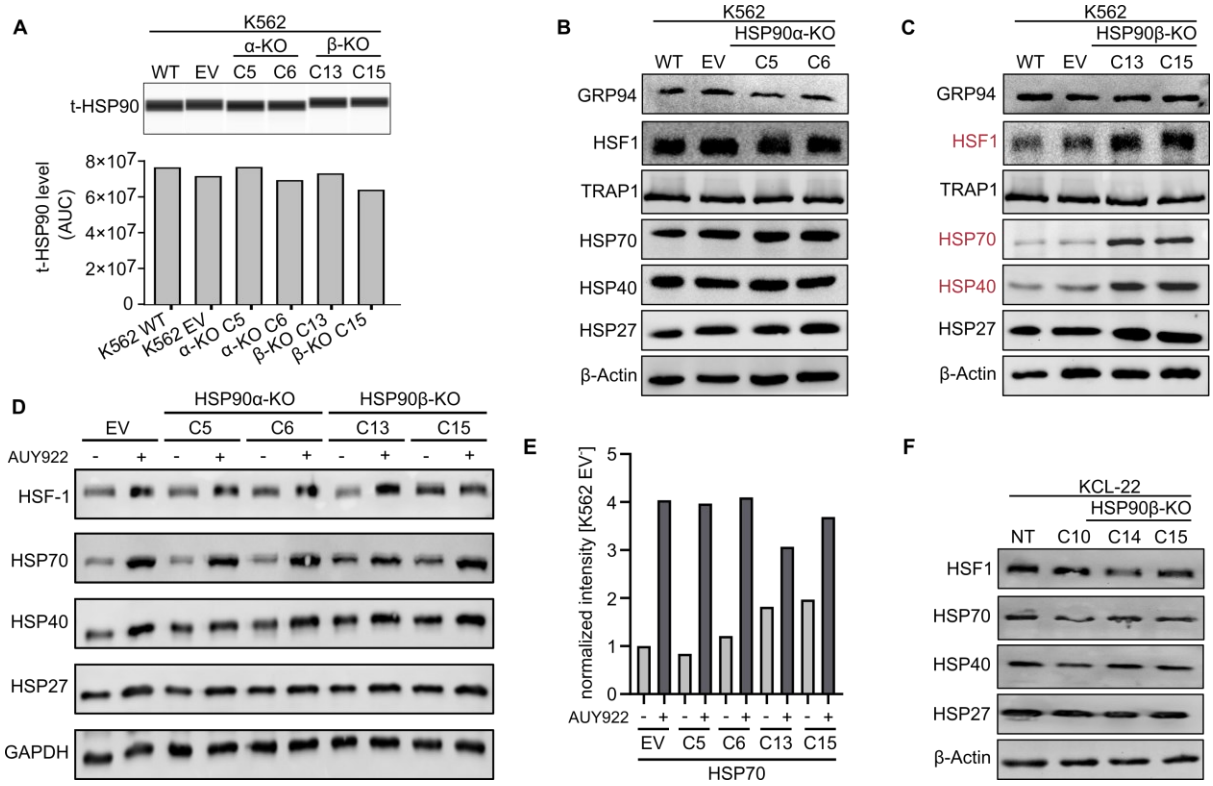


**Figure 11: Investigation of HSR.**

(**A**) JESS quantification showed no changes in the total HSP90 levels, indicating a strong balancing effect. (**B**) WB results showed no changes for HSR-related proteins in the HSP90α-KO K562 clones. (**C**) For the HSP90β-KO K562 clones, upregulation of HSF1, HSP70 and HSP40 could be seen. (**D**) WB analysis of HSP90α/β-KO cells after treatment with HSP90 NTD targeting inhibitor AUY922 (100 nM, 24h), known to induce HSR. (**E**) Quantification of the HSP70 levels after treatment with AUY922 (100 nM, 24h) revealed a higher basal level of HSP70 and a comparatively lower induction of HSP70 upregulation in the HSP90β-KO clones. (**F**) WB results showed no changes of HSR-related proteins in KCL-22 KO clones. Proteins with changes in the expression level are marked in red.

Other interesting proteins are co-chaperones required for HSP90 activity or client proteins. Previous studies reported that some clients of HSP90 are isoform dependent and have a specific binding preference.[50] In the HSP90-KO cell lines, no changes in the expression profile of CDK4, CDK6 and SURVIVIN could be observed. Also, no changes for the co-chaperones AHA1 and CDC37 could be observed. Of note, both HSP90α and HSP90β-KO K562 cells demonstrated higher levels of the co-chaperone FK06-binding protein 5 (FKBP5) (Figure 12A/B). Again, only changing targets were analysis in the KCL-22-KO clones, but no change in the FKBP5 expression level was observed (Figure 12C).

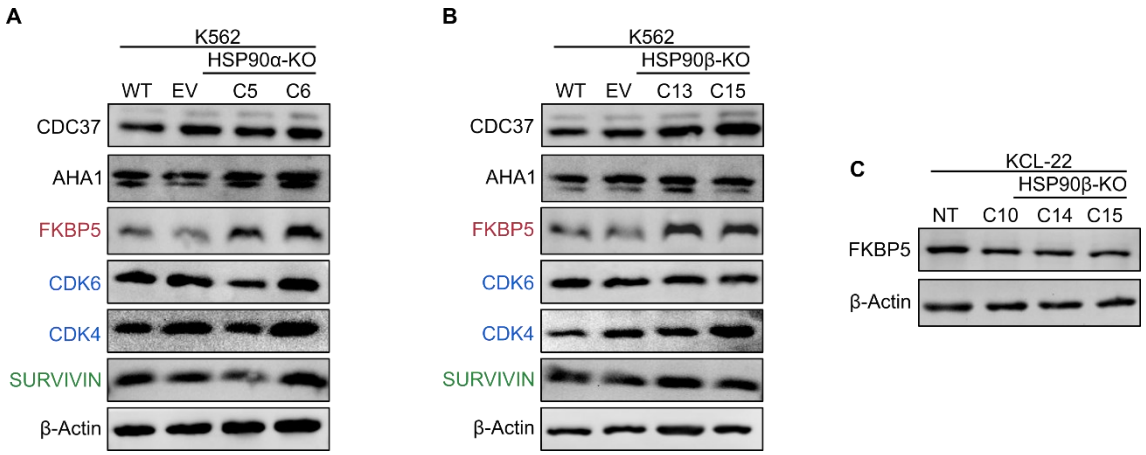


**Figure 12: Investigation of client and co-chaperone protein expression.**

(**A**) WB results showed upregulation of FKBP5 in both K562 KO models. No changes in HSP90-dependent clients, CDK4, CDK6, and SURVIVIN, could be detected. (**C**) WB results showed no changes in FKBP5 expression in KCL-22 KO clones. Proteins with changes in the expression level are marked in red. HSP90β-dependent clients are marked in blue and HSP90α-dependent clients are marked in green.

In summary, western blot analysis of HSP90α and HSP90β-KO cell lines revealed no changes in HSP90 isoform-dependent client proteins, like CDK4/6 and SURVIVIN. However, an induction of HSR in K562 HSP90β-KO clones was detected.

### 4.1.3 Generation of HSP90α/β-KD K562 cell lines

A transient small interfering RNA (siRNA) mediated knockdown (KD) in K562 cells was utilized to study the kinetic implications of the loss of HSP90α/β isoforms in the cells. For this purpose, the cells were cultivated in Accell siRNA delivery media, and the respective siRNA SMARTpool, containing four siRNAs, was used. Gene silencing using this method does not require transfection reagents or viruses and offers a fast modification. Pre-experiments with K562 cells revealed that the cultivation in Accell siRNA delivery media hinders the cells from growing, and an increase in cell density decreases cell viability. For this reason, the media was changed after 48 h to RPMI, supplemented with 10 % FCS, to let the cells recover. Cells were isolated and analysed after 96 h and after 192 h to gain more insights into the gene KD kinetics (Figure 13A).

At first, qPCR analysis was done to evaluate the performance of the gene KD. The data showed that mRNA levels of *HSP90AA1* in HSP90α-KD cells are 60 % lower after 96 h and 92 % lower after 192 h. The mRNA levels of *HSP90AB1* in HSP90β-KD cells are approximately 80 % lower after 96 h and 192 h. For the HSP90α-KD, no changes in the *HSP90AB1* mRNA levels was observed, whereas slightly higher mRNA levels of *HSP90AA1* after 192 h in the HSP90β-KD could be seen (Figure 13B).

Next, it was investigated if the knockdown also occurred on the protein level. JESS immunoassay showed a significant reduction of HSP90α and HSP90β after 96 h and after 192 h (Figure 13C).

The quantification revealed a significant ($p = 0.0003$; $p < 0.0001$) reduction of HSP90α after 96 h to 25 % and after 192 h to 5 % compared to the NT control. In the case of HSP90β, there was a non-significant reduction after 96 h to 75 % and a significant ($p = 0.0007$) reduction after 192 h to 27 % compared to the NT control (Figure 13D).

Previously, it was shown that an HSP90β-KO induced HSR in K562 cells by upregulating HSP90α, HSP70, and HSP40. Furthermore, it was shown that an HSP90β-KO consistently led to an upregulation of HSP90α in K562 and KCL-22 cells. Therefore, these proteins were also analysed for the HSP90β-KD.

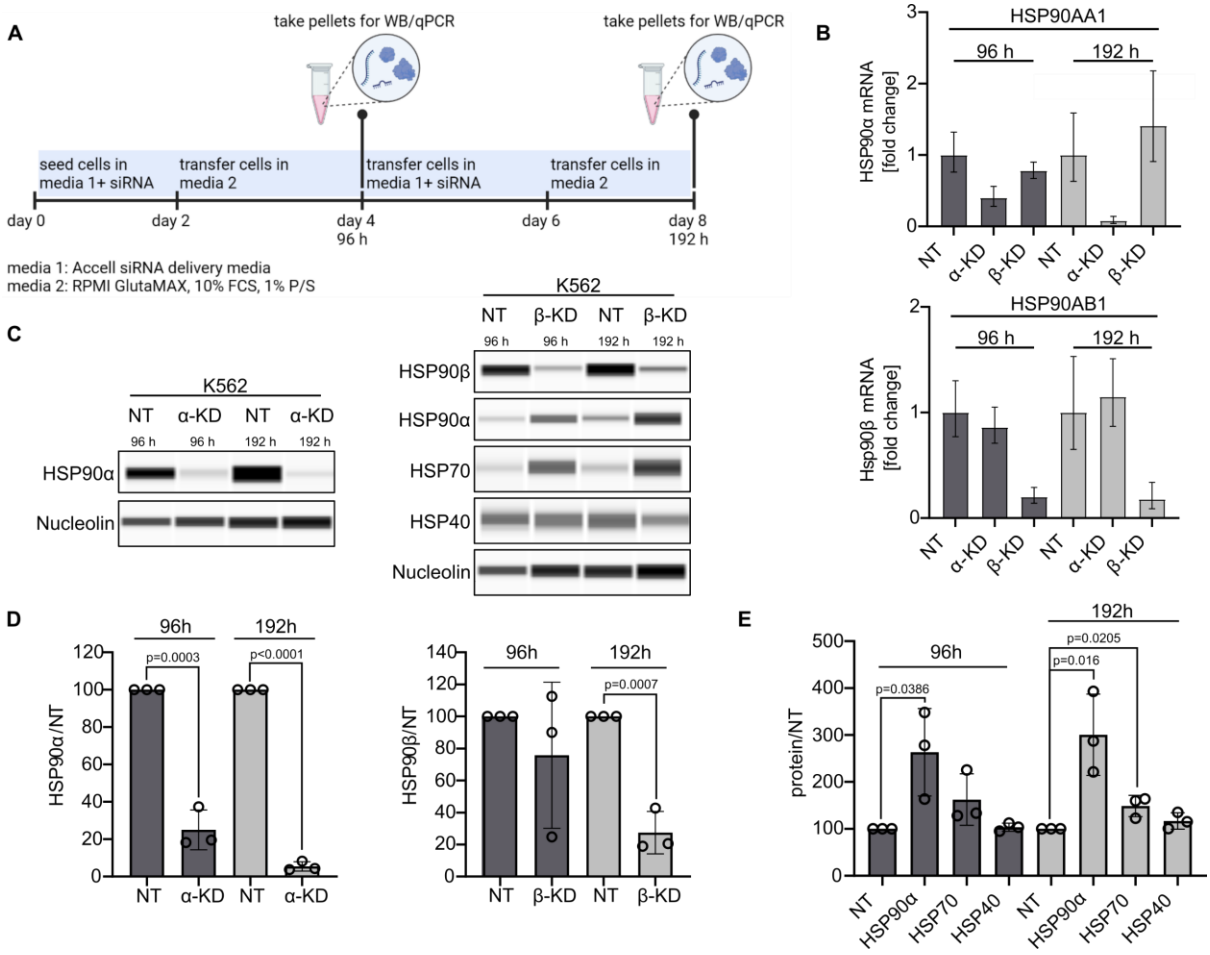


**Figure 13: Generation of HSP90α and HSP90β KD in K562 cells *via* siRNA silencing.**

(**A**) Schematic representation of siRNA silencing timeline. Cells were harvested at two different time points (96 h and 192 h) Figure: Created with BioRender.com. (**B**) qPCR data showed lower mRNA levels of *HSP90AA1* and *HSP90AB1* after 96 h and 192 h. Also, mRNA levels of *HSP90AA1* are slightly higher in HSP90β-KD cells after 192 h. Results are shown as means ± error (N = 4). (**C**) Representative images showing the JESS evaluation of HSP90α/β-KD cells. The HSP90α/β protein level was strongly reduced after 96h and 192h. The expression levels of HSP90α and HSP70 were increased, while the expression of HSP40 remained equal after the HSP90β-KD. (**D**) JESS quantification showed a gradual decrease of the HSP90α (HSP90β) level in HSP90α-KD (HSP90β-KD) cells. (**E**) JESS quantification showed significantly increased levels of HSP90α after 96 h and 192 h and significant increased levels of HSP70 after 192 h in HSP90β-KD cells. The quantifications are from 3 independent experiments (means ± SD). P values were determined by a two-tailed unpaired t-test.

There was a significant ($p = 0.0386$; $p = 0.016$) upregulation of HSP90α after 96 h to 263 % and after 192 h to 300 %. For HSP70, an initially non-significant upregulation to 162 % after 96 h and a significant ($p = 0.0205$) upregulation to 150 % after 192 h was observed. For HSP40, there was no change in the expression level after 96 h, and only a slight non-significant increase to 117 % after 192 h (Figure 13C/E).

In summary, siRNA-mediated KD of HSP90β resulted in an upregulation of HSP90α even after 96 h and an upregulation of HSP70 after 192 h, indicating HSR induction.

### 4.1.4 Investigation of BCR-ABL1 expression and related downstream signaling in HSP90α/β-KO K562 cell lines

HSP90 is extensively involved in the folding and stabilization of the translocated protein BCR-ABL1.[161] Therefore, a focused analysis of BCR-ABL1 and its downstream effector proteins were made. JESS analysis showed an increased level of $P210^{BCR\text{-}ABL1}$ for the HSP90α-KO clone C6. The same trend was observed for the phosphorylated form of BCR-ABL1, as it showed a significantly increased level in clone C6 ($p = 0.0013$) in comparison the EV. The STAT5a showed no striking changes in the HSP90α-KO clone, whereas p-STAT5a was significantly upregulated ($p = 0.0455$). There was a strong increase in the AKT and the p-AKT level in the HSP90α-KO clone C6. The CRK Like proto-oncogene (CRKL) slightly increased in the HSP90α-KO clone, whereas the phosphorylated form p-CRKL was strongly upregulated ($p = 0.0149$).

For the HSP90β-KO clone C15, a double band of BCR-ABL1 was observed, which was very weak in the K562 WT/EV and HSP90α-KO clone. This additional band was found to be indicative of an increase in $p190^{BCR\text{-}ABL1}$. In contrast to BCR-ABL1, the HSP90β-KO clone showed a strong reduction of the p-BCR-ABL1-, STAT5a- and p-STAT5a level. CRKL and p-CRKL were not altered in comparison to EV. For AKT and p-AKT, however, there was a strong increase in expression in the HSP90β-KO clone.

In conclusion, enhanced BCR-ABL1-mediated pro-survival signalling was observed in the HSP90α-KO cell lines *via* p-BCR-ABL1, p-CRKL and p-STAT5a, and reduced BCR-ABL1-mediated pro-survival signalling was observed in the HSP90β-KO cell lines, indicated by reduced expression levels of p-BCR-ABL1 and p-STAT5 (Figure 14A/B).

Since HSP90 is also involved in the subcellular localization of BCR-ABL1, HSP90-KO cell lines were fixed and prepared for immunofluorescence imaging.[162] The cells were stained with DAPI to visualize the nucleus and treated with a BCR-ABL1 antibody. Microscopic analysis showed a homogeneous distribution of BCR-ABL1 in the K562 EV cells. Increased BCR-ABL1 signal was measured in the HSP90α-KO cells, indicated by the red arrows. Furthermore, the BCR-ABL1 signal was observed to be increased at the edge of the cells. The BCR-ABL1 signal in the HSP90β-KO cells was comparable to the EV control cells (Figure 14C).

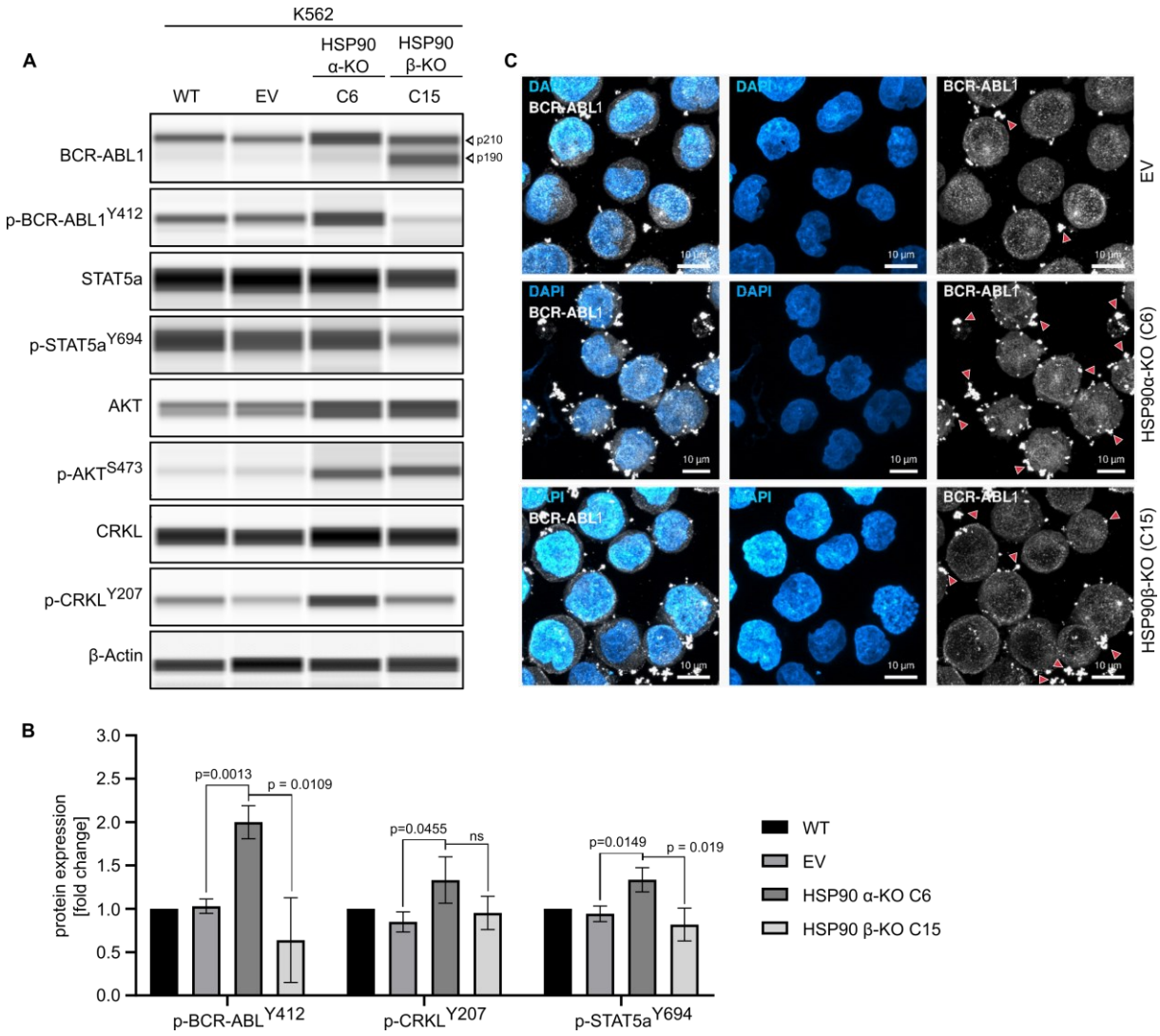


**Figure 14: Investigation of BCR-ABL1 signalling in HSP90α/β-KO K562 cells.**

(**A**) Automated WB analysis of BCR-ABL1 and p-BCR-ABL1$^{Y412}$ and their related downstream pro-survival effectors. (**B**) Quantification of three independent JESS runs of p-BCR-ABL, p-CRKL and p-STAT5a revealed significant increase of phosphorylated proteins in the HSP90α-KO clone. (**C**) Immunofluorescence imaging demonstrated a higher abundance of BCR-ABL1 foci (cytoplasmic/nucleocytoplasmic region) in HSP90α-KO cells than in HSP90β-KO or EV control cells. The BCR-ABL1 signal is highlighted by the red arrows. Immunofluorescence imaging was done by the colleague *Philip Gebing*. Results are shown as means ± SD of 3 independent experiments. P values were determined by a two-tailed unpaired t-test.

Taken together the observations indicates, that an HSP90α-KO promotes BCR-ABL1 signaling.

### 4.1.5 *In vitro* characterization of HSP90α/β-KO K562 and KCL-22 cells

After a detailed validation of the HSP90-KO cell lines on the protein level and analysis of the most important co-chaperones and clients, the next step was to analyse the leukemic cell growth. To this end, HSP90-KO cell lines were analysed in functional assays. For this purpose, a proliferation assay was performed by seeding the cells equally and measuring the viability and cell number every day. Subsequently, the viable cell number was plotted, and the data of the respective clones were pooled.

It was found that the HSP90β-KO cells behaved similarly to the EV control cells and that the proliferation was almost equal. The HSP90α-KO cells showed significantly ($p(t_{96h}) = 0.0092$) faster proliferation (Figure 15A).

CDK4 and CDK6 are clients of HSP90β and play a crucial role in cell cycle progression. Therefore, cell cycle analysis was performed by permeabilizing the cells, staining with propidium iodide (PI) and subsequent analysis by flow cytometry. Quantification of the FACS data showed no differences in the cell cycle sub-G1, S, G0/G1 and G2/M phases between the K562 EV cells and the HSP90α/β-KO cells (Figure 15B).

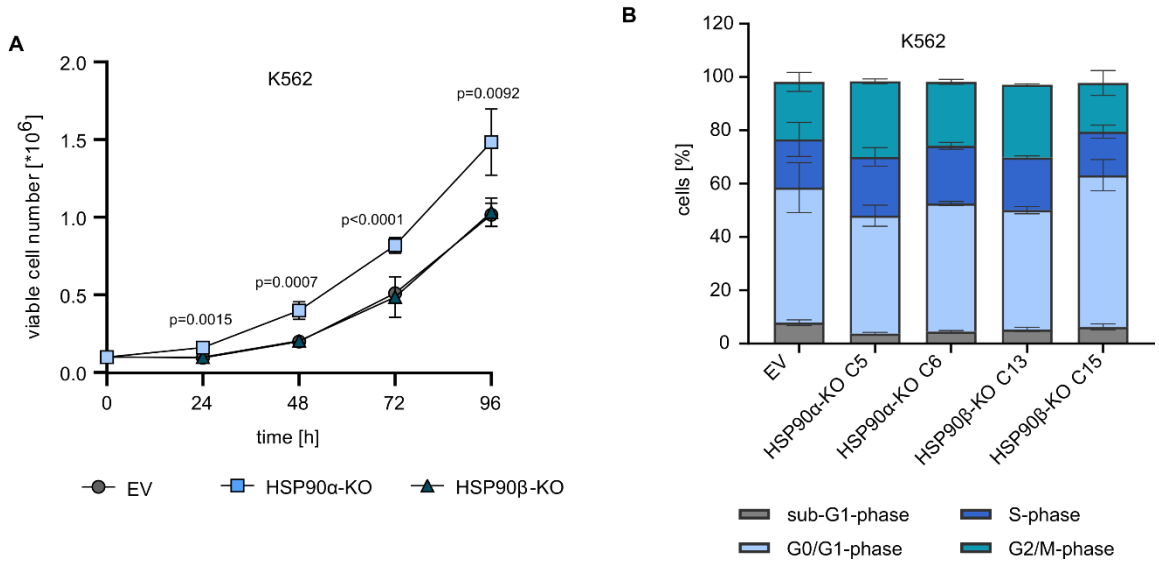


**Figure 15: Proliferation- and Nicoletti-assay for the *in vitro* characterization of HSP90α/β-KO K562 cells.** (**A**) Proliferation assay showed significantly faster proliferation of HSP90α-KO K562 cells. (**B**) Nicoletti assay showed no differences in the cell cycle sub-G1-, S-, G0/G1- and G2/M-phases between the K562 EV cells and the HSP90α/β-KO cells. Results are shown as means ± SD of 3 independent experiments. P values were determined by a two-tailed unpaired t-test.

Since the proliferation of the cell lines was altered, the cells' behaviour in methylcellulose-based media was investigated in more detail. The cells were highly diluted and added isolated to the plates in a semi-solid medium, so that colony formation had to occur from a single cell, and the colonies could be easily distinguished. After eight days of incubation, the colonies were evaluated under the microscope. The K562 WT/EV control cells showed good colony formation, and the colonies had sharp edges and a 3-dimensional structure. The HSP90α-KO cells formed comparably sized colonies, but these were less densely packed and did not have sharp edges. Rather, there was a greater distribution and migration of cells at the outer edge of the colonies. The HSP90β-KO cells formed smaller colonies, which were as densely packed as the colonies of the control cells (Figure 16A).

The colonies were also counted and normalized to the number of colonies formed by K562 WT cells. The results showed a non-significant increase in the number of colonies of the HSP90α-KO cells and a significant ($p = 0.0298$; $p = 0.0211$) decrease in the number of colonies in both HSP90β-KO clones (Figure 16B).

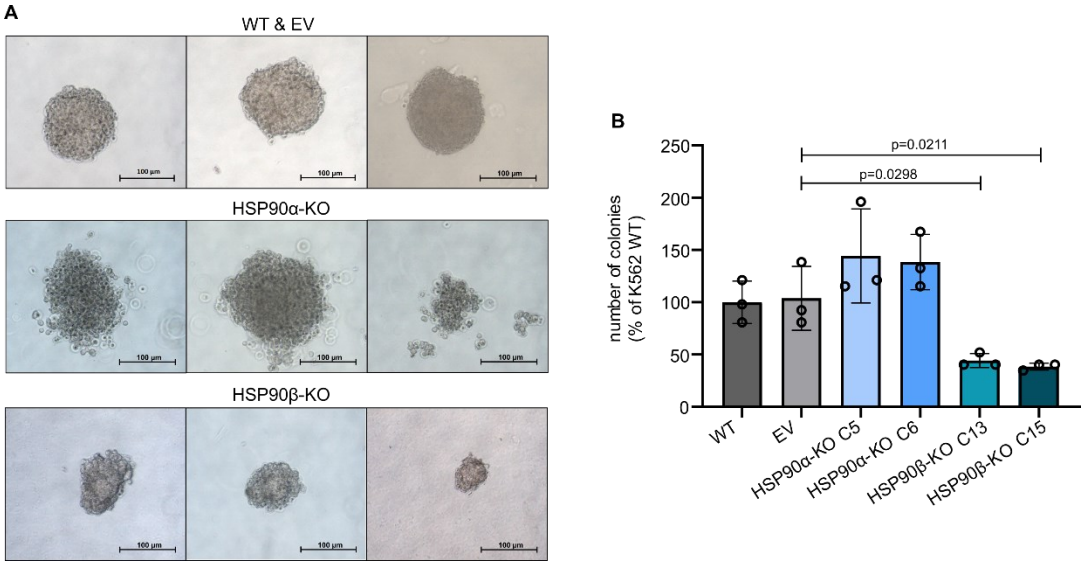


**Figure 16: CFU assay for the *in vitro* characterization of HSP90α/β-KO K562 cells.**

(**A**) Microscopic images of colonies in semi-solid media. (**B**) The number of colonies normalized to K562 WT cells. Results are shown as means ± SD of 3 independent experiments. P values were determined by a two-tailed unpaired t-test.

Similar assays were performed for the KCL-22 HSP90-KO cell lines to exclude cell line-specific effects. Measurement of cell proliferation again showed comparable growth of HSP90β-KO cells, whereas HSP90α-KO cells were proliferating significantly ($p(t_{115h}) = 0.0275$) faster (Figure 17A).

The HSP90-KO KCL-22 cell lines were also seeded in methylcellulose-based media and evaluated microscopically after six days of incubation. The KCL-22 NT cells formed 3-dimensional colonies with sharp edges. The HSP90α-KO cells formed partly larger colonies, which were mainly 2-dimensional. The HSP90β-KO cells formed comparably smaller colonies, which were as densely packed as the colonies of the KCL-22 NT cells (Figure 17B).

Colony counting showed a non-significant increase in the number of colonies of HSP90α-KO cells and a significantly ($p = 0.0295$; $p = 0.0448$) reduced number of colonies of HSP90β-KO clones C10 and C12. No reduced number of colonies was observed for HSP90β-KO clone C11 (Figure 17C).

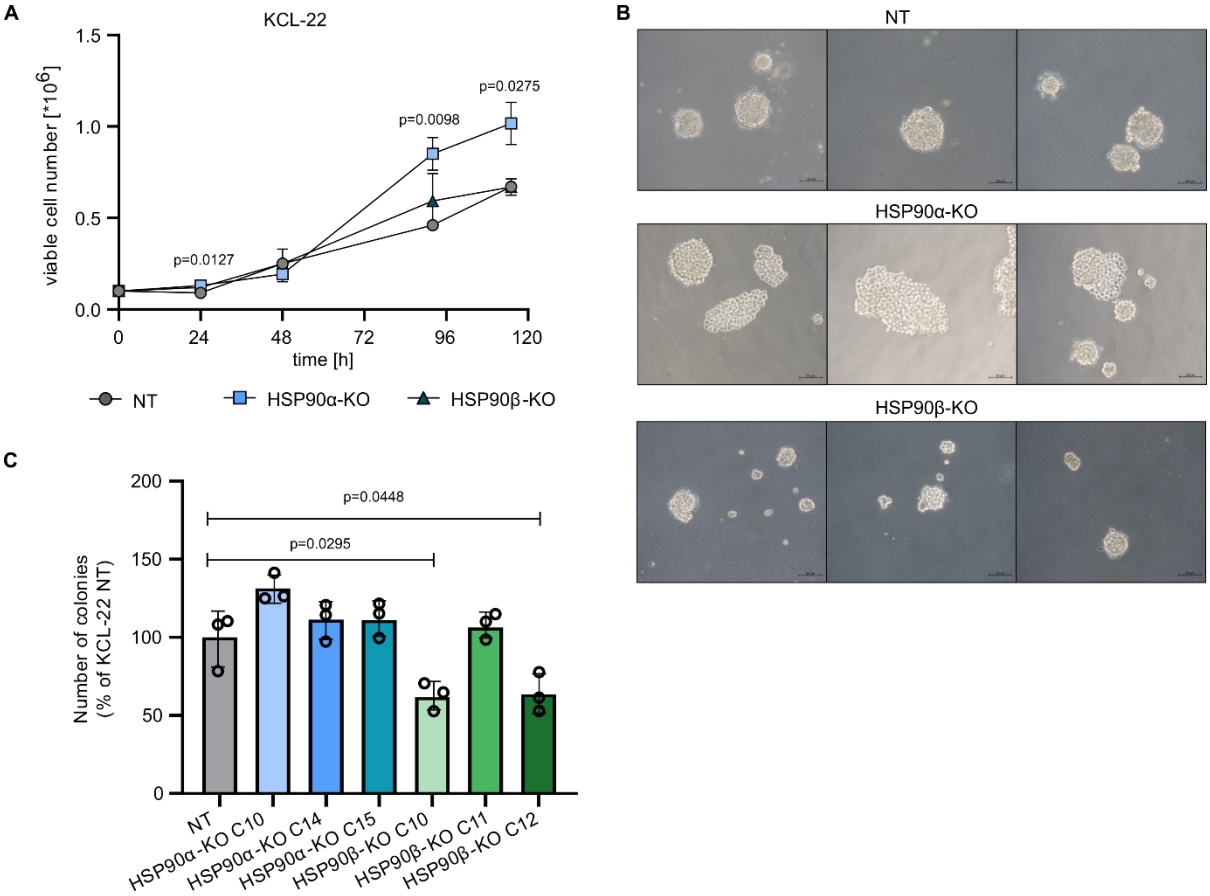


**Figure 17: Proliferation- and CFU-assay for the *in vitro* characterization of HSP90α/β-KO KCL-22 cells.** (**A**) Proliferation assay showed significantly faster proliferation of HSP90α-KO KCL-22 cells. (**B**) Microscopic images of colonies in semi-solid media. (**C**) The number of colonies normalized to KCL-22 NT cells. Results are shown as means ± SD of 3 independent experiments. P values were determined by unpaired t-test.

In conclusion, *in vitro* characterization revealed a consistent growth advantage of K562 and KCL-22 HSP90α-KO cells. Furthermore, CFU capability of HSP90β-KO cells was impaired in terms of colony number and size.

### 4.1.6 Exploring the *in vivo* engraftment capacity of HSP90α/β-KO K562 cells

Besides the *in vitro* characterization of the HSP90-KO cell lines, the *in vivo* transplantation efficiency should be exploited. For this purpose, extremely immunodeficient NOD scid gamma (NSG) mice (NOD.Cg-Prkdc$^{scid}$ Il2rg$^{tm1Wjl}$/SzJ from the Jackson Laboratory, RRID: IMSR_JAX:005557) were used. These mice harbour a severe combined immune deficiency (scid) mutation in the DNA repair complex protein PRKDC, which results in a deficiency of B- and T-cells. Furthermore, they have a deficiency in functional NK cells, resulting from the IL2rg$^{null}$ mutation, which prevents cytokine signaling.[163]

To successfully track the tumour cells in the mice, a chemiluminescent marker in the HSP90-KO cells was required. The visualization was achieved *via* bioluminescence imaging using the IVIS device. To this end, HSP90-KO K562 cells were genetically modified *via* viral transduction using a plasmid encoding for luciferase.

Positive cells were sorted for a high GFP signal, as the EV and the HSP90α-KO cells already harbour GFP. Next, the cells were monoclonal selected and validated by adding luciferin to lysed cells. Subsequently, 2.5 million Luciferase-GFP$^+$ HSP90α/β-KO or K562 EV cells were injected intravenously (i.v.) into the tail vein of NSG mice. Mice were checked for successful transplantation of leukemia cells after ten days and were visualized every five days and later every ten days *via* IVIS. Visualization was done until all mice died or had to be sacrificed due to their high leukemic burden (Figure 18A).

Analysis of the mice showed a different transplantation progression from day 15 on. In the EV control mice and the HSP90β-KO mice, signals were already measured predominantly in the spleen and the hind legs, whereas no signals were observed in the HSP90α-KO mice (Figure 18B). Also, in the further course, the EV control cells and the HSP90β-KO cells behaved comparably, whereas the HSP90α-KO cells showed a weaker signal. This trend was also observed on day 25 and day 35, and the difference between the cell lines became even more pronounced. On day 46, three mice from the control group and three from the HSP90β-KO group were dead, whereas all mice from the HSP90α-KO group were still alive.

Quantification of the region of interest (ROI) bioluminescence signal at day 35 showed a significant ($p = 0.0002$) reduction in the transplantation of HSP90α-KO cells compared to EV control cells (Figure 18C).

Besides the bioluminescence imaging for tracking engraftment, the survival of the mice was monitored. For the EV control mice, the first mouse had to be sacrificed after 35 days and the last after 46 days. For the mice transplanted with the HSP90α-KO cells, the first mouse had to be sacrificed after 55 days, and two survived for 68 days. The ones transplanted with the HSP90β-KO cells lived between 38 and 48 days. Most of them needed to be sacrificed due to health issues such as the formation of solid tumours and associated weight loss, weakness, and signs of paralysis.

For the HSP90β-KO mice, the median survival was 42 days, showing no significant difference. In contrast, HSP90α-KO mice survived a median of 67 days, significantly ($p = 0.0015$) longer than the control mice (Figure 18B).

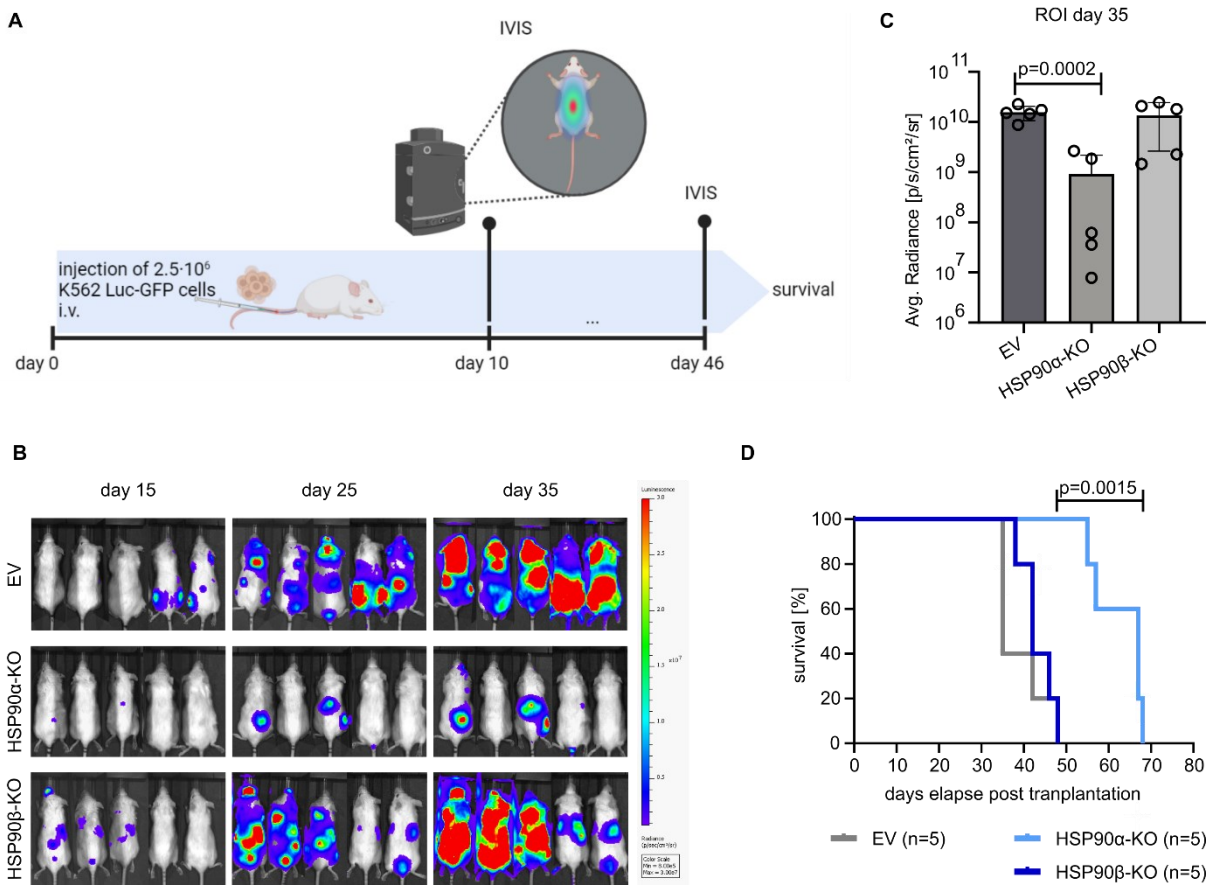


**Figure 18: *In vivo* evaluation of injected HSP90α/β-KO K562 cells.**

(**A**) Schematic representation of the workflow. NSG mice were transplanted with $2.5 \cdot 10^6$ Luciferase-GFP$^+$ HSP90α/β-KO or K562 EV cells intravenous. Figure: Created with BioRender.com. (**B**) Chemiluminescence images of mice on the days depicted outside the image panel (day 15 to 35). Visualization was done *via* IVIS. (**C**) The graph displays mean ± SD (n=5 mice/group) of the bioluminescence measurements of the region of interest (radiance; p/s/cm2/sr) at day 35. A significant reduction in the transplantation of HSP90α-KO cells compared to EV control cells was determined by a two-tailed unpaired t-test. (**D**) Kaplan-Meier survival curves showed a significantly prolonged overall survival of NSG mice transplanted with HSP90α-KO cells compared to HSP90β-KO or EV control cells. Results are shown from n=5 mice/group. P value was determined by the Log-rank Mantel-Cox test. *In vivo* evaluation of the HSP90-KO models, including injections and imaging, was done by the colleagues *Katerina Scharov* and *Jia-Wey Tu*.

To sum up the observations of the *in vivo* exploration, a growth repression of BCR-ABL1$^+$ cells upon HSP90α loss, as well as a prolonged survival of the mice was observed.

### 4.1.7 High-throughput drug screening of HSP90α/β-KO K562 cells

Combinational treatment of cancer cells by dual targeting represents a promising approach to overcome resistance and minimize toxicity, which may occur with single drug treatment. Drugs can interact with each other in different ways. On the one hand, they can have opposite effects when administered together, called drug antagonism. Furthermore, they can have an additive effect when the combined effect of two drugs is equal to the sum of the effects of the two drugs acting independently. In the best case, at least two drugs can have a greater effect than the sum of the two drugs alone, called drug synergism.[164]

Therefore, a high-throughput drug screening was done with the generated HSP90α/β-KO cell lines to identify novel therapeutic vulnerabilities. The library consisted of 93 inhibitors and contained chemotherapeutics and approved or in early to advanced stage clinical trials targeted inhibitors. The activity of the inhibitors was determined by CellTiter-Glo® assay. This assay identifies the living cell number by photometric quantification of ATP. Measurement of the luminescence signal, which is proportional to the ATP concentration, thus allows calculation of viability relative to DMSO-treated cells. The K562 HSP90α/β-KO cells and the K562 EV control were screened in biological triplicates, and then the half-maximal inhibitor concentration ($IC_{50}$) was calculated. Last, multiple t-tests were performed, and the calculated p-values were plotted against the fold changes in a volcano plot. Furthermore, the results of the respective HSP90α-KO and HSP90β-KO clones were pooled to improve the consistency of the resulting hits.

HSP90α-KO cells showed increased resistance toward treatment with Everolimus, Barasertib, Miransertib, and Gilteritinib (Figure 19A). Everolimus belongs to the drug class of mTOR inhibitors, Miransertib is an AKT inhibitor, Barasertib is an Aurora B kinase inhibitor, and Gilteritinib is a TKI belonging to the subgroup of AXL inhibitors.[165-167] It is striking that some drug classes are particularly well represented. In the case of Gilteritinib, the targets are tyrosine kinases, and in the case of Everolimus, Miransertib and Barasertib, the targets are serine/threonine kinases. HSP90α-KO cells showed increased sensitivity toward treatment with CI-994, Clofarabine, Aurora A inhibitor, KUNB31, Cytarabine, THZ1, and Staurosporine as the most significant hit (Figure 19A). CI-994 is a selective class I HDAC inhibitor, KUNB31 is an isoform-selective inhibitor of HSP90β, THZ1 is a CDK7 inhibitor, and cytarabine and clofarabine are both cytostatics.[168, 169] Staurosporine is a broad spectrum, a non-selective protein kinase inhibitor, including PKC, PKA and CaMK2.[170]

HSP90β-KO cells showed increased resistance toward treatment with KUNB31, Cytarabine, YKL-5-124, a CDK7 inhibitor and Ricolinostat, a selective HDAC6 inhibitor with some activity against HDAC 1, HDAC 2, and HDAC 3 (Figure 19B).[171] HSP90β-KO cells showed increased sensitivity toward treatment with PU-H71, Geldanamycin, AUY922 and BIIB021, which are all HSP90 inhibitors. An increased sensitivity could also be observed against Birinapant, which selectively inhibits the activity of inhibitor of apoptosis proteins (IAPs), such as X chromosome-linked IAP (XIAP) and cellular IAPs (c-IAP1/2). (Figure 19B).[172]

Taken together, HSP90α-KO cells were found hypersensitive toward CDK7i (THZ-1) and standard chemotherapeutics, whereas HSP90β-KO cells displayed hypersensitivity toward several HSP90i.

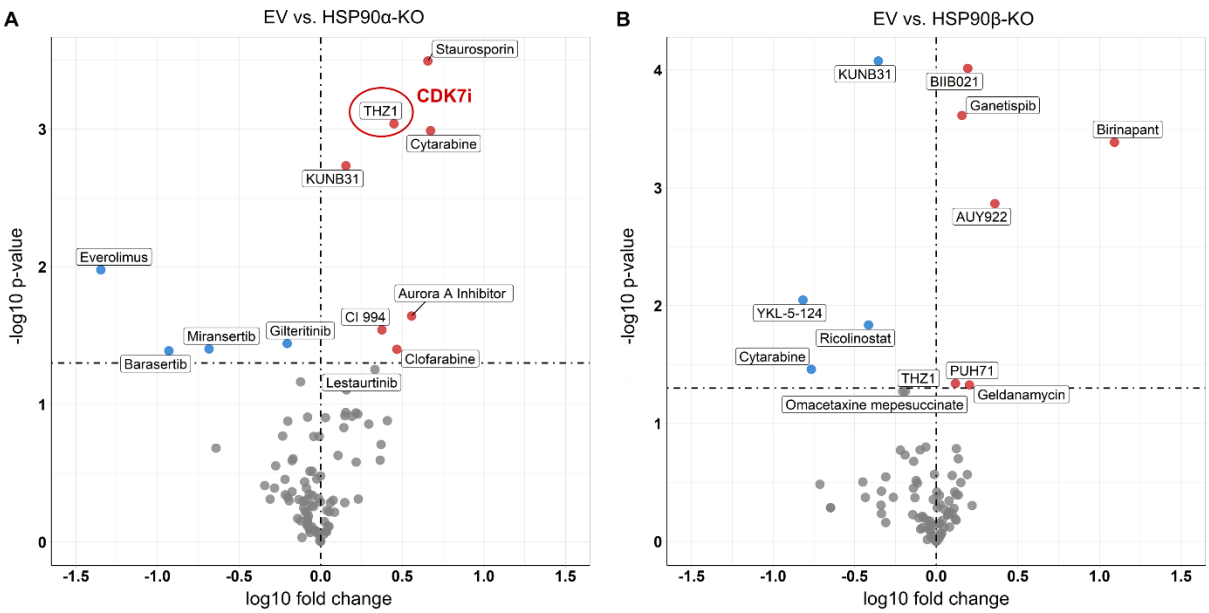


**Figure 19: Library drug screening to identify differences between K562 HSP90 KO and EV cell lines.**

(**A**) Volcano plot depicting the average $IC_{50}$ values (n=3 replicates) comparing EV and HSP90α-KO. The CDK7 inhibitor THZ1 is marked in red. (**B**) Volcano plot depicting the average $IC_{50}$ values (n=3 replicates) comparing EV and HSP90β-KO. In the upper left quadrant are the inhibitors with increased resistance (blue dots), and in the upper right quadrant are the inhibitors with increased sensitivity (red dots). The threshold was set at a p-value of 0.5 and a fold change greater/less than zero.

Subsequently, some of the identified targets were investigated on the protein level. In the K562 HSP90α-KO cells, an increased level of AKT was found, as already shown in chapter 4.1.4, for the downstream analysis of pro-survival signalling *via* BCR-ABL1. For Aurora A and Aurora B, there was no change in the expression level, and the phosphorylation status of pAurora A/B/C displayed no differences (Figure 20A). In the K562 HSP90β-KO cells, an increased level of XIAP and c-IAP1 was found (Figure 20B).

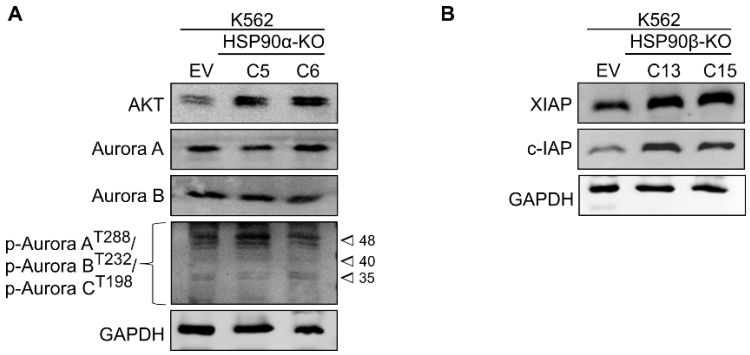


**Figure 20: Target investigation in K562 cells.**

(**A**) WB analysis of proteins in HSP90α-KO cells. Targets were selected based on the different sensitivity of the respective Inhibitor. (**B**) WB analysis of proteins in HSP90β-KO cells. Targets were selected based on the different sensitivity of the respective Inhibitor.

In line with the drug screening results, an increased AKT level resulted in an increased resistance against the AKT inhibitor Miransertib in the HSP90α-KO.

On the other hand, an increased level of XIAP and c-IAP1 resulted in an increased sensitivity against the inhibitor Birinapant in the HSP90β-KO cells. Moreover, HSP90β-KO cells exhibited increased sensitivity against all tested HSP90 inhibitors, except for the HSP90β selective inhibitor KUNB31.

#### 4.1.7.1 Investigation of CDK7 in HSP90α-KO cell lines

Increased sensitivity to a certain inhibitor provides a good starting point for developing a dual-treatment strategy. For this purpose, a focused study on the CDK7 inhibitor THZ1 was performed. The HSP90α-KO cells showed an $IC_{50}$ log10 fold change of 0.45 with a p-value of 0.000914. This represents an effective $IC_{50}$ fold change of 2.81 and implies an $IC_{50}$ reduction of 67 nM for K562 EV cells to 34 nM for K562 HSP90α-KO cells.

Initially, changes at the protein level were investigated, and a strong upregulation of CDK7 was found in the two HSP90α-KO clones. Subsequently, the CDK7 level in the two other HSP90-KO cell lines was examined to exclude the possibility of a cell line-specific effect. A strong upregulation of CDK7 in all three HSP90α-KO KCL-22 clones and an upregulation in the SUP-B15 HSP90α-KO cell pool could be identified (Figure 21A). Plates were designed to identify possible synergistic interactions between the CDK7i THZ1 and the inhibition of HSP90. To this end, the respective inhibitors were printed alone and in a combination matrix. PU-H71 was chosen as an HSP90 inhibitor. The cells were seeded onto the plates, and the evaluation *via* CTG was done after 72h. Drug combination cell viability data were used to calculate synergy scores with the SynergyFinder R package performed by *Julian Schliehe-Diecks*.[173] The zero-interaction potency (ZIP) method, which calculates the delta score matrix from a dose-response matrix, was chosen for the data representation. [174] The interpretation of the calculated synergy score depends on the value obtained. In the case of less than -10, it indicates an antagonistic interaction. In the case of -10 to 10, it indicates an additive interaction. In the case of larger than 10 it indicates a synergistic interaction. For example, a synergy score of 10 corresponds to 10% of response beyond expectation. For the combination of THZ1 and PU-H71, a synergy score of 18 was obtained in K562 WT and KCL-22 WT cells. This indicates a synergistic interaction between both drugs (Figure 21B/C).

Furthermore, K562 and KCL-22 Imatinib (TKI) resistant cell lines were tested to evaluate whether the combination approach with PU-H71 and THZ1 can address the resistant phenotype. A maximum synergy score of 13 in K562r and a synergy score of 30 in KCL-22r cells was obtained, which indicates a synergistic interaction between both drugs (Figure 21B/C). In addition, a synergistic behavior was observed in the Ponatinib (TKI) resistant pro-B cell line BA/F3 (maximum score = 40) and the Imatinib (TKI) resistant SUP-B15 cells (maximum score = 35) (Figure 21D).

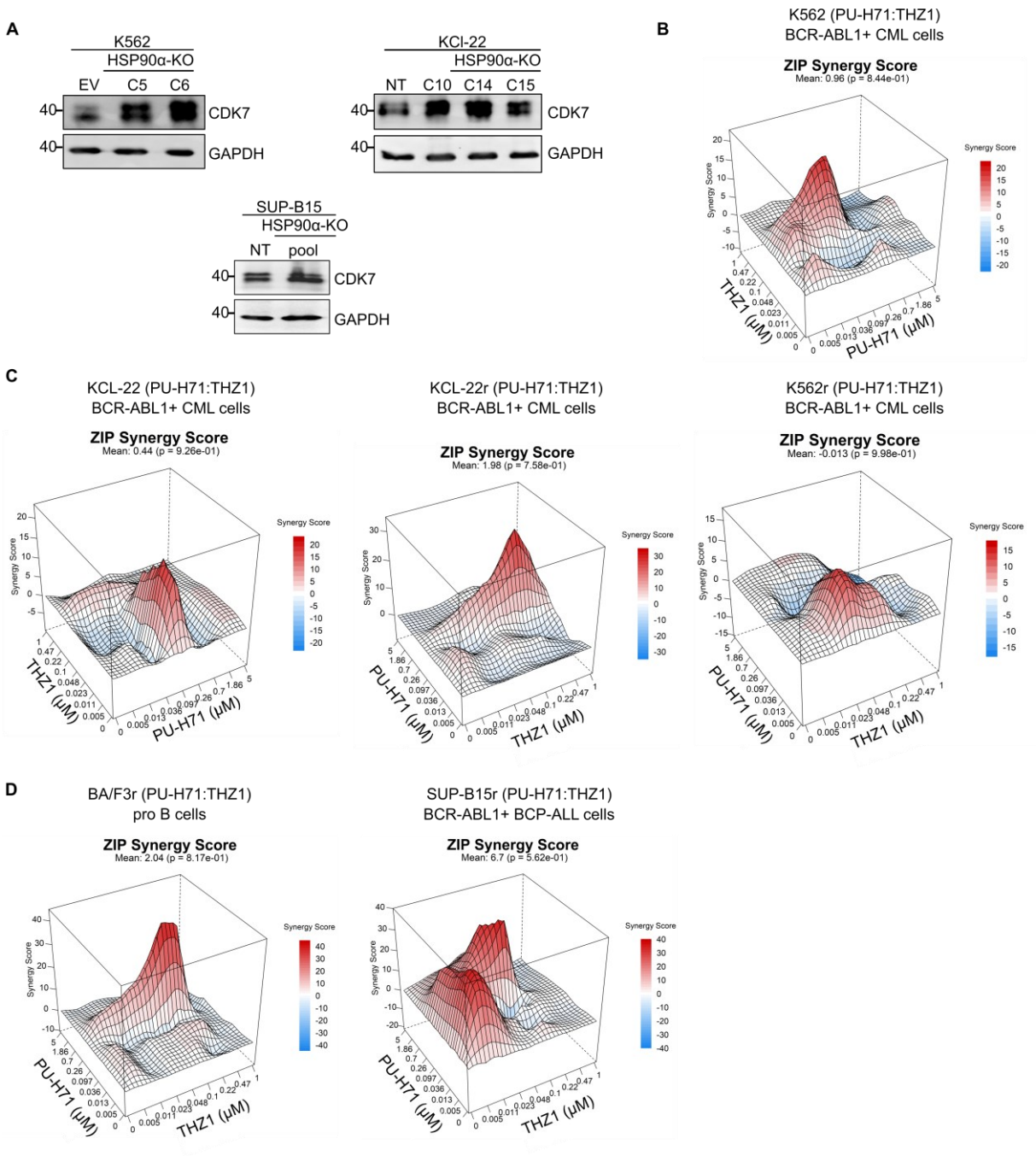


**Figure 21: Investigation of CDK7 in HSP90α-KO cell lines and synergy drug screening.**

(**A**) WB analysis of CDK7 in HSP90α-KO K562, KCL-22 and SUP-B15 cells. (**B**) Synergy drug screening combining the CDK7i THZ1 and the HSP90i PU-H71 in K562 WT and K562r (Imatinib resistant) cell lines. (**C**) Synergy drug screening combining the CDK7i THZ1 and the HSP90i PU-H71 in KCL-22 WT and KCL-22r (T315I, F317L; Imatinib resistant) cell lines. (**D**) Synergy drug screening in BA/F3r (T315I, Y272H; Ponatinib resistant) and SUP-B15r (T315I; Imatinib resistant) cell lines.

The results of the cell lines were subsequently validated in patient-derived cell lines obtained from three relapsed patients with BCR-ABL1$^{+}$ BCP-ALL. The leukemia cells were injected into NSG mice and isolated from bone marrow and spleen after successful transplantation. First, WB analysis was performed to determine the level of BCR-ABL1. All three patient cell lines were positive for P190$^{\text{BCR-ABL1}}$, whereas the control KCL-22 CML cell line was positive for P210$^{\text{BCR-ABL1}}$ (Figure 22A).

The smaller $P190^{BCR\text{-}ABL1}$ isoform is predominantly found in B-ALL cell lines. Furthermore, the leukemia cells were purified and used directly for ex vivo drug sensitivity assays. For this purpose, the cells were seeded onto the previously used plates with THZ1 and PU-H71 and measured after 72 h by CTG. Again, matrix data were used to calculate ZIP synergy scores, and visualization was done using the SynergyFinder R package. For the combination of THZ1 and PU-H71, a synergy score of 20 for patient one was obtained. For patient two, a synergy score of 21 and for patient three, a synergy score of 15 was obtained (Figure 22B-D). Subsequently, it was to be ensured that the combination treatment with PU-H71 and THZ1 is effective only or enhanced in leukemia cell lines. For this purpose, peripheral blood-derived mononuclear cells (PBMCs) were isolated from three healthy individuals and treated with PU-H71, THZ1, either alone or in combination. To monitor the effect of the treatment, apoptosis induction was measured using the Caspase-Glo® 3/7 assay. In this assay, a proluminescent caspase-3/7 DEVD-aminoluciferin substrate was used in combination with luciferase. The substrate gets cleaved in the cells by caspase 3/7 and the resulting product aminoluciferin served as substrate for luciferase, resulting in a luminescence signal. The measured luminescence signal is proportional to the amount of caspase 3/7.

PU-H71 was shown to increase caspase 3/7 activity 3.7-fold and THZ1 1.7-fold in K562 WT cells. Both inhibitors combined resulted in a 4.2-fold increase in caspase 3/7 activity. PBMCs showed a comparable increase in caspase activity by THZ1 of 2.3-, 2.1- and 1.6-fold, respectively. Treatment with PU-H71 showed a smaller effect in PBMCs and an increase of 2.3-, 1.6- and 2.2-fold, respectively. Combination treatment with PU-H71 and THZ1 increased caspase 3/7 activity in PBMCs by 2.2, 2.2, and 2.7-fold, respectively, resulting in a significantly reduced effect ($p < 0.0001$, $p = 0.0002$, and $p < 0.0001$) compared to K562 cells (Figure 22E).

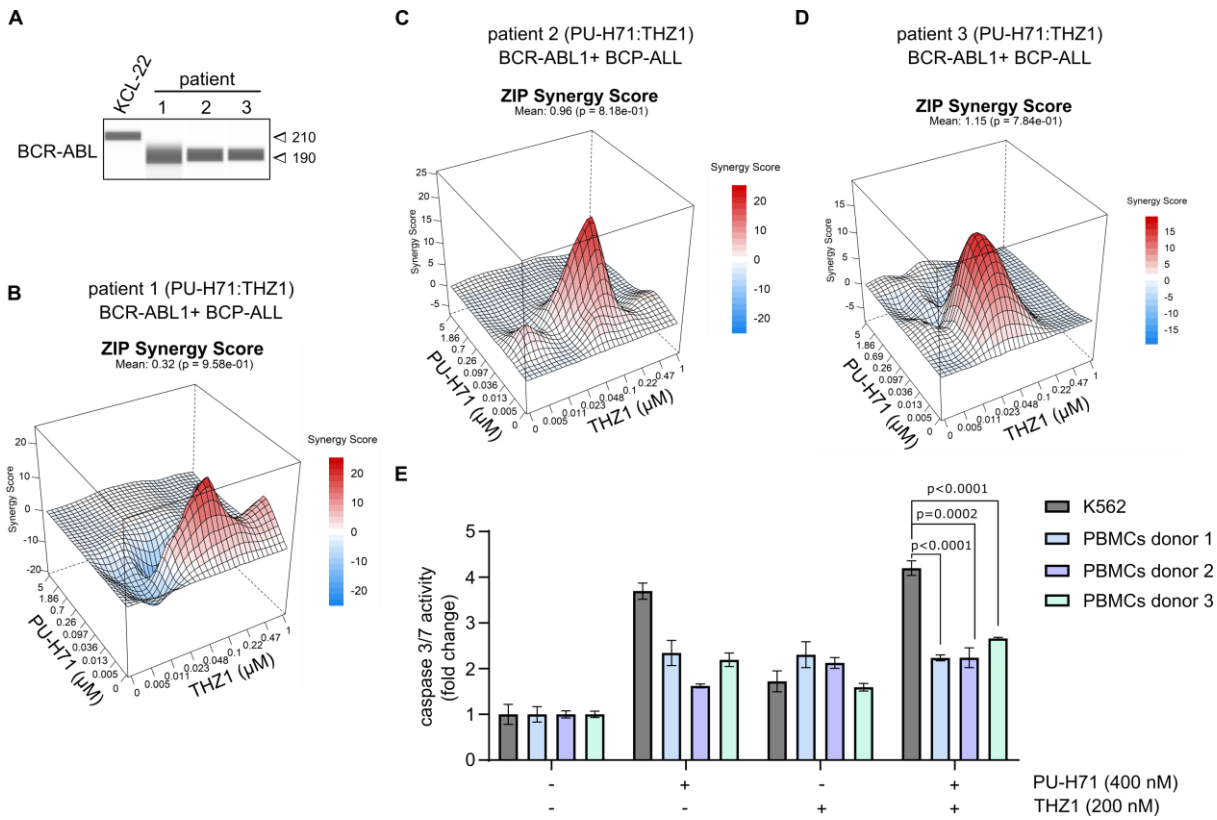


**Figure 22: Target validation in BCR-ABL1$^+$ BCP-ALL patient cells.**

(**A**) WB analysis revealed that all three patient cell lines are positive for P190$^{BCR-ABL1}$. (**B-C**) Synergy drug screening in three patient-derived BCR-ABL1$^+$ BCP-ALL cell lines combining the CDK7i THZ1 and the HSP90i PU-H71. (**E**) Caspase 3/7 glo assay was conducted following the treatment of PBMCs obtained from three healthy individuals. These cells were treated with PU-H71, THZ1, either alone or in combination, and their response was compared to that of leukemia K562 cells. Error bars ± SD of three independent replicates; p-values were calculated by unpaired two-tailed t-test.

Therefore, a synergistic interaction between both drugs (PU-H71 and THZ1) could be validated in patient-derived BCR-ABL1$^+$ BCP-ALL cells.

### 4.1.7.2 Mechanistic studies on combining HSP90i and CDK7i

Effector proteins were examined to elucidate the mechanistic background of the observed synergistic effect of PU-H71 and THZ1 to address HSP90 and CDK7. For this purpose, K562 and KCL-22 cell lines were treated with either PU-H71 or THZ1 alone or together. Concentration was determined from drug screening data and chosen to ensure that the viability was above 75% after treatment. After 24 h, cell viability and proliferation were checked, and pellets were taken. As an apoptotic marker, the level and the ratio between uncleaved and cleaved poly (ADP-ribose) polymerase (PARP) was checked.[175] Cleaved PARP, which facilitates cell degradation, is a target of several caspases and is one of the main cleavage targets of caspase 3.[176] Western blot analysis showed that single treatment with PU-H71 does not induce an increase in cleaved PARP. In contrast, single treatment with THZ1 induces a slight increase.

The dual treatment induces a greater increase in cleaved PARP levels, which is also associated with lower cell viability (Figures 23A/D).

Furthermore, the RNA polymerase II subunit (RPB1) levels were investigated since the C-terminal domain gets phosphorylated by CDK7 and inhibition with THZ1 directly affects RPB1 activity and, thus, gene transcription.[177] A decreased level of RPB1 was found in the THZ1-treated cells, and a highly decreased level of RPB1, especially p-RPB1, was found in the dual-treated cell lines. RPB1 is further associated with the transcription of HSR-related genes, such as HSP70.[178] Therefore, the induction of HSR in the treated cells was investigated. Treatment with PU-H71 showed induction of HSR mediated by upregulation of HSF1, HSP90α, HSP70, and HSP40 (Figure 23B/E). A single treatment with THZ1 did not affect HSR-related genes. The dual treatment with PU-H71 and THZ1 also showed no induction of HSR in K562 and KCL-22 cells, which was also shown by the quantification of Western blot replicates.

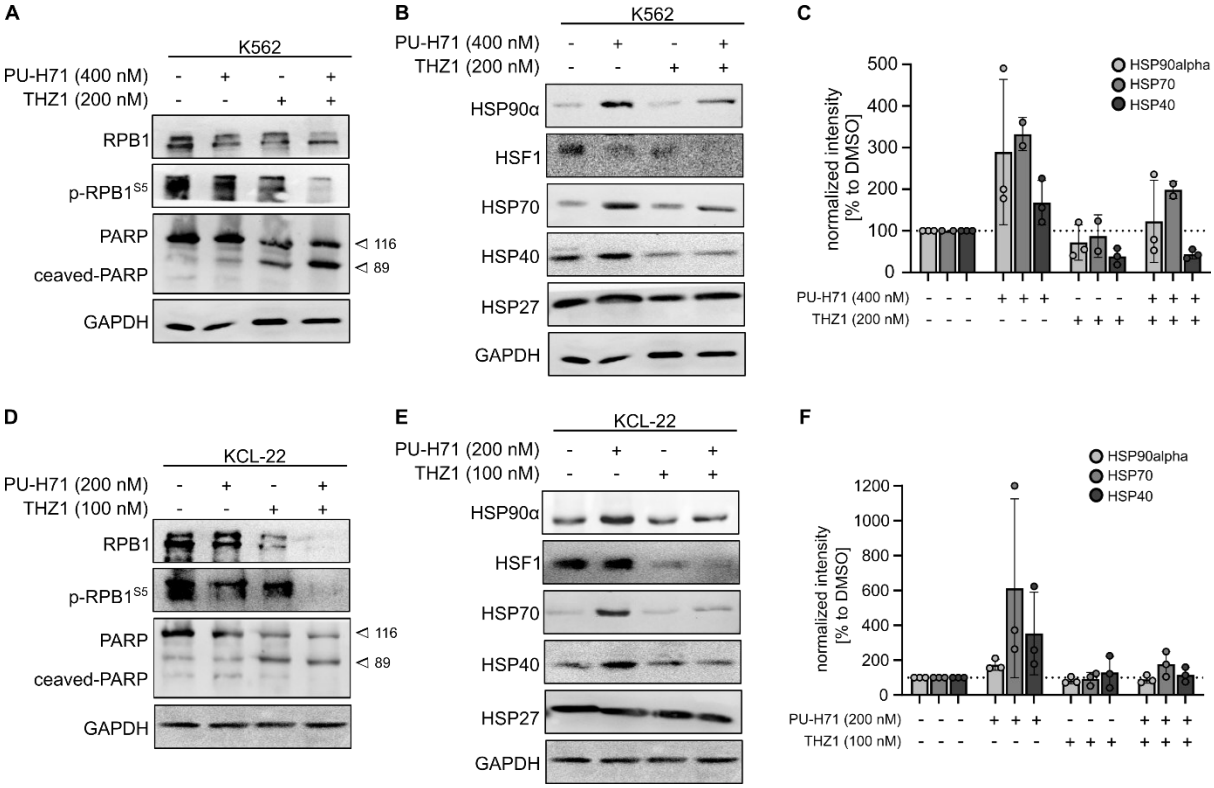


**Figure 23: Mechanistic studies on combining HSP90i and CDK7i in K562 and KCL-22 cell lines.**

(**A**) WB analysis revealed a strong reduction of RPB1 and p-RPB1$^{S5}$ with the dual treatment of PU-H71 and THZ1 in K562 cells. (**B**) WB analysis of the heat shock protein panel in K562 cells after treatment with PU-H71 and THZ1 alone or in combination revealed no HSR induction after the dual treatment. (**C**) Quantification of HSP90α, HSP70, and HSP40 in K562 cells. (**D**) WB analysis revealed a strong reduction of RPB1 and p-RPB1$^{S5}$ with the dual treatment of PU-H71 and THZ1 in KCL-22 cells. (**E**) WB analysis of the heat shock protein panel in KCL-22 cells after treatment with PU-H71 and THZ1 alone or in combination revealed no HSR induction after the dual treatment. (**F**) Quantification of HSP90α, HSP70, and HSP40 in KCL-22 cells. Error bars = SD of three independent replicates.

It could be seen that single treatment of K562 cells with PU-H71 resulted in an increase of HSP90α up to 290 %, of HSP70 up to 330 %, and of HSP40 up to 170 %. The dual treatment resulted in a slight increase of HSP90α up to 120 % and of HSP70 up to 200 %. The level of HSP40 was decreased to 44% (Figure 23 C). In KCL-22 cells, the treatment with PU-H71 led to an increase of HSP90α up to 170 %, of HSP70 up to 612 % and of HSP40 up to 350 %. In the dual treatment, the HSP90α level was 90 %, the HSP70 level was 176 %, and the HSP40 level was 115 % (Figure 23F).

The mechanism identified in the cell lines was subsequently verified in BCR-ABL1$^{+}$ B-ALL patient derived xenograft (PDX) cells. These were also treated alone or with PU-H71 and THZ1 together, and differentially expressed proteins were examined. Strong downregulation of RPB1 and p-RPB1 was found in THZ1 and dual-treated cells. Furthermore, as expected, induction of HSR mediated through HSP90α, HSP70, and HSP40 was observed in the PU-H71 treated cells (Figure 24A). Quantification revealed an increase of HSP90α up to 188 % of HSP70 up to 344 %, and of HSP40 up to 127 %. The dual treatment did not increase the HSR-related genes. On the contrary, the expression level of HSP90α, HSP70 and HSP40 was lower than in the DMSO-treated control cells (Figure 24B).

The expression level of total HSP90 and HSP70 was further examined by immunofluorescence staining, and microscopic analysis showed a significantly stronger fluorescence signal of HSP90 ($p = 0.0328$) and HSP70 ($p = 0.0035$) in the PU-H71 treated PDX cells. In contrast, no increased signal was observed in the dual-treated cells and the signal was significantly lower ($p_{HSP90} = 0.0269$; $p_{HSP70} = 0.0133$) in comparison to the PU-H71 treated cells (Figure 24C/D).

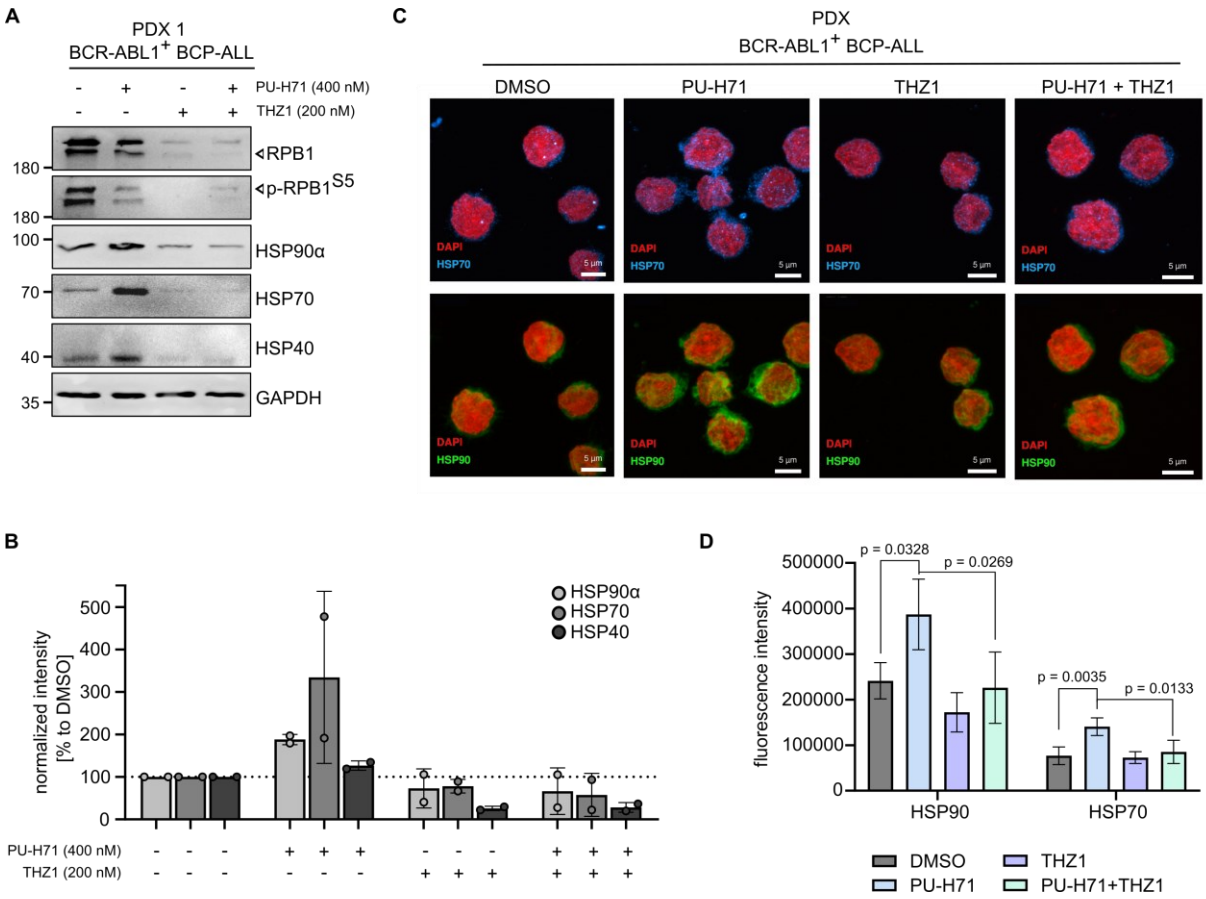


**Figure 24: Mechanistic studies on combining HSP90i and CDK7i in BCR-ABL1$^+$ B-ALL cells.**
(**A**) WB analysis revealed a strong reduction of RPB1 and p-RPB1$^{S5}$ and no HSR induction with the dual treatment of PU-H71 and THZ1 in the BCR-ABL1$^+$ patient cells. (**B**) Quantification of HSP90α, HSP70, and HSP40 in PDX cells. Error bars = SD of two independent replicates. (**C**) Immunofluorescence imaging demonstrated no HSR induction with the dual treatment of PU-H71 and THZ1 in the BCR-ABL1$^+$ patient cells. DAPI (red), HSP70 (AlexaFluor 488; blue), HSP90 (AlexaFluor 594; green). (**D**) Quantification of HSP90 and HSP70 using Fiji software. The process involved loading images, splitting composite images into individual channels, and creating a Z-projection from all slices with maximum intensity. Subsequently, the images were converted to grayscale by changing the current look-up table (LUT) to grayscale. Square regions were then placed around the cells, and the mean gray values were measured. To ensure accuracy, background values were subtracted from all measurements. Error bars = SD (n = 4); p-values were calculated by unpaired two-tailed t-test.

Taken together, dual treatment with PU-H71 and THZ1 causes suppression of HSR, leading to synergistic behaviour.

## 4.1.8 Proteogenomic profiling of HSP90α/β-KO K562 cell lines

Proteogenomic profiling enables a better understanding of the differences between the genetically modified K562 models and provides a comprehensive overview of protein expression and function. RNA sequencing (RNAseq) can be used to measure a wide variety of transcripts, but it can be difficult to distinguish between transcripts that are actually expressed and transcripts that are pseudogenes or artifacts of the sequencing process.

The mass spectrometry (MS) based proteome analysis is more sensitive and can identify and quantify proteins with high specificity, whereby the overall analysis can be improved.

#### 4.1.8.1 RNA sequencing (RNAseq) of HSP90α/β-KO K562 cell lines

RNA sequencing was carried out to investigate the transcriptomic disparities between the HSP90α/β-KO cell lines and the control cells. RNA sequencing was performed at the Biological-Medical Research Center (BMFZ) -Genomics & Transcriptomics Laboratory (GTL) at the HHU in Düsseldorf.

First, RNA was isolated, which was used to synthesize cDNA and for library amplification. The reads obtained after data processing were aligned to the Genome Reference Consortium Human Build 38 (GRCh38). To obtain an overview of the differentially expressed genes, they were plotted in a volcano plot with the log2 fold change against the negative log10 FDR. Differential RNA expression analysis revealed 2095 genes (1090 up- and 1005 down-regulated) with altered expression in the K562 HSP90α-KO cells compared to the control cells (Figure 25A). In contrast, 903 genes (368 up- and 535 down-regulated) were found to be altered in the K562 HSP90β-KO cells in comparison to the control cells (Figure 25B).

In the HSP90α-KO cells, the mRNA level of *HSP90α* was shown to be most significantly downregulated with a fold change of 0.125. The most upregulated hit with a fold change of 168.9 was observed to be the *androgen receptor* (*AR*). Also, the mRNA level of *lymphocyte cytosolic protein 2* (*LCP2*) was upregulated with a fold change of 6.06.

For the HSP90β-KO, the mRNA level of *carbonic anhydrase 2* (*CA2*) was mostly upregulated with a fold change of 90.51. In line with previously observed results from chapter 4.1.1 and 4.1.2, *HSP90α* was found to be upregulated with a fold change of 1.74. The mRNA level of *HSP90β* was slightly reduced with a fold change of 0.66. The most downregulated gene with a fold change of 0.0006 was *Prostaglandin Reductase 1* (*PTGR1*).

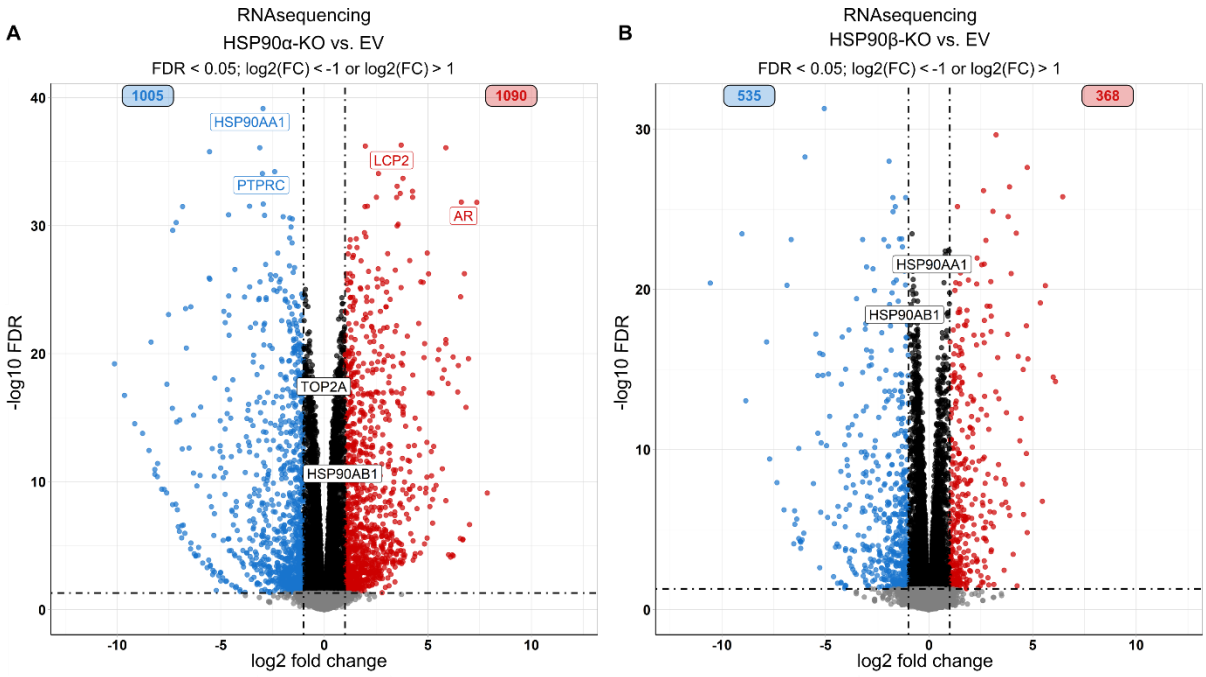


**Figure 25: RNA sequencing to identify differences between K562 HSP90 KO and EV cell lines.**
Volcano plots of the significantly (FDR < 0.05; log2(FC) < -1 or log2(FC) > 1) up- or down-regulated genes in the mRNA expression profile of (**A**) HSP90α-KO cells and (**B**) HSP90β-KO cells, in comparison to EV control cells. Grey dots represent genes that are not significantly regulated, while black dots represent significantly regulated genes below the log2(FC) threshold. Blue and Red dots represent significantly downregulated and upregulated genes, respectively.

All differentially expressed genes, including up- and downregulated ones, were subsequently analyzed by fast gene set enrichment analysis (fGSEA). For this purpose, the human Molecular Signatures Database (MSigDB) was used, which contains 33196 gene sets divided into different subgroups. This computational method calculates whether there are significant differences in defined gene sets between two conditions. The input was a gene set database and the molecular profile of the samples, herein K562 EV control and the respective HSP90-KO samples.
After filtering (10 % FDR), there were significant differences in the HSP90α-KO cells for gene sets that contain genes annotated by the same ontology term (C5: ontology gene sets), for gene sets that are curated from various sources, including online pathway databases and biomedical literature (C2: curated gene sets), and for hallmark gene sets (H: hallmark gene sets). In the HSP90α-KO cells, there was an upregulation of gene sets involved in the G protein-coupled receptor signalling and the MAPK cascade, including ERK signalling. Furthermore, there was an upregulation of gene sets involved in leukocyte, myeloid and mononuclear cell migration (Figure 26A). For the HSP90β-KO cells, there were significant differences for gene sets that contain genes annotated by the same ontology term (C5: ontology gene sets), including poor motor coordination (NES = -2), and basal ganglia calcification and visual loss (NES = 2) (Figure 26B).

Cluster profiler revealed no significant networks for the HPS90β-KO cells after filtering (10 % FDR), whereas in the HSP90α-KO cells, a huge and significant interaction network was found. The HSP90α-KO cells showed an upregulation of genes connected to the MAPK cascade, the regulation of ERK1 and ERK2, the cell motility, and the leukocyte development and function (Figure 26C).

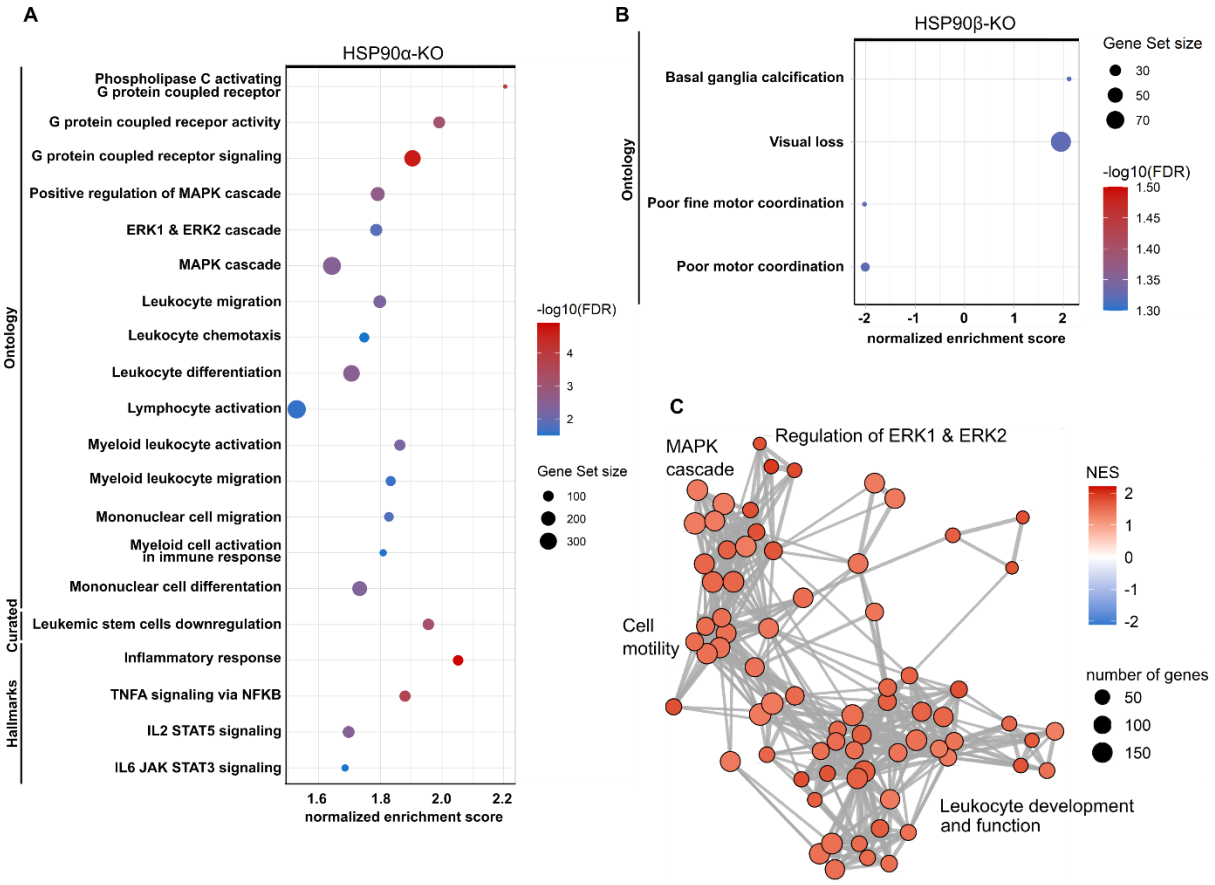


**Figure 26: Fast gene set enrichment analysis of differently expressed genes in the HSP90α/β-KO cells.** (**A**) Fast gene set enrichment analysis (fGSEA) showed significantly (FDR = 0.1) differentially regulated gene set signatures in HSP90α-KO cells. (**B**) Fast gene set enrichment analysis (fGSEA) showed significant (FDR = 0.1) differentially regulated gene set signatures in HSP90β-KO cells. (**C**) Gene clusters were obtained using Cluster profiler on the RNA-seq data of HSP90α-KO cells. Normalized enrichment scores (NES).

Gene set enrichment analysis (GSEA) revealed a significant enrichment of androgen receptor (AR) signalling and reactome FcεRI-mediated MAPK activation in the transcriptome of HSP90α-KO cells (Figure 27A/B).

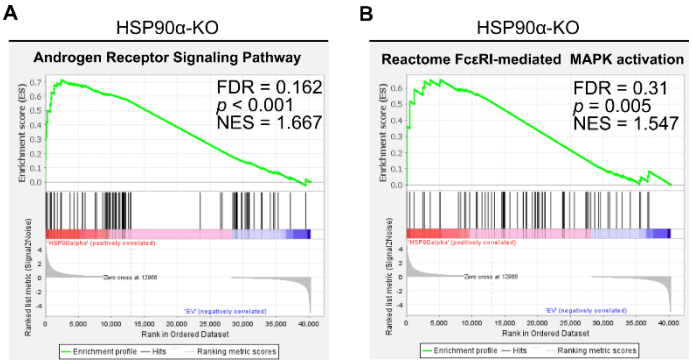


**Figure 27: Gene set enrichment analysis of differently expressed genes in the HSP90α-KO cells.**
(**A**) GSEA plot depicts a significant enrichment of androgen receptor (AR) signalling in the transcriptome of HSP90α-KO cells. (**B**) GSEA plot depicts a significant enrichment of reactome FcεRI-mediated MAPK activation in the transcriptome of HSP90α-KO cells.

In summary, RNA sequencing revealed differences in specific genes, like the downregulation of *PTPRC* and *HSP90AA1* and the upregulation of *LCP2* and *AR* in the HSP90α-KO cell lines. Furthermore, differences in gene sets associated with MAPK signaling cascade, cell motility- and immune-related signatures in the HSP90α-KO cell lines were found.

### 4.1.8.2 Mass spectrometry (MS) based proteome analysis of HSP90α/β-KO K562 cell lines

Mass spectrometry analysis was performed to analyse changes in the proteome between the HSP90-KO cell lines and the control cells. Quantitative LC-MS analysis was performed at the BMFZ - Molecular Proteomics Laboratory (MPL) at the HHU in Düsseldorf. To identify and quantify the peptides/proteins, the human sequence database from UniProtKB was used, and a total of 4676 protein groups were identified in the K562 cells (FDR = 0.01). To obtain an overview of the differentially expressed proteins, they were plotted in a volcano plot with the log2 fold change against the negative log10 p-value. Differential protein expression analysis revealed 375 proteins (180 up- and 195 down-regulated) with altered expression in the HSP90α-KO cells compared to the control cells (Figure 28A). In contrast, 213 proteins (103 up- and 110 down-regulated) were found to be altered in the HSP90β-KO cells in comparison to the control cells (Figure 28B).

As expected, in the HSP90α-KO, HSP90α was shown to be the most significant downregulated hit with a fold change of 0.014. Downregulated as well was protein tyrosine phosphatase (PTPRC or CD45). The most significant upregulated hit with a fold change of 17.47 was observed to be LCP2. Upregulated as well was DNA topoisomerase 2 α (TOP2A).

For the HSP90β KO, HSP90AB2P, a pseudogene, was the most significant downregulated hit with a fold change of 0.002. Furthermore, HSP90β was found to be downregulated with a fold change of 0.38. The most significant upregulated hit with a fold change of 25 was observed to be CA2. In line with previously observed results from chapters 4.1.1 and 4.1.2, HSP90α and HSP70 (HSPA1A) were upregulated with a fold change of 2.36 and 2.45, respectively.

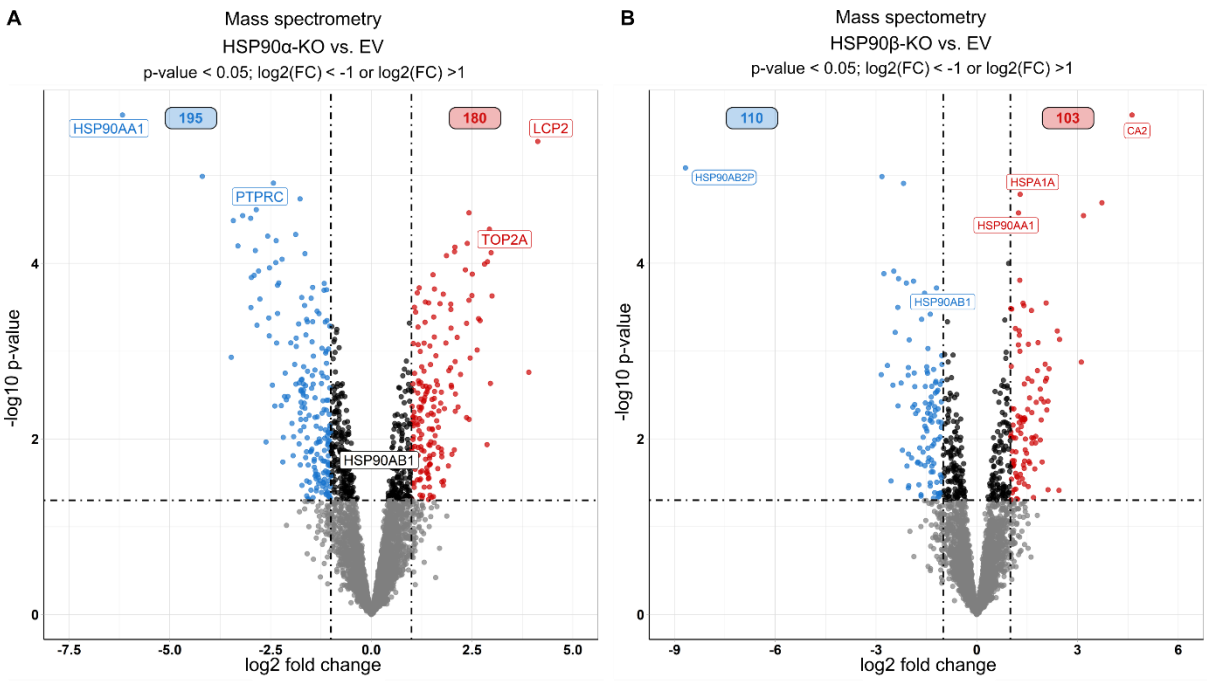


**Figure 28: Mass spectrometry-based proteome analysis to identify differences between K562 HSP90 KO and EV cell lines.**

Volcano plots of the significantly (p-value < 0.05; log2(FC) < -1 or log2(FC) > 1) up- or down-regulated proteins in (**A**) HSP90α-KO cells and (**B**) HSP90β-KO cells, in comparison to EV control cells. Grey dots represent genes that are not significantly regulated, while black dots represent significantly regulated genes below the log2(FC) threshold. Blue and Red dots represent significantly downregulated and upregulated proteins, respectively.

All differentially expressed proteins, including up- and downregulated ones, were subsequently examined in more detail by fGSEA. After filtering (20% FDR), there were no significantly enriched gene sets with either negative or positive NES for the HSP90β-KO cells. For the HSP90α-KO cells, significant differences were shown for gene sets that contain genes annotated by the same ontology term (C5: ontology gene sets) and for gene sets that are curated from various sources, including online pathway databases and biomedical literature (C2: curated gene sets). In the HSP90α-KO cells, there was an upregulation of gene sets involved in the cell cycle. In addition, an upregulation was found for chromosomal organization, DNA repair, cell division, chromosome segregation, and the mitotic cell cycle process (Figure 29A). Downregulation of gene sets related to the NADH dehydrogenase complex, oxidative phosphorylation, and respiratory electron transport were found. Cluster profilers revealed the downregulation of energy metabolism (Figure 29B).

In the next step, the RNA sequencing and mass spectrometry data were compared, and the top hits, as well as overlapping targets, were compared by log fold change and FDR values. LCP2 and TOP2A were consistently upregulated on mRNA and protein levels in the HSP90α-KO. The *androgen receptor*, on the other hand, was only detected in the RNA sequencing analysis. HSP90AB1 was not significantly changing on the mRNA and protein level.

HSP90AA1, PTPRC, and glucose-6-phosphate dehydrogenase (G6PD) were consistently downregulated (Figure 29C).

In HSP90β-KO cells, CA2 and HSP90AA1 were upregulated, and HSP90AB1 was consistently downregulated on the mRNA and protein level. HSPA1A (HSP70) was found to be upregulated on the protein level, whereas on the mRNA level, it was downregulated (Figure 29D).

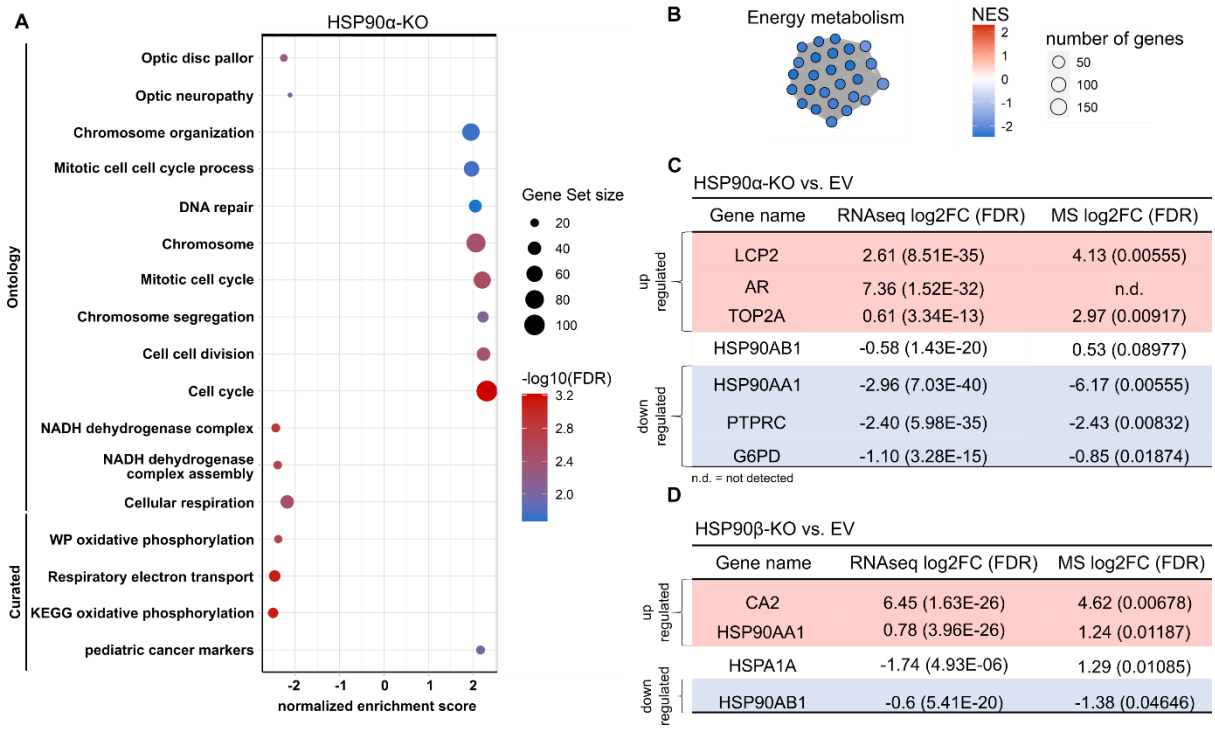


**Figure 29: Fast gene set enrichment analysis of differently expressed proteins in the HSP90α-KO cells.**
(**A**) fGSEA showed significantly (FDR = 0.2) differentially regulated gene set signatures in HSP90α-KO cells. (**B**) Gene clusters were obtained using Cluster profiler on the RNA-seq data of HSP90α-KO cells. Normalized enrichment scores (NES). (**C-D**) Table with log FC values comparing RNAseq and MS analysis in the HSP90α/β-KO cells.

The top-hit LCP2 and TOP2A were subsequently validated *via* WB, and both proteins were found to be strongly upregulated. Both proteins were also examined in the HSP90α-KO KCL-22 clones and the HSP90α-KO SUP-B15 pool cells to exclude cell line-specific effects. A slight upregulation of TOP2A and a strong upregulation of LCP2 was observed in the KCL-22 clones. A strong upregulation of LCP2 and TOP2A was also observed in the SUP-B15 pool cells (Figure 30A).

To address TOP2A, the inhibitor mitoxantrone can be used. This inhibitor is commonly used as a cytostatic agent in cancer treatment, including AML.[179, 180] To identify a possible synergistic interaction between the TOP2Ai mitoxantrone and the inhibition of HSP90, plates were designed with the respective inhibitor alone and with a combination matrix. PU-H71 was again chosen as an HSP90 inhibitor. K562 and KCL-22 cells were seeded onto the plates, and the evaluation *via* CTG was done after 72h. Drug combination cell viability data were used to calculate synergy scores.

For the combination of mitoxantrone and PU-H71, a synergy score of 20 was obtained in K562. In the KCL-22 cells, a synergy score of 32 was obtained, indicating a synergistic interaction between both drugs (Figure 30B-C).

The obtained results of the cell lines were subsequently validated in patient-derived cell lines. These cells were obtained from two relapsed patients with BCR-ABL1$^{+}$ BCP-ALL. For this purpose, the cells were seeded onto the previously used plates with mitoxantrone and PU-H71 and measured after 72 h by CTG. Again, matrix data were used to calculate ZIP synergy scores, and visualization was done using the SynergyFinder R package. For the combination of mitoxantrone and PU-H71, synergy scores of 20 for patient one and 40 for patient two were obtained (Figure 30D-E).

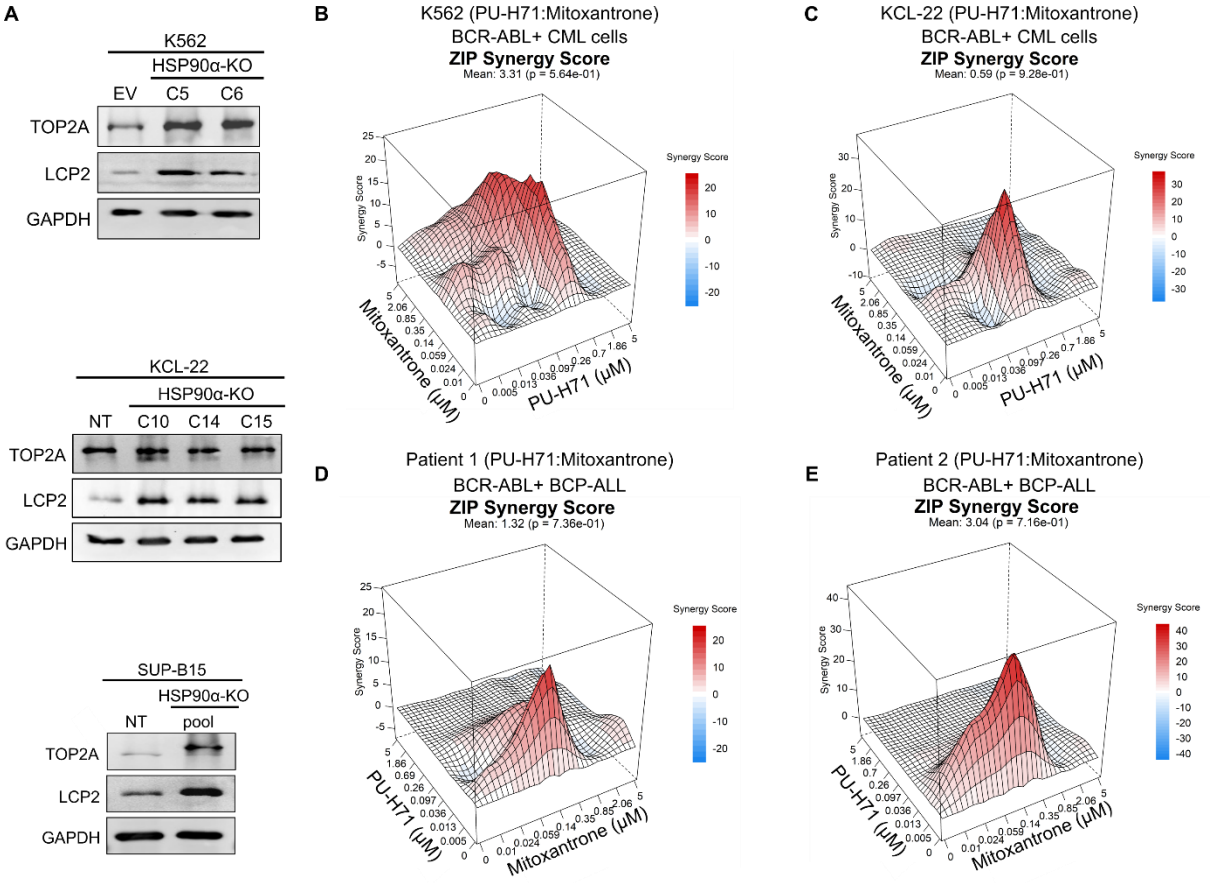


**Figure 30: Target validation in HSP90α-KO K562, KCL-22 and SUP-B15 cell lines and synergy screening.** (**A**) WB analysis showed a consistent upregulation of TOP2A and LCP2 in all HSP90α-KO clones. (**B-C**) Synergy drug screening in K562 and KCL-22 cell lines combining the TOP2Ai mitoxantrone and the HSP90i PU-H71. (**D-E**) Synergy drug screening in two patient-derived BCR-ABL1$^{+}$ BCP-ALL cell lines combining the TOP2Ai mitoxantrone and the HSP90i PU-H71.

Therefore, a synergistic interaction between both drugs could be validated in patient-derived BCR-ABL1$^{+}$ BCP-ALL cells.

Taken together the observations indicates, that dual targeting of HSP90 and TOP2A offers a promising therapeutic combination.

#### 4.1.8.3 MS-based Secretome analysis of HSP90α/β-KO K562 cell lines

Quantitative MS-based secretome analysis was performed to analyse changes in secreted proteins in the extracellular space between the HSP90-KO cell lines and the control cells. The cells were washed and incubated for 12 h in a serum-free medium to exclude contamination by serum proteins in the cell culture medium.

To identify and quantify the peptides/proteins, the human sequence database from Uni-ProtKB was used, and a total of 2051 protein groups were identified in the K562 cells (FDR = 0.01). Differentially expressed proteins were plotted in a volcano plot with the log2 fold change against the negative log10 p-value. Differential protein expression analysis revealed 149 proteins (87 up- and 62 down-regulated) with altered expression in the HSP90α-KO cells compared to the control cells (Figure 31A). In contrast, 124 proteins (57 up- and 49 down-regulated) were found to be altered in the HSP90β-KO cells in comparison to the control cells (Figure 31B).

In the secretome of the HSP90α-KO cells, HSP90α was shown to be the most significant downregulated hit with a fold change of 0.00088. The most significant upregulated hit with a fold change of 36.43 was observed to be Insulin-like growth factor-binding protein 2 (IGFBP2).

TOP2A was slightly upregulated, whereas LCP was not detected in the secretome of HSP90α-KO cells. PTPRC was significantly downregulated (Figures 31A/C). Another protein, HSPA5, a member of the HSP70 family, was found to be downregulated.[181]

In the secretome of the HSP90β-KO cells, HSP90AB2P was the most significant downregulated hit with a fold change of 0.019, closely followed by HSP90AB1 with a fold change of 0.027. In line with previously observed results, HSP90α was upregulated in the secretome with a fold change of 2.44. The most significant upregulated hit with a fold change of 136.13 was echinoderm microtubule-associated protein-like 4 (EML4). CA2 was significantly upregulated as well (Figure 31B/D).

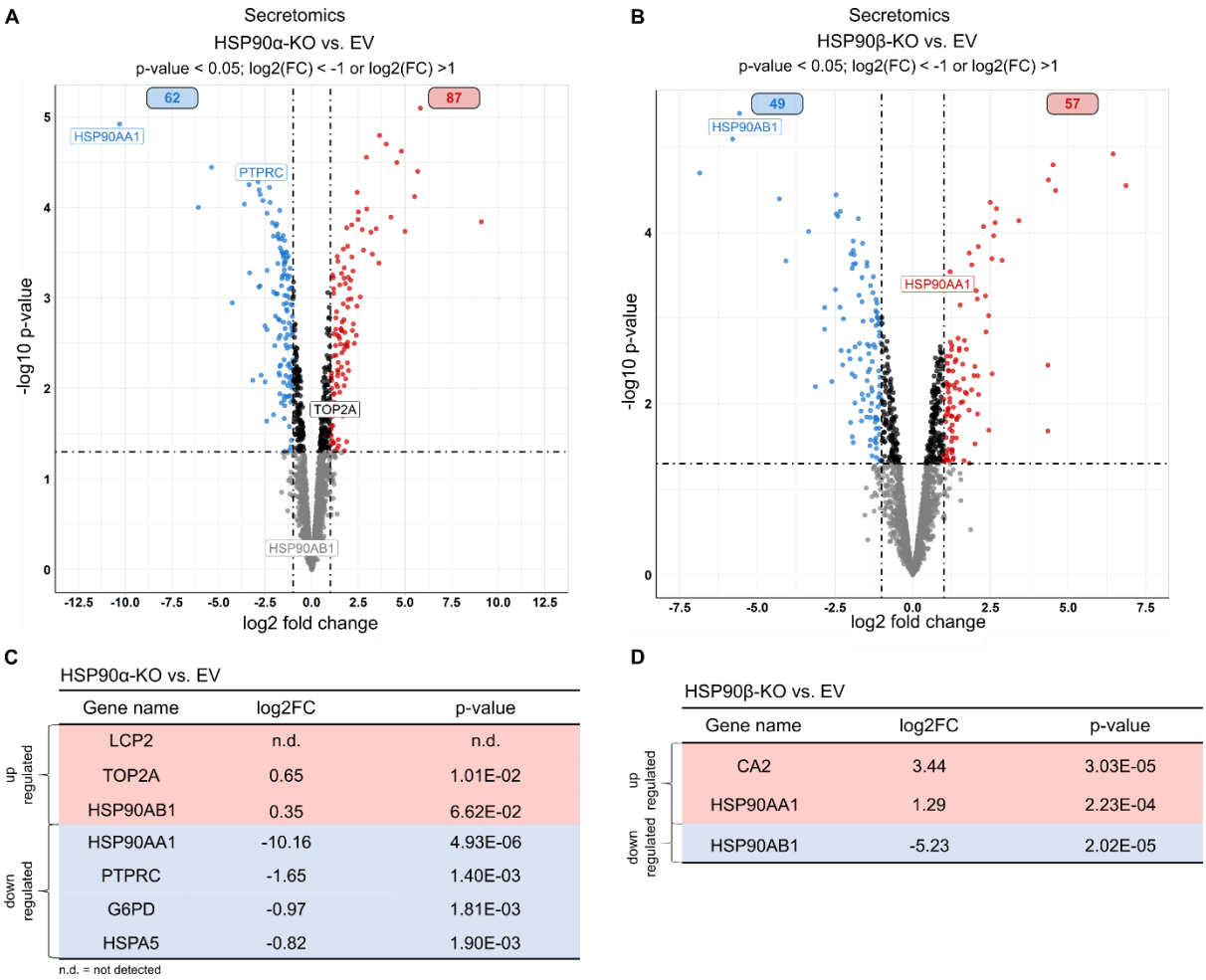


C

HSP90α-KO vs. EV

| | Gene name | log2FC | p-value |
|---|---|---|---|
| up regulated | LCP2 | n.d. | n.d. |
| up regulated | TOP2A | 0.65 | 1.01E-02 |
| up regulated | HSP90AB1 | 0.35 | 6.62E-02 |
| down regulated | HSP90AA1 | -10.16 | 4.93E-06 |
| down regulated | PTPRC | -1.65 | 1.40E-03 |
| down regulated | G6PD | -0.97 | 1.81E-03 |
| down regulated | HSPA5 | -0.82 | 1.90E-03 |

n.d. = not detected

D

HSP90β-KO vs. EV

| | Gene name | log2FC | p-value |
|---|---|---|---|
| up regulated | CA2 | 3.44 | 3.03E-05 |
| up regulated | HSP90AA1 | 1.29 | 2.23E-04 |
| down regulated | HSP90AB1 | -5.23 | 2.02E-05 |

**Figure 31: Secretome analysis to identify differences between K562 HSP90 KO and EV cell lines.**

Volcano plots of the significantly (p-value < 0.05; log2(FC) < -1 or log2(FC) > 1) up- or down-regulated proteins in (**A**) HSP90α-KO cells and (**B**) HSP90β-KO cells, in comparison to EV control cells. Grey dots represent genes that are not significantly regulated, while black dots represent significantly regulated genes below the log2(FC) threshold. Blue and Red dots represent significantly downregulated and upregulated proteins, respectively.

Comparing the secreted proteins with previously analysed transcriptome and proteome in the cells, consistent downregulation of HSP90AA1 and PTPRC was observed. Furthermore, a consistent upregulation of TOP2A was detected in the HSP90α-KO cell lines.

### 4.1.8.4 Investigating PTPRC (CD45) and LCK signaling

PTPRC was consistently downregulated in RNA sequencing data, the proteome, and in the secretome of HSP90α-KO cells. PTPRC, in the following referred to as CD45, is a transmembrane protein that is predominantly expressed in hematopoietic cells and functions as a tyrosine phosphatase, which is essential for regulating the balance of protein phosphorylation.[182]

Extracellular antibody staining using a CD45-APC tagged antibody and subsequent FACS analysis was performed to validate lower levels of the surface protein CD45. Compared to the histogram of the stained K562 EV control cells, the peak of the HSP90α-KO clones was shifted to a lower signal (Figure 32A). For the KCL-22 HSP90α-KO clones C10 and C14, a small shift to a lower signal could be observed, whereas no shift for C15 could be observed (Figure 32B).

As an orthogonal approach, CD45 protein levels were explored *via* WB analysis. It was validated that the CD45 protein level in the K562 and KCL-22 HSP90α-KO clones was strongly reduced compared to the control cells. Since CD45, with its phosphatase activity, can dephosphorylate and thereby activate or inactivate proteins of the SRC family, effector proteins were investigated.[183]

The total level of SRC was slightly reduced in the HSP90α-KO clones in both cell lines. Furthermore, there was a distinct increase in the p-SRC$^{Y416}$ (activating phosphorylation) level in KCL-22 cells. In the K562 cells, the phosphorylated species could not be detected. For the tyrosine kinase LYN and p-LYN$^{Y507}$ (inactivating phosphorylation), no altered expression could be observed in both cell lines.

For the protein kinase LCK, a very low expression level was found in both cell lines and only a slight increase of total LCK was detected in the KCL-22 HSP90α-KO cells. Investigation of the inactivating phosphorylation p-LCK$^{Y505}$ revealed a slight increase in the K562 HSP90α- KO cells and a strong increase in the KCL-22 HSP90α-KO cells. Investigation of the activating phosphorylation p-LCK$^{Y394}$ revealed no differences in the K562 cells, but a strong increase in the KCL-22 HSP90α-KO cells (Figure 32C-D).

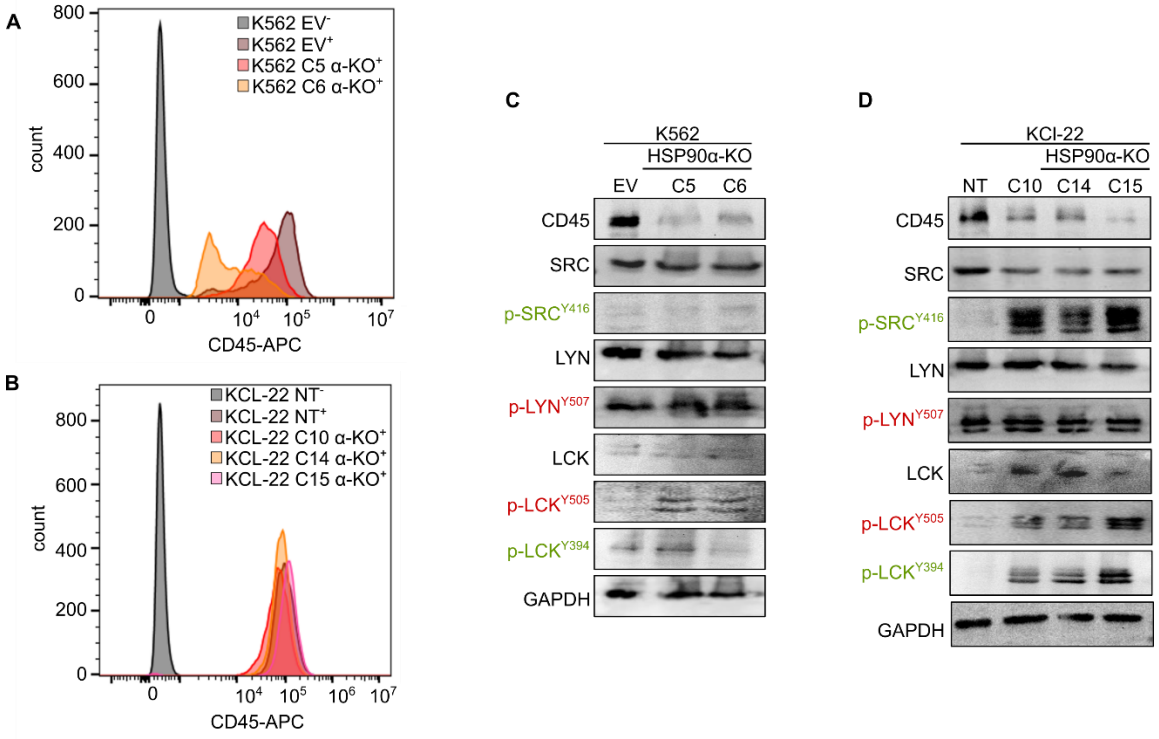


**Figure 32: FACS data of CD45 stained K562 and KCL-22 cells and downstream signalling analysis of CD45.** K562 EV and K562 HSP90α-KO cells (**A**), KCL-22 NT and KCL-22 HSP90α-KO cells (**B**) were stained with CD45-APC conjugated antibody and analysed *via* FACS. K562 HSP90α-KO cells (**C**) and KCL-22 HSP90α-KO cells (**D**) were analysed for the downstream SRC family proteins of CD45 *via* WB. Green-marked entities represent activating phosphorylation sited, and red-marked entities represent inactivating phosphorylation sites.

To sum up the observations for CD45 and downstream signaling analysis, a strong and consistent downregulation of CD45 in K562 and KCL-22 cell lines could be detected, which was in line with previously observed transcriptomic and proteomic data. Furthermore, downstream analysis revealed an increased level of p-LCK$^{Y505}$.

## 4.2 Characterization of small molecule HSP90 inhibitors

### 4.2.1 Identification of C-terminal HSP90 dimerization inhibitors

Selective targeting of HSP90 with small molecules, especially with C-terminal inhibitors, offers a promising approach in tumour therapy. The rational development and evaluation of the peptidomimetic aminoxyrone (AX) demonstrated the efficacy of this inhibitor class *in vitro* and *in vivo* using CML cell lines and patient-derived CML cells and no induction of HSR.[75] The efficacy of AX is based on the ability to fold into a unique $2_8$-helical conformation, whereby the α-aminoxy hexapeptide can mimic the HSP90 dimerization hot spot residues (I688, Y689, I692, and L696), which localize on α-helix H5 and account for most of the protein dimerization energy.[75] Dimerization is essential for the activity of HSP90. Based on this knowledge, small molecule inhibitors were subsequently designed and synthesized by the working group *Gohlke* and *Kurz*, which should also address the HSP90 CTD dimerization interface. The following data presented for compound **1a** are published in *Bhatia, S. et. al*.[159]

For this purpose, a compound library based on a tripyrimidonamide scaffold was synthesized and subsequently, the cytotoxic ability against the leukemia cell line K562 was evaluated *via* CTG. The pre-selection was performed by colleagues from the working group *Bhatia*. Computational binding mode predictions showed that tripyrimidonamides could adopt the required confirmation and mimic the side chain orientation of an α-helix (Figure 33A). The lead structure of the first generation HSP90 CTD dimerization inhibitor **1a** revealed an IC50 value of 4.55 µM against the CML cell line K562 (Figure 33B, Entry 1). The tripyrimidonamide **1a** mimics the hot spots I688, I692, and L696. Subsequently, derivatives of **1a** were prepared, including compound **1b**, which was obtained by removing the benzoyl group from ring C of **1a** (Figure 33B, Entry 2). Compound **1b** was found to have enhanced antileukemic activity with an IC50 value of 2.26 µM against the CML cell line K562. Further biological studies showed that **1a** and **1b** also exhibit anti-proliferative activity against other leukemia subgroups, such as AML, B-ALL and patient-derived cells (data not shown). In general, **1b** showed increased activity over **1a**. Furthermore, the antileukemic activity of **1b** was shown in Imatinib-resistant K562 cells (data not shown). Neither compound induced HSR, indicated by no increase in HSP70, HSP40, and HSP27 (data not shown).

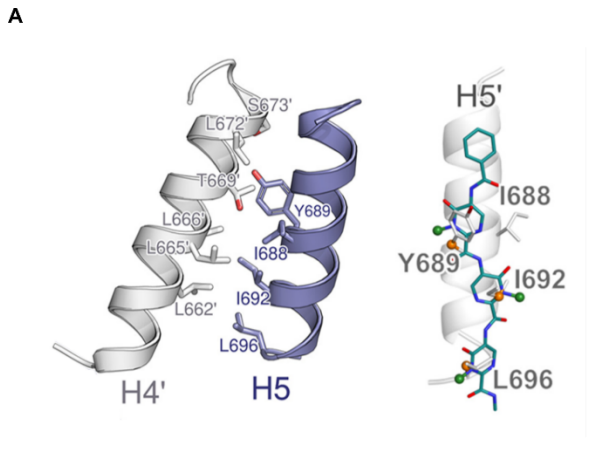


| entry | name | R | $IC_{50}$ K562 [µM] |
|---|---|---|---|
| 1 | **1a** (LSK82) | 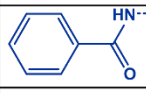 | 4.55 |
| 2 | **1b** (VWK147) | $H_2N$ ---- | 2.26 |

**Figure 33: Structure and predicted binding mode of α-helix mimetics.**

(**A**) Left: residues forming the CTD dimerization interface located on helices H4, H4′, H5, and H5′. Right: predicted binding mode of tripyrimidonamides at the C-terminal dimerization domain of HSP90α. Figure adapted from Bhatia, S. *et al.*[159] (**B**) $IC_{50}$ values for the K562 cell line after treatment with the indicated tripyrimidonamides **1a** and **1b**.

Due to the poor physicochemical properties of the two tripyrimidonamides, structural optimization was subsequently carried out, mainly to improve solubility and to simplify the structure. This was accomplished by introducing a basic N,N-dimethylaminoethyle group on ring A, as well as scaffold hopping from the tripyrimidonamide to the bipyrimidonamide and bipyrimidinamide structure type. The bipyrimidonamide **2**, functionalized with an *iso*-butyl (R1) and a *sec*-butyl (R2) side chain, showed comparable antileukemic activity with an $IC_{50}$ value of 2.26 µM (Table 22A). Finally, modification to the bipyrimidinamide **3** increased the activity, and an $IC_{50}$ value of 1.56 µM could be achieved (Table 22B).

**Table 22:** $IC_{50}$ values for the K562 cell line after treatment with (**A**) the bipyrimidonamide **2** and (**B**) the bipyrimidinamide **3**.

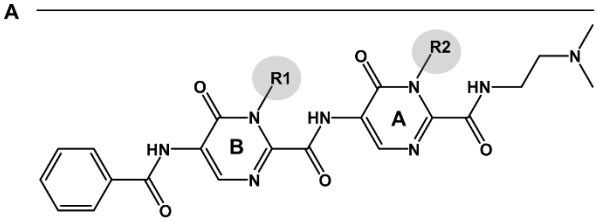


| entry | name | R1 | R2 | $IC_{50}$ K562 [µM] |
|---|---|---|---|---|
| 1 | **2** (VWK346) | 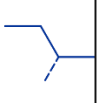 |  | 2.26 |

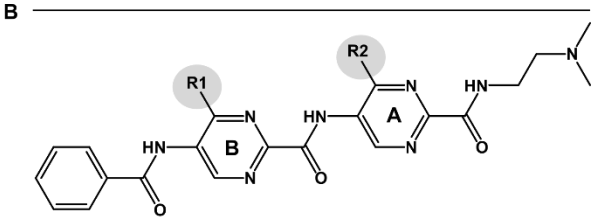


| entry | name | R1 | R2 | $IC_{50}$ K562 [µM] |
|---|---|---|---|---|
| 1 | **3** (VWK141) | 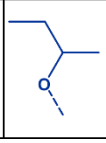 | 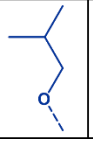 | 1.56 |

Taken together, small molecule HSP90 inhibitors based on α-helix mimetics could be synthesized with antileukemic activity against the CML cell line K562 in the low µM range. Scaffold hopping and structural modifications led to a 3-fold increased cytotoxic activity and improved biophysical properties.

### 4.2.2 Mode of action (MoA) of HSP90 CTD inhibitors

A thermal shift assay, which is used to detect the thermostability of a protein, was performed to investigate the mode of action of the compounds.[184] The heating of a recombinant protein leads to denaturation, which can be monitored using the fluorescent protein-dye SYPRO orange. This dye binds to hydrophobic side chains, which gets exposed during protein reorientation during denaturation. The addition of small molecules that bind to the target protein usually leads to stabilization and thus to an increase in the melting temperature (Tm).[185]

Measurement of HSP90 stabilization upon ligand binding in a thermal shift assay has previously been reported.[186]

The use of known N-terminal HSP90 inhibitors in combination with NTD-HSP90 leads to significant ($p < 0.0001$) stabilization and an increase in melting temperature ($\Delta Tm_{Geldanamycin}$: +3.36 °C; $\Delta Tm_{Tanespimycin}$: +3.64 °C; $\Delta Tm_{AUY922}$: +3.27 °C; $\Delta Tm_{PU\text{-}H71}$: +3.73 °C) (Figure 34A). The use of the known C-terminal HSP90 inhibitor CmA1 in combination with CTD-HSP90 leads to a stabilization and a significant ($p = 0.0046$) increase of the melting temperature by 4.24 °C (Figure 34B).

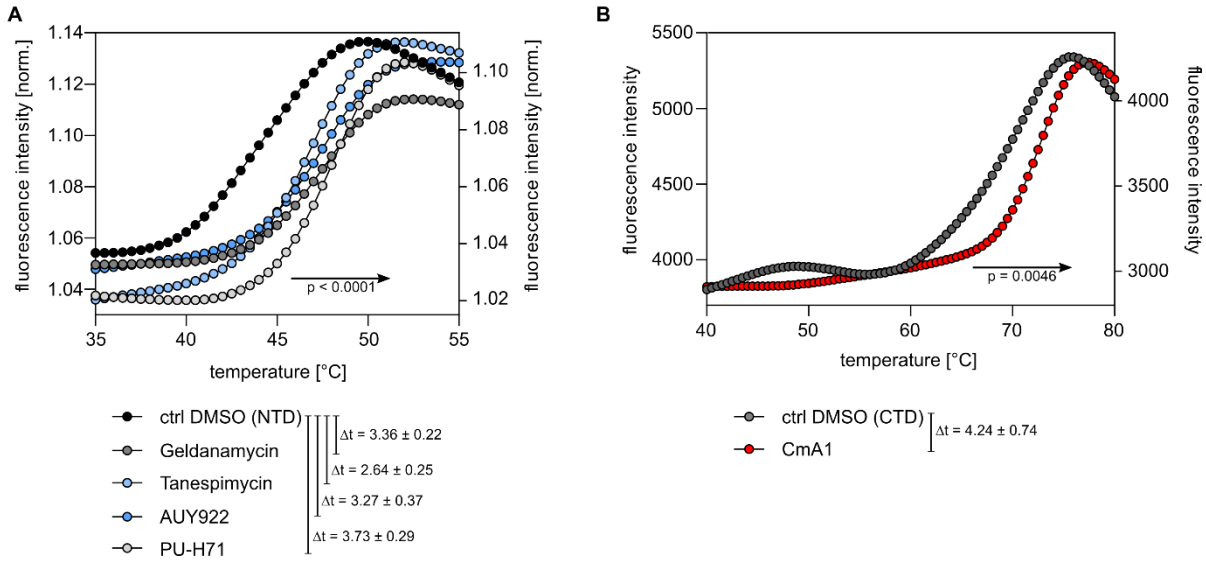


**Figure 34: Thermal shift assay with reference NTD/CTD HSP90i.**

(**A**) Thermal protein degradation curves using recombinant GST-NTD-HSP90 with N-terminal inhibitors Geldanamycin, Tanespimycin, AUY922 and PU-H71. HSP90 NTDi induced a significant positive shift, indicating protein stabilization. (**B**) Thermal protein degradation curves using recombinant His-CTD-HSP90 with the C-terminal inhibitor Coumermycin A1. CmA1 induced a significant positive shift, indicating protein stabilization. Results are shown as means (N = 6). P values were determined by unpaired t-test by comparing Tm values.

The use of the experimental inhibitors in combination with CTD-HSP90 led to a significant reduction in the melting temperature and, thus, to the destabilization of HSP90. Adding tripyrimidonamides **1a** and **1b** resulted in a negative shift of -8.45 °C and -8.43 °C (Figure 35A/B).

The use of bipyrimidonamide **2** resulted in a shift of -3.74 °C, and with adding bipyrimidinamide **3**, a shift of -6.07 °C could be observed (Figure 35B/C). The destabilization can be explained by the fact that the inhibitors presumably lead to a disruption of the CTD dimer.

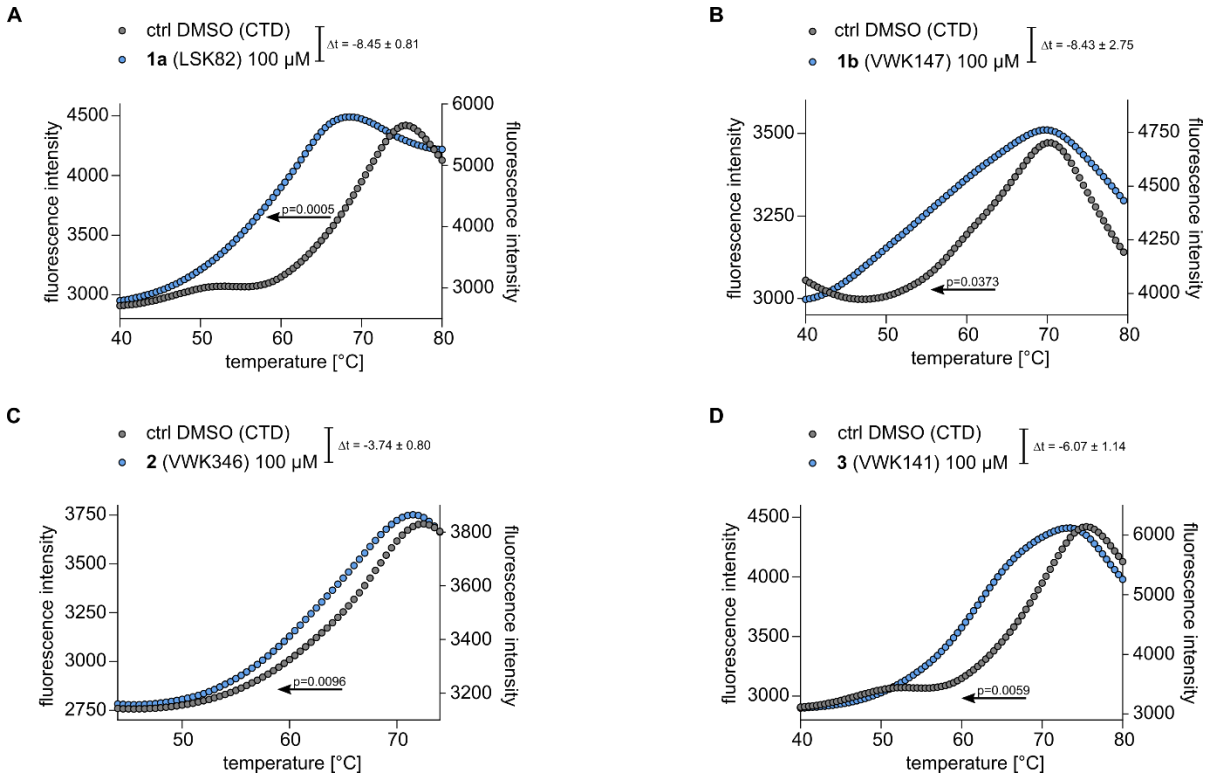


**Figure 35: Thermal shift assay with experimental CTD HSP90i.**

Thermal protein degradation curves using recombinant His-CTD-HSP90 with experimental inhibitors **1a** (**A**), **1b** (**B**), **2** (**C**) and **3** (**D**). All inhibitors induced a significant negative shift, indicating protein destabilization. Results are shown as means (N = 3). P values were determined by unpaired t-test by comparing Tm values.

The inhibitors were evaluated in an orthogonal assay to verify the assumption of dimer disruption. For this purpose, a crosslinker assay was established, which allows the chemical crosslinking of proteins and, thus, the analysis of the oligomeric state. The crosslinker used is bis(sulfosuccinimidyl)suberate ($BS^3$), which contains an amine-reactive N-hydroxysulfosuccinimide (NHS) ester at each end of an 8-carbon spacer arm. These esters can react with primary amines in the side chains of lysine residues and thus capture the dominant oligomerized state of the protein, despite denaturation during sample preparation. In the case of HSP90, an analysis should be made for monomers, dimers, and higher oligomers and visualization was done *via* western blot analysis. Assessment of HSP90 dimerization using $BS^3$ crosslinking has previously been reported.[187, 188]

Without the addition of $BS^3$, almost exclusively monomeric CTD-HSP90α was present. The addition of BS3 decreased the amount of monomeric HSP90α and increased the amount of dimeric and oligomeric (> 180 kDa) HSP90α. Treatment with the N-terminal inhibitor Tanespimycin caused no change because it does not bind to the C-terminal domain of HSP90α.

In contrast, treatment with the C-terminal inhibitor CmA1 led to an increase of monomers, and slightly reduced dimers and oligomers, as previously described in the literature.[188, 189]
Adding **1a** resulted in a decreased amount of HSP90α dimer and an increased amount of oligomers with increasing the concentration to 25 µM and 50 µM. Inhibitor **1b** showed a lower oligomer level and a distinct concentration-dependent reduction of dimers at a concentration of 20 µM and 50 µM. The compound-induced oligomerization of HSP90α with adding inhibitors **2** and **3** was markedly stronger, especially at a concentration of 50 µM. Inhibitor **2** showed an apparent reduction of dimers, whereas inhibitor **3** showed less dimer disruption. The monomer levels remained largely unaffected (Figure 36).

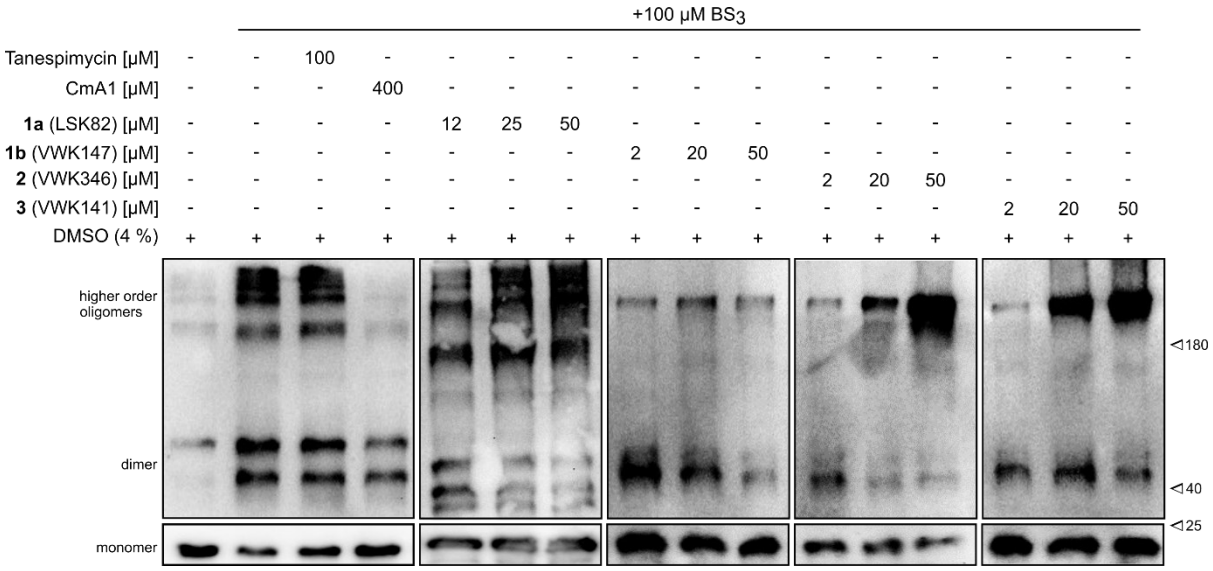


**Figure 36: BS[3] crosslinker assay followed by WB revealing HSP90α dimer disruption.**
Presented are HSP90 monomers (21 kDa), dimers (42 kDa), and higher order oligomers (> 180 kDa).

Evaluation of the experimental HSP90 inhibitors in the thermal shift binding assay showed that the compounds interact with the CTD of HSP90 and that binding to HSP90 lead to a reduction in thermostability. Further investigation using a crosslinker assay showed that the compounds lead to a reduction of HSP90 dimers and an enrichment of HSP90 oligomers. Taken together, these studies indicate that the novel HSP90 inhibitors address the CTD dimerization interface.

### 4.2.3 Characterization of CTD HSP90i in an HSP90 activity-based assay

The previously performed assays provided insight into the binding mode of the experimental inhibitors to HSP90. A thermal shift based binding assay showed that the α-helix mimetics bind to the CTD of HSP90 and lead to a dimer disruption as indicated by the negative thermal shift and the crosslinker assay. In the following, it should be investigated if the compounds inhibit HSP90 chaperone function. For this purpose, the luciferase refolding assay was established, which can be used to study the HSP90 folding capacity as previously described.[188, 190, 191]

For this assay, recombinant firefly luciferase was used, which in the folded, active state catalyses the ATP-dependent oxidation of D-luciferin under light emission. The chaperone-mediated renaturation of firefly luciferase has previously been reported. The concentration of HSP90 and HSP70 correlate with the ATP-dependent restoration of luciferase activity.[192]

The first step was to optimize the thermal denaturation of luciferase. After all buffer conditions and concentrations were optimized, the reference and experimental inhibitors were tested and related to the maximum renaturation under untreated conditions. An incubation of eight minutes at 38 °C was the optimal condition, and the luciferase activity dropped to about 2%. Many factors are essential for the successful renaturation of luciferase, including optimal ATP, $Mg^{2+}$ and $K^{+}$ concentration. Furthermore, the lysate is important, and in this setup, rabbit reticulocyte lysate was used. The special characteristic of this lysate is that it contains abundant quantities of heat shock proteins like HSP90, HSP70, and STI1/HOP. Furthermore, it contains relevant co-chaperones for protein folding. The measurable light emission is proportional to the luciferase activity and, thus, indirectly to the activity of HSP90.

The pre-incubation with the N-terminal HSP90i Tanespimycin, PU-H71, and AUY922 significantly ($p < 0.0001$, $p = 0.0002$ $p < 0.0001$) reduced the amount of renatured luciferase to 37%, 56%, and 35%, respectively. Incubation with the C-terminal HSP90i CmA1 significantly ($p < 0.0001$) reduced the amount of renatured luciferase to 11%. The maximal inhibition referred to in the following was calculated by subtracting the recovered luciferase activity [%] of the respective inhibitor from the maximal luciferase activity of 100 %.

Treatment with **1a** exhibited maximal HSP90 inhibition of 56% at 100 µM, and inhibitor **1b** achieved maximal HSP90 inhibition of 57% at 100 µM. Treatment with **2** achieved maximal HSP90 inhibition of 54% at 100 µM, and treatment with **3** achieved maximal HSP90 inhibition of 48% at 100 µM.

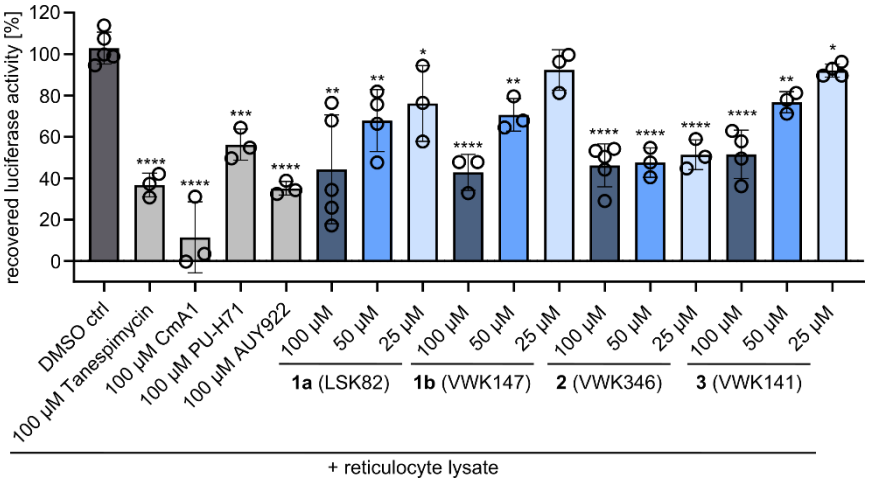


**Figure 37: Luciferase refolding assay revealing HSP90 on-target efficacy.**

Results are shown as means ± SD. P values were determined by a two-tailed unpaired t-test. *p ≤ 0.05; **p ≤ 0.01; ***p ≤ 0.001; ****p ≤ 0.0001.

Overall, all inhibitors induced a concentration-dependent inhibition of HSP90 (Figure 37). The luciferase refolding assay demonstrated that the experimental CTD HSP90 inhibitors lead to a decrease in luciferase refolding. These findings provided the assumption that the novel inhibitors, in addition to binding to HSP90, lead to inhibition of HSP90 chaperone activity.

### 4.2.4 High-throughput drug screening of compounds 2 and 3

The activity of the two most advanced compounds, **2** and **3,** were tested in a variety of leukemia cell lines and were compared to reference NTD HSP90i. For this purpose, the leukemia cell lines were plated on the compound library plates, incubated for 72 h and subsequently measured *via* CTG. Drug sensitivity scores (DSS) were then calculated, determined by the integral over the dose range exceeding a certain activity minimum. In some cases, the calculated $IC_{50}$ value may be identical, but the dose-response curves may show significant differences, making the DSS more meaningful. Subsequently, the differential DSS, calculated from the difference between the drug response quantified in patient cells or cancer cell lines and the average drug response of (healthy) control samples, was further calculated. This provides the opportunity to compare inhibitors with widely divergent efficacy and to identify those that are effective over a relatively broad therapeutic window.[193]

Healthy placental cord blood derived $CD34^+$ hematopoietic stem cells served as control cells. Analysis of Inhibitor **2** showed significantly ($p = 0.0068$) higher dDSS than the reference HSP90i in T-ALL cell lines. In B-ALL cell lines, there was a more significant ($p = 0.0002$) efficacy of Inhibitor **2**. The same trend was seen for inhibitor **3**, with significantly ($p = 0.0031$) higher dDSS in the T-ALL cell lines. Inhibitor **3** also showed significantly ($p < 0.0001$) higher dDSS in the B-ALL cell lines. Strikingly, both inhibitors showed much higher dDSS, especially in the SEM (relapse B-ALL, t(4;11) KMT2A-AFF1) and the NALL-1 (PAX5-$ETV6^+$) cell line (Figure 38A).

Furthermore, the two inhibitors were tested against a variety of PDX leukemia samples. Inhibitor **2** had a significantly higher dDSS in high-hyperdiploid B-ALL cells (HHD), ETV6-RUNX1 and T-ALL patient cells. In contrast, inhibitor **3** had significantly higher dDSS in BCR-ABL1, HHD and transcription factor 3 (TCF3)-rearranged patient cells (Figure 38B).

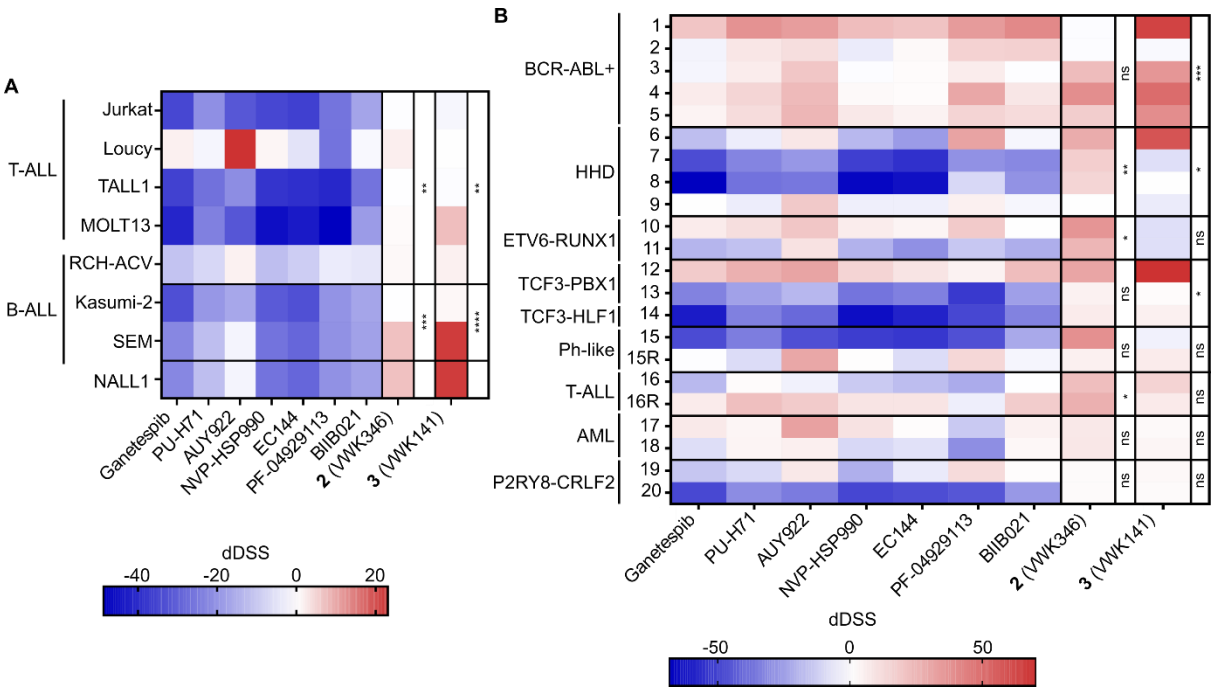


**Figure 38: Heat maps showing the differential drug sensitivity score (dDSS).**

(**A**) Heat map showed the dDSS of reference HSP90i and inhibitor **2** and **3** for T-ALL and B-ALL cell lines. (**B**) Heat map showing the dDSS of reference HSP90i and inhibitors **2** and **3** for PDX cell lines. P values were determined by a two-tailed unpaired t-test combining all dDSS from the reference Inhibitors and all dDSS from Inhibitor **2** and **3**. *p ≤ 0.05; **p ≤ 0.01; ***p ≤ 0.001; ****p ≤ 0.0001.

In summary, both compounds showed significantly higher dDSS in T-ALL and B-ALL cell lines compared to standard N-terminal HSP90 inhibitors. Furthermore, both compounds showed high antileukemic activity in PDX cell lines with different preferences to various genetic subgroups. In general, the bipyrimidonamide **2** and the bipyrimidinamide **3** offer a promising structural motif as novel CTD HSP90 inhibitors.

## 4.3 Characterization of HSP90 targeting PROTACs

### 4.3.1 Generation of K562-HiBiT cells *via* gene knock-in (KI)

To assess intracellular protein expression within a cellular context while minimizing interference with cellular processes, the implementation of HiBiT technology proves highly advantageous. This innovative approach enables the examination of proteins at their endogenous level, retaining their original promoter conditions. To achieve this, a CRISPR/CAS9 knock-in can be utilized to introduce an 11 bp tag to the target protein, facilitating its detection without disrupting cellular functionality.[194]

To generate stable HSP90α/β HiBiT-tagged K562 cells, the transient method *via* ribonucleoprotein (RNP) nucleofection was used. In this case, recombinant CAS9, two gRNAs for each isoform targeting a section at the C-terminal end of the proteins, and respective single-strand oligodeoxynucleotide (ssODNs), containing the HiBiT sequence was used (Figure 39A). The presence of the ssODN enables homologous recombination (HR) in cells after the CAS9-mediated DNA cut. The genetically modified cell pool was afterwards evaluated by WB analysis. To this end, a HiBiT antibody was used and successful insertion of the HiBiT-tag to the endogenous protein HSP90 could be validated, as the occurring band was at the right size with around 90 kDa (Figure 39B). Afterwards, the cells were monoclonal selected and growing clones were isolated. Genetically modified clones were validated using the Nano-Glo® HiBiT lytic detection system containing the complementing polypeptide LgBiT. By adding this reagent to the cells, the LgBiT unit interacts with the HiBiT unit at the protein and forms the luminescent NanoBit® enzyme. The resulting luminescence signal is proportional to the amount of HiBiT-tagged protein. Three clones were isolated from each pool, and it could be seen that unedited K562 cells and some clones do not show any signal (g1C1, g2C1, g2C2). For further experiments, one positive clone with HiBiT-tagged HSP90α (g2C2) and one clone with HiBiT-tagged HSP90β (g1C2) was chosen, and the insertion was validated *via* Sanger sequencing (Figure 39C).

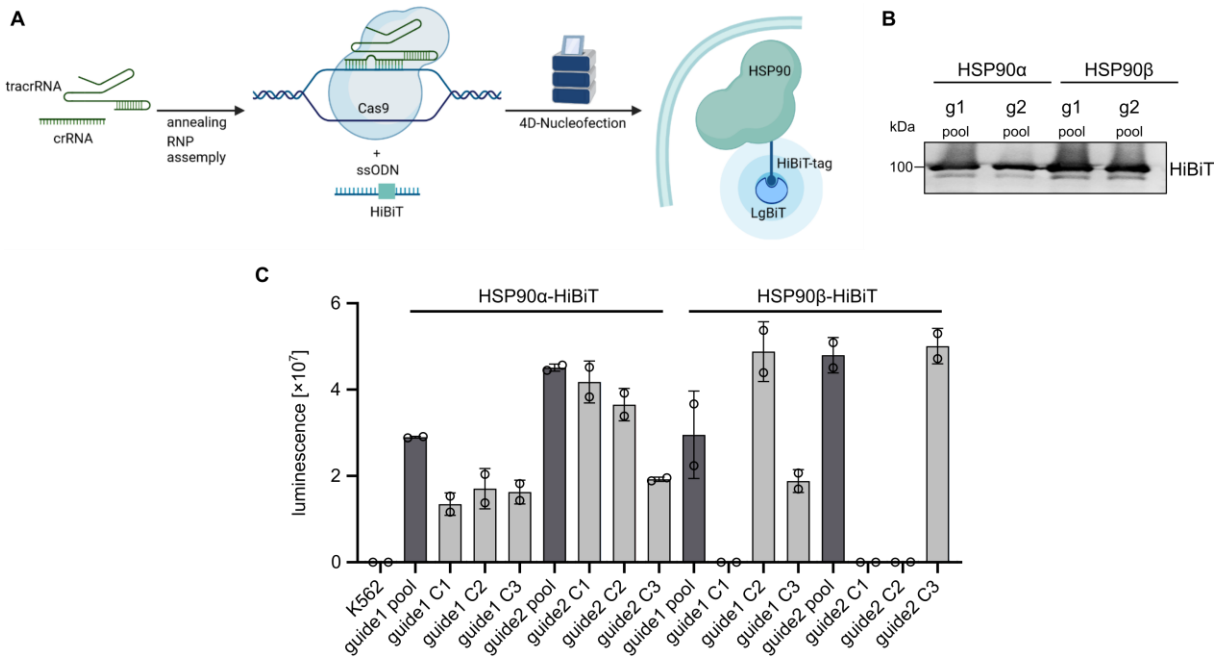


**Figure 39: Generation of HSP90-HiBiT tagged K562 cells *via* gene KI using RNP nucleofection.**

(**A**) Schematic representation of RNP nucleofection using the respective gRNAs and ssODN donor templates. Figure: Created with BioRender.com. (**B**) WB results with anti-HiBiT antibody showing a successful integration of the HiBiT-tag to the endogenous protein at the right size around 90kDa. (**C**) Nano-Glo HiBiT lytic detection assay of K562 pool cells compared to monoclonal cells. Positive clones g2C2 (HSP90α) and g1C2 (HSP90β) were Sanger-validated and selected for further experiments. Results are shown as means ± SD.

### 4.3.2 Selection and characterization of HSP90 PROTACs

PROTAC technology enables targeted protein degradation and can overcome problems associated with traditional protein inhibition. The design and synthesis of the PROTACs was done by the working group *Hansen*. The HSP90 inhibitor Geldanamycin was used as a starting point. Geldanamycin is an established N-terminal HSP90 inhibitor used as a fluorescence probe in commercial assays. The knowledge of the existing crystal structure of HSP90 with FITC labelled GM offers descriptive possibilities for a structure-based design. For the development of PROTACs, the inhibitor needs to be chemically modified, and the binding affinity and specificity must be maintained. The following data presented for compound **4** are published in *Wurnig, S. et. al.*[195] Starting from the crystal structure, it can be seen that the C-17 atom is solvent exposed and thus represents an ideal exit vector to add a linker. Subsequently, a series of potential PROTACs was synthesized with varying lengths of alkyl- or PEG-based linkers. Furthermore, a CRBN-recruiting, pomalidomide-derived ligand was chosen for the E3 ligase. The pre-selection, including Western Blot analysis and the fluorescence polarization (FP) assay, was performed by the colleague *Niklas Dienstbier*. K562 cells were treated with all potential PROTACs at 1 µM, incubated for 24h and harvested to perform a pre-selection. Quantitative JESS was used to evaluate the expression level of HSP90α, HSP90β and total HSP90. In general, degradation of both isoforms was found to be weak at 1 µM of PROTACs. The relatively strongest degradation was obtained with **4** (SW10-1-1).

Therefore, this compound with a PEG2-based linker was selected for further analysis (Figure 40A). To determine the on-target binding affinity, a fluorescence polarization assay was performed. This assay is based on the competition of FITC-labelled GM for binding to purified recombinant HSP90α. The results showed that **4** binds to the ATP binding pocket of HSP90α-NTD with only slightly lower affinity than GM. Subsequently, K562 cells were treated with the degrader **4** in a concentration range between 31 nM and 375 nM, incubated for 24h and harvested. Quantitative JESS was used to evaluate the expression level of HSP90α and HSP90β. HSP90α was strongly degraded mainly at low concentrations between 31 nM and 125 nM, with a maximum degradation of 56.8 % at 125 nM. With higher PROTAC concentration between 188 nM and 375 nM, HSP90α increased to 77 % of the initial level. HSP90β gradually degraded with increasing concentration of PROTAC until a plateau was reached with a maximum degradation of around 33 % (Figure 40B/C).

The effect of **4** was then tested in an orthogonal assay using the K562 HiBiT target lines. Cells were treated with the degrader **4** in a concentration range between 15 nM and 250 nM, incubated for 24 h and analyzed with the Nano-Glo® HiBiT lytic detection system. It was found that HSP90α was getting more degraded than HSP90β at low concentrations and that a maximum degradation of 40.58 % was reached at 125 nM. Subsequently, the level of HSP90α increased to 81 % of the initial level. The HSP90β level decreased continuously and reached a maximum degradation of 43.13 % at 250 nM (Figure 40D).

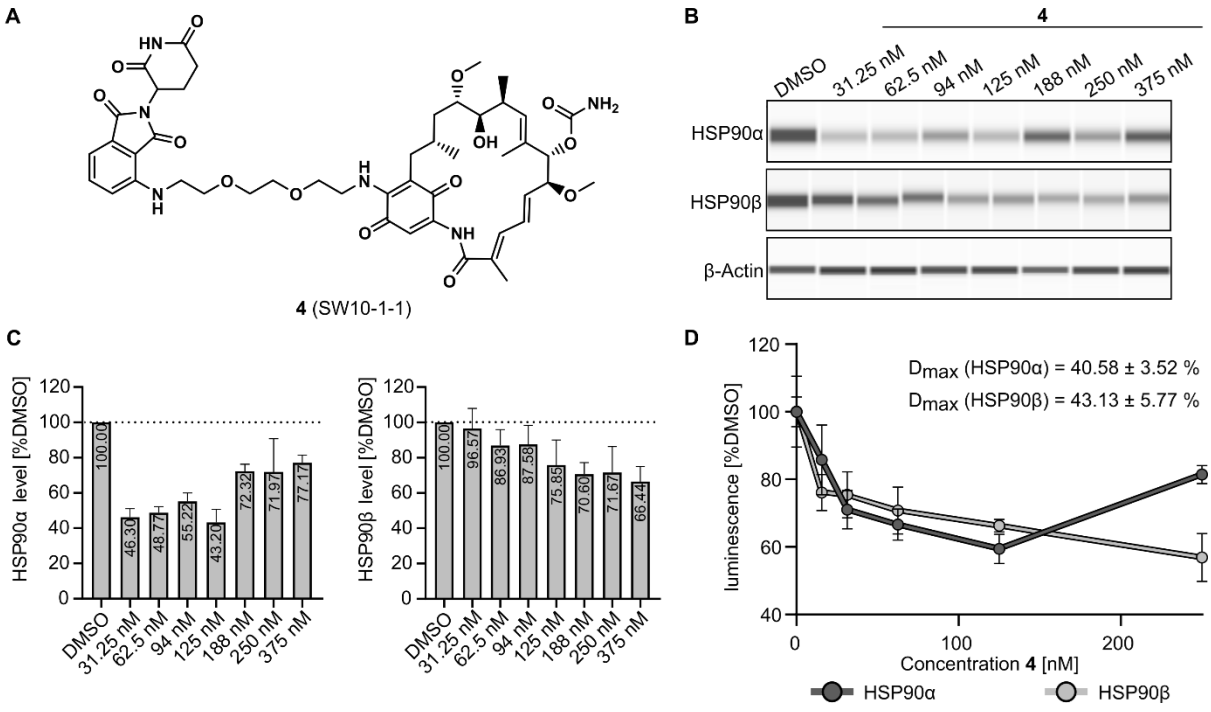


**Figure 40: Evaluation of 4 (SW10-1-1) in HSP90-HiBiT tagged K562 cell lines.**

(**A**) Chemical structure of **4**. (**B**) Representative image of JESS results shows HSP90α/β levels with increasing concentration of the degrader **4**. (**C**) Quantification of JESS results. Results are shown as means ± SD (N = 3). (**D**) Luminescence signal of HSP90-HiBiT tagged K562 cell lines treated with **4**.

Both methods gave comparable results, and the same trend that HSP90α gets strongly degraded at low concentrations and the level starts to increase again at higher concentrations of PROTAC and that HSP90β decreases more delayed at higher concentrations of PROTAC was observed. The evaluation of **4** in HSP90-HiBiT tagged K562 cell lines, including the treatment with the proteasome inhibitor MG132 and the CRBN ligand pomalidomide was done in collaboration with the Master student *Julian Hogenkamp*.

To exclude the possibility that **4** non-specifically induces a reduction of HSP90, a non-degrading control **nc-4** (nc-SW10-1-1) was synthesized. This control has a modification on the piperidine-2,6-dione moiety of the CRBN ligand by introducing a methyl group at the nitrogen, which enables the compound to still bind to HSP90 but not to CRBN. Evaluation by HiBiT lytic assay showed no degradation of HSP90β with 100 nM and 200 nM of **nc-4**. For HSP90α, it was observed that there is a significant upregulation at 100 nM to 140 % and at 200 nM to 145 %. Furthermore, the N-terminal HSP90 inhibitor Geldanamycin was used as a control. The treatment with Geldanamycin also resulted in a constant HSP90β level of around 100 % and a strong upregulation of HSP90α. The level of HSP90α increased to approximately 130 % (Figure 41A).

Competition experiments were performed to investigate the mechanism of PROTAC-induced degradation of HSP90. For this purpose, the CRBN ligand pomalidomide was used on the one hand and the proteasome inhibitor MG132 on the other. The HSP90-HiBiT tagged K562 cell lines were treated with 200 nM **4** and different concentrations of pomalidomide (100 nM to 2000 nM).

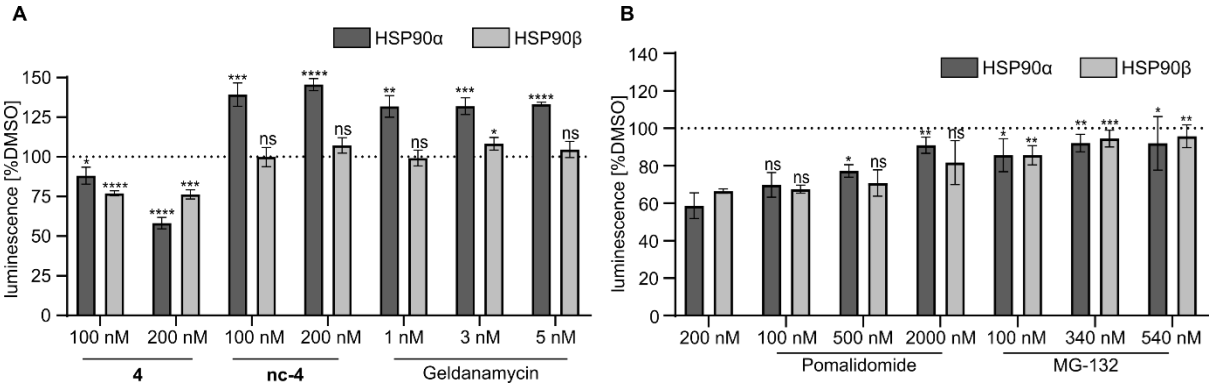


**Figure 41: Evaluation of 4 in HSP90-HiBiT tagged K562 cell lines**

(**A**) HiBiT lytic assay using **4**, **nc-4** and Geldanamycin. (**B**) HiBiT lytic assay using the proteasome inhibitor MG132 and the CRBN ligand pomalidomide to show that **4** degrade HSP90 *via* the ubiquitin-proteasome pathway and ternary complex formation. Results are shown as means ± SD of 3 independent experiments. P values were determined by a two-tailed unpaired t-test. *p ≤ 0.05; **p ≤ 0.01; ***p ≤ 0.001; ****p ≤ 0.0001.

The evaluation with the HiBiT lytic assay showed a gradual increase of HSP90 in a dose-dependent manner under the influence of pomalidomide. The HSP90α level could be almost restored and reached 90 % (Figure 41B).

Furthermore, cells were treated with 200 nM **4** and different concentrations of MG-132 (100 nM to 540 nM). Inhibition of the proteasome resulted in a significant increase in HSP90α/β. HSP90α reached a maximum of 95 % and HSP90β of 96 % from the initial value (Figure 41B). In summary, the most promising GM-based HSP90 PROTAC **4** effectively degraded both HSP90α and HSP90β *via* the ubiquitin proteasome pathway and ternary complex formation.

# 5. Discussion

Since discovering the anti-tumour activity of the natural product Geldanamycin, HSP90 has gained considerable importance as a cancer target. Although HSP90 gets abundantly expressed in all cells and is essential for cell survival, differences between HSP90 in cancer cells and HSP90 in non-transformed cells have been identified and have contributed significantly to the understanding and development of cancer drugs. In many tumour cells, induction of HSP90-mRNA and -protein occurs, resulting in increased HSP90 expression levels.[196, 197] Furthermore, tumour cells exhibit increased dependence due to more difficult survival conditions in the harsh tumour microenvironment. HSP90 is strongly activated in tumour cells, for example, by post-translational modifications, which can lead to different localizations of HSP90 by secretion into the extracellular space.[198, 199]

The distinct roles of HSP90α/β and the incorporation into a variety of complex signal networks is not fully understood.[46] A better understanding of the two cytosolic isoforms HSP90α/β will enable a contribution to developing new inhibitor classes and therapeutic approaches.

## 5.1 HSP90α/β isoforms in BCR-ABL1$^+$ leukemia

### 5.1.1 HSP90β-KO/KD induces upregulation of HSP90α in K562 cells

Most studies related to HSP90 are done with pan-HSP90 inhibitors or transient knockdown models, which address both cytosolic isoforms equally. Studies that address HSP90α/β isoform-specific roles, for example, concerning client proteins, use isoform-selective HSP90i or transient knockdown approaches. In this work, therefore, HSP90α and HSP90β isoform-specific knockout models were generated and biologically characterized in leukemia-relevant cell lines using CRISPR/CAS9 technology.

It was shown that the loss of HSP90α does not affect the HSP90β level, whereas the loss of HSP90β induces overexpression of the HSP90α isoform at the mRNA and protein levels (Figure 9C/D and 10C/D). The stress-inducible HSP90α isoform can be regulated much more rapidly than the HSP90β isoform because of the 5′ flanking sequences that contain multiple heat shock elements and are involved in the inducible gene expression of HSP90α.[200] Therefore, it was expected that the cells would counteract the stress of HSP90β deletion and compensate for the loss by upregulating HSP90α to maintain the total HSP90 level. A more detailed characterization of the effect of the knockouts on HSR showed that not only HSP90α was upregulated in K562 cells but also HSF1, HSP70, and HSP40 (Figure 11C). Accordingly, HSR was shown to be an HSP90β-isoform-specific response. Nevertheless, the induction of HSR in the HSP90α-KO cells was still possible and as strong as in the control cells, mainly due to the overexpression of HSP70 (Figure 11D/E).

HSP90-KD models in K562 cells further showed that the upregulation of HSP90α in the HSP90β-KO cells was not a time-dependent effect, as there was also an upregulation of HSP90α and HSP70 in the HSP90β-KD cell lines already after 96 h and 192 h on protein level (Figure 13C/E).

Interestingly, no changes in the expression of previously reported HSP90-isoform-dependent client proteins, such as CDK4, CDK6, and SURVIVIN, were observed (Figure 12A/B). With HSP90-isoform selective inhibitors, downregulation of client proteins could be observed in previously reported studies.[50] This suggests that the generation of an HSP90-KO causes a long-term adaptation that involves the acquisition of the functions of the other isoform. Inhibitor treatment may not result in compensation due to the short response time. This strong compensatory ability of the two HSP90 isoforms has been described previously.[201]

### 5.1.2 HSP90α-KO leads to faster proliferation *in vitro*

The *in vitro* characterization of the K562 and KCL-22 HSP90-KO cell lines revealed a significantly faster proliferation of HSP90α-KO cell lines and a different colony formation capability (Figure 15A, 16, and 17).

This can be explained by the decisive role of HSP90β in stabilizing BCR-ABL1 and maintenance of the localization in the cytoplasm. The CC domain of BCR-ABL1 can bind to HSP90β and, when bound, prevents the transport of BCR-ABL1 into the nucleus. Nucleus-trapped BCR-ABL1 leads to reduced proliferation and apoptosis.[162] In the case of HSP90α-KO cell lines, only HSP90β is available in the cells, resulting in increased stabilization of BCR-ABL1. This leads to increased activation of BCR-ABL1 tyrosine kinase in the cytoplasm. In line, Western blot analysis revealed increased BCR-ABL1 expression and enhanced downstream signalling *via* p-STAT5a and p-CRKL (Figure 14).

Another explanation for the increased proliferation of HSP90α-KO cell lines could be the lower levels of CD45 tyrosine phosphatase. This transmembrane protein is mainly expressed by hematopoietic cells and can activate or inactivate various signalling processes.[202] Using RNA sequencing, mass spectrometry and secretome analysis, a consistent down-regulation of CD45 was identified (Figure 25A, 28A, and 31A). Downstream analysis revealed that this leads to increased levels of activated p-SRC$^{Y416}$ due to decreased dephosphorylation by CD45 (Figure 32D). Activated SRC (p-SRC$^{Y416}$) can then facilitate cell survival *via* AKT or induce enhanced proliferation *via* MAPK signalling. An increased AKT level could also be observed in the HSP90α-KO cell lines (Figure 14A).

Another factor that has an impact on proliferation is LCP2. Lymphocyte cytosolic protein 2 was consistently upregulated at the mRNA and protein levels in the HSP90α-KO cells. It was present 6-fold higher on mRNA and 17.5-fold higher on protein level, making it the strongest and most significant hit in mass spectrometry analysis (Figure 25A and 28A).

Activation of LCP2 can lead to various downstream responses, including activation of the MAPK signalling cascade.[203] These results align with the results found by fGSEA and Cluster Profiler analysis of RNA sequencing data, where the MAPK signalling cascade, including ERK1/ERK2 signalling, was upregulated in the HSP90α-KO cell lines (Figure 26A/C). Likewise, GSEA showed enrichment of the FcεRI-mediated MAPK activation gene set (Figure 27B). Taken together, activation of the MAPK signalling cascade leads to migration, differentiation, and proliferation. [204]

Alternatively, the *in vitro* characterization of the K562 and KCL-22 HSP90β-KO cell lines demonstrated no alterations in proliferation when compared to their respective controls (Figure 15A and 17A). Nevertheless, the elimination of the HSP90β isoform resulted in a notable decrease in colony formation capability and reduced size of colonies (Figure 16 and 17B/C). Due to the absence of HSP90β in the cells, BCR-ABL1 gets less stabilized, which also leads to significantly weaker BCR-ABL1 signalling *via* p-BCR-ABL1. Furthermore, lower levels of STAT5a and weaker pSTAT5a signalling were observed, which is also due to the destabilization of $p210^{BCR\text{-}ABL1}$, because $p210^{BCR\text{-}ABL1}$ shows a significantly stronger activation of the STAT5 transcription factor.[205] Moreover, HSP90β-KO revealed an increase in the $P190^{BCR\text{-}ABL1}$ isoform (Figure 14). The observed reduction in both, the number and size of colonies, following the loss of the HSP90β isoform in BCR-ABL1$^+$ leukemia cells may serve as a plausible explanation for this phenomenon.

### 5.1.3 Prolonged survival of mice injected with HSP90α-KO cells

In addition to the *in vitro* characterization of the HSP90-KO cell lines, the cells were injected into NSG mice, and the engraftment was monitored. The *in vitro* behaviour of the cell lines is interesting for the analysis of molecular mechanisms and provides information about the response to genetic modification. *In vivo* characterization, on the other hand, is indispensable in terms of biological effects and the transfer and incorporation into the clinical context.

Based on the *in vitro* results, it was initially hypothesized that the HSP90β-KO cell lines might distribute more slowly due to reduced colony-forming ability, and the HSP90α-KO cell lines may distribute more rapidly due to increased proliferation. Interestingly, a slowed engraftment of the HSP90α-KO cell lines was observed in the mice (Figure 18). These results highlight the strong differences between the behaviour of the cell lines in cell culture and a living, complex organism and demonstrate the restricted transfer.

Among others, secreted proteins play a crucial role in this complex system. Secretome analyses of HSP90-KO cell lines showed, as expected that HSP90α is not secreted in HSP90α-KO cell lines (Figure 31A).

In non-modified cells, however, HSP90α is expressed extracellularly and is a mediator of tumour cell invasion and plays an important role in cell motility and cancer metastasis.[206-209] Furthermore, less HSPA5 protein, a member of the HSP70 family, was found in the secretome of HSP90α-KO cell lines (Figure 31C). In addition to HSP90α, extracellular HSP70 may also drive tumour metastasis and progression.[210, 211]

Taken together, the strong reduction of extracellular heat shock proteins, especially HSP90α, may have an inhibitory effect on the rapidity of tumour engraftment and distribution of leukemia cells in mice and, thus, a positive effect on survival.

Another important factor for the *in vivo* investigation is the anti-tumour immune response. Although the mouse line used is highly immunodeficient with a deficiency of B- and T-cells and a deficiency in functional NK cells, they have a reduced function of the innate immune system. This non-specific immune defence includes immune cells such as macrophages, dendritic cells, and neutrophils.[212] Accordingly, after injection into the mice, there may be a partial and attenuated immune response against the different HSP90-KO cell lines with altered effects.

LCP2 has emerged as a novel prognostic biomarker for immune cell infiltration into the tumour microenvironment.[213] As mentioned, LCP2 was upregulated in HSP90α-KO cells at the mRNA and protein levels (Figure 25A and 28A). *In vitro*, the increased LCP2 level may contribute to enhanced cell proliferation mediated *via* MAPK signalling. *In vivo* studies showed a positive correlation between LCP2 and tumour-infiltrating immune cells.[214] This was particularly evident for B-cells, $CD8^+$ T-cells and $CD4^+$ T-cells, which play no role in the NSG mice, but also for macrophages, neutrophils and dendritic cells found in the used mice. A high expression level of LCP2, as found in the HSP90α-KO cell lines, can thus lead to increased infiltration of immune cells, and thus decelerate tumour engraftment.

Another factor that plays an important role *in vivo* are the surface markers on the cells. Such antigen surface structures can subsequently influence a variety of signalling cascades intracellularly. In the HSP90α-KO cell lines, PTPRC, also called CD45, was downregulated in all proteogenomic analyses, after which western blot and FACS analyses confirmed the findings (Figure 29C, 31C, and 32). The studies in this work further revealed that the decreased level of CD45 resulted in an increased level of inactivated p-$LCK^{Y505}$ (Figure 32C/D). In the inactive state, LCK cannot initiate or drive pro-proliferative, migratory, and angiogenic processes.[215, 216] Thus, HSP90α-KO cell lines may be less capable of metastasis. This hypothesis is also supported by the fact that an increased level of CD45 is associated with a poor prognosis of the patients. It has been shown that CD45 acts as a risk factor for patients with AML.[217]

Accordingly, a lower level of CD45 may lead to a decreased distribution of K562 HSP90α-KO cell lines in mice and, thus, to prolonged survival.

### 5.1.4 Drug screening of HSP90α/β-KO cells

The process of drug screening enabled the identification of inhibitors targeting other classes of targets that are dependent on the HSP90α/β isoforms. Enhanced sensitivity played a pivotal role in recognizing potential synergistic partners during this screening. HSP90α-KO cells were found to be differentially sensitive (more resistant) to the drug class of tyrosine kinase inhibitors, including Barasertib (Aurora B kinase), Gilteritinib (TKI belonging to the subgroup of AXL inhibitors), Miransertib (AKT), and Everolimus (mTOR) (Figure 19A).

For the HSP90β-KO, HSP90 inhibitors, including Geldanamycin, PU-H71, AUY922, Ganetespib, and BIIB021, were the most striking. The HSP90β-KO cell lines were more sensitive towards the treatment with these inhibitors (Figure 19B). Since only HSP90α was still present in these cell lines, which was upregulated by the HSP90β-KO as compensation, indicating increased dependence, the cells are more sensitive to HSP90 inhibition. Interestingly, HSP90β-KO cell lines showed increased resistance to the HSP90 inhibitor KUNB31 (Figure 19B). This inhibitor is HSP90β specific and, therefore, cannot address its target.[50]

The most pronounced $IC_{50}$ fold change, indicating the greatest sensitization due to HSP90β-KO, was observed for Birinapant, a potent inhibitor of c-IAP1/2 and a less potent inhibitor of XIAP.[218] Interestingly, c-IAP1 and XIAP were shown to be upregulated in the HSP90β-KO cell lines, although c-IAP1 is an HSP90β-specific client (Figure 20B). Previous studies have shown that the loss of HSP90β leads to the degradation of c-IAP1.[219] Despite the complete loss of HSP90β in the KO cell lines, protein overexpression occurred in these studies. c-IAP1 and c-IAP2 regulate the pro-survival canonical NF-κB pathway, which became more important with increased dependency in the cell lines due to the HSP90β-KO. Inhibition with Birinapant leads to degradation of c-IAP1, caspase activation, and PARP cleavage.[220, 221]

### 5.1.5 CDK7i is a novel therapeutic vulnerability upon HSP90α loss

Another inhibitor identified by drug screening that showed increased sensitivity in the HSP90α-KO cell lines is THZ1, a CDK7 inhibitor (Figure 19A). In the HSP90α-KO cell lines, an increased level of CDK7, on the one hand, and an enhanced AR signalling in the transcriptome, on the other hand, could be found (Figure 21A and 27A). Furthermore, a synergistic behaviour between HSP90 and CDK7 inhibitors could be validated (Figure 21 and 22B/C/D).

CDK7 is part of the transcription factor IIH protein complex and plays a crucial role in AR signalling. First, CDK7 phosphorylates the C-terminal domain of RNA polymerase II, which leads to disruption of the CTD and the mediator and releases RNA polymerase II from the promoter-proximal pause.

Furthermore, CDK7 phosphorylates the kinase CDK9, which then, in complex with pTEFb, also phosphorylates the CTD of RNA polymerase II, ultimately inducing the release of RNA polymerase II from the promoter, allowing transcriptional elongation.[222]

Furthermore, CDK7 is involved in the modulation of AR activity *via* MED1. The presence of AR in the nucleus and binding to distal enhancers or super-enhancers causes recruitment of the mediator complex, which interacts with RNA polymerase II and the preinitiation complex, including TFIIH. This leads to chromatin looping to the promoter and ultimately promotes transcription.

To fulfil its role as a transcription factor in the nucleus, AR needs to undergo nuclear trafficking. Under normal circumstances, this occurs through binding a ligand and the subsequent dimerization of AR and disruption of the HSP90-AR complex.[223] HSP90 generally leads to the stabilization of AR in the cytoplasm. However, the exact mechanism is not entirely understood, and possibly dissociation of the AR-HSP90 complex, even ligand independently, already leads to the nuclear transport of AR.[224] This ligand-independent reaction could be induced by HSP90-KO or HSP90 inhibition. Loss of HSP90α thus can lead to an increased accumulation of AR in the nucleus. Activation of this pathway can induce pro-survival effects, which can be circumvented by CDK7 inhibition (Figure 42).

Furthermore, there is a link to the expression of heat shock genes, as the expression is controlled at the level of polymerase II elongation. In response to heat shock, for example, induced by HSP90 inhibition, polymerase II gets recruited to the heat shock loci.[225, 226] Inhibition and inactivation of CDK7 thus results in decreased levels of transcriptionally active polymerase II along heat shock genes, as the kinase is essential for activation.[227]

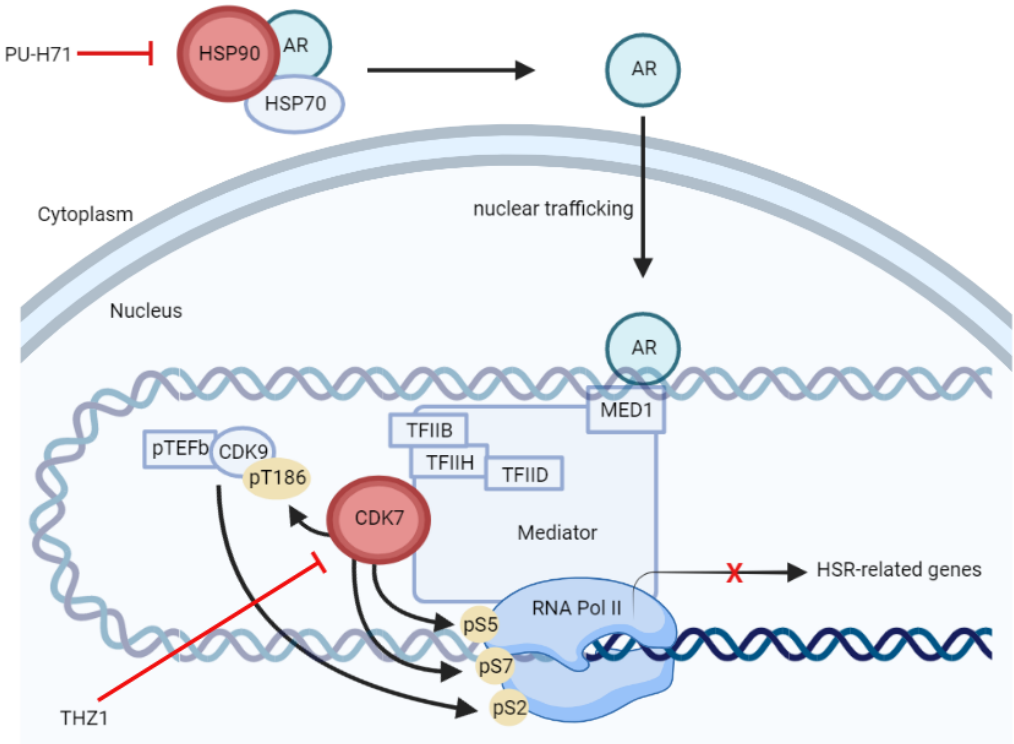


**Figure 42: Proposed mechanism of how co-targeting of HSP90α and CDK7 can result in a synergistic effect.** Dual targeting of HSP90 and CDK7 results in the inhibition of RNA polymerase II elongation and no increasement in HSR-related proteins, allowing HSP90i to act more effectively and synergistically with CDK7i. Figure: Created with BioRender.com, modified from X. Li et. al.[228] and used under CC BY 4.0.

Co-targeting of HSP90α and CDK7 showed a complete loss of phosphorylated RNA polymerase II and no induction of HSR-related genes, like HSP90α, HSP70, and HSP40 (Figure 23 and 24). In contrast, single treatment with PU-H71 caused the induction of HSR as an escape mechanism, which the combinational treatment could suppress. Thus, co-targeting of HSP90 and CDK7 leads to a synergistic effect and offers a promising approach to overcome HSP90i-associated resistances and limitations.

Furthermore, the investigations in this work showed that the combination approach with PU-H71 and THZ1 provides a treatment option in refractory or relapsed leukemia cells of patients with clinically relevant BCR-ABL1 mutations. Also, a synergistic behavior in TKI resistant cell lines (Imatinib and Ponatinib) could be measured, allowing the potential use as secondary treatment after failure of TKI inhibitors or to overcome TKI-induced mutations in BCR-ABL1 (Figure 21B/C/D). In PBMCs from healthy individuals, the combination treatment did not respond (Figure 22E). This offers a promising therapeutic window for the use of the inhibitors in further *in vivo* applications.

## 5.2 Small molecule HSP90 C-terminal dimerization inhibitors

The targeting of HSP90 with small molecules has received considerable attention in recent years, especially regarding its use in various subtypes of leukemia with poor prognosis. The importance increased due to the role of HSP90 as a chaperone for clients, such as BCR-ABL1, relevant in CML or B-ALL.[114]

Despite the development of various N-terminal HSP90i, difficulties in advanced clinical trials continue to occur due to side effects, such as ocular toxicity.[229] In general, the use of the NTD HSP90i class causes the initiation of HSR.[138, 139]

Addressing HSP90 *via* the C-terminal domain offers a promising approach to circumvent the drawbacks of NTD HSP90 inhibitors. Previous studies showed that C-terminal HSP90 inhibitors exhibit anti-proliferative activity in prostate, breast cancer, and ewing sarcoma tumour cell lines *via* allosteric inhibition.[188, 230] Subsequently, the first protein-protein interaction HSP90 CTD inhibitor was developed by cooperation partners, which disrupts the dimerization of HSP90. The peptide-based inhibitor AX further showed no initiation of HSR and promising efficacy in Ph-like and BCR-ABL1$^+$ BCP-ALL cell lines, among others.

The small molecule HSP90i in this work were designed to bind to the C-terminal domain of HSP90. They were synthesized to prevent the dimerization necessary for HSP90 activity by mimicking the HSP90 dimerization hot spot residues similar to AX.[231]

As an initial small molecule inhibitor, compound **1a** was obtained, which showed an antileukemic activity of 4.55 µM in K562 cells (Figure 33B). Small modifications resulted in **1b** with a two-fold improved activity of 2.26 µM in K562 cells (Figure 33B). In a thermal shift assay, the experimental inhibitors **1a** and **1b** induced a strong negative shift of -8 °C (Figure 35A/B).

Accordingly, the compounds did not stabilize HSP90-CTD as initially expected and as observed with CmA1 but destabilized HSP90-CTD (Figure 34B). Therefore, a different MoA can be defined. In the apo state, HSP90-CTD forms a dimer, and the addition of the inhibitors results in a loss of stabilizing subunit interactions and disruption of the CTD dimer.[232] Interestingly, only one melting curve was observed after the addition of the inhibitors, which indicates either a complete disruption of the dimers and a complete presence of monomers or a non-specific destabilization. A non-specific effect is also indicated by the melting curve merely starting earlier, but the peak maximum does not shift strongly.

Furthermore, experimental inhibitors **1a** and **1b** show a loss of dimers in the BS3 crosslinker assay (Figure 36). Compound **1a** also induces a strong oligomerization of HSP90 CTD to species even larger than the tetrameric form. Compound **1b** does not show this oligomerization. Both compounds inhibited the activity of HSP90 in a luciferase refolding assay, showing similar profiles with increased inhibitory activity with higher inhibitor concentrations (Figure 37). By scaffold hopping, bipyrimidonamide-based structures and bipyrimidinamide-based structures were synthesized. Initially, this did not improve the antileukemic activity and an $IC_{50}$ value of 2.26 µM was obtained for compound **2** in K562 cells (Table 22A). However, compound **3** showed a three-fold improvement in activity with an $IC_{50}$ value in the low µmolar range (1.56 µM) (Tabel 22B). Furthermore, introducing a basic N,N-dimethylaminoethyl group at the C-terminus of ring A improved the physicochemical properties of both inhibitors **2** and **3** regarding solubility. In the thermal shift assay, both experimental inhibitors produced a negative shift, which was weaker for compound **2** at -3.74 °C and again improved for compound **3** at -6.07 °C (Figure 35C/D). Both compounds induced a dimer loss in the BS3 crosslinker assay and a strong oligomerization of HSP90 CTD to species larger than the tetrameric form (Figure 36). Overall, the advanced series of inhibitors was also shown to inhibit the dimerization of HSP90. Compound **3** inhibited the activity of HSP90 in a luciferase refolding assay and showed increased inhibitory activity with increasing inhibitor concentration, like compounds **1a** and **1b**. Compound **2**, on the other hand, showed strong inhibition of HSP90 already at 25 µM, which could not be significantly increased by increasing the concentration (Figure 37). The drug screening showed that the experimental inhibitors **2** and **3** have significantly increased and thus improved dDSS compared to the reference HSP90-NTD inhibitors in ALL cell lines (Figure 38A). Furthermore, they were also convincing for PDX samples with different genetic lesions (Figure 38B). For example, inhibitor **2** showed significantly increased efficacy in ETV6-RUNX1$^+$ cells (most common inter-chromosomal alteration with 25%), and HHD cells (in 30 % of all pediatric BCP-ALL) have particular significance in childhood BCP-ALL. Inhibitor **3**, however, showed improved efficacy in BCR-ABL1$^+$ leukemia.

This is the case even though the experimental CTD HSP90i show significantly lower $IC_{50}$ values and can be explained by the fact that the experimental inhibitors show no or very low activity against the healthy $CD34^+$ control cells. In contrast, the NTD HSP90i show partially increased toxicity. Thus, significantly better results can be achieved with experimental inhibitors **2** and **3**, as they have higher selectivity towards leukemia cells and offer an excellent therapeutic window.

## 5.3 HSP90 PROTACs

Targeting proteins with PROTACs to modulate protein function *via* target degradation has gained significant importance in recent years and has already succeeded in clinical applications. Since the targeting of HSP90, especially with conventional NTD HSP90i, triggers HSR and leads to an upregulation of HSP90 itself, PROTAC technology offers promising opportunities. Selective degradation of HSP90 may allow circumvention of the side effects that occur with small molecule inhibitors. To date, there has been only one study concerning HSP90 that has designed and evaluated BIIB021-based PROTACs. This study investigated the degradation of total HSP90, and no isoform-specific classification or specification was performed.[233] In this work, HSP90 PROTACs were designed based on Geldanamycin and induced degradation using a CRBN-recruiting, pomalidomide-derived ligand.

The most promising degrader **4** showed binding to HSP90 in mechanistic studies *via* FP-assay and degradation of HSP90α and HSP90β. Isoform-specific analysis showed that at lower concentrations (< 125 nM), HSP90α gets primarily degraded, whereas, at higher concentrations (> 125 nM), HSP90β gets more degraded (Figure 40B/C). In this concentration range, an increased HSP90α level was also detected. Genetically modified HiBiT K562 cell lines showed the same trend in an orthogonal system (Figure 40D). Also, a specific degradation using a non-degrading control and degradation *via* the ubiquitin-proteasome pathway and the recruitment of CRBN could be confirmed (Figure 41). Furthermore, PROTAC **4** showed anti-proliferative activity in K562 cells, with an $IC_{50}$ value in the low µmolar range. This rather high value can be explained by the maximum degradation of HSP90α and HSP90β of only 40.58 % and 43.13 %, respectively. As shown in Chapter 4.1.1, an isoform-specific deletion *via* HSP90α- or HSP90β-KO is not lethal for the cells, and therefore cell death occurs due to a complete HSP90α/β deletion. Furthermore, it could be observed that the increase of PROTAC concentration, which induced a stronger degradation of HSP90β, resulted in higher levels of HSP90α (Figure 40B/C). These results show strong similarities to the findings obtained with the HSP90β-KO cell lines, which also upregulated HSP90α. This escape mechanism can also be observed upon treatment with small molecule inhibitors but is much more pronounced. The treatment with an NTD HSP90i results in a several-fold expression level increase of HSP90α, whereas PROTAC treatment still leads to a lower HSP90α level.[234]

Overall, this work was the first demonstration of a Geldanamycin-based HSP90 degrader and its evaluation concerning HSP90α and HSP90β.

# 6. Outlook

## 6.1 HSP90α and β isoforms in BCR-ABL1$^+$ leukemia

In this section, the generation of genetic knockout models for both HSP90 cytosolic isoforms (α and β) was undertaken for the first time, aimed at deciphering the precise roles of these isoforms in BCR-ABL1$^+$ leukemia cell lines. Numerous *in vitro* and *in vivo* experiments, proteogenomic profiling, including RNA sequencing, mass spectrometry, and secretome analysis, allowed a detailed characterization of the isoform-specific deletions.

Future investigations could explore the reversibility of HSP90α/β-KO-specific effects on proliferation, colony-forming ability, and the expression of effector and client proteins. To perform so-called rescue experiments, it would be necessary to genetically modify the KO cell lines by introducing the corresponding HSP90 isoform. This approach facilitates the subsequent examination of whether the wild-type phenotype can be restored, providing crucial support for the hypothesis that the observed phenotype is a consequence of genetic impairment.

HSP90α-KO also resulted in prolonged mouse survival and slowed tumour cell distribution. Proteogenomic profiling revealed that one factor affecting tumour metastasis and progression was the loss of HSP90α secretion. Furthermore, the upregulation of LCP2 levels was observed upon the ablation of the HSP90α isoform. This upregulation may contribute to an increased infiltration of immune cells, thereby potentially impeding tumor spread. Investigation of immune activation upon loss of HSP90α isoform should be conducted through the utilization of immunocompetent mouse models.

In this work, drug screening of HSP90-KO cell lines identified an approach for the combinatorial treatment of BCR-ABL1$^+$ cell lines. Increased sensitivity of HSP90α-KO cell lines to the CDK7 inhibitor THZ1 was found. Further studies showed that combining the HSP90 inhibitor PU-H71 and THZ1 resulted in synergistic lethality in the cell lines. This is based on suppressing the resistance and escape mechanism, the induction of HSR mediated *via* treatment with PU-H71 alone. In the following, it would be interesting to investigate whether other CDK7 inhibitors in advanced clinical trials, such as (covalent CDK7i) YKL-5-124 and (non-covalent CDK7i) SY-5609, act synergistically in combination with HSP90 inhibitors and whether this is also due to suppression of HSR. Since the proposed mechanism is based on the activation of RNA Pol II, there would be another approach to verify this. Activation may also occur *via* phosphorylation by CDK9 (pS2) beside phosphorylation by CDK7 (pS5 and pS7). Thus, treatment with the CDK9 inhibitor AZD4573 could provide further insights into the underlying mechanism. In addition to the use of inhibitors, genetic knockdown or knockout approaches can also be used. For this purpose, generating and characterising CDK7 KD cell lines would be useful.

This would allow an even more precise delimitation, excluding and overcoming off-target effects and non-specificity of inhibitors. The next essential step involves in vivo tests, where leukemia cell engrafted mice would undergo treatment with the combination approach and be compared to those treated with a single reagent. SY-5609, a CDK7 inhibitor, and Pimitespib, an HSP90 inhibitor, would be suitable candidates for this experiment, given their advanced clinical trial phases.

Taken together, this study offers a comprehensive understanding of the roles and significance of the two cytosolic HSP90 isoforms. The identified differences in molecular signaling associated with HSP90 cytosolic isoforms (α and β) will significantly influence the future development of therapeutic strategies for addressing BCR-ABL1$^+$ leukemia characterized by abnormal HSP90 protein expression. Moreover, this research introduces an innovative approach by concurrently targeting HSP90 and CDK7 to overcome the HSR induction triggered by HSP90 inhibitors.

## 6.2 Small molecule HSP90 C-terminal dimerization inhibitors

This study introduces first-in-class HSP90 C-terminal dimerization inhibitors, representing a hitherto unexplored mechanism of action (MoA) within small-molecule HSP90 inhibitors. These experimental inhibitors have demonstrated noteworthy success in terms of their antileukemic activity. Nevertheless, the tripyrimidonamide-, bipyrimidonamide-, and bipyrimidinamide-based inhibitors (**1a**, **1b**, **2**, and **3**) have $IC_{50}$ values in the low µmolar range and are thus still several steps away from the $IC_{50}$ values of the NTD HSP90i. In this work, it could be shown that scaffold hopping and further structural modifications improved the inhibitors' activity and solubility. Therefore, research on new structural analogues is ongoing. In the following, it would be interesting to validate further the new structure analogues concerning MoA and to characterize the binding mode in more detail. For this purpose, it would be an option to perform co-crystallization experiments to obtain a crystal structure of HSP90-CTD with the bound inhibitor. Furthermore, it would be important to test the inhibitors for *in vivo* applications, including solubility- and dose-tolerance studies. Subsequently, leukemia-engrafted mouse models could be treated with these inhibitors to see if they reduce the tumour burden and prolong or improve the survival of the mice.

Recent research has primarily emphasized the development of HSP90β-selective inhibitors. However, this study reveals that selectively deleting or reducing HSP90β induces the HSR and upregulates HSP90α, potentially compromising the efficacy of HSP90 inhibitors and prompting an escape mechanism. Consequently, there is a need to characterize or specifically modify inhibitors for HSP90α selectivity. In summary, this work contributes to enhancing small molecule C-terminal dimerization inhibitors with antileukemic activity.

## 6.3 HSP90 PROTACs

A first-in-class series of GM-based HSP90 degraders was presented in this work. The most promising degrader showed a maximal degradation of 40.58 % of HSP90α and 43.13 % of HSP90β, and it could be validated that the degradation proceeds *via* ternary complex formation and the ubiquitin-proteasome pathway. In the future, it would be interesting to prepare other structure analogues to analyse whether the degradation activity can be improved using the GM-based HSP90 degraders. Moreover, obtaining optimized degraders that can keep HSP90α levels low would be very important, preventing the occurring escape mechanism. Furthermore, it would be interesting to investigate the biological effects of HSP90 degradation concerning HSP90 clients or co-chaperones. Functional assay, such as colony formation assay, could also be performed. Additionally, it would be important to evaluate the HSP90 PROTACs for *in vivo* applications. This would first require solubility and dose-tolerance studies since the PROTACs generally have a high molecular weight and, afterwards, efficacy studies.

# Attachment

## List of Figures

## List of Tables

# Author contributions to manuscripts

I. Title: Co-targeting HSP90 alpha and CDK7 overcomes resistance against HSP90 inhibitors in BCR-ABL1+ leukemia cells

Published: 06 December 2023 in Cell Death & Disease

Contribution: Melina Vogt shares first authorship. She collected data by performing western blots, JESS, synergy drug screening, library drug screening, FACS, and CFU assays. Furthermore, she generated the HSP90α/β-KO cell lines (K562, KCL22, and SUP-B15) *via* CRISPR/CAS9 gene Knockout and the siRNA mediated HSP90α/β-KD K562 cell lines and performed cell culturing and treatment. She further performed the statistical analysis of the data and prepared all figures (Figure 1-6; suppl. Figures 1-6).

II. Title: Development of a first-in-class small molecule inhibitor of the C-terminal HSP90 dimerization

Published: 27 April 2022 in ACS Central Science

Contribution: Melina Vogt performed the biochemical and biophysical characterization of the lead compound 5b by performing thermal shift assays, luciferase refolding assays, and crosslinker assays. In addition, she did the recombinant expression of h-HSP90α NTD protein (amino acids 9–236) in *E. coli*. She further performed the statistical analysis of the data and prepared the according figure panels (Figure 3b, 3d, 5a).

III. Title: Development of the first Geldanamycin-Based HSP90 Degraders

Published: 28 June 2023 in Frontiers in Chemistry

Contribution: Melina Vogt shares first authorship. She did the biological characterization of the lead compound 3a and the respective control nc-3a by performing NanoGlo lytic assays and JESS. Furthermore, she generated the HSP90α/β HiBiT-tagged K562 cell lines via CRISPR/CAS9 gene Knock-in and performed cell culturing and treatment. She performed the statistical analysis of the data, prepared the according figure panels (Figure 2-3), and wrote the original draft for the biological section.

# Literature


(1) Sterbefälle 2021 der ICD-10, Statistisches Bundesamt (Destatis), 2022. www .destatis.de/DE/Themen/Gesellschaft-Umwelt/Gesundheit/Todesursachen/Tabellen/gestorbene_anzahl.html Last access: 28.01.2024

(2) Macconaill, L. E.; Garraway, L. A. Clinical implications of the cancer genome. *J Clin Oncol* **2010**, *28* (35), 5219-5228. DOI: 10.1200/jco.2009.27.4944 From NLM.

(3) Robert Koch Institut, Zentrum für Krebsregisterdaten, Leukämien, ICD-10 C91-C95. https://www.krebsdaten.de/Krebs/DE/Content/Krebsarten/Leukaemien/leukaemien_node.htmll Last access: 18.01.2024

(4) American Cancer Society (2022, January 12). Key Statistics for Childhood Leukemia. https://www.cancer.org/cancer/leukemia-in-children/about/key-statistics.html Last access: 18.01.2024

(5) Swerdlow SH, Campo E, Harris NL, Jae ES, Pileri SA, Stein H, Thiele J (Eds.) WHO Classification of Tumours of Haematopoietic and Lymphoid Tissues, Revised 4th ed.; IARC: Lyon, France, 2017.

(6) Albrecht, T. A. Physiologic and psychological symptoms experienced by adults with acute leukemia: an integrative literature review. *Oncol Nurs Forum* **2014**, *41* (3), 286-295. DOI: 10.1188/14.Onf.286-295 From NLM.

(7) American Cancer Society, Phases of Chronic Myeloid Leukemia (2018, June 19), https://www.cancer.org/cancer/chronic-myeloid-leukemia/detection-diagnosis-staging/staging.html Last access: 18.01.2024

(8) Arber, D. A.; Orazi, A.; Hasserjian, R.; Thiele, J.; Borowitz, M. J.; Le Beau, M. M.; Bloomfield, C. D.; Cazzola, M.; Vardiman, J. W. The 2016 revision to the World Health Organization classification of myeloid neoplasms and acute leukemia. *Blood* **2016**, *127* (20), 2391-2405. DOI: 10.1182/blood-2016-03-643544 From NLM.

(9) Kondo, M. Lymphoid and myeloid lineage commitment in multipotent hematopoietic progenitors. *Immunol Rev* **2010**, *238* (1), 37-46. DOI: 10.1111/j.1600-065X.2010.00963.x From NLM.

(10) Jagannathan-Bogdan, M.; Zon, L. I. Hematopoiesis. *Development* **2013**, *140* (12), 2463-2467. DOI: 10.1242/dev.083147 From NLM.

(11) Siegel, R. L.; Miller, K. D.; Jemal, A. Cancer statistics, 2019. *CA Cancer J Clin* **2019**, *69* (1), 7-34. DOI: 10.3322/caac.21551 From NLM.

(12) Buitenkamp, T. D.; Izraeli, S.; Zimmermann, M.; Forestier, E.; Heerema, N. A.; van den Heuvel-Eibrink, M. M.; Pieters, R.; Korbijn, C. M.; Silverman, L. B.; Schmiegelow, K.; et al. Acute lymphoblastic leukemia in children with Down syndrome: a retrospective analysis from the Ponte di Legno study group. *Blood* **2014**, *123* (1), 70-77. DOI: 10.1182/blood-2013-06-509463 (acccessed 7/24/2023).

(13) Wagener, R.; Elitzur, S.; Brozou, T.; Borkhardt, A. Functional damaging germline variants in ETV6, IKZF1, PAX5 and RUNX1 predisposing to B-cell precursor acute lymphoblastic leukemia. *European Journal of Medical Genetics* **2023**, *66* (4), 104725. DOI: https://doi.org/10.1016/j.ejmg.2023.104725.

(14) Stieglitz, E.; Loh, M. L. Genetic predispositions to childhood leukemia. *Ther Adv Hematol* **2013**, *4* (4), 270-290. DOI: 10.1177/2040620713498161 From NLM.

(15) Greaves, M. A causal mechanism for childhood acute lymphoblastic leukaemia. *Nature Reviews Cancer* **2018**, *18* (8), 471-484. DOI: 10.1038/s41568-018-0015-6.

(16) Rowley, J. D. The critical role of chromosome translocations in human leukemias. *Annu Rev Genet* **1998**, *32*, 495-519. DOI: 10.1146/annurev.genet.32.1.495 From NLM.

(17) Rowley, J. D. A New Consistent Chromosomal Abnormality in Chronic Myelogenous Leukaemia identified by Quinacrine Fluorescence and Giemsa Staining. *Nature* **1973**, *243* (5405), 290-293. DOI: 10.1038/243290a0.

(18) Nowell, P. C.; Hungerford, D. A.; Nowell, P. C. A minute chromosome in human chronic granulocytic leukemia. *Science* **1960**, *132*, 1497.

(19) Melo, J. The diversity of BCR-ABL fusion proteins and their relationship to leukemia phenotype [editorial; comment]. *Blood* **1996**, *88* (7), 2375-2384. DOI: 10.1182/blood.V88.7.2375.bloodjournal8872375 (acccessed 12/20/2022).
(20) Minciacchi, V. R.; Kumar, R.; Krause, D. S. Chronic Myeloid Leukemia: A Model Disease of the Past, Present and Future. *Cells* **2021**, *10* (1). DOI: 10.3390/cells10010117 From NLM.
(21) Burmeister, T.; Schwartz, S.; Bartram, C. R.; Gökbuget, N.; Hoelzer, D.; Thiel, E. Patients' age and BCR-ABL frequency in adult B-precursor ALL: a retrospective analysis from the GMALL study group. *Blood* **2008**, *112* (3), 918-919. DOI: https://doi.org/10.1182/blood-2008-04-149286.
(22) Papaemmanuil, E.; Gerstung, M.; Bullinger, L.; Gaidzik, V. I.; Paschka, P.; Roberts, N. D.; Potter, N. E.; Heuser, M.; Thol, F.; Bolli, N.; et al. Genomic Classification and Prognosis in Acute Myeloid Leukemia. *New England Journal of Medicine* **2016**, *374* (23), 2209-2221. DOI: 10.1056/NEJMoa1516192.
(23) Robak, T.; Wierzbowska, A. Current and emerging therapies for acute myeloid leukemia. *Clinical Therapeutics* **2009**, *31*, 2349-2370. DOI: https://doi.org/10.1016/j.clinthera.2009.11.017.
(24) Capdeville, R.; Buchdunger, E.; Zimmermann, J.; Matter, A. Glivec (STI571, imatinib), a rationally developed, targeted anticancer drug. *Nat Rev Drug Discov* **2002**, *1* (7), 493-502. DOI: 10.1038/nrd839 From NLM.
(25) Silver, R. T.; Woolf, S. H.; Hehlmann, R.; Appelbaum, F. R.; Anderson, J.; Bennett, C.; Goldman, J. M.; Guilhot, F.; Kantarjian, H. M.; Lichtin, A. E.; et al. An evidence-based analysis of the effect of busulfan, hydroxyurea, interferon, and allogeneic bone marrow transplantation in treating the chronic phase of chronic myeloid leukemia: developed for the American Society of Hematology. *Blood* **1999**, *94* (5), 1517-1536. From NLM.
(26) Reddy, E. P.; Aggarwal, A. K. The ins and outs of bcr-abl inhibition. *Genes Cancer* **2012**, *3* (5-6), 447-454. DOI: 10.1177/1947601912462126 From NLM.
(27) Hasford, J.; Baccarani, M.; Hoffmann, V.; Guilhot, J.; Saussele, S.; Rosti, G.; Guilhot, F.; Porkka, K.; Ossenkoppele, G.; Lindoerfer, D.; et al. Predicting complete cytogenetic response and subsequent progression-free survival in 2060 patients with CML on imatinib treatment: the EUTOS score. *Blood* **2011**, *118* (3), 686-692. DOI: 10.1182/blood-2010-12-319038 (acccessed 12/20/2022).
(28) Mahon, F. o.-X.; Belloc, F.; Lagarde, V. r.; Chollet, C.; Moreau-Gaudry, F. o.; Reiffers, J.; Goldman, J. M.; Melo, J. V. MDR1 gene overexpression confers resistance to imatinib mesylate in leukemia cell line models. *Blood* **2003**, *101* (6), 2368-2373. DOI: 10.1182/blood.V101.6.2368 (acccessed 12/22/2022).
(29) Donato, N. J.; Wu, J. Y.; Stapley, J.; Gallick, G.; Lin, H.; Arlinghaus, R.; Talpaz, M. BCR-ABL independence and LYN kinase overexpression in chronic myelogenous leukemia cells selected for resistance to STI571. *Blood* **2003**, *101* (2), 690-698. DOI: 10.1182/blood.V101.2.690 (acccessed 12/22/2022).
(30) Alves, R.; Gonçalves, A. C.; Rutella, S.; Almeida, A. M.; De Las Rivas, J.; Trougakos, I. P.; Sarmento Ribeiro, A. B. Resistance to Tyrosine Kinase Inhibitors in Chronic Myeloid Leukemia-From Molecular Mechanisms to Clinical Relevance. *Cancers (Basel)* **2021**, *13* (19). DOI: 10.3390/cancers13194820 From NLM.
(31) le Coutre, P.; Tassi, E.; Varella-Garcia, M.; Barni, R.; Mologni, L.; Cabrita, G. a.; Marchesi, E.; Supino, R.; Gambacorti-Passerini, C. Induction of resistance to the Abelson inhibitor STI571 in human leukemic cells through gene amplification. *Blood* **2000**, *95* (5), 1758-1766. DOI: 10.1182/blood.V95.5.1758.005a41_1758_1766 (acccessed 12/22/2022).
(32) Gorre, M. E.; Mohammed, M.; Ellwood, K.; Hsu, N.; Paquette, R.; Rao, P. N.; Sawyers, C. L. Clinical Resistance to STI-571 Cancer Therapy Caused by BCR-ABL Gene Mutation or Amplification. *Science* **2001**, *293* (5531), 876-880. DOI: doi:10.1126/science.1062538.

(33) Shamroe, C. L.; Comeau, J. M. Ponatinib:A New Tyrosine Kinase Inhibitor for the Treatment of Chronic Myeloid Leukemia and Philadelphia Chromosome–Positive Acute Lymphoblastic Leukemia. *Annals of Pharmacotherapy* **2013**, *47* (11), 1540-1546. DOI: 10.1177/1060028013501144.
(34) Cortes, J. E.; Kantarjian, H.; Shah, N. P.; Bixby, D.; Mauro, M. J.; Flinn, I.; O'Hare, T.; Hu, S.; Narasimhan, N. I.; Rivera, V. M.; et al. Ponatinib in Refractory Philadelphia Chromosome–Positive Leukemias. *New England Journal of Medicine* **2012**, *367* (22), 2075-2088. DOI: 10.1056/NEJMoa1205127.
(35) Nicolini, F. E.; Basak, G. W.; Kim, D.-W.; Olavarria, E.; Pinilla-Ibarz, J.; Apperley, J. F.; Hughes, T.; Niederwieser, D.; Mauro, M. J.; Chuah, C.; et al. Overall survival with ponatinib versus allogeneic stem cell transplantation in Philadelphia chromosome-positive leukemias with the T315I mutation. *Cancer* **2017**, *123* (15), 2875-2880. DOI: https://doi.org/10.1002/cncr.30558.
(36) Shah, N. P.; Nicoll, J. M.; Nagar, B.; Gorre, M. E.; Paquette, R. L.; Kuriyan, J.; Sawyers, C. L. Multiple BCR-ABL kinase domain mutations confer polyclonal resistance to the tyrosine kinase inhibitor imatinib (STI571) in chronic phase and blast crisis chronic myeloid leukemia. *Cancer Cell* **2002**, *2* (2), 117-125. DOI: https://doi.org/10.1016/S1535-6108(02)00096-X.
(37) Baccarani, M. Treatment-free remission in chronic myeloid leukemia: floating between expectation and evidence. *Leukemia* **2017**, *31* (4), 1015-1016. DOI: 10.1038/leu.2017.20.
(38) Kantarjian, H. M.; Shah, N. P.; Cortes, J. E.; Baccarani, M.; Agarwal, M. B.; Undurraga, M. S.; Wang, J.; Kassack Ipiña, J. J.; Kim, D.-W.; Ogura, M.; et al. Dasatinib or imatinib in newly diagnosed chronic-phase chronic myeloid leukemia: 2-year follow-up from a randomized phase 3 trial (DASISION). *Blood* **2012**, *119* (5), 1123-1129. DOI: 10.1182/blood-2011-08-376087 (acccessed 12/20/2022).
(39) Kantarjian, H. M.; Hochhaus, A.; Saglio, G.; De Souza, C.; Flinn, I. W.; Stenke, L.; Goh, Y.-T.; Rosti, G.; Nakamae, H.; Gallagher, N. J.; et al. Nilotinib versus imatinib for the treatment of patients with newly diagnosed chronic phase, Philadelphia chromosome-positive, chronic myeloid leukaemia: 24-month minimum follow-up of the phase 3 randomised ENESTnd trial. *The Lancet Oncology* **2011**, *12* (9), 841-851. DOI: https://doi.org/10.1016/S1470-2045(11)70201-7.
(40) Cortes, J. E.; Gambacorti-Passerini, C.; Deininger, M. W.; Mauro, M. J.; Chuah, C.; Kim, D. W.; Dyagil, I.; Glushko, N.; Milojkovic, D.; le Coutre, P.; et al. Bosutinib Versus Imatinib for Newly Diagnosed Chronic Myeloid Leukemia: Results From the Randomized BFORE Trial. *J Clin Oncol* **2018**, *36* (3), 231-237. DOI: 10.1200/jco.2017.74.7162 From NLM.
(41) Sakurai, M.; Kikuchi, T.; Karigane, D.; Kasahara, H.; Matsuki, E.; Hashida, R.; Yamane, Y.; Abe, R.; Koda, Y.; Toyama, T.; et al. Renal dysfunction and anemia associated with long-term imatinib treatment in patients with chronic myelogenous leukemia. *International Journal of Hematology* **2019**, *109* (3), 292-298. DOI: 10.1007/s12185-019-02596-z.
(42) Hochhaus, A.; Larson, R. A.; Guilhot, F.; Radich, J. P.; Branford, S.; Hughes, T. P.; Baccarani, M.; Deininger, M. W.; Cervantes, F.; Fujihara, S.; et al. Long-Term Outcomes of Imatinib Treatment for Chronic Myeloid Leukemia. *New England Journal of Medicine* **2017**, *376* (10), 917-927. DOI: 10.1056/NEJMoa1609324.
(43) Whitesell, L.; Lindquist, S. L. HSP90 and the chaperoning of cancer. *Nature reviews. Cancer* **2005**, *5* (10), 761-772. DOI: 10.1038/nrc1716 From NLM.
(44) Calderwood, S. K.; Gong, J. Heat Shock Proteins Promote Cancer: It's a Protection Racket. *Trends Biochem Sci* **2016**, *41* (4), 311-323. DOI: 10.1016/j.tibs.2016.01.003 From NLM.
(45) Donnelly, A.; Blagg, B. S. Novobiocin and additional inhibitors of the Hsp90 C-terminal nucleotide-binding pocket. *Curr Med Chem* **2008**, *15* (26), 2702-2717. DOI: 10.2174/092986708786242895 From NLM.

(46) Sreedhar, A. S.; Kalmár, E.; Csermely, P.; Shen, Y. F. Hsp90 isoforms: functions, expression and clinical importance. *FEBS Lett* **2004**, *562* (1-3), 11-15. DOI: 10.1016/s0014-5793(04)00229-7 From NLM.
(47) Voss, A. K.; Thomas, T.; Gruss, P. Mice lacking HSP90beta fail to develop a placental labyrinth. *Development* **2000**, *127* (1), 1-11. DOI: 10.1242/dev.127.1.1 From NLM.
(48) Grad, I.; Cederroth, C. R.; Walicki, J.; Grey, C.; Barluenga, S.; Winssinger, N.; De Massy, B.; Nef, S.; Picard, D. The Molecular Chaperone Hsp90α Is Required for Meiotic Progression of Spermatocytes beyond Pachytene in the Mouse. *PLOS ONE* **2011**, *5* (12), e15770. DOI: 10.1371/journal.pone.0015770.
(49) Taherian, A.; Krone, P. H.; Ovsenek, N. A comparison of Hsp90alpha and Hsp90beta interactions with cochaperones and substrates. *Biochem Cell Biol* **2008**, *86* (1), 37-45. DOI: 10.1139/o07-154 From NLM.
(50) Khandelwal, A.; Kent, C. N.; Balch, M.; Peng, S.; Mishra, S. J.; Deng, J.; Day, V. W.; Liu, W.; Subramanian, C.; Cohen, M.; et al. Structure-guided design of an Hsp90β N-terminal isoform-selective inhibitor. *Nature Communications* **2018**, *9* (1), 425. DOI: 10.1038/s41467-017-02013-1.
(51) Peterson, L. B.; Eskew, J. D.; Vielhauer, G. A.; Blagg, B. S. The hERG channel is dependent upon the Hsp90α isoform for maturation and trafficking. *Mol Pharm* **2012**, *9* (6), 1841-1846. DOI: 10.1021/mp300138n From NLM.
(52) Didelot, C.; Lanneau, D.; Brunet, M.; Bouchot, A.; Cartier, J.; Jacquel, A.; Ducoroy, P.; Cathelin, S.; Decologne, N.; Chiosis, G.; et al. Interaction of heat-shock protein 90 beta isoform (HSP90 beta) with cellular inhibitor of apoptosis 1 (c-IAP1) is required for cell differentiation. *Cell Death Differ* **2008**, *15* (5), 859-866. DOI: 10.1038/cdd.2008.5 From NLM.
(53) Grammatikakis, N.; Vultur, A.; Ramana, C. V.; Siganou, A.; Schweinfest, C. W.; Watson, D. K.; Raptis, L. The Role of Hsp90N, a New Member of the Hsp90 Family, in Signal Transduction and Neoplastic Transformation*. *Journal of Biological Chemistry* **2002**, *277* (10), 8312-8320. DOI: https://doi.org/10.1074/jbc.M109200200.
(54) Lee, C.-T.; Graf, C.; Mayer, F. J.; Richter, S. M.; Mayer, M. P. Dynamics of the regulation of Hsp90 by the co-chaperone Sti1. *The EMBO Journal* **2012**, *31* (6), 1518-1528. DOI: https://doi.org/10.1038/emboj.2012.37.
(55) Onuoha, S. C.; Coulstock, E. T.; Grossmann, J. G.; Jackson, S. E. Structural Studies on the Co-chaperone Hop and Its Complexes with Hsp90. *Journal of Molecular Biology* **2008**, *379* (4), 732-744. DOI: https://doi.org/10.1016/j.jmb.2008.02.013.
(56) Mielczarek-Lewandowska, A.; Hartman, M.; Czyz, M. Inhibitors of HSP90 in melanoma. *Apoptosis* **2020**, *25*. DOI: 10.1007/s10495-019-01577-1.
(57) Blagosklonny, M. V.; Toretsky, J.; Neckers, L. Geldanamycin selectively destabilizes and conformationally alters mutated p53. *Oncogene* **1995**, *11* (5), 933-939. From NLM.
(58) O'Keeffe, B.; Fong, Y.; Chen, D.; Zhou, S.; Zhou, Q. Requirement for a kinase-specific chaperone pathway in the production of a Cdk9/cyclin T1 heterodimer responsible for P-TEFb-mediated tat stimulation of HIV-1 transcription. *J Biol Chem* **2000**, *275* (1), 279-287. DOI: 10.1074/jbc.275.1.279 From NLM.
(59) Miyata, Y.; Nakamoto, H.; Neckers, L. The therapeutic target Hsp90 and cancer hallmarks. *Curr Pharm Des* **2013**, *19* (3), 347-365. DOI: 10.2174/138161213804143725 From NLM.
(60) Pick, E.; Kluger, Y.; Giltnane, J. M.; Moeder, C.; Camp, R. L.; Rimm, D. L.; Kluger, H. M. High HSP90 Expression Is Associated with Decreased Survival in Breast Cancer. *Cancer Research* **2007**, *67* (7), 2932-2937. DOI: 10.1158/0008-5472.Can-06-4511 (acccessed 7/17/2023).
(61) Su, J. M.; Hsu, Y. Y.; Lin, P.; Chang, H. Nuclear Accumulation of Heat-shock Protein 90 Is Associated with Poor Survival and Metastasis in Patients with Non-small Cell Lung Cancer. *Anticancer Res* **2016**, *36* (5), 2197-2203. From NLM.
(62) Normant, E.; Paez, G.; West, K. A.; Lim, A. R.; Slocum, K. L.; Tunkey, C.; McDougall, J.; Wylie, A. A.; Robison, K.; Caliri, K.; et al. The Hsp90 inhibitor IPI-504 rapidly

lowers EML4–ALK levels and induces tumor regression in ALK-driven NSCLC models. *Oncogene* **2011**, *30* (22), 2581-2586. DOI: 10.1038/onc.2010.625.
(63) Park, J. M.; Kim, Y.-J.; Park, S.; Park, M.; Farrand, L.; Nguyen, C.-T.; Ann, J.; Nam, G.; Park, H.-J.; Lee, J.; et al. A novel HSP90 inhibitor targeting the C-terminal domain attenuates trastuzumab resistance in HER2-positive breast cancer. *Molecular Cancer* **2020**, *19* (1), 161. DOI: 10.1186/s12943-020-01283-6.
(64) Choi, Y. J.; Kim, S. Y.; So, K. S.; Baek, I.-J.; Kim, W. S.; Choi, S. H.; Lee, J. C.; Bivona, T. G.; Rho, J. K.; Choi, C.-M. AUY922 Effectively Overcomes MET- and AXL-Mediated Resistance to EGFR-TKI in Lung Cancer Cells. *PLOS ONE* **2015**, *10* (3), e0119832. DOI: 10.1371/journal.pone.0119832.
(65) Hanahan, D.; Weinberg, R. A. The Hallmarks of Cancer. *Cell* **2000**, *100* (1), 57-70. DOI: 10.1016/S0092-8674(00)81683-9 (acccessed 2022/11/23).
(66) Hanahan, D.; Weinberg, Robert A. Hallmarks of Cancer: The Next Generation. *Cell* **2011**, *144* (5), 646-674. DOI: https://doi.org/10.1016/j.cell.2011.02.013.
(67) Daver, N.; Schlenk, R. F.; Russell, N. H.; Levis, M. J. Targeting FLT3 mutations in AML: review of current knowledge and evidence. *Leukemia* **2019**, *33* (2), 299-312. DOI: 10.1038/s41375-018-0357-9.
(68) Yao, Q.; Nishiuchi, R.; Li, Q.; Kumar, A. R.; Hudson, W. A.; Kersey, J. H. FLT3 Expressing Leukemias Are Selectively Sensitive to Inhibitors of the Molecular Chaperone Heat Shock Protein 90 through Destabilization of Signal Transduction-Associated Kinases. *Clinical Cancer Research* **2003**, *9* (12), 4483-4493. (accessed 7/25/2023).
(69) Bonvini, P.; Gastaldi, T.; Falini, B.; Rosolen, A. Nucleophosmin-Anaplastic Lymphoma Kinase (NPM-ALK), a Novel Hsp90-Client Tyrosine Kinase: Down-Regulation of NPM-ALK Expression and Tyrosine Phosphorylation in ALK+ CD30+ Lymphoma Cells by the Hsp90 Antagonist 17-Allylamino,17-demethoxygeldanamycin1. *Cancer Research* **2002**, *62* (5), 1559-1566. (accessed 7/25/2023).
(70) Coustan-Smith, E.; Kitanaka, A.; Pui, C.; McNinch, L.; Evans, W.; Raimondi, S.; Behm, F.; Arico, M.; Campana, D. Clinical relevance of BCL-2 overexpression in childhood acute lymphoblastic leukemia. *Blood* **1996**, *87* (3), 1140-1146. DOI: 10.1182/blood.V87.3.1140.bloodjournal8731140 (accessed 7/25/2023).
(71) Allen, A.; Gill, K.; Hoehn, D.; Sulis, M.; Bhagat, G.; Alobeid, B. C-myc protein expression in B-cell acute lymphoblastic leukemia, prognostic significance? *Leuk Res* **2014**, *38* (9), 1061-1066. DOI: 10.1016/j.leukres.2014.06.022 From NLM.
(72) Žáčková, M.; Moučková, D.; Lopotová, T.; Ondráčková, Z.; Klamová, H.; Moravcová, J. Hsp90 - a potential prognostic marker in CML. *Blood Cells, Molecules, and Diseases* **2013**, *50* (3), 184-189. DOI: https://doi.org/10.1016/j.bcmd.2012.11.002.
(73) Peng, C.; Brain, J.; Hu, Y.; Kong, L.; Grayzel, D.; Pak, R.; Read, M.; Li, S. IPI-504, a Novel, Orally Active HSP90 Inhibitor, Prolongs Survival of Mice with BCR-ABL T315I CML and B-ALL. *Blood* **2006**, *108* (11), 2183-2183. DOI: 10.1182/blood.V108.11.2183.2183 (accessed 7/25/2023).
(74) Wu, L. X.; Xu, J. H.; Zhang, K. Z.; Lin, Q.; Huang, X. W.; Wen, C. X.; Chen, Y. Z. Disruption of the Bcr-Abl/Hsp90 protein complex: a possible mechanism to inhibit Bcr-Abl-positive human leukemic blasts by novobiocin. *Leukemia* **2008**, *22* (7), 1402-1409. DOI: 10.1038/leu.2008.89 From NLM.
(75) Bhatia, S.; Diedrich, D.; Frieg, B.; Ahlert, H.; Stein, S.; Bopp, B.; Lang, F.; Zang, T.; Kröger, T.; Ernst, T.; et al. Targeting HSP90 dimerization via the C terminus is effective in imatinib-resistant CML and lacks the heat shock response. *Blood* **2018**, *132* (3), 307-320. DOI: 10.1182/blood-2017-10-810986 From NLM.
(76) Sanchez, J.; Carter, T. R.; Cohen, M. S.; Blagg, B. S. J. Old and New Approaches to Target the Hsp90 Chaperone. *Curr Cancer Drug Targets* **2020**, *20* (4), 253-270. DOI: 10.2174/1568009619666191202101330 From NLM.

(77) Prodromou, C.; Roe, S. M.; O'Brien, R.; Ladbury, J. E.; Piper, P. W.; Pearl, L. H. Identification and Structural Characterization of the ATP/ADP-Binding Site in the Hsp90 Molecular Chaperone. *Cell* **1997**, *90* (1), 65-75. DOI: 10.1016/S0092-8674(00)80314-1 (accessed 2022/11/22).
(78) Whitesell, L.; Mimnaugh, E. G.; De Costa, B.; Myers, C. E.; Neckers, L. M. Inhibition of heat shock protein HSP90-pp60v-src heteroprotein complex formation by benzoquinone ansamycins: essential role for stress proteins in oncogenic transformation. *Proc Natl Acad Sci U S A* **1994**, *91* (18), 8324-8328. DOI: 10.1073/pnas.91.18.8324 From NLM.
(79) Sharma, S. V.; Agatsuma, T.; Nakano, H. Targeting of the protein chaperone, HSP90, by the transformation suppressing agent, radicicol. *Oncogene* **1998**, *16* (20), 2639-2645. DOI: 10.1038/sj.onc.1201790.
(80) Roe, S. M.; Prodromou, C.; O'Brien, R.; Ladbury, J. E.; Piper, P. W.; Pearl, L. H. Structural Basis for Inhibition of the Hsp90 Molecular Chaperone by the Antitumor Antibiotics Radicicol and Geldanamycin. *Journal of Medicinal Chemistry* **1999**, *42* (2), 260-266. DOI: 10.1021/jm980403y.
(81) Muller, P. Y.; Milton, M. N. The determination and interpretation of the therapeutic index in drug development. *Nature Reviews Drug Discovery* **2012**, *11* (10), 751-761. DOI: 10.1038/nrd3801.
(82) Supko, J. G.; Hickman, R. L.; Grever, M. R.; Malspeis, L. Preclinical pharmacologic evaluation of geldanamycin as an antitumor agent. *Cancer Chemotherapy and Pharmacology* **1995**, *36* (4), 305-315. DOI: 10.1007/BF00689048.
(83) Tanespimycin in Treating Women With Refractory Locally Advanced or Metastatic Breast Cancer, ClinicalTrials.gov Identifier: NCT00096109
(84) Efficacy and Safety of IPI-504 With Trastuzumab Pretreated, Locally Advanced or Metastatic HER2 Positive Breast Cancer, ClinicalTrials.gov Identifier: NCT00817362
(85) Alvespimycin Hydrochloride in Treating Patients With Relapsed Chronic Lymphocytic Leukemia, Small Lymphocytic Lymphoma, or B-Cell Prolymphocytic Leukemia, ClinicalTrials.gov Identifier: NCT01126502
(86) A Study of Tanespimycin (KOS-953) in Patients With Relapsed-refractory Multiple Myeloma (TIME-2), ClinicalTrials.gov Identifier: NCT00514371
(87) Austin, C.; Pettit, S. N.; Magnolo, S. K.; Sanvoisin, J.; Chen, W.; Wood, S. P.; Freeman, L. D.; Pengelly, R. J.; Hughes, D. E. Fragment screening using capillary electrophoresis (CEfrag) for hit identification of heat shock protein 90 ATPase inhibitors. *J Biomol Screen* **2012**, *17* (7), 868-876. DOI: 10.1177/1087057112445785 From NLM.
(88) A Phase 3 Study of Ganetespib in Combination With Docetaxel Versus Docetaxel Alone in Patients With Advanced NSCLC (Galaxy 2), ClinicalTrials.gov Identifier: NCT01798485
(89) Open-label Study of STA-9090 for Patients With Metastatic Breast Cancer, ClinicalTrials.gov Identifier: NCT01273896
(90) STA-9090(Ganetespib) in Patients With Unresectable Stage III or Stage IV Melanoma, ClinicalTrials.gov Identifier: NCT01551693
(91) STA-9090 for Treatment of AML, CML, MDS and Myeloproliferative Disorders, ClinicalTrials.gov Identifier: NCT00858572
(92) A Phase 1 Study of the HSP90 Inhibitor, STA-9090 in Subjects With Acute Myeloid Leukemia, Acute Lymphoblastic Leukemia and Blast-phase Chronic Myelogenous Leukemia, ClinicalTrials.gov Identifier: NCT00964873
(93) An Open-label, Randomized Phase II Study to Evaluate the Efficacy of AUY922 vs Pemetrexed or Docetaxel in NSCLC Patients With EGFR Mutations, ClinicalTrials.gov Identifier: NCT01646125
(94) Study of Hsp90 Inhibitor AUY922 for the Treatment of Patients With Refractory Gastrointestinal Stromal Tumor, ClinicalTrials.gov Identifier: NCT01404650
(95) HSP90 Inhibitor, AUY922, in Patients With Primary Myelofibrosis (PMF), Post-Polycythemia Vera Myelofibrosis (Post-PV MF), Post-Essential Thrombocythemia

Myelofibrosis (Post-ET MF), and Refractory PV/ET, ClinicalTrials.gov Identifier: NCT01668173
(96) A Phase I-Ib/II Study to Determine the Maximum Tolerated Dose (MTD) of AUY922 Alone and in Combination With Bortezomib, With or Without Dexamethasone, in Patients With Relapsed or Refractory Multiple Myeloma., ClinicalTrials.gov Identifier: NCT00708292
(97) Chiosis, G.; Lucas, B.; Shtil, A.; Huezo, H.; Rosen, N. Development of a Purine-Scaffold Novel Class of Hsp90 Binders that Inhibit the Proliferation of Cancer Cells and Induce the Degradation of Her2 Tyrosine Kinase. *Bioorganic & Medicinal Chemistry* **2002**, *10* (11), 3555-3564. DOI: https://doi.org/10.1016/S0968-0896(02)00253-5.
(98) He, H.; Zatorska, D.; Kim, J.; Aguirre, J.; Llauger, L.; She, Y.; Wu, N.; Immormino, R. M.; Gewirth, D. T.; Chiosis, G. Identification of Potent Water Soluble Purine-Scaffold Inhibitors of the Heat Shock Protein 90. *Journal of Medicinal Chemistry* **2006**, *49* (1), 381-390. DOI: 10.1021/jm0508078.
(99) PU-H71 With Nab-paclitaxel (Abraxane) in Metastatic Breast Cancer, ClinicalTrials.gov Identifier: NCT03166085
(100) The First-in-human Phase I Trial of PU-H71 in Patients With Advanced Malignancies, ClinicalTrials.gov Identifier: NCT01393509
(101) Pillarsetty, N.; Jhaveri, K.; Taldone, T.; Caldas-Lopes, E.; Punzalan, B.; Joshi, S.; Bolaender, A.; Uddin, M. M.; Rodina, A.; Yan, P.; et al. Paradigms for Precision Medicine in Epichaperome Cancer Therapy. *Cancer Cell* **2019**, *36* (5), 559-573.e557. DOI: 10.1016/j.ccell.2019.09.007 (accessed 2022/11/23).
(102) Zong, H.; Gozman, A.; Caldas-Lopes, E.; Taldone, T.; Sturgill, E.; Brennan, S.; Ochiana, Stefan O.; Gomes-DaGama, Erica M.; Sen, S.; Rodina, A.; et al. A Hyperactive Signalosome in Acute Myeloid Leukemia Drives Addiction to a Tumor-Specific Hsp90 Species. *Cell Reports* **2015**, *13* (10), 2159-2173. DOI: 10.1016/j.celrep.2015.10.073 (accessed 2023/07/24).
(103) Shimomura, A.; Yamamoto, N.; Kondo, S.; Fujiwara, Y.; Suzuki, S.; Yanagitani, N.; Horiike, A.; Kitazono, S.; Ohyanagi, F.; Doi, T.; et al. First-in-Human Phase I Study of an Oral HSP90 Inhibitor, TAS-116, in Patients with Advanced Solid Tumors. *Molecular Cancer Therapeutics* **2019**, *18* (3), 531-540. DOI: 10.1158/1535-7163.Mct-18-0831 (accessed 7/25/2023).
(104) Ohkubo, S.; Kodama, Y.; Muraoka, H.; Hitotsumachi, H.; Yoshimura, C.; Kitade, M.; Hashimoto, A.; Ito, K.; Gomori, A.; Takahashi, K.; et al. TAS-116, a highly selective inhibitor of heat shock protein 90α and β, demonstrates potent antitumor activity and minimal ocular toxicity in preclinical models. *Mol Cancer Ther* **2015**, *14* (1), 14-22. DOI: 10.1158/1535-7163.Mct-14-0219 From NLM.
(105) CHAPTER-GIST-301 trial: A RANDOMIZED, DOUBLE-BLIND, PLACEBO-CONTROLLED, MULTICENTER TRIAL OF TAS-116 IN PATIENTS WITH ADVANCED GASTROINTESTINAL STROMAL TUMOR, CHAPTER; The molecular chaperone heat shock protein 90 (HSP90) inhibitor, Pimitespib, Japic CTI-184094.
(106) Wang, L.; Zhang, Q.; You, Q. Targeting the HSP90–CDC37–kinase chaperone cycle: A promising therapeutic strategy for cancer. *Medicinal Research Reviews* **2022**, *42* (1), 156-182. DOI: https://doi.org/10.1002/med.21807.
(107) Butler, L. M.; Ferraldeschi, R.; Armstrong, H. K.; Centenera, M. M.; Workman, P. Maximizing the Therapeutic Potential of HSP90 Inhibitors. *Molecular Cancer Research* **2015**, *13* (11), 1445-1451. DOI: 10.1158/1541-7786.Mcr-15-0234 (accessed 1/16/2024).
(108) Kryeziu, K.; Bruun, J.; Guren, T. K.; Sveen, A.; Lothe, R. A. Combination therapies with HSP90 inhibitors against colorectal cancer. *Biochim Biophys Acta Rev Cancer* **2019**, *1871* (2), 240-247. DOI: 10.1016/j.bbcan.2019.01.002 From NLM.

(109) Donahue, K.; Xie, H.; Li, M.; Gao, A.; Ma, M.; Wang, Y.; Tipton, R.; Semanik, N.; Primeau, T.; Li, S.; et al. Diptoindonesin G is a middle domain HSP90 modulator for cancer treatment. *Journal of Biological Chemistry* **2022**, *298* (12). DOI: 10.1016/j.jbc.2022.102700 (accessed 2024/01/16).
(110) Gao, J.; Fan, M.; Xiang, G.; Wang, J.; Zhang, X.; Guo, W.; Wu, X.; Sun, Y.; Gu, Y.; Ge, H.; et al. Diptoindonesin G promotes ERK-mediated nuclear translocation of p-STAT1 (Ser727) and cell differentiation in AML cells. *Cell Death & Disease* **2017**, *8* (5), e2765-e2765. DOI: 10.1038/cddis.2017.159.
(111) Zhang, F. Z.; Ho, D. H.-H.; Wong, R. H.-F. Triptolide, a HSP90 middle domain inhibitor, induces apoptosis in triple manner. *Oncotarget* **2018**, *9* (32).
(112) Soti, C.; Vermes, A.; Haystead, T. A.; Csermely, P. Comparative analysis of the ATP-binding sites of Hsp90 by nucleotide affinity cleavage: a distinct nucleotide specificity of the C-terminal ATP-binding site. *Eur J Biochem* **2003**, *270* (11), 2421-2428. DOI: 10.1046/j.1432-1033.2003.03610.x From NLM.
(113) Marcu, M. G.; Schulte, T. W.; Neckers, L. Novobiocin and related coumarins and depletion of heat shock protein 90-dependent signaling proteins. *Journal of the National Cancer Institute* **2000**, *92* (3), 242-248. DOI: 10.1093/jnci/92.3.242 From NLM.
(114) An, W. G.; Schulte, T. W.; Neckers, L. M. The heat shock protein 90 antagonist geldanamycin alters chaperone association with p210bcr-abl and v-src proteins before their degradation by the proteasome. *Cell Growth Differ* **2000**, *11* (7), 355-360. From NLM.
(115) Roe, S. M.; Ali, M. M. U.; Meyer, P.; Vaughan, C. K.; Panaretou, B.; Piper, P. W.; Prodromou, C.; Pearl, L. H. The Mechanism of Hsp90 Regulation by the Protein Kinase-Specific Cochaperone p50cdc37. *Cell* **2004**, *116* (1), 87-98. DOI: https://doi.org/10.1016/S0092-8674(03)01027-4.
(116) Gray, P. J., Jr.; Stevenson, M. A.; Calderwood, S. K. Targeting Cdc37 Inhibits Multiple Signaling Pathways and Induces Growth Arrest in Prostate Cancer Cells. *Cancer Research* **2007**, *67* (24), 11942-11950. DOI: 10.1158/0008-5472.Can-07-3162 (accessed 8/1/2023).
(117) Zhang, T.; Hamza, A.; Cao, X.; Wang, B.; Yu, S.; Zhan, C.-G.; Sun, D. A novel Hsp90 inhibitor to disrupt Hsp90/Cdc37 complex against pancreatic cancer cells. *Molecular Cancer Therapeutics* **2008**, *7* (1), 162-170. DOI: 10.1158/1535-7163.Mct-07-0484 (accessed 12/22/2022).
(118) Abbas, S.; Bhoumik, A.; Dahl, R.; Vasile, S.; Krajewski, S.; Cosford, N. D. P.; Ronai, Z. e. A. Preclinical Studies of Celastrol and Acetyl Isogambogic Acid in Melanoma. *Clinical Cancer Research* **2007**, *13* (22), 6769-6778. DOI: 10.1158/1078-0432.Ccr-07-1536 (accessed 12/6/2022).
(119) Zhang, T.; Hamza, A.; Cao, X.; Wang, B.; Yu, S.; Zhan, C.; Sun, D. Mol. Cancer Ther. **2008**.
(120) Westerheide, S. D.; Bosman, J. D.; Mbadugha, B. N. A.; Kawahara, T. L. A.; Matsumoto, G.; Kim, S.; Gu, W.; Devlin, J. P.; Silverman, R. B.; Morimoto, R. I. Celastrols as Inducers of the Heat Shock Response and Cytoprotection. *Journal of Biological Chemistry* **2004**, *279* (53), 56053-56060. DOI: 10.1074/jbc.M409267200 (accessed 2022/12/06).
(121) Yu, Y.; Hamza, A.; Zhang, T.; Gu, M.; Zou, P.; Newman, B.; Li, Y.; Gunatilaka, A. A. L.; Zhan, C.-G.; Sun, D. Withaferin A targets heat shock protein 90 in pancreatic cancer cells. *Biochemical Pharmacology* **2010**, *79* (4), 542-551. DOI: https://doi.org/10.1016/j.bcp.2009.09.017.
(122) Belofsky, G. N.; Jensen, P. R.; Fenical, W. Sansalvamide: A new cytotoxic cyclic depsipeptide produced by a marine fungus of the genus Fusarium. *Tetrahedron Letters* **1999**, *40* (15), 2913-2916. DOI: https://doi.org/10.1016/S0040-4039(99)00393-7.
(123) Vasko, R. C.; Rodriguez, R. A.; Cunningham, C. N.; Ardi, V. C.; Agard, D. A.; McAlpine, S. R. Mechanistic Studies of Sansalvamide A-Amide: An Allosteric

Modulator of Hsp90. *ACS Medicinal Chemistry Letters* **2010**, *1* (1), 4-8. DOI: 10.1021/ml900003t.
(124) Ardi, V. C.; Alexander, L. D.; Johnson, V. A.; McAlpine, S. R. Macrocycles That Inhibit the Binding between Heat Shock Protein 90 and TPR-Containing Proteins. *ACS Chemical Biology* **2011**, *6* (12), 1357-1366. DOI: 10.1021/cb200203m.
(125) Horibe, T.; Kohno, M.; Haramoto, M.; Ohara, K.; Kawakami, K. Designed hybrid TPR peptide targeting Hsp90 as a novel anticancer agent. *Journal of Translational Medicine* **2011**, *9* (1), 8. DOI: 10.1186/1479-5876-9-8.
(126) Rahimi, M. N.; McAlpine, S. R. Protein–protein inhibitor designed de novo to target the MEEVD region on the C-terminus of Hsp90 and block co-chaperone activity. *Chemical Communications* **2019**, *55* (6), 846-849, 10.1039/C8CC07576J. DOI: 10.1039/C8CC07576J.
(127) Ratzke, C.; Mickler, M.; Hellenkamp, B.; Buchner, J.; Hugel, T. Dynamics of heat shock protein 90 C-terminal dimerization is an important part of its conformational cycle. *Proceedings of the National Academy of Sciences* **2010**, *107* (37), 16101-16106. DOI: doi:10.1073/pnas.1000916107.
(128) Ciglia, E.; Vergin, J.; Reimann, S.; Smits, S. H. J.; Schmitt, L.; Groth, G.; Gohlke, H. Resolving Hot Spots in the C-Terminal Dimerization Domain that Determine the Stability of the Molecular Chaperone Hsp90. *PLOS ONE* **2014**, *9* (4), e96031. DOI: 10.1371/journal.pone.0096031.
(129) Diedrich, D.; Moita, A. J. R.; Rüther, A.; Frieg, B.; Reiss, G. J.; Hoeppner, A.; Kurz, T.; Gohlke, H.; Lüdeke, S.; Kassack, M. U.; et al. α-Aminoxy Oligopeptides: Synthesis, Secondary Structure, and Cytotoxicity of a New Class of Anticancer Foldamers. *Chemistry – A European Journal* **2016**, *22* (49), 17600-17611. DOI: https://doi.org/10.1002/chem.201602521.
(130) Koren, J., 3rd; Blagg, B. S. J. The Right Tool for the Job: An Overview of Hsp90 Inhibitors. *Adv Exp Med Biol* **2020**, *1243*, 135-146. DOI: 10.1007/978-3-030-40204-4_9 From NLM.
(131) Eccles, S. A.; Massey, A.; Raynaud, F. I.; Sharp, S. Y.; Box, G.; Valenti, M.; Patterson, L.; de Haven Brandon, A.; Gowan, S.; Boxall, F.; et al. NVP-AUY922: a novel heat shock protein 90 inhibitor active against xenograft tumor growth, angiogenesis, and metastasis. *Cancer Res* **2008**, *68* (8), 2850-2860. DOI: 10.1158/0008-5472.Can-07-5256 From NLM.
(132) Lee, C.; Park, H.-K.; Jeong, H.; Lim, J.; Lee, A.-J.; Cheon, K. Y.; Kim, C.-S.; Thomas, A. P.; Bae, B.; Kim, N. D.; et al. Development of a Mitochondria-Targeted Hsp90 Inhibitor Based on the Crystal Structures of Human TRAP1. *Journal of the American Chemical Society* **2015**, *137* (13), 4358-4367. DOI: 10.1021/ja511893n.
(133) Mishra, S. J.; Khandelwal, A.; Banerjee, M.; Balch, M.; Peng, S.; Davis, R. E.; Merfeld, T.; Munthali, V.; Deng, J.; Matts, R. L.; et al. Selective Inhibition of the Hsp90α Isoform. *Angewandte Chemie International Edition* **2021**, *60* (19), 10547-10551. DOI: https://doi.org/10.1002/anie.202015422.
(134) Mishra, S. J.; Liu, W.; Beebe, K.; Banerjee, M.; Kent, C. N.; Munthali, V.; Koren, J., III; Taylor, J. A., III; Neckers, L. M.; Holzbeierlein, J.; et al. The Development of Hsp90β-Selective Inhibitors to Overcome Detriments Associated with pan-Hsp90 Inhibition. *Journal of Medicinal Chemistry* **2021**, *64* (3), 1545-1557. DOI: 10.1021/acs.jmedchem.0c01700.
(135) Barna, J.; Csermely, P.; Vellai, T. Roles of heat shock factor 1 beyond the heat shock response. *Cellular and Molecular Life Sciences* **2018**, *75* (16), 2897-2916. DOI: 10.1007/s00018-018-2836-6.
(136) Pincus, D. Regulation of Hsf1 and the Heat Shock Response. In *HSF1 and Molecular Chaperones in Biology and Cancer*, Mendillo, M. L., Pincus, D., Scherz-Shouval, R. Eds.; Springer International Publishing, 2020; pp 41-50.

(137) Westerheide, S. D.; Morimoto, R. I. Heat Shock Response Modulators as Therapeutic Tools for Diseases of Protein Conformation *. *Journal of Biological Chemistry* **2005**, *280* (39), 33097-33100. DOI: 10.1074/jbc.R500010200 (accessed 2022/11/25).
(138) Bagatell, R.; Paine-Murrieta, G. D.; Taylor, C. W.; Pulcini, E. J.; Akinaga, S.; Benjamin, I. J.; Whitesell, L. Induction of a Heat Shock Factor 1-dependent Stress Response Alters the Cytotoxic Activity of Hsp90-binding Agents1. *Clinical Cancer Research* **2000**, *6* (8), 3312-3318. (accessed 12/20/2022).
(139) McCollum, A. K.; TenEyck, C. J.; Sauer, B. M.; Toft, D. O.; Erlichman, C. Up-regulation of Heat Shock Protein 27 Induces Resistance to 17-Allylamino-Demethoxygeldanamycin through a Glutathione-Mediated Mechanism. *Cancer Research* **2006**, *66* (22), 10967-10975. DOI: 10.1158/0008-5472.Can-06-1629 (accessed 12/20/2022).
(140) Peron, M.; Bonvini, P.; Rosolen, A. Effect of inhibition of the Ubiquitin-Proteasome System and Hsp90 on growth and survival of Rhabdomyosarcoma cells in vitro. *BMC Cancer* **2012**, *12* (1), 233. DOI: 10.1186/1471-2407-12-233.
(141) O'Connell, B. C.; O'Callaghan, K.; Tillotson, B.; Douglas, M.; Hafeez, N.; West, K. A.; Stern, H.; Ali, J. A.; Changelian, P.; Fritz, C. C.; et al. HSP90 Inhibition Enhances Antimitotic Drug-Induced Mitotic Arrest and Cell Death in Preclinical Models of Non-Small Cell Lung Cancer. *PLOS ONE* **2014**, *9* (12), e115228. DOI: 10.1371/journal.pone.0115228.
(142) Yuno, A.; Lee, M.-J.; Lee, S.; Tomita, Y.; Rekhtman, D.; Moore, B.; Trepel, J. B. Clinical Evaluation and Biomarker Profiling of Hsp90 Inhibitors. In *Chaperones: Methods and Protocols*, Calderwood, S. K., Prince, T. L. Eds.; Springer New York, 2018; pp 423-441.
(143) Siegelin, M. D. Inhibition of the mitochondrial Hsp90 chaperone network: A novel, efficient treatment strategy for cancer? *Cancer Letters* **2013**, *333* (2), 133-146. DOI: https://doi.org/10.1016/j.canlet.2013.01.045.
(144) Hayat, U.; Elliott, G. T.; Olszanski, A. J.; Altieri, D. C. Feasibility and safety of targeting mitochondria for cancer therapy – preclinical characterization of gamitrinib, a first-in-class, mitochondriaL-targeted small molecule Hsp90 inhibitor. *Cancer Biology & Therapy* **2022**, *23* (1), 117-126. DOI: 10.1080/15384047.2022.2029132.
(145) Rouhi, A.; Miller, C.; Grasedieck, S.; Reinhart, S.; Stolze, B.; Döhner, H.; Kuchenbauer, F.; Bullinger, L.; Fröhling, S.; Scholl, C. Prospective identification of resistance mechanisms to HSP90 inhibition in KRAS mutant cancer cells. *Oncotarget* **2016**, *8* (5).
(146) Rouhi, A.; Miller, C.; Grasedieck, S.; Reinhart, S.; Stolze, B.; Döhner, H.; Kuchenbauer, F.; Bullinger, L.; Fröhling, S.; Scholl, C. Prospective identification of resistance mechanisms to HSP90 inhibition in KRAS mutant cancer cells. *Oncotarget* **2017**, *8* (5), 7678-7690. DOI: 10.18632/oncotarget.13841 From NLM.
(147) Chatterjee, S.; Huang, E. H.; Christie, I.; Kurland, B. F.; Burns, T. F. Acquired Resistance to the Hsp90 Inhibitor, Ganetespib, in KRAS-Mutant NSCLC Is Mediated via Reactivation of the ERK-p90RSK-mTOR Signaling Network. *Mol Cancer Ther* **2017**, *16* (5), 793-804. DOI: 10.1158/1535-7163.Mct-16-0677 From NLM.
(148) Sakamoto, K. M.; Kim, K. B.; Kumagai, A.; Mercurio, F.; Crews, C. M.; Deshaies, R. J. Protacs: Chimeric molecules that target proteins to the Skp1–Cullin–F box complex for ubiquitination and degradation. *Proceedings of the National Academy of Sciences* **2001**, *98* (15), 8554-8559. DOI: doi:10.1073/pnas.141230798.
(149) Ocaña, A.; Pandiella, A. Proteolysis targeting chimeras (PROTACs) in cancer therapy. *Journal of Experimental & Clinical Cancer Research* **2020**, *39* (1), 189. DOI: 10.1186/s13046-020-01672-1.
(150) Bondeson, D. P.; Crews, C. M. Targeted Protein Degradation by Small Molecules. *Annual Review of Pharmacology and Toxicology* **2017**, *57* (1), 107-123. DOI: 10.1146/annurev-pharmtox-010715-103507.

(151) Kleiger, G.; Mayor, T. Perilous journey: a tour of the ubiquitin–proteasome system. *Trends in Cell Biology* **2014**, *24* (6), 352-359. DOI: https://doi.org/10.1016/j.tcb.2013.12.003.
(152) Burslem, G. M.; Crews, C. M. Proteolysis-Targeting Chimeras as Therapeutics and Tools for Biological Discovery. *Cell* **2020**, *181* (1), 102-114. DOI: https://doi.org/10.1016/j.cell.2019.11.031.
(153) Dale, B.; Cheng, M.; Park, K. S.; Kaniskan, H.; Xiong, Y.; Jin, J. Advancing targeted protein degradation for cancer therapy. *Nat Rev Cancer* **2021**, *21* (10), 638-654. DOI: 10.1038/s41568-021-00365-x From NLM.
(154) Park, J.; Cho, J.; Song, E. J. Ubiquitin-proteasome system (UPS) as a target for anticancer treatment. *Arch Pharm Res* **2020**, *43* (11), 1144-1161. DOI: 10.1007/s12272-020-01281-8 From NLM.
(155) Samarasinghe, K. T. G.; Crews, C. M. Targeted protein degradation: A promise for undruggable proteins. *Cell Chemical Biology* **2021**, *28* (7), 934-951. DOI: 10.1016/j.chembiol.2021.04.011 (accessed 2022/12/13).
(156) Trial of ARV-110 in Patients With Metastatic Castration Resistant Prostate Cancer (mCRPC), ClinicalTrials.gov Identifier: NCT03888612
(157) A Phase 1/2 Trial of ARV-471 Alone and in Combination With Palbociclib (IBRANCE®) in Patients With ER+/HER2- Locally Advanced or Metastatic Breast Cancer (mBC), ClinicalTrials.gov Identifier: NCT04072952
(158) Nalawansha, D. A.; Crews, C. M. PROTACs: An Emerging Therapeutic Modality in Precision Medicine. *Cell Chemical Biology* **2020**, *27* (8), 998-1014. DOI: 10.1016/j.chembiol.2020.07.020 (accessed 2022/12/13).
(159) Bhatia, S.; Spanier, L.; Bickel, D.; Dienstbier, N.; Woloschin, V.; Vogt, M.; Pols, H.; Lungerich, B.; Reiners, J.; Aghaallaei, N.; et al. Development of a First-in-Class Small-Molecule Inhibitor of the C-Terminal Hsp90 Dimerization. *ACS Central Science* **2022**, *8* (5), 636-655. DOI: 10.1021/acscentsci.2c00013.
(160) Abel, T.; El Filali, E.; Waern, J.; Schneider, I. C.; Yuan, Q.; Münch, R. C.; Hick, M.; Warnecke, G.; Madrahimov, N.; Kontermann, R. E.; et al. Specific gene delivery to liver sinusoidal and artery endothelial cells. *Blood* **2013**, *122* (12), 2030-2038. DOI: 10.1182/blood-2012-11-468579 From NLM.
(161) Shiotsu, Y.; Soga, S.; Akinaga, S. Heat Shock Protein 90-antagonist Destabilizes Bcr-Abl/HSP90 Chaperone Complex. *Leukemia & Lymphoma* **2002**, *43* (5), 961-968. DOI: 10.1080/10428190290021371.
(162) Peng, Y.; Huang, Z.; Zhou, F.; Wang, T.; Mou, K.; Feng, W. Effect of HSP90AB1 and CC domain interaction on Bcr-Abl protein cytoplasm localization and function in chronic myeloid leukemia cells. *Cell Communication and Signaling* **2021**, *19* (1), 71. DOI: 10.1186/s12964-021-00752-9.
(163) The Jackson Laboratory, https://www.jax.org/strain/005557, Last access: 20.03.2023
(164) Chou, T.-C. Theoretical Basis, Experimental Design, and Computerized Simulation of Synergism and Antagonism in Drug Combination Studies. *Pharmacological Reviews* **2006**, *58* (3), 621. DOI: 10.1124/pr.58.3.10.
(165) Dumont, F. J. Everolimus. Novartis. *Current opinion in investigational drugs (London, England : 2000)* **2001**, *2* (9), 1220-1234. From NLM.
(166) Yu, Y.; Savage, R. E.; Eathiraj, S.; Meade, J.; Wick, M. J.; Hall, T.; Abbadessa, G.; Schwartz, B. Targeting AKT1-E17K and the PI3K/AKT Pathway with an Allosteric AKT Inhibitor, ARQ 092. *PLoS One* **2015**, *10* (10), e0140479. DOI: 10.1371/journal.pone.0140479 From NLM.
(167) Boss, D. S.; Witteveen, P. O.; van der Sar, J.; Lolkema, M. P.; Voest, E. E.; Stockman, P. K.; Ataman, O.; Wilson, D.; Das, S.; Schellens, J. H. Clinical evaluation of AZD1152, an i.v. inhibitor of Aurora B kinase, in patients with solid malignant tumors. *Annals of oncology : official journal of the European Society for Medical Oncology* **2011**, *22* (2), 431-437. DOI: 10.1093/annonc/mdq344 From NLM.

(168) El-Subbagh, H. I.; Al-Badr, A. A. Chapter 2 - Cytarabine. In *Profiles of Drug Substances, Excipients and Related Methodology*, Brittain, H. G. Ed.; Vol. 34; Academic Press, 2009; pp 37-113.
(169) Pui, C.-H.; Jeha, S.; Kirkpatrick, P. Clofarabine. *Nature Reviews Drug Discovery* **2005**, *4*, 369+, Article. (accessed 2023/3/24/). From Gale Gale OneFile: Health and Medicine.
(170) Meggio, F.; Donella Deana, A.; Ruzzene, M.; Brunati, A. M.; Cesaro, L.; Guerra, B.; Meyer, T.; Mett, H.; Fabbro, D.; Furet, P.; et al. Different susceptibility of protein kinases to staurosporine inhibition. Kinetic studies and molecular bases for the resistance of protein kinase CK2. *Eur J Biochem* **1995**, *234* (1), 317-322. DOI: 10.1111/j.1432-1033.1995.317_c.x From NLM.
(171) Cosenza, M.; Civallero, M.; Marcheselli, L.; Sacchi, S.; Pozzi, S. Ricolinostat, a selective HDAC6 inhibitor, shows anti-lymphoma cell activity alone and in combination with bendamustine. *Apoptosis* **2017**, *22* (6), 827-840. DOI: 10.1007/s10495-017-1364-4.
(172) Chang, Y.-C.; Cheung, C. H. A. An Updated Review of Smac Mimetics, LCL161, Birinapant, and GDC-0152 in Cancer Treatment. *Applied Sciences* **2021**, *11* (1), 335.
(173) Zheng, S.; Wang, W.; Aldahdooh, J.; Malyutina, A.; Shadbahr, T.; Tanoli, Z.; Pessia, A.; Tang, J. SynergyFinder Plus: Toward Better Interpretation and Annotation of Drug Combination Screening Datasets. *Genomics, Proteomics & Bioinformatics* **2022**, *20* (3), 587-596. DOI: https://doi.org/10.1016/j.gpb.2022.01.004.
(174) Yadav, B.; Wennerberg, K.; Aittokallio, T.; Tang, J. Searching for Drug Synergy in Complex Dose-Response Landscapes Using an Interaction Potency Model. *Comput Struct Biotechnol J* **2015**, *13*, 504-513. DOI: 10.1016/j.csbj.2015.09.001 From NLM.
(175) Oliver, F. J.; de la Rubia, G.; Rolli, V.; Ruiz-Ruiz, M. C.; de Murcia, G.; Murcia, J. M.-d. Importance of Poly(ADP-ribose) Polymerase and Its Cleavage in Apoptosis: LESSON FROM AN UNCLEAVABLE MUTANT. *Journal of Biological Chemistry* **1998**, *273* (50), 33533-33539. DOI: 10.1074/jbc.273.50.33533 (accessed 2023/03/20).
(176) Nicholson, D. W.; Ali, A.; Thornberry, N. A.; Vaillancourt, J. P.; Ding, C. K.; Gallant, M.; Gareau, Y.; Griffin, P. R.; Labelle, M.; Lazebnik, Y. A.; et al. Identification and inhibition of the ICE/CED-3 protease necessary for mammalian apoptosis. *Nature* **1995**, *376* (6535), 37-43. DOI: 10.1038/376037a0.
(177) Olson, C. M.; Liang, Y.; Leggett, A.; Park, W. D.; Li, L.; Mills, C. E.; Elsarrag, S. Z.; Ficarro, S. B.; Zhang, T.; Düster, R.; et al. Development of a Selective CDK7 Covalent Inhibitor Reveals Predominant Cell-Cycle Phenotype. *Cell Chemical Biology* **2019**, *26* (6), 792-803.e710. DOI: https://doi.org/10.1016/j.chembiol.2019.02.012.
(178) Bunch, H. RNA polymerase II pausing and transcriptional regulation of the HSP70 expression. *European Journal of Cell Biology* **2017**, *96* (8), 739-745. DOI: https://doi.org/10.1016/j.ejcb.2017.09.003.
(179) Thomas, X.; Archimbaud, E. Mitoxantrone in the treatment of acute myelogenous leukemia: a review. *Hematol Cell Ther* **1997**, *39* (4), 63-74. DOI: 10.1007/s00282-997-0163-8 From NLM.
(180) Abu Saleh, M.; Solayman, M.; Hoque, M. M.; Khan, M. A.; Sarwar, M. G.; Halim, M. A. Inhibition of DNA Topoisomerase Type IIα (TOP2A) by Mitoxantrone and Its Halogenated Derivatives: A Combined Density Functional and Molecular Docking Study. *BioMed research international* **2016**, *2016*, 6817502. DOI: 10.1155/2016/6817502 From NLM.
(181) Hendershot, L. M.; Valentine, V. A.; Lee, A. S.; Morris, S. W.; Shapiro, D. N. Localization of the gene encoding human BiP/GRP78, the endoplasmic reticulum cognate of the HSP70 family, to chromosome 9q34. *Genomics* **1994**, *20* (2), 281-284. DOI: 10.1006/geno.1994.1166 From NLM.
(182) Holmes, N. CD45: all is not yet crystal clear. *Immunology* **2006**, *117* (2), 145-155. DOI: https://doi.org/10.1111/j.1365-2567.2005.02265.x.
(183) Roach, T.; Slater, S.; Koval, M.; White, L.; Cahir McFarland, E. D.; Okumura, M.; Thomas, M.; Brown, E. CD45 regulates Src family member kinase activity associated

with macrophage integrin-mediated adhesion. *Curr Biol* **1997**, *7* (6), 408-417. DOI: 10.1016/s0960-9822(06)00188-6 From NLM.
(184) Niesen, F. H.; Berglund, H.; Vedadi, M. The use of differential scanning fluorimetry to detect ligand interactions that promote protein stability. *Nature Protocols* **2007**, *2* (9), 2212-2221. DOI: 10.1038/nprot.2007.321.
(185) Huynh, K.; Partch, C. L. Analysis of Protein Stability and Ligand Interactions by Thermal Shift Assay. *Current Protocols in Protein Science* **2015**, *79* (1), 28.29.21-28.29.14. DOI: https://doi.org/10.1002/0471140864.ps2809s79.
(186) Huang, R.; Ayine-Tora, D. M.; Muhammad Rosdi, M. N.; Li, Y.; Reynisson, J.; Leung, I. K. H. Virtual screening and biophysical studies lead to HSP90 inhibitors. *Bioorganic & Medicinal Chemistry Letters* **2017**, *27* (2), 277-281. DOI: https://doi.org/10.1016/j.bmcl.2016.11.059.
(187) Allan, R. K.; Mok, D.; Ward, B. K.; Ratajczak, T. Modulation of Chaperone Function and Cochaperone Interaction by Novobiocin in the C-terminal Domain of Hsp90: EVIDENCE THAT COUMARIN ANTIBIOTICS DISRUPT Hsp90 DIMERIZATION . *Journal of Biological Chemistry* **2006**, *281* (11), 7161-7171. DOI: 10.1074/jbc.M512406200 (accessed 2023/07/26).
(188) Goode, K. M.; Petrov, D. P.; Vickman, R. E.; Crist, S. A.; Pascuzzi, P. E.; Ratliff, T. L.; Davisson, V. J.; Hazbun, T. R. Targeting the Hsp90 C-terminal domain to induce allosteric inhibition and selective client downregulation. *Biochim Biophys Acta Gen Subj* **2017**, *1861* (8), 1992-2006. DOI: 10.1016/j.bbagen.2017.05.006 From NLM.
(189) Allan, R. K.; Mok, D.; Ward, B. K.; Ratajczak, T. Modulation of Chaperone Function and Cochaperone Interaction by Novobiocin in the C-terminal Domain of Hsp90: EVIDENCE THAT COUMARIN ANTIBIOTICS DISRUPT Hsp90 DIMERIZATION. *Journal of Biological Chemistry* **2006**, *281* (11), 7161-7171. DOI: https://doi.org/10.1074/jbc.M512406200.
(190) McConnell, J. R.; Alexander, L. A.; McAlpine, S. R. A heat shock protein 90 inhibitor that modulates the immunophilins and regulates hormone receptors without inducing the heat shock response. *Bioorganic & Medicinal Chemistry Letters* **2014**, *24* (2), 661-666. DOI: https://doi.org/10.1016/j.bmcl.2013.11.059.
(191) Galam, L.; Hadden, M. K.; Ma, Z.; Ye, Q.-Z.; Yun, B.-G.; Blagg, B. S. J.; Matts, R. L. High-throughput assay for the identification of Hsp90 inhibitors based on Hsp90-dependent refolding of firefly luciferase. *Bioorganic & Medicinal Chemistry* **2007**, *15* (5), 1939-1946. DOI: https://doi.org/10.1016/j.bmc.2007.01.004.
(192) Schumacher, R. J.; Hurst, R.; Sullivan, W. P.; McMahon, N. J.; Toft, D. O.; Matts, R. L. ATP-dependent chaperoning activity of reticulocyte lysate. *Journal of Biological Chemistry* **1994**, *269* (13), 9493-9499. DOI: https://doi.org/10.1016/S0021-9258(17)36908-9.
(193) Yadav, B.; Pemovska, T.; Szwajda, A.; Kulesskiy, E.; Kontro, M.; Karjalainen, R.; Majumder, M. M.; Malani, D.; Murumägi, A.; Knowles, J.; et al. Quantitative scoring of differential drug sensitivity for individually optimized anticancer therapies. *Scientific Reports* **2014**, *4* (1), 5193. DOI: 10.1038/srep05193.
(194) Schwinn, M. K.; Machleidt, T.; Zimmerman, K.; Eggers, C. T.; Dixon, A. S.; Hurst, R.; Hall, M. P.; Encell, L. P.; Binkowski, B. F.; Wood, K. V. CRISPR-Mediated Tagging of Endogenous Proteins with a Luminescent Peptide. *ACS Chemical Biology* **2018**, *13* (2), 467-474. DOI: 10.1021/acschembio.7b00549.
(195) Wurnig, S.; Vogt, M.; Hogenkamp, J.; Dienstbier, N.; Borkhardt, A.; Bhatia, S.; Hansen, F. K. Development of the first geldanamycin-based HSP90 degraders. *Frontiers in Chemistry* **2023**, *11*, Original Research. DOI: 10.3389/fchem.2023.1219883.
(196) Whitesell, L.; Lindquist, S. L. HSP90 and the chaperoning of cancer. *Nature Reviews Cancer* **2005**, *5* (10), 761-772. DOI: 10.1038/nrc1716.
(197) Zagouri, F.; Sergentanis, T. N.; Nonni, A.; Papadimitriou, C. A.; Michalopoulos, N. V.; Domeyer, P.; Theodoropoulos, G.; Lazaris, A.; Patsouris, E.; Zogafos, E.; et al. Hsp90

in the continuum of breast ductal carcinogenesis: Evaluation in precursors, preinvasive and ductal carcinoma lesions. *BMC Cancer* **2010**, *10* (1), 353. DOI: 10.1186/1471-2407-10-353.

(198) Kamal, A.; Thao, L.; Sensintaffar, J.; Zhang, L.; Boehm, M. F.; Fritz, L. C.; Burrows, F. J. A high-affinity conformation of Hsp90 confers tumour selectivity on Hsp90 inhibitors. *Nature* **2003**, *425* (6956), 407-410. DOI: 10.1038/nature01913.

(199) Yang, Y.; Rao, R.; Shen, J.; Tang, Y.; Fiskus, W.; Nechtman, J.; Atadja, P.; Bhalla, K. Role of Acetylation and Extracellular Location of Heat Shock Protein 90α in Tumor Cell Invasion. *Cancer Research* **2008**, *68* (12), 4833-4842. DOI: 10.1158/0008-5472.Can-08-0644 (accessed 2/2/2023).

(200) Zhang, S.-l.; Yu, J.; Cheng, X.-k.; Ding, L.; Heng, F.-y.; Wu, N.-h.; Shen, Y.-f. Regulation of human hsp90α gene expression. *FEBS Letters* **1999**, *444* (1), 130-135. DOI: https://doi.org/10.1016/S0014-5793(99)00044-7.

(201) Tang, X.; Chang, C.; Mosallaei, D.; Woodley, D. T.; Schönthal, A. H.; Chen, M.; Li, W. Heterogeneous Responses and Isoform Compensation the Dim Therapeutic Window of Hsp90 ATP-Binding Inhibitors in Cancer. *Mol Cell Biol* **2022**, *42* (2), e0045921. DOI: 10.1128/mcb.00459-21 From NLM.

(202) Courtney, A. H.; Shvets, A. A.; Lu, W.; Griffante, G.; Mollenauer, M.; Horkova, V.; Lo, W. L.; Yu, S.; Stepanek, O.; Chakraborty, A. K.; et al. CD45 functions as a signaling gatekeeper in T cells. *Sci Signal* **2019**, *12* (604). DOI: 10.1126/scisignal.aaw8151 From NLM.

(203) Koretzky, G. A.; Abtahian, F.; Silverman, M. A. SLP76 and SLP65: complex regulation of signalling in lymphocytes and beyond. *Nature Reviews Immunology* **2006**, *6* (1), 67-78. DOI: 10.1038/nri1750.

(204) Zhang, W.; Liu, H. T. MAPK signal pathways in the regulation of cell proliferation in mammalian cells. *Cell Research* **2002**, *12* (1), 9-18. DOI: 10.1038/sj.cr.7290105.

(205) Reckel, S.; Hamelin, R.; Georgeon, S.; Armand, F.; Jolliet, Q.; Chiappe, D.; Moniatte, M.; Hantschel, O. Differential signaling networks of Bcr-Abl p210 and p190 kinases in leukemia cells defined by functional proteomics. *Leukemia* **2017**, *31* (7), 1502-1512. DOI: 10.1038/leu.2017.36 From NLM.

(206) Eustace, B. K.; Sakurai, T.; Stewart, J. K.; Yimlamai, D.; Unger, C.; Zehetmeier, C.; Lain, B.; Torella, C.; Henning, S. W.; Beste, G.; et al. Functional proteomic screens reveal an essential extracellular role for hsp90α in cancer cell invasiveness. *Nature Cell Biology* **2004**, *6* (6), 507-514. DOI: 10.1038/ncb1131.

(207) Stellas, D.; El Hamidieh, A.; Patsavoudi, E. Monoclonal antibody 4C5 prevents activation of MMP2 and MMP9 by disrupting their interaction with extracellular HSP90 and inhibits formation of metastatic breast cancer cell deposits. *BMC Cell Biology* **2010**, *11* (1), 51. DOI: 10.1186/1471-2121-11-51.

(208) Tsutsumi, S.; Scroggins, B.; Koga, F.; Lee, M. J.; Trepel, J.; Felts, S.; Carreras, C.; Neckers, L. A small molecule cell-impermeant Hsp90 antagonist inhibits tumor cell motility and invasion. *Oncogene* **2008**, *27* (17), 2478-2487. DOI: 10.1038/sj.onc.1210897.

(209) Zou, M.; Bhatia, A.; Dong, H.; Jayaprakash, P.; Guo, J.; Sahu, D.; Hou, Y.; Tsen, F.; Tong, C.; O'Brien, K.; et al. Evolutionarily conserved dual lysine motif determines the non-chaperone function of secreted Hsp90alpha in tumour progression. *Oncogene* **2017**, *36* (15), 2160-2171. DOI: 10.1038/onc.2016.375.

(210) Kaur, J.; Das, S. N.; Srivastava, A.; Ralhan, R. Cell surface expression of 70 kDa heat shock protein in human oral dysplasia and squamous cell carcinoma: correlation with clinicopathological features. *Oral Oncology* **1998**, *34* (2), 93-98. DOI: https://doi.org/10.1016/S1368-8375(97)00055-9.

(211) Farkas, B.; Hantschel, M.; Magyarlaki, M.; Becker, B.; Scherer, K.; Landthaler, M.; Pfister, K.; Gehrmann, M.; Gross, C.; Mackensen, A.; et al. Heat shock protein 70 membrane expression and melanoma-associated marker phenotype in primary and metastatic melanoma. *Melanoma Research* **2003**, *13* (2).

(212) Zhou, Q.; Facciponte, J.; Jin, M.; Shen, Q.; Lin, Q. Humanized NOD-SCID IL2rg–/– mice as a preclinical model for cancer research and its potential use for individualized cancer therapies. *Cancer Lett* **2014**, *344* (1), 13-19. DOI: 10.1016/j.canlet.2013.10.015 From NLM.
(213) zou, s.; Ye, J.; Zou, S.; Tan, J.; Wei, Y.; Xu, J. LCP2 expression is correlated with an abundance of immune infiltrates and is a potential prognostic biomarker in lung adenocarcinoma. Research Square: 2023.
(214) Wang, Z.; Peng, M. A novel prognostic biomarker LCP2 correlates with metastatic melanoma-infiltrating CD8+ T cells. *Scientific Reports* **2021**, *11* (1), 9164. DOI: 10.1038/s41598-021-88676-9.
(215) Ren, H.; Fang, J.; Ding, X.; Chen, Q. Role and inhibition of Src signaling in the progression of liver cancer. *Open Life Sciences* **2016**, *11* (1), 513-518. DOI: doi:10.1515/biol-2016-0067 (accessed 2023-04-07).
(216) Xiong, J.; Wu, J. S.; Mao, S. S.; Yu, X. N.; Huang, X. X. Effect of saracatinib on pulmonary metastases from hepatocellular carcinoma. *Oncol Rep* **2016**, *36* (3), 1483-1490. DOI: 10.3892/or.2016.4968 From NLM.
(217) Ye, N.; Cai, J.; Dong, Y.; Chen, H.; Bo, Z.; Zhao, X.; Xia, M.; Han, M. A multi-omic approach reveals utility of CD45 expression in prognosis and novel target discovery. *Frontiers in Genetics* **2022**, *13*, Original Research. DOI: 10.3389/fgene.2022.928328.
(218) Krepler, C.; Chunduru, S. K.; Halloran, M. B.; He, X.; Xiao, M.; Vultur, A.; Villanueva, J.; Mitsuuchi, Y.; Neiman, E. M.; Benetatos, C.; et al. The novel SMAC mimetic birinapant exhibits potent activity against human melanoma cells. *Clin Cancer Res* **2013**, *19* (7), 1784-1794. DOI: 10.1158/1078-0432.Ccr-12-2518 From NLM.
(219) Didelot, C.; Lanneau, D.; Brunet, M.; Bouchot, A.; Cartier, J.; Jacquel, A.; Ducoroy, P.; Cathelin, S.; Decologne, N.; Chiosis, G.; et al. Interaction of heat-shock protein 90β isoform (HSP90β) with cellular inhibitor of apoptosis 1 (c-IAP1) is required for cell differentiation. *Cell Death & Differentiation* **2008**, *15* (5), 859-866. DOI: 10.1038/cdd.2008.5.
(220) Allensworth, J. L.; Sauer, S. J.; Lyerly, H. K.; Morse, M. A.; Devi, G. R. Smac mimetic Birinapant induces apoptosis and enhances TRAIL potency in inflammatory breast cancer cells in an IAP-dependent and TNF-α-independent mechanism. *Breast Cancer Res Treat* **2013**, *137* (2), 359-371. DOI: 10.1007/s10549-012-2352-6 From NLM.
(221) Varfolomeev, E.; Goncharov, T.; Vucic, D. Roles of c-IAP proteins in TNF receptor family activation of NF-κB signaling. *Methods Mol Biol* **2015**, *1280*, 269-282. DOI: 10.1007/978-1-4939-2422-6_15 From NLM.
(222) Russo, J. W.; Nouri, M.; Balk, S. P. Androgen Receptor Interaction with Mediator Complex Is Enhanced in Castration-Resistant Prostate Cancer by CDK7 Phosphorylation of MED1. *Cancer Discovery* **2019**, *9* (11), 1490-1492. DOI: 10.1158/2159-8290.Cd-19-1028 (accessed 2/17/2023).
(223) Azad, A. A.; Zoubeidi, A.; Gleave, M. E.; Chi, K. N. Targeting heat shock proteins in metastatic castration-resistant prostate cancer. *Nature Reviews Urology* **2015**, *12* (1), 26-36. DOI: 10.1038/nrurol.2014.320.
(224) Tien, A. H.; Sadar, M. D. Keys to unlock androgen receptor translocation. *Journal of Biological Chemistry* **2019**, *294* (22), 8711-8712. DOI: 10.1074/jbc.H119.009180 (accessed 2023/02/17).
(225) Gerber, M.; Tenney, K.; Conaway, J. W.; Conaway, R. C.; Eissenberg, J. C.; Shilatifard, A. Regulation of Heat Shock Gene Expression by RNA Polymerase II Elongation Factor, Elongin A. *Journal of Biological Chemistry* **2005**, *280* (6), 4017-4020. DOI: https://doi.org/10.1074/jbc.C400487200.
(226) Smith, E. R.; Winter, B.; Eissenberg, J. C.; Shilatifard, A. Regulation of the transcriptional activity of poised RNA polymerase II by the elongation factor ELL. *Proceedings of the National Academy of Sciences* **2008**, *105* (25), 8575-8579. DOI: doi:10.1073/pnas.0804379105.

(227) Schwartz, B. E.; Larochelle, S.; Suter, B.; Lis, J. T. Cdk7 is required for full activation of Drosophila heat shock genes and RNA polymerase II phosphorylation in vivo. *Mol Cell Biol* **2003**, *23* (19), 6876-6886. DOI: 10.1128/mcb.23.19.6876-6886.2003 From NLM.
(228) Li, X.-P.; Qu, J.; Teng, X.-Q.; Zhuang, H.-H.; Dai, Y.-H.; Yang, Z.; Qu, Q. The Emerging Role of Super-enhancers as Therapeutic Targets in The Digestive System Tumors. *International Journal of Biological Sciences* **2023**, *19* (4), 1036-1048, Review. DOI: 10.7150/ijbs.78535.
(229) Zhou, D.; Liu, Y.; Ye, J.; Ying, W.; Ogawa, L. S.; Inoue, T.; Tatsuta, N.; Wada, Y.; Koya, K.; Huang, Q.; et al. A rat retinal damage model predicts for potential clinical visual disturbances induced by Hsp90 inhibitors. *Toxicology and Applied Pharmacology* **2013**, *273* (2), 401-409. DOI: https://doi.org/10.1016/j.taap.2013.09.018.
(230) Zajec, Ž.; Dernovšek, J.; Gobec, M.; Tomašič, T. In Silico Discovery and Optimisation of a Novel Structural Class of Hsp90 C-Terminal Domain Inhibitors. *Biomolecules* **2022**, *12* (7), 884.
(231) Pearl, L. H.; Prodromou, C. Structure and Mechanism of the Hsp90 Molecular Chaperone Machinery. *Annual Review of Biochemistry* **2006**, *75* (1), 271-294. DOI: 10.1146/annurev.biochem.75.103004.142738.
(232) Seetoh, W.-G.; Abell, C. Disrupting the Constitutive, Homodimeric Protein–Protein Interface in CK2β Using a Biophysical Fragment-Based Approach. *Journal of the American Chemical Society* **2016**, *138* (43), 14303-14311. DOI: 10.1021/jacs.6b07440.
(233) Liu, Q.; Tu, G.; Hu, Y.; Jiang, Q.; Liu, J.; Lin, S.; Yu, Z.; Li, G.; Wu, X.; Tang, Y.; et al. Discovery of BP3 as an efficacious proteolysis targeting chimera (PROTAC) degrader of HSP90 for treating breast cancer. *Eur J Med Chem* **2022**, *228*, 114013. DOI: 10.1016/j.ejmech.2021.114013 From NLM.
(234) Duerfeldt, A. S.; Blagg, B. S. J. Hsp90 inhibition: Elimination of shock and stress. *Bioorganic & Medicinal Chemistry Letters* **2010**, *20* (17), 4983-4987. DOI: https://doi.org/10.1016/j.bmcl.2010.06.108.